Synthesis, Characterization and Applications of Persistent Radical Systems

Jose Luis Muñoz Gómez

Tesis Doctoral

Programa de doctorado de Ciencia de Materiales

Directores

José Vidal Gancedo and Jaume Veciana Miró

Departament de Química
Facultat de Ciències

2015

Memoria presentada para aspirar al grado de doctor por:

Jose Luis Muñoz Gómez

Visto Bueno:

José Vidal Gancedo

Jaume Veciana Miró

en Bellaterra, a dd de Enero de 2015

JOSÉ VIDAL GANCEDO Tenured Scientist and **JAUME VECIANA MIRÓ**, Research Professor, of the Spanish National Research Council at the Materials Science Institute of Barcelona (ICMAB-CSIC)

CERTIFY

That **Jose Luis Muñoz Gómez**, "licenciado" in Chemistry, has performed, under their management, the research work entitled **"Synthesis, characterization and applications of persistent radical systems ".** This work has been performed under the mark of the Materials Science Ph. D. program of the Chemistry Department of the Autonomous University of Barcelona.

An in witness whereof this is signed by

Directors		UAB Tutor
José Vidal Gancedo	Jaume Veciana Miró	Jordi Marquet Cortés

PhD Student

Jose Luis Muñoz Gómez

FECHA: dd, mm, 2015

¿Qué es "real"? ¿De qué modo definirías "real"? Si te refieres a lo que puedes sentir, a lo que puedes oler, a lo que puedes saborear y ver, entonces el término "real" son señales eléctricas interpretadas por tu cerebro.

Morfeo

A mi madre, mi hermano y mi tío Ton.

Agradecimientos

En primer lugar me gustaría agradecer al programa $JAE-PreDoc$ del Consejo Superior de Investigaciones Científicas (CSIC) por la beca que me ha permitido llevar a cabo el trabajo que hoy se presenta y a mis directores de tesis José Vidal y Jaume Veciana. Por extensión quiero agradecer a todos los miembros del grupo Nanomol los buenos y no tan buenos momentos pasados en este tiempo, particularmente a Vega por el tiempo dedicado la Resonancia Paramagnética y por su gran caligrafía; Ole tu caligrafía. Una persona que merece una especial mención es mi querido Amable, aunque pocas veces lo he llamado así. Tú has aguantado mis mejores momentos y has sufrido los peores, pero si me tengo que quedar con alguien del grupo, sin duda te escogería a tí. GRACIAS Amable por todo. Otro sufridor destacable sin duda ha sido César que aparte ha sido un gran soporte y de gran ayuda. Gracias a tí también.

El hecho de que queden separados el resto no implica, ni mucho menos, que los considere menos importantes a María Aguado y sus omisiones, Eva Samanes y sus imitaciones de mis siglas, Queral y las camisetas, Elisa (a la que forcé a cambiar de despacho) y el grupo del café. A Paco Vera con quien empecé en el laboratorio y con quien he tenido tantas largar y provechosas conversaciones de química, tú sí que vales. Espero no olvidar a nadie si cito por despachos, a Davide, Ajay y Francesc de arriba, Mat, Victor, Ingrid, Lydia, Isaac, Serena, Mildrey, Ariadna, Evelyn, Nuria, Santi, Stamatis, Sergi y Antonio de los despachos diferentes al mío. La gente de mi despacho, siendo por orden Javi, Elena, Freddy, , Inés, Manel (valenciano corrupto), Lourdes, Dolores, Toni, Dolores, Dayana, Elena Gonca y Raphael. Espero que a los que aún estais os vaya todo bien por el ICMAB y a los que no estaís que vayan muy bien todos los proyectos.

De la gente de fuera del grupo pero de dentro del ICMAB me gustaría mencionar, sin lugar a dudas a los David's Cristina, Marta, Romen, Arancha, Angela, Wojtek y el crack Josep. A la gente de administración, especialmente a Pietat, Trini, Carme y Vicente y a toda la gente que seguro me dejo y que tengo mucho cariño. Mi más sincero agradecimiento a Ildefonso, Angel y Eva, pues de ellos he aprendido prácticamente todo lo que sé de Polarización Dinámica y a María Rosa Sebastián con quien aprendí cómo preparar dendrímeros de fosforo.

Para continuar me gustaría mencionar a Enrique Pedroso y Vicente Marchán con

quienes dí mis primeros pasos como investigador y quienes ayudaron a poner los cimientos del investigador que soy hoy; gracias a vosotros y a todo el grupo 10-O del que guardo grandes recuerdos. Si los cimientos se pusieron en el grupo 10-O, sin lugar a dudas una parte muy importante me la ha aportado Enantia y en particular Yohan, gracias.

Hay dos personas del laboratorio omitidas a conciencia, Witold (Polish para los amigos) y Carlos (axo pijo), a ellos, junto con Vickitrón, Eve, Tom y Hector (mi calvo favorito) les he de agradecer momentos tanto dentro como fuera del laboratorio, especialmente los de fuera: las partidas, las cenas, las salidas en grupo, el cuidado de Cáprica cuando no estoy.

Los incondicionales que siempre están cuando los necesitas, Jessica, Mireia, Berta, Andrea, Montse, Magda y alguno ms que se me olvida, gracias por el soporte psicologico, sin vosotros estaría encerrado en Sant Boi. A los incondicionales del rio David (cuantas disculpas te debo), Rubén ferrer (castigo para tí), el nuevo pudiente Sergio, Rubén Dario, Adel (no más fotos). No quiero olvidar a los que me han acompaado en el pasado en mi vida Rubén culpable en parte de que me embarcase en esta aventura, el friki de Carlos, el altramú Miguel y especialmente a Luis quien ha soportado los momentos de histeria del proceso de escritura con un aplomo envidiable, quien ha organizado los viajes a la costa brava de desconexión, con una generosidad sin límites, GRACIAS (I love you an egg).

Para acabar quiero recordar que esta tesis se la quiero dedicar a mi madre, mi hermano (aunque no te tenga cerca siempre te tengo en mente) y a mi tío Ton, quien fue una gran persona, ojalá me pareciese más a él.

Pido disculpas si he olvidado mencionar a alguien, pero teniendo en cuenta el poco tiempo que he tenido para escribirlos creo que estan los ms importantes.

Summary

During the last decades many techniques for molecular structure studies have been developed. Nuclear Magnetic Spectroscopy (NMS), in particular, is an important technique that has achieved a widespread use for the identification and characterization of molecules of interest in chemistry and biochemistry. Moreover, magnetic resonance imaging (MRI) is one of the best non invasive clinical imaging methods used in medicine which takes benefit of the NMS principles. One of the main limitations of Nuclear Magnetic Resonance (NMR) is its intrinsic low sensitivity. NMR signal is proportional to nuclear polarization, P, which is governed by the Boltzmann distribution of nuclear spins. In order to overcome this intrinsic limitation some instrumental improvements have appeared in the last few decades as the development of cryogenically cooled probes and the availability of higher magnetic field superconducting magnets.

Additionally, several methods to enhance the nuclear polarization have been also developed and are in constant expansion. Among them, the most extended ones are optical pumping, *para*-hydrogen induced polarization (PHIP) and dynamic nuclear polarization (DNP). All these methods are based on hyperpolarization, that is a general term that describes a system in which the distribution of populations has been disturbed to create an excess of populations in one energetic level, thus boosting the net magnetization of the system. Dynamic nuclear polarization (DNP) has emerged as one of the most general methods for nuclear hyperpolarization. DNP is a technique that requires the presence in the sample of a paramagnetic compound, a glassing agent and the analyte, the target of polarization. In this Thesis we have developed several new paramagnetic compounds based on organic persistent radicals covering from monoradicals of three different families (TEMPO, BDPA and PTM) to biradicals combining such monoradicals.

In the present Thesis we have been synthesized and characterized several monoradicals of three families of compounds (PTM, BDPA and TEMPO). The possible application of three BDPA derivatives as polarizing agents has been explored. The results obtained for two of them are promising as they improve the sample preparation conditions with respect the non functionalized BDPA, reducing the time necessary to perform the DNP experiment and open the possibility to be eliminated during the transference process in order to avoid a further loss of polarization. It has recently been proposed that mixed biradicals based on trityl radicals and nitroxide radicals are

potentially the best biradical candidates for attaining the maximal DNP enhancements. Under the light of these studies, we performed the synthesis and characterization of a few biradicals, not only those that joins trityl and nitroxide but other that mix carbon centered radicals of the same family or the different family too. The possible application of some of them as a polarizing agents were tested obtaining good results for a some of them.

Another methodology to obtain hyperpolarized nuclei of low gyromagnetic constant is the use of Magic Angle Spinning-Dynamic Nuclear Polarization (MAS-DNP). In this technique, the hyperpolarized compound usually are the hydrogen atoms of water that transfer their polarization to low gyromagnetic nuclei by the double resonance performed by the Cross Polarization. The paramagnetic compounds that are used to polarize hydrogen nuclei in general are TEMPO biradicals. As we synthesized a monoradical of TEMPO, we performed the synthesis and characterization of three TEMPO biradicals (TEMPO=TEMPO, TEMPOesterTEMPO and TEMPOamidoTEMPO), the water enhancements tests were performed in Dr. Bodenhausen laboratory (Switzerland). The enhancements obtained indicated that the biradicals with greater couplings generates lower polarization levels and with them lower enhancement.

In general, MRI is limited to systems with a large bulk magnetization, such as that provided by water in tissues. Imaging of other nuclei is possible, but challenging. These shortcomings are the result of both the gyromagnetic ratios and natural abundances of the other active nuclei. More specifically, protons have a relatively high gyromagnetic ratio compared to other nuclei. The gyromagnetic ratio controls the difference in the energy levels of the system, and the larger the energy difference, the larger the polarization is obtained because of the Boltzmann distribution. Since other nuclei such as carbon, nitrogen or phosphorus have smaller gyromagnetic ratios, they have smaller energy level differences and thus smaller net polarizations. While spectroscopic applications of nuclei other than protons using NMR are possible, imaging of the other nuclei (especially *in vivo*) is nearly impossible.

The low sensibility of MRI of low gyromagnetic constant nuclei can be improved by hyperpolarization techniques. On the other hand, the improvements on water imaging, apart from differences in the local water content of different tissues which generates an intrinsic contrast, the basic contrast in the MR images mainly results from regional differences in the intrinsic relaxation times T_1 and T_{02}, each of which can be independently chosen to dominate image contrast. However, the intrinsic contrast provided by the water T_1 and T_2 and changes in their values brought about by tissue pathology are often too limited to enable a sensitive and specific diagnosis. For that reason, increasing use is made of MRI contrast agents that alter the image contrast following their administration. The degree and location of the contrast changes provide substantial diagnostic information. Certain contrast agents are predominantly used to shorten the T_1 relaxation time and these are mainly based on low-molecular weight chelates of

gadolinium ion Gd^{3+}. The research in organic radical contrast agents would provide an alternative to highly toxic gadolinium-based contrast agents. However, the intrinsically low paramagnetic relaxivity of nitroxides (in part due to their low spin of 1/2) has prevented their widespread application as a MRI contrast agent.

The challenge in the development of new contrast agents for MRI is the design and synthesis of paramagnetic compounds of moderate molecular size that possess long *in vivo* lifetimes, high water solubility and high ^1H water relaxivities. The use of dendrimers makes possible to enhance water solubility by addition of surface polar groups and increase the total spin by the interaction among them on the dendrimer surface. Dendrimers introduce to the contrast agent system the possibility to change the molecule size, as long as we use different generations, providing specific size-bio distribution. In that way, low molecular weight (small sizes) compounds are quickly eliminated by kidneys. On the other hand, larger molecular weight molecules (big sizes) present low permeability through the vascular wall and remain in blood vessels for long time. In this sense radical dendrimers are a versatile molecules that allow control the final size of the contrast agent to ensure the desired bio distribution, controlling the lifetimes and excretion. Thus, we have synthesized and characterized a series of radical dendrimers. The water solubility was tested with the purpose of studying their behavior as a contrast agents in water media. Only Gc_0amidoTEMPO, PROXYL-Lys(Gc_x)OLi and PROXYL-Tyr(Gc_x)OLi, were water soluble; so the measurement of the water relaxivities were performed only for them. The obtained results for tyrosine dendrimers showed a dendritic effect on the relaxivities which opens the door of this family of compounds as a promising metal-free contrast agents.

Contents

Abbreviations

Å: Ångström unit.
ACN: Acetonitrile.
AcOH: Acetic Acid.
B_0: External Magnetic Field.
BA-BDPA: 4-((fuoren-9-yl)(fuoren-9-ylidene)methyl)phenyl)methanol radical.
BAm-BDPA: 4-((fuoren-9-yl)(fuoren-9-ylidene)methyl)phenyl)methanamine radical.
BDPA: 1,3-bis(diphenylene)-2-phenylallyl radical.
BDPAamidoTEMPO: N-(4-((fluoren-9-yl)(fluoren-9-ylidene)methyl)benzyl)-2-(2,2,6,6-tetramethylpiperidin-4-ylidene-1oxyl)acetamide biradical.
BDPAesterTEMPO: O-(4-((fluoren-9-yl)(fluoren-9-ylidene)methyl)benzyl)-2-(2,2,6,6-tetramethylpiperidin-4-ylidene-1oxyl)acetate biradical.
BDPA=TEMPO: (trans)-4-(1,3-bis(diphenylene)-2-phenylallyl)-1,3-bis(diphenylene)-2-phenylallyl biradical
BDPA=TEMPO:(trans)-4-(2,2,6,6-tetramethyl-1-piperidinyloxyl)-1,3-bis(diphenylene)-2-phenylallyl biradical.
BiTEMPO: General term for biradicals with two TEMPO moieties.
BOC: tert-butyloxycarbonyl protecting group.
br: broad.
brs: broad singlet.
CE: Cross Effect.
CP: Cross polarization.
CV: Cyclic voltamperometry.
d: doublet.
DBU: 1,8-Diazabicyclo[5.4.0]undec-7-ene.
DCC: Dicyclohexylcarbodiimide.
DCI: Diisopropylcarbodiimide.
DCM: Dichlorometane.
DIBAL-H: Diisobutylaluminum hydride.
DIEA: N,N-Diisopropylethylamine.
DMA: Dimethylacetamide.
DMAP: 4-(Dimethylamino)pyridine.
DMF: Dimethylformamide.

DMSO: Dimethyl sulfoxide.
DNP: Dynamic Nuclear Polarization.
DPPH: 2,2-Diphenyl-1-picrylhydrazyl radical.
EPR.: Electron Paramagnetic Resonance.
eq.: Equivalent.
Et_2O: Diethyl ether.
AcOEt: Ethyl acetate.
Fc: Ferrocene.
G: Gauss, magnetic field unit.
GPC: Gel Permeation chromatography.
HABT: 1-Hydroxy-7-aza-benzotriazole.
HATU: 1-[Bis(dimethylamino)methylene]-1H-1,2,3-triazolo[4,5-b]pyridinium 3-oxid hexafluorophosphate.
HOBT: 1-Hydroxybenzotriazole.
HP: Hyperpolarized.
HPLC: High Performance Liquid Chromatography.
Hx: Hexane.
I: Angular momentum.
I_{HP}: Intensity of the hyperpolarized NMR peak.
I_{Th}: Intensity of the thermal NMR peak.
IR-ATR: Infrared spectroscopy-Attenuated Total Reflectance.
GALVINOXYL: 2,6-Di-tert-butyl--(3,5-di-tert-butyl-4-oxo-2,5-cyclohexadien-1-ylidene) -p-tolyloxy radical
GBCAs: gadolinium-based contrast agents.
Gc_x: Dendrimer of x generation ended in chlorine.
Gc'_x: Dendrimer of x generation ended in aldehyde.
HOMO: Highest Occupied Molecular Orbital.
HP MR: Hyperpolarized Magnetic resonance.
LUMO: Lowest Unoccupied Molecular Orbital.
m: multiplet.
MALDI-TOF: Matrix-Assisted Laser Desorption/ Ionization-Time Of Fly.
MAS: Magic Angle Spinning.
MeOH: Methanol.
MNP: Magnetic Nanoparticles.
MRI: Magnetic Resonance Imaging.
MS: Mass Spectrometry.
m/z: Mass to charge ratio.
nm: nanometer.
NMP: N-methyl pirrolidone.
NMR: Nuclear Magnetic Resonance.
NMS: Nuclear Magnetic Spectroscopy.

ORCAs: Organic Radical Contrast Agents.
OX63: Tris8-carboxyl-2,2,6,6 tetra[2-(1-hydroxyethyl)]-benzo(1,2-d:4,5-d)bis(1,3) dithiole-4-ylmethyl sodium salt radical.
PCC: Piridinium chlorocromate.
PTM: Perchlorotriphenylmethyl radical.
PTMamidoTEMPO: N-(4-2,3,5,6-(tetrachlorophenyl)bis(pentachlorophenyl)methyl) -2-(2,2,6,6-tetramethylpiperidin-4-ylidene-1oxyl)acetamide biradical.
PTMesterTEMPO: O-(4-2,3,5,6-(tetrachlorophenyl)bis(pentachlorophenyl)methyl) -2-(2,2,6,6-tetramethylpiperidin-4-ylidene-1oxyl)acetate biradical.
PTM=BDPA: (trans)-4(4-2,3,5,6-(tetrachlorophenyl)bis(pentachlorophenyl)methyl) -(1,3-bis(diphenylene)-2-phenylallyl) biradical.
PTM=PTM: 4-(trans)-(4-2,3,5,6-(tetrachlorophenyl)bis(pentachlorophenyl)methyl) -(4-2,3,5,6-(tetrachlorophenyl)bis(pentachlorophenyl)methyl) biradical .
PTM=TEMPO:(trans)-4-(2,2,6,6-tetramethyl-1-piperidinyloxyl)-2,3,5,6-(tetrachlorophenyl) bis(pentachlorophenyl)methyl biradical.
PTM=TEMPE: (trans)-4-(2,2,6,6-tetramethyl-1-piperidine)-2,3,5,6 (tetrachlorophenyl) bispentachlorophenyl) methyl radical.
PROXYL: 2,2,5,5-tetramethylpyrrolidin-1-oxyl radical.
r_1: Longitudinal relaxivity.
r_2: Transverse relaxivity.
RF: Radio-frequency.
s: singlet.
SE: Solid Effect.
SOMO: Singly Occupied Molecular Orbital.
t: triplet.
td: triplet of doubles.
T: Tesla (magnetic induction units).
TEMPO=TEMPO: 2,2,2',2',6,6,6',6'-octamethyl-4,4'-bipiperidyliden-oxyl.
TM: Thermal Mixing.
TTM: Tris-(2,4,6-trichlorophenyl)methyl radical.
T_c: Build-up time constant (DNP parameter).
T_1: Longitudinal relaxation time or Spin-Lattice relaxation time.
T_2: Transverse relaxation time or Spin-Spin relaxation time.
TBAI: tetrabutylammonium iodide $n\mathrm{BuN_4}^+\mathrm{I}^-$.
$\mathrm{TBAPF_6}$: Tetrabutylammonium hexafluorophosphate. $n\mathrm{BuN_4}^+\mathrm{PF_6}^-$
TE: Time Echo.
TEMPO: (2,2,6,6-Tetramethylpiperidin-1-yl)oxyl radical.
TEMPOamidoTEMPO: 2-(2,2,6,6-tetramethylpiperidin-4-ylidene-1-oxyl)-N-((2,2,6,6-tetramethylpiperidin-4-ylidene-1-oxyl)methyl)acetamide biradical.
TEMPOesterTEMPO: 2-(2,2,6,6-tetramethylpiperidin-4-ylidene-1-oxyl)-O-((2,2,6,6-tetramethylpiperidin-4-ylidene-1-oxyl)methyl)acetate biradical.

TFA: Trifluoroacetic acid.
THF: Tetrahydrofuran.
UV-Vis: ultraviolet-visible spectrophotometry.
Verdacyl: Family of radicals derivaticed from 1,2,4,5-tetrazine.
δ: Chemical shift (ppm).
ϵ: Enhancement of the NMR signal.
γ: Giromagnetic constant.
$\omega_{0\mathrm{I}}$: Nuclear magnetic Frequency.
^{31}P: ^{31}P NMR spectrum with $\{^1\mathrm{H}\}$ deengaged.
^{13}C: ^{13}C NMR spectrum with $\{^1\mathrm{H}\}$ deengaged.
[1-^{13}C]piruvic acid: Piruvic acid with the C_1 labeled with ^{13}C.
[2-^{13}C]acetone: Acetone with the C_2 labeled with ^{13}C.

Chapter 1

Introduction

1.1 Nuclear Magnetic Resonance. Brief overview

One of the most useful techniques to study materials, among other fields, that has emerged during the last years is Nuclear Magnetic Resonance (NMR). NMR not only allows the study of the binding among atoms but also the study of surfaces [2–4] in a broad among of materials of the spatial distribution in 3D structures, cells [5,6] or their internal structures. [7] Moreover, its medical applications has revolutionized the study on the field. [8,9] Some possible improvements related with the sensitivity of the technique are under study and deals with magnetic compounds as the previously mentioned organic free radicals that can be endogenous [10] or, the more common case, exogenous.

Nuclear spin is the basis of all magnetic resonance (MR) research. The concept of spin is challenging and abstract, and it is mainly a convention developed to describe experimentally an evidence. Spin is a form of an angular momentum that is not produced by a rotation of the particle, but rather it is an intrinsic property of the particle itself. Spin behaves as expected from a classical description of a rotating object but fits the quantum mechanical descriptions of angular momentum. The total angular momentum of a particle with a spin, with 2I+1 possible sublevels,takes values following values $[\mathrm{I(I+1)}]^{\frac{1}{2}}$, where I is the spin quantum number, that depends on the nature of the particle. The applications described here deal with systems containing spins $\frac{1}{2}$, and therefore, the focus of this Introduction will be solely centered on $\frac{1}{2}$ spin systems.

Nuclear magnetic resonance is based on the interaction of a nuclear spin with an external magnetic field, referred to as $\mathrm{B_0}$. This interaction causes the spin to feel a torque, forcing it to precess around the magnetic field ($\mathrm{B_0}$). The size of the torque experienced by the spin depends both on the characteristics of the spin as well as the size of the magnetic field. Therefore, the rate at which the spin precesses depends on the magnetic field and the characteristics of the nucleus. Taking into account all these factors, the frequency of the precession (ω_0) is given by the Larmor equation:

$$\omega_0 = \gamma \times (1 - \sigma)\mathrm{B_0} \tag{1.1}$$

where γ is the gyromagnetic ratio (2.68×10^8 rad/s/Tesla for ^{1}H), a characteristic of the nucleus, and σ is the shielding constant due to the electrons orbiting around the nucleus.

For spin $\frac{1}{2}$ nuclei, there are two stationary states, one aligned with the magnetic field and another anti parallel with respect to the magnetic field. The magnetic moment can assume any orientation, but unless it is in one of these two states, it precesses. The difference in energy between those two states is given by the Larmor frequency ($\hbar\omega_0$). At room temperature this number is very small compared to kT, and there is only a slight excess of spins aligned along the magnetic field (*i. e.* in the lower energy level) compared to those aligned against the field (in the higher energy level) if the nuclei has a positive gyromagnetic ratio. The slight excess of spins aligned in one direction yields a net magnetic moment, which is the signal detected in an NMR experiment. The excess of spins in the lower energy level is quite small (often approximately 1 ppm), and therefore, the net magnetization is not negligible. Bloch[11] showed that for any ensemble of spins with I= $\frac{1}{2}$, the net magnetization is given by:

$$\mathrm{M_0} = \frac{\rho_0\gamma^2\hbar^2\mathrm{B_0}}{4\kappa\mathrm{T}} \tag{1.2}$$

where ρ_0 is the spin density, κ is the Boltzmann constant, $1.380\times\ 10^{-23}$ JK^{-1}, $\hbar$ is Planck's constant divided by 2π, 1.054×10^{-34} Js, and T is the temperature in Kelvin. By taking the vector sum over all spins, the behavior of the spins in a magnetic field can be described by the Bloch equations.[11]

$$\frac{d\mathrm{M_x}}{d\mathrm{t}} = \gamma(\mathrm{M_y B_0} + \mathrm{M_z B_1 sin}(\omega\mathrm{t})) - \frac{\mathrm{M_x}}{\mathrm{T_2}} \tag{1.3}$$

$$\frac{d\mathrm{M_y}}{d\mathrm{t}} = \gamma(-\mathrm{M_x B_0} + \mathrm{M_z B_1 sin}(\omega\mathrm{t})) - \frac{\mathrm{M_y}}{\mathrm{T_2}} \tag{1.4}$$

$$\frac{d\mathrm{M_z}}{d\mathrm{t}} = \gamma(\mathrm{M_x B_1 sin}(\omega\mathrm{t}) + \mathrm{M_y B_1 cos}(\omega\mathrm{t})) - \frac{\mathrm{M_z} - \mathrm{M_0}}{\mathrm{T_1}} \tag{1.5}$$

where $\mathrm{M_x}$, $\mathrm{M_y}$ and $\mathrm{M_z}$ are the x, y and z components, respectively, of the macroscopic magnetization of the sample placed in a magnetic field $\mathrm{B_0}$. $\mathrm{B_1}$ is the applied magnetic field created by an RF pulse, and $\mathrm{T_1}$ and $\mathrm{T_2}$ are the longitudinal and transverse relaxation times, respectively. The longitudinal relaxation time indicates the time it takes for $\mathrm{M_z}$ to be restored to its equilibrium value of $\mathrm{M_0}$. $\mathrm{T_1}$ relaxation is the result of non-radiative interactions between the spin system and the lattice, which connects the spin system with the external world. Relative to other types of spectroscopies, $\mathrm{T_1}$ is fairly slow (usually on the order of seconds), reflecting the weak interactions between the spins and their environment. $\mathrm{T_2}$ relaxation comes from the spin-spin interactions, which cause the Larmor frequency of the spins to change and dephasing the magnetization.

Many MR experiments can be developed correctly using a vector diagram representation, where the behavior of the system under different conditions (such as those from

magnetic field imperfections), be drawn and understood simply. For example, a spin echo experiment is outlined in **Figure 1.1**. In this sequence, the net magnetization is initially oriented along the net magnetic field (the z-direction). A 90°-x RF pulse is applied to the sample, which rotates the magnetization vector into the xy plane. The magnetization is allowed to precess, where the vector rotates around the net magnetic field at the Larmor frequency and becomes dephased due to T_2. The time that the spins are allowed to freely precess is referred to as the echo time, TE. TE is usually defined as the time between the 90° pulse and the center of the echo. After a time TE/2, 180° RF pulse is applied, which reverses the evolution and causes a refocusing of the signal TE/2 later.[12–14]

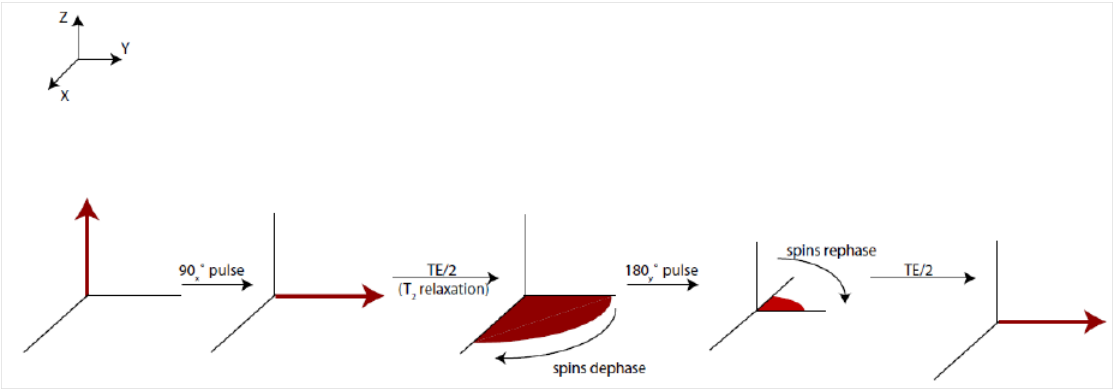

Figure 1.1: Vector diagram of a spin echo experiment. The 90°-x pulse takes the magnetization vector from +z to +y. While in the plane, the spins dephase during TE/2 due to T_2 relaxation. The 180°y pulse reverses the dephasing, causing a refocusing after TE/2.

The term "molecular imaging" has been used to describe techniques that directly or indirectly monitor and record the spatiotemporal distribution of molecular species or cellular processes for biochemical, biologic, diagnostic, or therapeutic applications.[13] A variety of imaging methods fit this description, including positron emission tomography (PET), single photon emission computed tomography (SPECT), optical imaging, and Raman spectroscopy. Relevant results have been evolved since the earliest SPECT camera, developed in the 1960s, up to the hundreds of PET tracers now described in the literature. Magnetic resonance imaging (MRI)which is based on nuclear magnetic resonance (NMR), was developed for clinical use on the 1980s for study structural aspects of tissues. More recently, this technique has provided functional insights due to several MRI innovations. Indeed, *in vivo* magnetic resonance spectroscopy (MRS), using gadolinium (Gd) chelates or magnetic nanoparticles (MNP), as contrast agents, to name a few, have permitted interrogation of basic cellular mechanisms at the molecular level. One limitation of MRS techniques is its low sensitivity. In order to overcome the lack of sensibility, the use of contrast agents (based on paramagnetic compounds as Gd(III) or organic free radicals) for ^{1}H visualization or hyperpolarization techniques (which requires a endogenous[10] or exogenous paramagnetic compound) for nuclei with

low giromagnetic constant (γ) as ^{13}C or ^{15}N are in development.

1.1.1 Magnetic Resonance with Contrast Agents

Signal intensity in most of the MRI experiments steams largely from the local value of the longitudinal relaxation rate, $1/T_1$, and the transverse rate $1/T_2$ of water protons contained in tissues. Signal tends to increase with increasing $1/T_1$ and decrease with increasing $1/T_2$. Pulse sequences that emphasize changes in $1/T_1$ are referred as T_1-weighted, and the opposite is called for T_2-weighted scans. Contrast agents (**Chapter 7**) are generally used to increase both $1/T_1$ and $1/T_2$ to vary degrees depending on their nature and the applied magnetic field. Contrast agents such as complexed Gadolinium (III) (positive contrast agents) that increase $1/T_1$ and $1/T_2$ values by roughly similar amounts are used to get T_1-weighted images since the percentage change in $1/T_1$ in tissue is much greater than in $1/T_2$. On the other hand, iron nanoparticles (negative contrast agents) generally lead to a much larger increase in $1/T_2$ than in $1/T_1$ and are used to get T_2-weighted scans.

Longitudinal and transverse relaxivity values, r_1 and r_2 refer to the amount of increase in $1/T_1$ and $1/T_2$, respectively obtained, per millimolar concentration of the contrast agent. T_1-agents usually have r_2/r_1 ratios of 1-2, whereas the values for T_2-agents, such as iron oxide particles, are higher than 10.

Advances in MRI have strongly favored the use of T_1-agents such as gadolinium (III) chelates, although new T_1-agents starts to be developed. The choice of Gd(III) chelates from other lanthanides derivatives, Dysprosium (III) or Holmium (III) with seven unpaired electrons are unexpected due to the symmetry of its electronic states leads to a slower spin relaxation.[24]

The presence of a paramagnetic compounds will increase the longitudinal and transverse relaxation rates, $1/T_1$ and $1/T_2$ of solvent nuclei. Diamagnetic and paramagnetic relaxation rates are additive and given by the Equation:

$$(1/T_i)_{obs} = (1/T_i)_d + (1/T_i)_p \qquad i = 1, 2 \tag{1.6}$$

where $(1/T_i)_{obs}$ is the observed solvent relaxation rate and the subscripts d and p refer to diamagnetic and paramagnetic contributions, respectively. The paramagnetic contribution is dependent on the concentration of paramagnetic species. Relaxivity, r_i (normally expressed in units of $mM^{-1}s^{-1}$), is defined as the slope of the concentration dependence. Thus a plot of $(1/T_i)_{obs}$ versus concentration of paramagnetic species would give the relaxivity as the slope of the plot.

$$(1/T_i)_{obs} = (1/T_i)_d + r_i[\text{radical}] \qquad i = 1, 2 \tag{1.7}$$

The origin of paramagnetic relaxation enhancement is generally divided into two components, the inner-sphere and the outer-sphere,

$$(1/T_i)_p = (1/T_i)_{\text{inner-sphere}} + (1/T_i)_{\text{outer-sphere}} \qquad i = 1, 2 \tag{1.8}$$

The inner-sphere relaxation refers to the relaxation enhancement of a solvent molecule directly coordinated to the paramagnetic compound, while the outer-sphere relaxation refers to relaxation enhancement of solvent molecules in the second coordination sphere and beyond (i.e., bulk solvent). This separation is used in an attempt to explain observed relaxivities in terms of existing theories. The emphasis will be on the longitudinal relaxation rate ($1/\mathrm{T}_1$) enhancement of water hydrogen atoms since this is the effect which is of the most interesting one in many MRI applications.

Equations relating the lifetime, chemical shift, and relaxation rates of solvent molecules in the inner sphere are given in **Equations 1.9 - 1.11**.

$$\frac{1}{\mathrm{T}_1^{\mathrm{IS}}} = \frac{\mathrm{qP}_m}{\mathrm{T}_{1m} + \tau_m} \tag{1.9}$$

$$\frac{1}{\mathrm{T}_2^{\mathrm{IS}}} = \mathrm{qP}_m \frac{1}{\tau_m} \left[\frac{\mathrm{T}_{2m}^{-1}(\tau_m^{-1} + \mathrm{T}_{2m}^{-1}) + \Delta\omega_m^2}{(\tau_m^{-1} + \mathrm{T}_{2m}^{-1})^2 + \Delta\omega_m^2} \right] \tag{1.10}$$

$$\Delta\omega_{\mathrm{obs}}^{\mathrm{IS}} = \mathrm{qP}_m \left[\frac{\Delta\omega_m}{(1 + \tau_m \mathrm{T}_{2m}^{-1})^2 + \tau_m^2 \Delta\omega_m^2} \right] \tag{1.11}$$

Where IS superscript refers to inner-sphere, P_m is the mole fraction of bond solvent nuclei, "q" is the number of bond water (or solvent) nuclei per paramagnetic center (i.e., the hydration number), τ_m is the lifetime of the solvent molecule in the complex (τ_m is the reciprocal of the solvent exchange rate, k_{ex}). The "m" subscript refers to the shift or relaxation rate of the solvent molecule in the inner-sphere and $\Delta\omega$ refers to the chemical shift difference between the paramagnetic complex and a diamagnetic reference.

From **Equation 1.9**, it is possible to see that if the water exchange rate is fast enough such that $\tau_m \ll \mathrm{T}_{1m}$, then the relaxation rate enhancement experienced by the bulk solvent will depend on the relaxation rate enhancement for the coordinated solvent molecule ($1/\mathrm{T}_{1m}$).

The outer-sphere relaxation arises from the translational diffusion of water molecules near the paramagnetic centers. Water molecules and the paramagnetic centers are often treated as hard spheres, and the outer-sphere relaxation rates are described by **Equations 1.12**.

$$\frac{1}{\mathrm{T}_2^{\mathrm{OS}}} = C[3j(\omega_I) + 7j(\omega_I)] \tag{1.12}$$

$$\frac{1}{\mathrm{T}_2^{\mathrm{OS}}} = C[2 + 1.5j(\omega_I) + 6.5j(\omega_I)] \tag{1.13}$$

$$C = \left(\frac{32\pi}{405}\right)\gamma_{\mathrm{I}}^2\gamma_{\mathrm{S}}^2\hbar^2 S(S+1)\left(\frac{\mathrm{N_A}M}{1000\mathrm{aD}}\right)$$

$$j(\omega) = Re\{[1 + \frac{1}{4}[i\omega\tau_{\mathrm{D}} + (\tau_{\mathrm{D}}/\mathrm{I}_{1\mathrm{e}}]^{\frac{1}{2}}]/[1 + [i\omega\tau_{\mathrm{D}} + (\tau_{\mathrm{D}}/\mathrm{I}_{1\mathrm{e}}]^{\frac{1}{2}}] + \frac{4}{9}[i\omega\tau_{\mathrm{D}} + (\tau_{\mathrm{D}}/\mathrm{I}_{1\mathrm{e}}] + \frac{1}{9}[i\omega\tau_{\mathrm{D}} + (\tau_{\mathrm{D}}/\mathrm{I}_{1\mathrm{e}}]^{\frac{3}{2}}]\}$$

where $\mathrm{N_A}$ is the Avogadro's number, M is the concentration of paramagnetic species, a is the distance of closest approach of the water molecule and paramagnetic specie, D is the sum of the diffusion constants of water and the paramagnetic species, and τ_{D} is a diffusional correlation time, given by $\tau_{\mathrm{D}} = a^2/D$.

Several groups have explored the potential use of conjugated large dendrimers as a new class of macromolecular MRI agents. Dendrimers (**Chapter 6**) are tree-shape, oligomerical structures prepared by reiterative reaction sequences starting from smaller "core" molecules. The highly branched, nearly monodisperse structure of dendrimer have led to a number of interesting molecular attributes for this class of macromolecules. The potential advantages of Gd(III) chelate dendrimers conjugates include the fact that dendrimers have uniform surface chemistry and minimal molecular weight distribution and shape variations, *e. g.* see Tacke *et al.*[25]

Metal-free organic radical contrast agents (ORCAs) would provide an alternative to high toxic gadolinium-based contrast agents (GBCAs). Although GBCAs are well tolerated by the majority of the patients, patients with impaired kidney function are reported to increase risk of developing a serious adverse reaction named nephrogenic systemic fibrosis (NSF).[26] Since the first report of this adverse effect in renal dialysis patients and its association with gadolinium,[27,28] guidelines for the administration of GBCAs have been issued and implemented worldwide to minimize the risk of NFS.

Conceptually, antibodies or other tissue-specific molecules may be combined with dendrimers and paramagnetic centers to provide disease-specific MRI agents. The challenge with regard to deliver sufficient quantity of paramagnetic label is substantial.[29] However, a number of interesting reports have appeared describing the preparation and characterization of targeted agents which contain a significant number of gadolinium atoms.[30]

1.1.2 Magnetic Resonance with Hyperpolarized Nuclei

As already mentioned, one limitation of MRS is low sensitivity. Magnetic resonance is inherently an insensitive technique, and thereby, magnetic resonance imaging is limited to study nuclei with a large bulk magnetization, such as water in tissues. Imaging of other nuclei is possible, but more challenging. These shortcomings are the result of the gyromagnetic ratio value and natural abundance of the other nuclei. More specifically, protons have a relatively high gyromagnetic ratio compared to other nuclei. The gyromagnetic ratio controls the difference in the energy levels of the system, and the larger the energy difference, the larger would be the polarization achieved because of the Boltzmann distribution. The polarization of a sample can be defined as the difference in populations between the two energy levels (N↑ and N↓) :[31]

$$\mathrm{P} = \frac{\mathrm{N}\uparrow - \mathrm{N}\downarrow}{\mathrm{N}\uparrow + \mathrm{N}\downarrow} \tag{1.14}$$

The populations in each energy level, N ↑ and N ↓, are determined by the energy difference between them, given by the Boltzmann distribution:

$$\frac{\mathrm{N}\uparrow}{\mathrm{N}\downarrow} = e^{-\Delta E/\kappa \mathrm{T}} \tag{1.15}$$

where ΔE is the energy difference between the two states, κ is the Boltzmann constant and T is the temperature in Kelvin. The magnitude of the observable magnetization is:

$$\mathrm{M}_0 = \frac{1}{2}\mathrm{N}_\mathrm{s}\gamma\hbar\mathrm{P} \tag{1.16}$$

With N_s equal to the number of spins in the sample. At thermal equilibrium, in the presence of an external magnetic field, B_0, the polarization, P, is given by:

$$\mathrm{P} = \tanh\left(\frac{\gamma\hbar\mathrm{B}_0}{2\kappa\mathrm{t}}\right) \tag{1.17}$$

Since other nuclei different of proton, such as carbon, nitrogen or phosphorus, have smaller gyromagnetic ratios, they have smaller energy level differences and thus smaller net polarizations. While spectroscopic applications of nuclei other than proton using NMR are possible, imaging of the other nuclei (especially *in vivo*) is nearly impossible. An illustrative example is given in **Figure 1.2**.

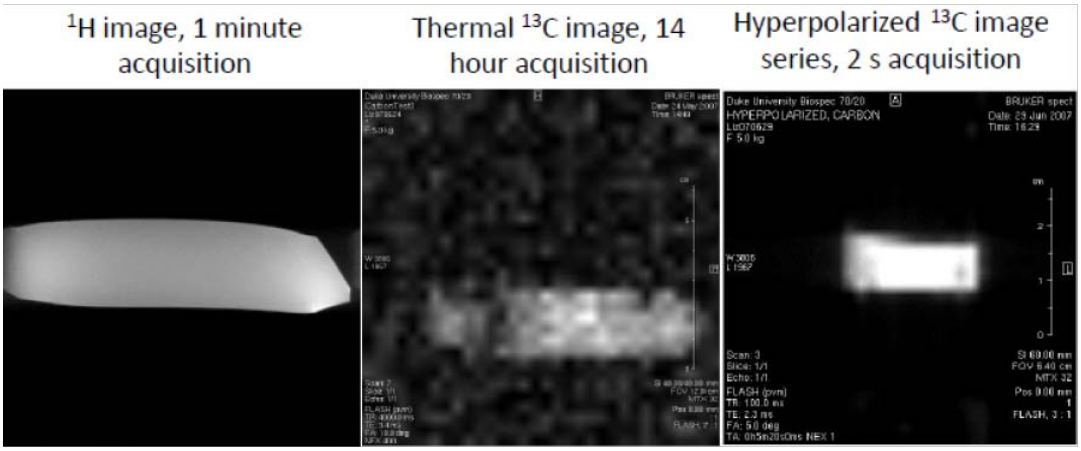

Figure 1.2: Comparison of signal intensity of ^{1}H water (left), thermally polarized ^{13}C urea (middle) and hyperpolarized ^{13}C urea (right). The proton image was acquired using a FLASH sequence in less than 1 minute, while the thermally polarized carbon image required 14 hours of averaging in order to acquire enough signal to make an image. The hyperpolarized carbon image series (right) has sufficient signal to allow acquisition in 2s using a FLASH sequence. Note that the slice for the hyperpolarized image was acquired using a different slice orientation than the proton and thermally polarized carbon images.

In the carbon image shown in **Figure 1.2** middle, the sample contains a concentrated ^{13}C labeled urea. Since the natural abundance of ^{13}C is 1%, we have significantly increased our signal by labeling 98% of the carbons. Yet, under these conditions, it still took 14 hours to get an image, and the quality of the image is very low. Thereby imaging smaller concentrations of non-proton nuclei, such as those *in vivo*, is nearly impossible.

The use of non-^{1}H nuclei in MRS, in particular ^{13}C, has been partially motivated by the limited chemical shift range ($\Delta\delta \approx 10$ ppm) of metabolites of interest in the ^{1}H spectrum.[32] Deconvolution of the many metabolite resonances in the ^{1}H spectrum is difficult. Additionally, strong signals from ^{1}Hs of water and lipids, relative to those of relevant metabolites, overwhelm the spectrum and are difficult to suppress.[33–35] Several strategies have been employed to overcome these limitations and are nowadays commonly applied to *in vitro* NMR applications, but this are relatively new for *in vivo* imaging and have been facilitated by the proliferation of high field strength magnets (3 T and 7 T). In contrast to the crowded ^{1}H spectrum, peaks corresponding to ^{13}C metabolites of interest occur over a much larger range, approximately 200 ppm. However, as previously mentioned, ^{13}C applications *in vivo* have been limited by both nuclear features and the low concentrations of interrogated metabolites. The natural abundance of ^{13}C, the NMR-active isotope, is only 1.1%. In addition, the gyromagnetic ratio (γ) of ^{13}C is only 1/4 that of ^{1}H, which further limits sensitivity. Finally, in contrast to water (60-70% of the human body), in which the concentration of ^{1}H is approximately 110M, the most concentrated metabolites (for example, ascorbate and lactate) are present in the mM range *in vivo*. Accordingly, MRI/MRS of endogenous

^{13}C is not possible at reasonable imaging times. Fortunately, HP MR has recently emerged as a way to dramatically improve sensitivity, with signal enhancements in solution routinely observed on the order of 104 for a variety of small molecules.[36–41]

The imaging of other non-proton nuclei for different applications, such as mapping ventilation/perfusion in the lungs using Xe or He,[42] pH measurements[43], and enzyme flux measurements[44,45], is only possible using hyperpolarized nuclei. There are several techniques for achieving hyperpolarization, including optical pumping for noble gases,[31] para-hydrogen induced polarization,[46] and dynamic nuclear polarization.[47]

All hyperpolarization work presented in this Thesis was done using dynamic nuclear polarization (DNP). Dynamic nuclear polarization is a technique that has been well studied in the physics community since 1958[48]. Until recently, it was limited to systems such as coal, for use in high energy physics, and to study micro-ordering in the μK temperature regime.[49] Technical advances in the engineering of magnets proves and microwave sources have transformed DNP into a practical method for the creation of hyperpolarized samples.[47] This technique and the experiments that were carried out will be explained in **Chapter 5** whereas the preparation of the paramagnetic species necessary to perform the experiments are explained in **Chapter 3** for monoradicals or **Chapter 4** for biradicals.

1.1.3 Organic radicals

Open-shell molecules such as radicals, carbenes, and electronically excited-state molecules are generally quite reactive.[15] These short lived species play a crucial role in many molecular transformations and also in materials science. Since the last century, significant developments in the chemistry of open-shell molecules have been achieved. Most of these developments were originated by the preparation of long lived open-shell molecules.[16] The creative design of ligands and substitents have made it possible to increase the lifetimes of such reactive molecules or even isolate them. In chemistry, a radical (or more precisely, a free radical) is neutral or charged (genative or possitive) with an open shell electronic structure with unpaired number of valence electrons, so they are paramagnetic substances.

With some exceptions, the open shell configuration make free radicals highly chemically reactive species towards other substances, or even towards themselves. Free radicals will often spontaneously dimerize or polymerize if they come in contact other react species. Most radicals are reasonably stable but only at very low concentrations in inert media or in vacuum. However, there are some examples of long-lived radicals that play an important role in some daily aspects as combustion[17], atmospheric chemistry polymerization[18], biochemistry[19], and many other chemical processes. For example, in living organisms, the free radicals superoxide and nitric oxide and their reaction products regulate many important processes, such as the control of vascular tone and thus the blood pressure. They also play a key role in the intermediary metabolism of various biological compounds. Such radicals can even be messengers in a process

dubbed redox signaling.

Radicals can be divided into classes in accordance with the kinetics of their bimolecular self-reactions and on the basis of their structural electronic properties. Three classes of radicals are recognized according with their kinetics: Transient radicals undergo bimolecular self-reactions at, or close to, the diffusion-controlled limit. Persistent radicals undergo much slower bimolecular self-reactions and slow, or no, unimolecular decay reactions. Stable radicals do not undergo such reactions at ambient temperatures (or if they go, the rates are negligible). There are two main classes of radicals according with their structural/electronic characteristics. The vast majority of organic radicals have their unpaired electrons occupying an orbital perpendicular to the local molecular framework. Such species are classified as π radicals. On the contrast, if the electron is occupying an orbital lying in the local framework, such species are classified as σ radicals.

The prime example of a stable radical is molecular dioxygen (O_2). Another common example is nitric oxide (NO). There are examples of thiazyl radicals, which show low reactivity and remarkable thermodynamic stability with only a very limited extent of a π resonance stabilization .[20,21] Most stable or persistent radical compounds are π radicals. Their longevity is due to steric crowding around the radical center, which makes it physically difficult for the radical to react with another molecule.[22] Examples of these radicals include Gomberg's triphenylmethyl radical, nitroxides, (general formula R_2NO) such as TEMPO, nitronyl nitroxides, phenoxy radicals, azephenylenyls and radicals derived from PTM (perchlorotriphenylmethyl radical) and TTM (tris(2,4,6-trichlorophenyl)methyl radical) **Figure 1.3**.[23]
Another way to have persistent radicals consist of increasing the delocalization of the unpaired electron. Radicals like Nitronyl nitroxides present delocalization of the unpaired electron between the nitrogen and oxigen atoms.

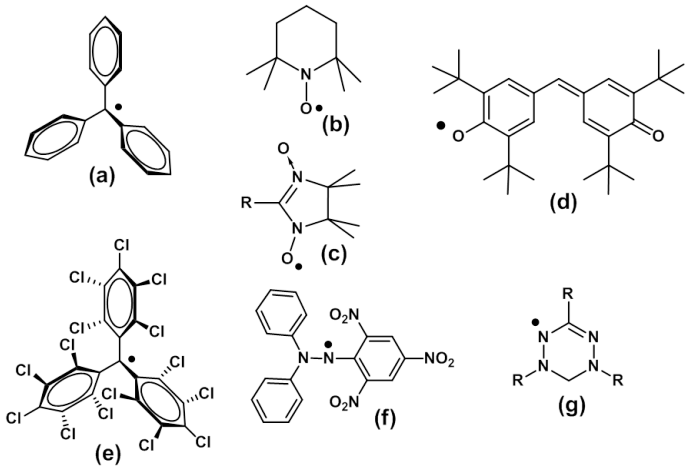

Figure 1.3: Some examples of persistent radical: a) Gomberg's triphenylmethyl radical, b) TEMPO radical, c) Nitronyl nitroxide radical, d) Galvinoxyl radical, e) PTM radical, f) DPPH radical and g) Verdazyl radical.

A very important tool to study radicals is Electron Paramagnetic Resonance (EPR). It is a spectroscopic technique useful for molecules with unpaired electrons. The basic concepts of EPR are analogous to those of nuclear magnetic resonance. However in EPR, electron spins are excited instead of the spin of atomic nuclei. This technique provides information about the electronic and molecular structure of the paramagnetic centers (see Appendice C).

Bibliography

[1] Kinoshita M. *Jpn. J. Appl. Phys.*, 33:p.5718, **1994**.

[2] Kobayashi T., Lafon O., Thankamony A.S.L., Slowing I.I., Kandel K., Carnevale D., Vitzthum V., Vezin H., Amoureux J.-P., Bodenhausen G., and Pruski M. *Phys. Chem. Chem. Phys.*, 15:p.5553, **2013**.

[3] Lelli M., Lesage A., Caporini M.A., Vitzthum V., Miéville P., Hé roguel F., Rascón F., Roussey A., Thieuleux C., Boualleg M., Veyre L., Bodenhausen G., Copéret C., and Emsley L. *J. Am. Chem. Soc.*, 133:p.2104, **2011**.

[4] Lesage A., Lelli D., Gajan D., Caporini M.A., Vitzthum V., Miéville P., Alauzun J., Roussey A., Thieuleux C., Mehdi A., Bodenhausen G., Copéret C., and Emsley L. *J. Am. Chem. Soc.*, 132:p.15459, **2010**.

[5] Bayro M.J., Debelouchina G.T., Eddy M.T., Birkett N.R., MacPhee C.E., Rosay M., Maas W.E., Dobson C.M., and Griffin R.G. *J. Am. Chem. Soc.*, 133:p.13967, **2011**.

[6] Linden a. H., Lange S., Franks W.T., Akbey U., Specker E., van Rossum B.-J., and Oschkinat H. *J. Am. Chem. Soc.*, 133:p.19266, **2011**.

[7] Gelis I., Vitzthum V., Dhimole N., Caporini M.A., Schedlbauer A., Carnevale D., Connell S.R., Fucini P., and Bodenhausen G. *J. Biomol. NMR*, 56:p.85, **2013**.

[8] Lingwood M.D., Siaw T.A., Sailasuta N., Abulseoud O.A., Chan H.R., Ross B.D., Bhattacharya P., and Han S. *Radiology*, 265(2):p.418, **2012**.

[9] Keshari K. R. and Wilson D. M. *Chem. soc. Rev.*, 43:p.1627, **2014**.

[10] Maly T., Cui D., Griffin R.G., and Miller A.-F. *J. Phys. Chem. B*, 116:p.7055, **2012**.

[11] Bloch F. *Nuclear Induction*, 70:p.460, **1946**.

[12] Haacke E.M., Brown R.W., Thompson M.R., and Venkatesan R. *Magnetic Resonance Imaging: Physical Principles and Sequence Design*. Wiley-Liss, **1999**.

[13] Keeler J. *Understanding NMR Spectroscopy*. Wiley, **2005**.

[14] Levitt M. *Spin Dynamics: Basics of Nuclear Magnetic Resonance*. Wiley, **2008**.

[15] Moss R.A., Platz M.S., and Jones M.Jr. *Reactive Intermediate Chemistry*. Wiley-Interscience, New york, **2004**.

[16] Hicks R.G. *In Stable Radicals*. John Wiley & Sons, New york, **2010**.

[17] Walker R.W. *Symposium (International) on Combustion*, 22(1):p.883, **1989**.

[18] Yndall G.S., Cox R.A., Granier C., Lesclaux R., Moortgat G.K., Pilling M. J.M., Ravishankara A.R., and T.J. Wallington. *Journal of Geophysical Research: Atmospheres*, 106(D11):p.12157, **2001**.

[19] Halliwell B. Wiley-VCH Verlag GmbH and Co. KGaA, **2006**.

[20] Richard T. O. John Wiley and Sons, Inc., **2007**.

[21] Rawson J., Banister A., and Lavender I. *Adv. Heterocycl. Chem.*, 62:p.137, **1995**.

[22] Griller D. and Ingold K.U. *Acc. Chem. Res.*, 9(1):p.13, **1976**.

[23] Lomnicki S., Truong H., Vejerano E., and Dellinger B. *Environ. Sci. Technol.*, 42(13):p.4982, **2008**.

[24] Banci L., Bertini I., and Luchinat C. *Nuclear and Electron Relaxation*. Wiley-VCH, **1991**.

[25] Tacke J., Adam G., Claben H., Muhler A., Prescher A., and Gunther R.W. *Magn. Reson. Imaging*, 7:p.678, **1997**.

[26] Braverman I.M. and Cowpe S. *F1000 Med. Rep.*, 2:p.84, **2010**.

[27] Grobner T. *Nephrol. Dial. Transplant.*, 21:p.1104, **2006**.

[28] Marckmann P., Skov L., Rossen D.A., Damholt M.B., Heaf J.G., and Thomsen H.S. *J. Am. Chem. Soc. Nephrol.*, 17:p.2359, **2006**.

[29] Nunn A.D., Linder K., and Tweedle M. *Quart. J. Nuc. Med.*, 7:p.678, **1997**.

[30] Wu C., Brechbiel M.W., Kozak R.W., and Gansow O.A. *Bioorg. Med. Chem. Lett.*, 41:p.155, **1994**.

[31] Goodson B.M. *J. Magn. Reson.*, 155(2):p.157, **2002**.

[32] Zhu H. and Barker P.B. *Methods Mol. Biol.*, 711:p.203, **2011**.

[33] Haase A., Frahm J., Hanicke W., and Matthaei D. *Phys. Med. Biol.*, 30:p.341, **1985**.

[34] Prost E., Sizun P., Piotto M., and Nuzillard J.M. *J. Magn. Reson.*, 159:p.76, **2002**.

[35] Smith M.A., Gillen J., McMahon M.T., Baker P.B., and Golay X. *Magn. Reson. Med.*, 54:p.691, **2005**.

[36] Mugler J.P., Driehuys B., Brookeman J.R., Cates G.D., Berr S.S., Bryant R.G., Daniel T.M., deLange E.E., Downs J.H., Erickson C.J., Happer W., Hinton D.P., Kassel N.F., Maier T., Phillips C.D., Saam B.T., Sauer K.L., and Wagshul M.E. *Cancer Research*, 68(20):p.8607, **2008**.

[37] Golman K., Zant R., Lerche M., Pehrson R., and Ardenkjær-Larsen J.H. *Cancer Research*, 103(30):p.1127, **2006**.

[38] Golman K. and Petersson J.S. *Academic Radiology*, 13(8):p.932, **2006**.

[39] Hurd R.E., Yen Y.F., Mayer D., Chen A., Wilson D., Kohler S., Bok R., Vigneron D., Kurhanewicz J., Tropp J., Spielman D., and Pfefferbaum A. *Magn. Reson. Med.*, 63(5):p.1137, **2010**.

[40] Park I., Larson P.E.Z., Zierhut M.L., Hu S., Bok R., Ozawa T., Kurhanewicz J., Vigneron D.B., VandenBerg S.R., James C.D., and Nelson S.J. *Neuro-Oncology*, 12(2):p.133, **2010**.

[41] Tyler D.J., Schroeder M.A., Cochlin L.E., Clarke K., and Radda G.K. *Appl. Magn. Reson.*, 34(3):p.133, **2008**.

[42] Mugler J.P., Driehuys B., Brookeman J.R., Cates G.D., Berr S.S., Bryant R.G., Daniel T.M., deLange E.E., Downs J.H., Erickson C.J., Happer W., Hinton D.P., Kassel N.F., Maier T., Phillips C.D., Saam B.T., Sauer K.L., and Wagshul M.E. *Magn. Reson. Med.*, 37(6):p.809, **1997**.

[43] Schroeder M.A., Swietach P., Atherton H.J., Gallagher F.A., Lee P., Radda G.K., Clarke K., and Tyler D.J. *Cardiovascular Research*, 86(1):p.82, **2010**.

[44] Merritt M.E., Harrison C., Storey C., Jeffrey F.M., Sherry A.D., and Malloy C.R. *Proceedings of the National Academy of Sciences of the United States of America*, 104(50):p.19773, **2007**.

[45] Schroeder M.A., Cochlin L.E., Heather L.C., Clarke K., Radda G.K., Tyler D.J., and Shulman R.G. *Proceedings of the National Academy of Sciences of the United States of America*, 105(33):p.12051, **2008**.

[46] Bowers C.R. and Weitekamp D.P. *J. Am. Chem. Soc.*, 109(18):p.5141, **1987**.

[47] Ardenkjær-Larsen J.H., Fridlund B., Gram A., Hansson G., Hansson L., Lerche M.H., Servin R., Thaning M., and Golman K. *Proceedings of the National Academy of Sciences of the United States of America*, 100(18):p.10158, **2003**.

[48] Abragam A. and Goldman M. *Reports on Progress in Physics*, 41(3):p.395, **1978**.

[49] Goldman M. *Appl. Magn. Reson.*, 34(3):p.219, **2008**.

Chapter 2

Objectives

The main objective of the present thesis is the preparation of paramagnetic systems in order to improve the sensitivity of the Nuclear Magnetic Resonance (NMR).

To afford this ambitious objective, an accurate study of the mechanisms to improve NMR was done. The two main mechanisms to improve the sensitivity are, on one hand, to modify the time of relaxation of nuclei, and on the other hand, to hyperpolarize the spin system. The modification of the relaxation time is mainly employed for reducing the relaxation time of ^{1}H (high giromagnetic constant γ) of water. The great majority of materials used in this approach nowadays are paramagnetic chelates of gadolinium (III) that, in addition, allow the visualization of selected areas of the body in MRI studies due to its biodistribution. However they show high level of toxicity. On the other hand, the visualization of nuclei of low giromagnetic constant as ^{13}C or ^{15}N is more challenging. The hyperpolarization techniques present a good option to perform the study of these kinds of nuclei. In order to hyperpolarize nuclei some techniques have been developed, being Dynamic Nuclear Polarization (DNP) the more important one. DNP technique requires performing a paramagnetic compound. With this knowledge, the objectives to afford the main objective were:

- To synthesize water soluble dendrimers which incorporate radicals on their surface. To achieve this goal, phosphorous dendrimers built from the hexachlorocyclotriphosphacene core up to the third generation ended in aldehyde were synthesized. On the other hand, the synthesis of the radical or their modification had to be performed in order to be incorporated on the dendrimer surface. Dendrimers functionalized with organic radicals were characterized and their water solubility tested.

- To perform the phantom MRI experiments in order to determine the relaxivity of each dendrimer with the purpose of evaluating their possible application as contrast agents.

- To prepare monoradicals of three different families (PTM, BDPA and TEMPO), characterize them and synthesize biradicals using them. The target birradicals

include the three families in order to obtain PTM-PTM, BDPA-BDPA, TEMPO-TEMPO, PTM-BDPA, PTM-TEMPO and BDPA-TEMPO biradicals and their characterization.

- To explore their potential application in DNP as polarizing agents of ^{13}C. In general, [1-^{13}C]pyruvic acid is the source of ^{13}C target with the purpose of performing future *in vivo* metabolomic studies, although [2-^{13}C]acetone were used for some biradical systems due to increasing interest of surface studies with DNP are appearing. Moreover, the study of BiTEMPO radicals in MAS-DNP where nuclei with high gyromagnetic constant (H) are polarized is desired to be tested by the *cross polarization* to obtain hyperpolarized nuclei of low giromagnetic ratio.

Chapter 3

Monoradicals

3.1 Introduction

Since the first synthetic organic free radical, triphenylmethyl radical, was identified by Moses Gomberg[8] in 1900, some persistent radicals have been isolated and characterized. In general, persistent organic radicals show one or more of the next characteristics: steric crowding of the radical center, extended π system to delocalize the radical in an extended SOMO (Single Occupied Molecular Orbital) and/or, electrostatic repulsion for the charged radicals (cation-radicals or anion-radical). They can be arranged taking into account the atom over which is mainly located the unpaired electron: Carbon centered radicals (*e.g.* trityl radicals: triphenylmethyl, perchlorotriphenylmethyl (PTM), OX63 or 1,3-bisdiphenylene-2-phenylallyl (BDPA)), nitrogen centered radicals (*e.g.* verdazyl or DPPH), N-oxide radicals (*e.g.* TEMPO, PROXYL or nitronyl nitroxide) or oxigen centered radicals (*e.g.* galvinoxyl). Due to the anisotropy of those radicals and the hyperfine interaction among the electron with different atoms, the EPR spectrum obtained for each family is very different. For examples of each of them, see **Figure 3.1**.

In the present Thesis we have obtained and studied several carbon centered radicals (perchlortriphenylmetyl radical (PTM) derivatives and 1,3-bis(diphenylene)-2-phenylallyl radical (BDPA) derivatives). On the other hand, the N-oxide radicals with six member ring was also employed; like 2,2,6,6- tetramethylpiperidin-1-oxyl TEMPO derivatives and 2,2,5,5- tetramethyl pyrrolidin-1-oxyl(PROXYL) derivatives. The nuclear magnetic resonance applications were explored using such derivatives as a monoradical, biradicals (combination of two of them) or polyradicals (combination of some of them, always using the same radical in each polyradical).

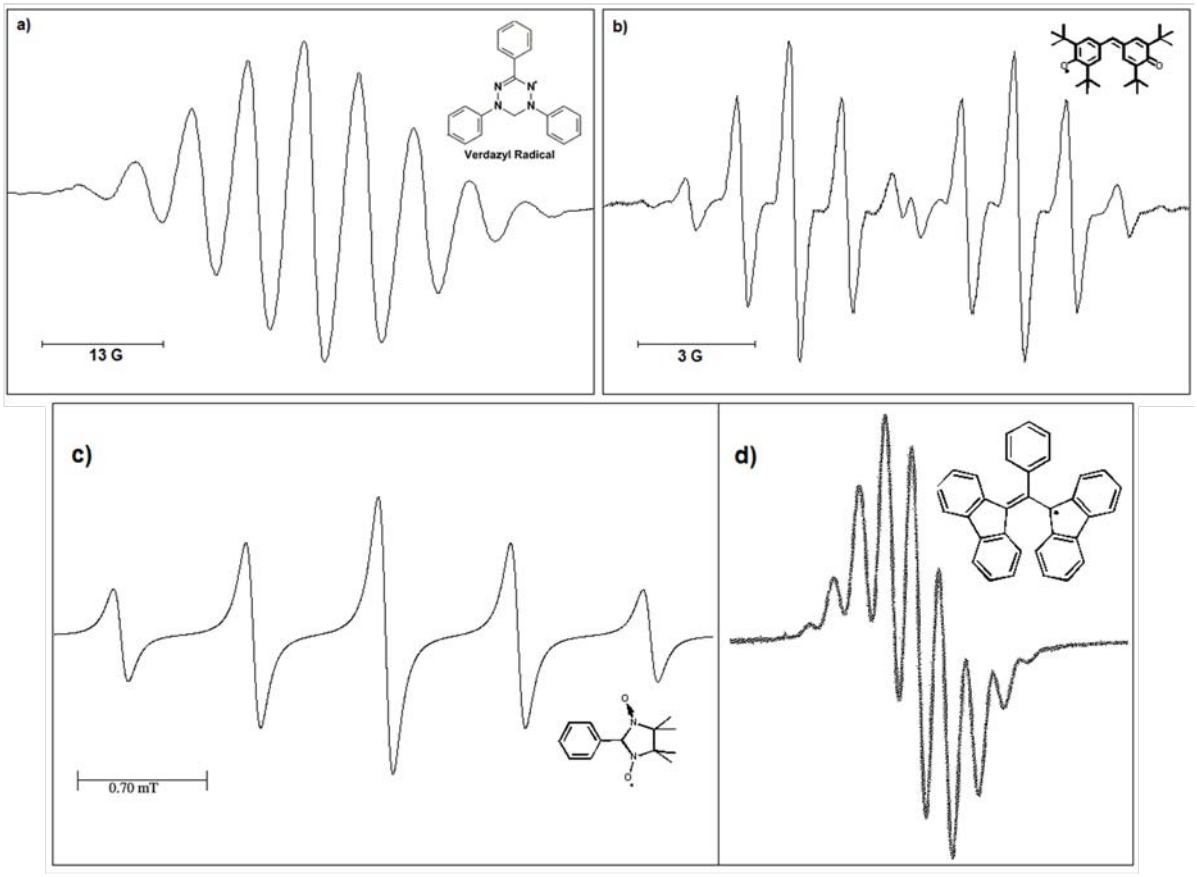

Figure 3.1: X-band EPR of a) Verdazyl, b) Galvinoxyl, c) Nitronyl nitroxide and d) BDPA radicals.

3.2 Synthesis of monoradicals

3.2.1 Perchlorotriphenylmetyl radical (PTM) derivatives

After Moses Gomberg reported the existence of a stable, trivalent organic free radical [8] which challenged the prevailing belief that carbon could only have four chemical bonds, research aimed at understanding and developing these radicals continued to thrive and permeated various fields of science including medicine and industrial applications. [9] However, it is known that some radicals and diradicals are short-lived and very reactive species (the half-life of triphenylmethyl radicals in aerated solution may be as low as a fraction of a second). Studies have also shown that these reactive radicals become stable and chemically inert upon perchlorination. [10–13]

In light of this endeavor, highly chlorinated mono-, di-, and triarylmethanes were developed and since then they have become the most valuable chemical precursors of inert free radicals with estimated half-lives in the order of 100 years in solid state. [11] These studies have been regarded as both promising and significant. [10] As a result, the synthesis of perchlorinated trityl radical has become an immense undertaking with

promising applications.

The synthesis of the hydrocarbon PTMCH$_2$Br, **4** (**Chapter 8**, Experimental Details) that allowed us the preparation of many PTM radical derivatives implied four synthetic steps (**Scheme 3.1**). The first step consisted of the preparation of the Grignard reagent of 4-bromotoluene and its addition to benzophenone in anhydrous ether, obtaining the triaryl alcohol core of PTM (**1**).[14] Secondly, the alcohol was reduced in presence of hot formic acid to the corresponding triphenylmethane (**2**).[15] Second to last step implied the perchloration of all rings with the BMC reagent ($AlCl_3$ and S_2Cl_2) in SO_2Cl_2, so the perchlorotriphenylmethane (**3**) was obtained.[16] The last step consisted of a radical bromination of the methyl group assisted with white light which allowed us to obtain the αH-PTM derivative (**4**).[17]

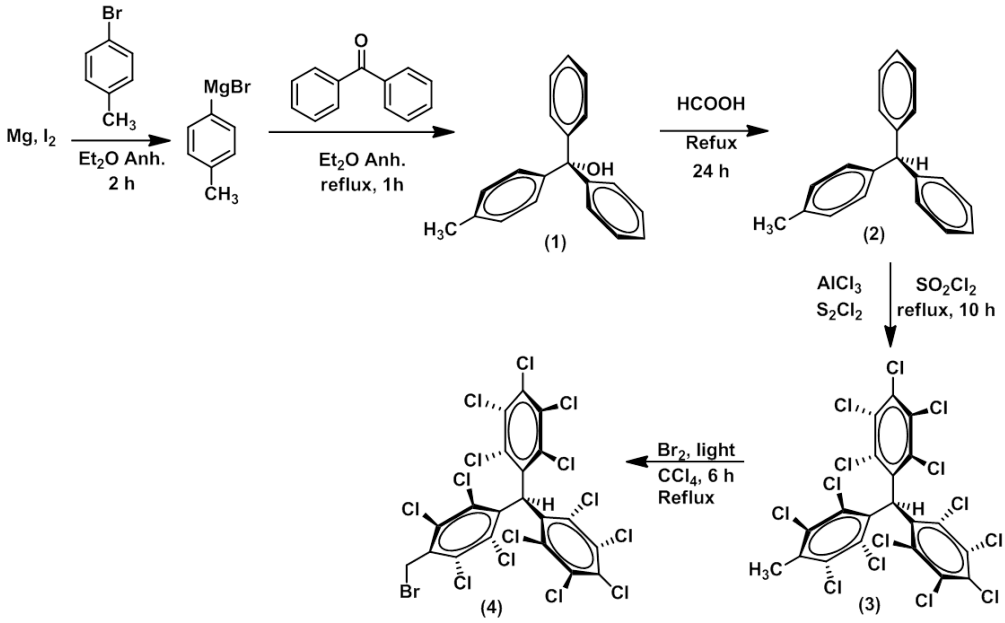

Scheme 3.1: Synthetic scheme of αH-PTMCH$_2$Br (**4**).

Once we obtained the precursor αH-PTMCH$_2$Br (**4**), we performed some modifications on it in order to obtain the different αH-PTM derivatives that were used for the synthesis of biradicals or polyradicals. With this purpose the PTM functionalized with alcohol **5**, aldehyde **6**, amine **8** (obtained through the phtalate intermediate **7**), and phosphonate **9** were prepared (see **Scheme 3.2**).

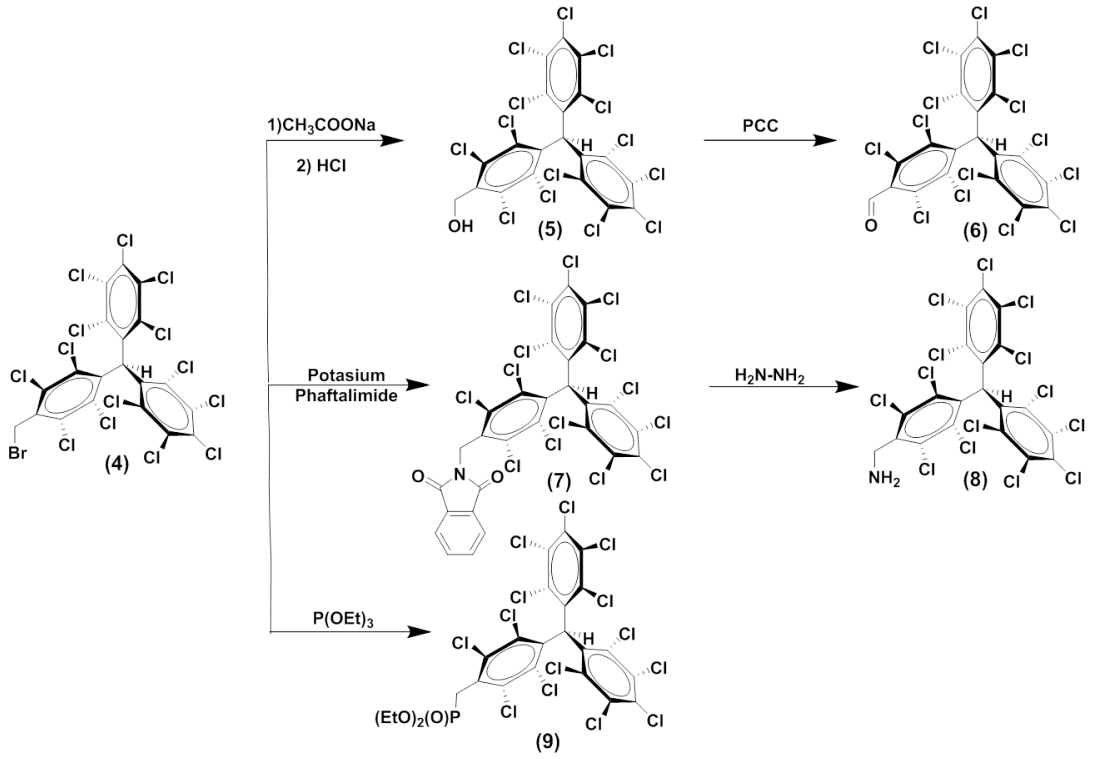

Scheme 3.2: Synthetic scheme of PTM derivatives form αH-PTMCH$_2$Br (**4**).

The αH-PTMCH$_2$Br (**4**) was used to prepare the benzyl alcohol derivative αH-PTMCH$_2$OH (**5**), (**Scheme 3.3**). The preparation of this alcohol goes through a slow nucleophilic substitution of the bromine by an acetate anion that takes three days. The acetate intermediate, that can be isolated, was then hydrolyzed by treatment with aqueous HCl to the desired alcohol with a high yield (94%).

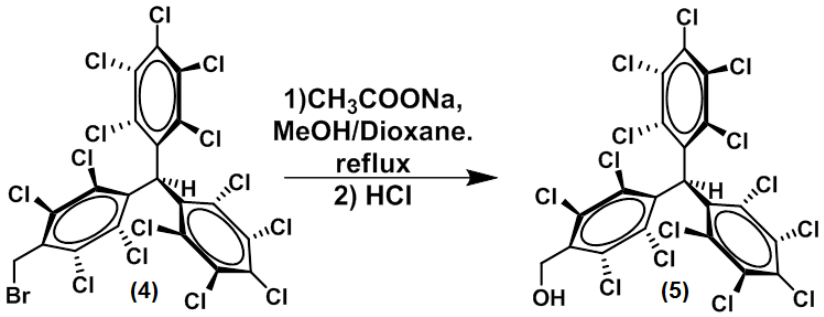

Scheme 3.3: Synthesis of αH-PTMCH$_2$OH (**5**).

The αH-PTMCH$_2$OH (**5**) can be used to obtain the corresponding aldehyde αH-PTM-CHO (**6**) (**Scheme 3.4**). The oxidation was performed under mild conditions, using as oxidant pyridinium chlorochromate (PCC) in dichlorometane. It is a fast

reaction which only needs to be filtered through silica gel in order to eliminate the metal salts affording the desired aldehyde with a good yield (85%).

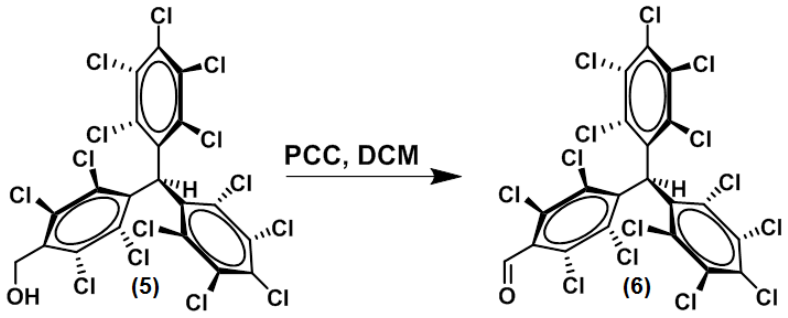

Scheme 3.4: Synthesis of αH-PTM-CHO (**6**).

The αH-PTMCH$_2$Br (**4**) can be also employed in the preparation of the phtalimido derivative **7** (**Scheme 3.5**). With this purpose, the αH-PTMCH$_2$Br (**4**) was dissolved in hot anhydrous DMF in presence of potasium phtalimide for 16 hours. After that, the product was purified. The isolated pure product (Yield: 86%) was characterized by NMR and MALDI-TOF.

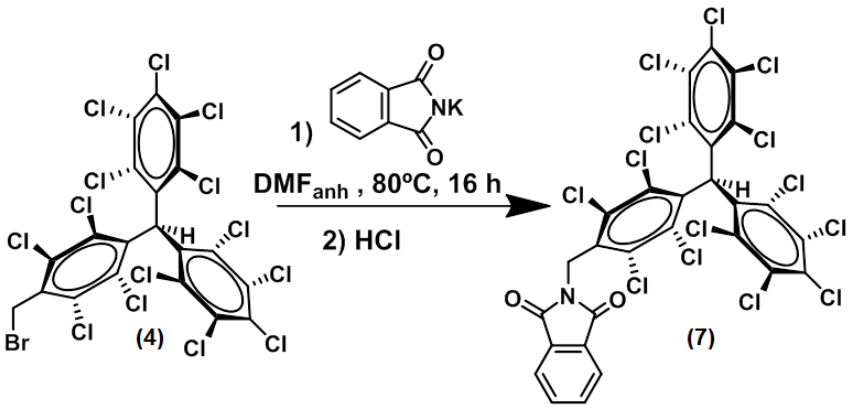

Scheme 3.5: Synthesis of phtalimido derivative of αH-PTMCH$_2$-phtalate (**7**).

The phtalimido derivative **7** can easily deliver the benzyl amino derivative **8** (αH-PTMCH$_2$NH$_2$) by treatment with hydrazine in ethanol (**Scheme 3.6**). In this reaction, the phthalhydrazide subproduct precipitates, so it can be easily removed by filtration. The organic phase can be then purified to afford the desired product with a high yield (85%).

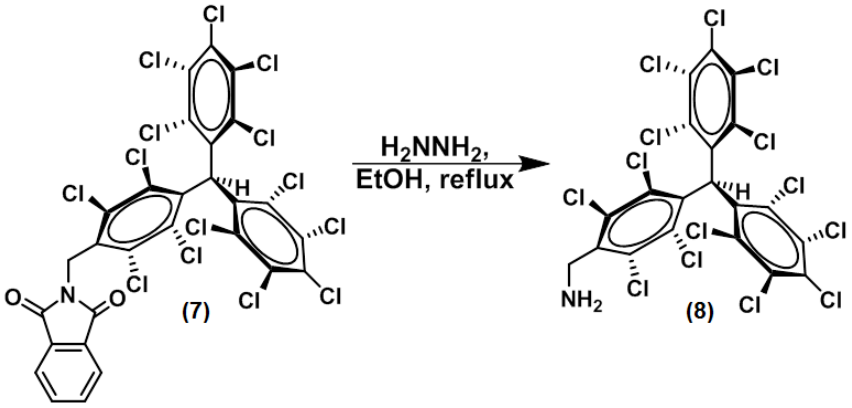

Scheme 3.6: Synthesis of αH-PTMCH$_2$NH$_2$ (**8**).

The synthesis of the phosphonate derivative **9** (**Scheme 3.7**) took place by refluxing the αH-PTMCH$_2$Br (**4**) derivative for three hours in triethyl phosphite, obtaining the desired compound in the α-H form with high yield (80%). The product was stored for its use in subsequent Wittig-Horner-Hemmons reactions which allowed us to form biradicals and polyradicals by its double bond binding to other structures.

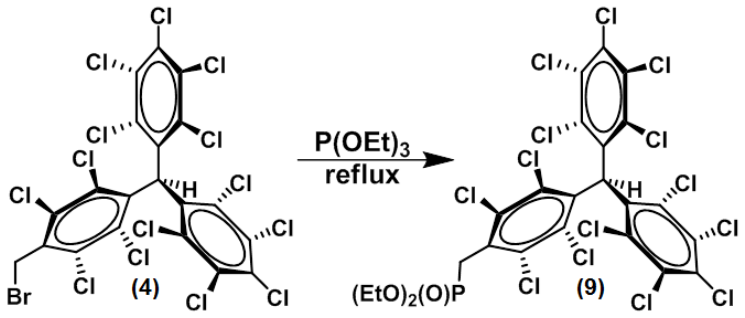

Scheme 3.7: Synthesis of αH-PTM phosphonate (**9**).

Concerning the PTM radical derivatives, all of them can be prepared by treatment of the corresponding αH-PTM derivative with tetrabutylammonium hydroxide as a base obtaining the anion derivative in anhydrous THF and then oxidazing it with $AgNO_3$ to the radical. The carbanion formation and its oxidation to radical was easily monitored by UV-Vis (**Figure 3.2**) as PTM carbanions show a strong absorption band at around 560 nm whereas the radicals show its characteristic band at around 385 nm.[18] With this knowledge, the anion formation were controlled by the appearance of the characteristic band at around 560 nm and the basic treatment was maintained until the stabilization of the absorbance was achieved. The radical formation can be monitored by the reduction of the absorbance of the latter band until its complete extinction and the concomitant of the radical band at 385 nm. The PTM monoradical anion is purple and the radical is found to be red. As an example, **Figure 3.2** shows the transformation of

αH-PTMCH$_2$OH (**5**) to the corresponding PTMCH$_2$OH radical (**5r**) through the anion.

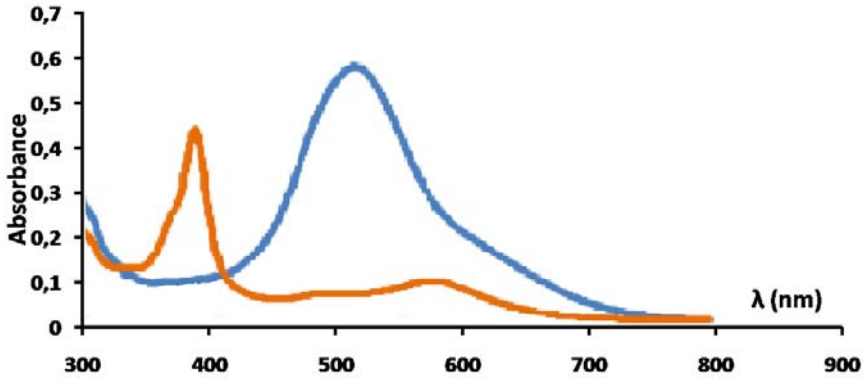

Figure 3.2: UV-Vis absorption spectrum of PTM carbanion (in blue) and PTM radical (in orange) of αH-PTMCH$_2$OH.

The EPR characterization of PTM monoradicals derivatives shows the same pattern as long as they are not conjugated with any substituent through a double bond. They show a central line and a few less intense lines related with the interaction of the electron with naturally abundant ^{13}C isotope at the α-carbon, the *bridge* and *orto*-carbons ones (**Figure 3.3**). In the case of PTMs conjugated with a double bond at the para position radicals show two main lines due to the coupling of the electron with the closest double bond proton and further couplings related with the ^{13}C atoms.

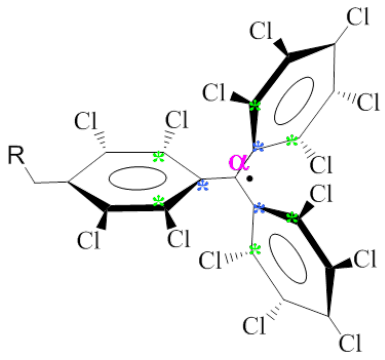

Figure 3.3: Carbon atoms of the PTM derivatives which interact with the unpaired electron, the α-carbon (in pink), the *bridge* head carbons (in blue) and the *orto*-carbons (in green).

As an example, **Figure 3.4a** shows the experimental EPR spectrum of PTM-CH$_2$OH (**5r**) monoradical. An expansion of it and the simulation (**Figure 3.4b**) shows the characteristic lines due to ^{13}C hyperfine couplings. The parameters obtained from the simulation were: g: 2.00258 and ΔH_{pp}: 1.49 G. The hyperfine couplings were: α-carbon (1, a_α= 29.8 G), *bridge* carbons (3, a_b= 12.5 G), and *ortho* carbons (6, a_o= 10.4 G).

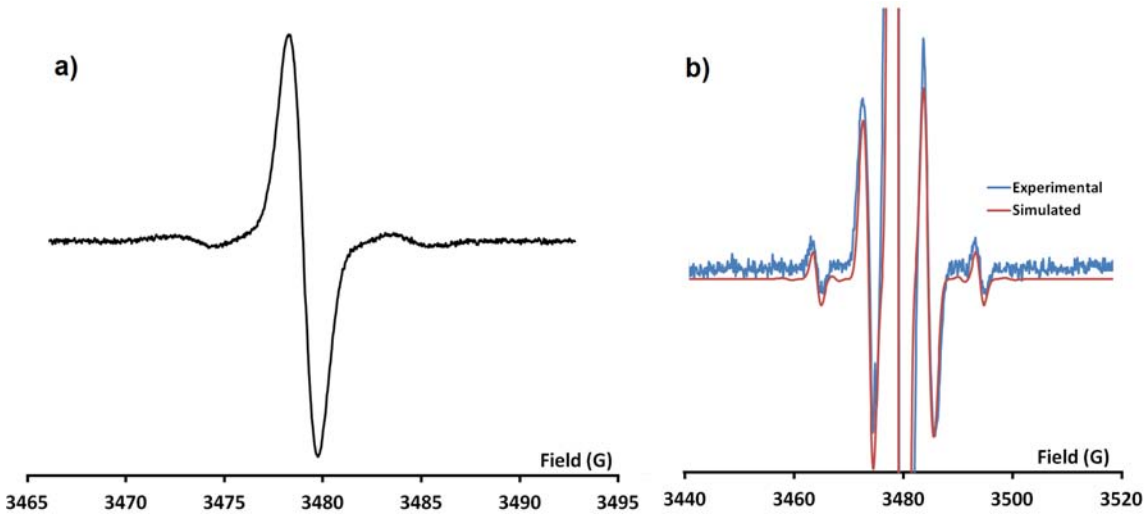

Figure 3.4: a) Liquid solution EPR spectrum of PTM-CH_2OH radical (**5r**) b) Experimental (blue) and simulated (red) expansion spectrum of PTM-CH_2OH radical (**5r**). Both spectra were recorded in DCM/Toluene 1/1.

The experimental frozen solution EPR spectrum of PTM-CH_2OH radical (**5r**) is shown in **Figure 3.5**, in this case due to the low anisotropy of PTM radical and the broad EPR line the spectrum appears as one broad line. The values of the g tensor were obtained by simulation (g_{xx}: 2.0017, g_{yy}: 2.0017 and g_{zz}: 2.0055). The experimental ΔH_{pp} was found to be 6.1 G that is the typical value for a frozen solution of a PTM monoradical and is in agreement with the simulated one (ΔH_{pp_x}=ΔH_{pp_y}: 5.0 G; ΔH_{pp_z}: 6.5 G). On the other hand, in the literature can be found the principal components of the g tensor for some PTM species that are similar to those obtained in the simulation.[19]

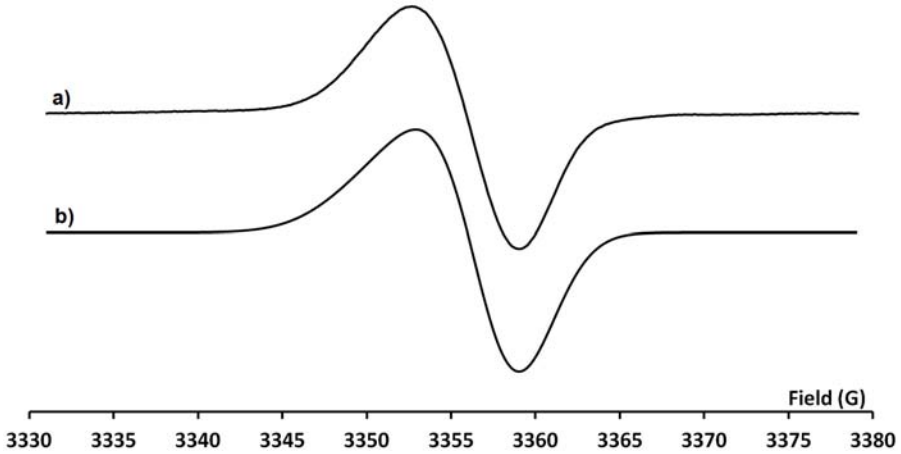

Figure 3.5: Frozen soltution EPR of PTM-CH_2OH (**5r**) in DCM/Toluene 1/1 at 120 K, a) experimental and b) simulated.

3.2.2 1,3-Bis(diphenylene)-2-phenylallyl radical (BDPA) derivatives

BDPA (**10**) was firstly synthesized by the Koelsch's method (**Scheme 3.8** blue path).[20] It involves the formation of an alcohol, the displacement of the hydroxyl group with HCl to form the chloride derivative, and the removal of the chlorine atom with mercury. On the other hand, the method developed by Kuhn and Neugebeauer (**Scheme 3.8** red path)[21] involves a conjugate addition of the fluorene anion to the bromine derivative, followed by a one electron oxidation of the stable carbanion intermediate. The later method was chosen to synthesize some functionalized BDPA derivatives because it requires fewer steps and provides higher yields.

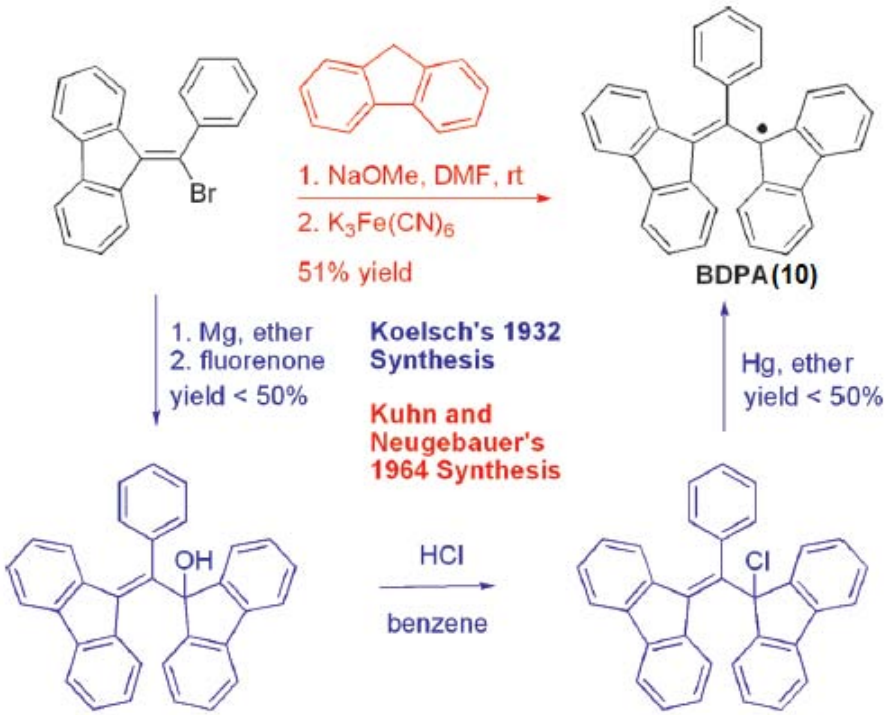

Scheme 3.8: BDPA synthetic methods.[22]

Efforts to synthesize BDPA derivatives have been carried out by different research groups.[23,24] Kuhn[21] reported a few halogenated BDPA derivatives and, Fox[25] reported the synthesis of BDPA derivatives with methoxy, cyano, and nitro groups at the 4-position of the phenyl ring. On the other hand, previously synthesized biradicals containing BDPA have been limited to molecules containing two BDPA radicals linked through the phenyl ring.[21]

The reactivity of the BDPA radical complicates its incorporation in biradicals. Although the radical is remarkably stable to oxygen in the solid state[20] and has been reported to be indefinitely stable to oxygen in solution with the exclusion of light, its

photoreactivity produces a variety of oxidation products in solution.[25] Additionally, solutions of the radical are reduced to give the corresponding carbanion when exposed to strong bases, such as hydroxide or alkoxide. Moreover, BDPA also reacts with strong acids.[20] On the other hand, this radical is stable in the dark but only in a few solvents[25] being benzene the best option for keeping it in solution. The nature of the photochemical decomposition of BDPA in presence of oxygen has been probed by product analysis and kinetics being the resulting products, in the case of dichloromethane, those indicated in **Figure 3.6a**.

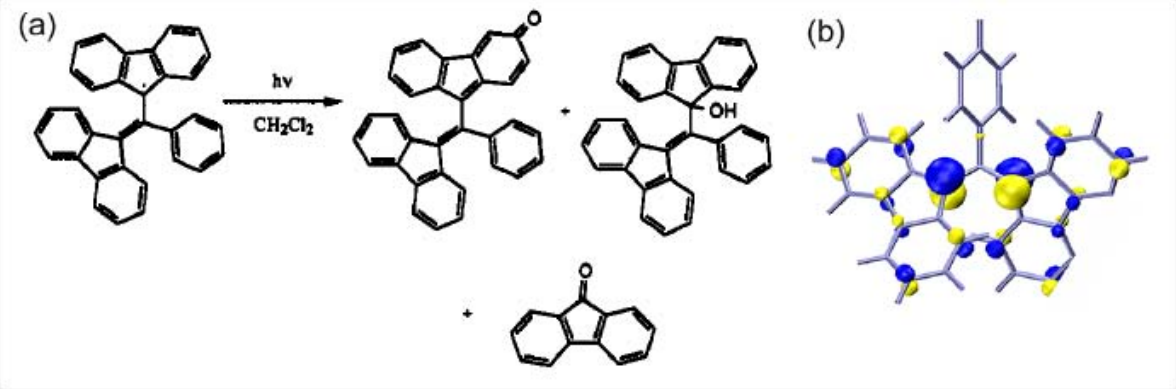

Figure 3.6: a) Scheme of photochemical decomposition of BDPA in DCM b) Calculated isodensity representation of the singly occupied molecular orbital of BDPA.[26]

Interestingly, the unpaired electron of BDPA is delocalized throughout the fluorenyls rings, but it is not appreciably delocalized into the phenyl one as can be see in the representation of the calculated singly occupied molecular orbital (**Figure 3.6b**.)[26,27]

Synthesis of BDPA-Br (**14**), BDPA-CN (**19**) and BDPA-COOH (**26**)

In the present work the synthesis of BDPA derivatives substituted at the 4-position of the phenyl ring was carried out following the Kuhn and Neugebeauer methodology,[21] as it is illustrated in **Scheme 3.9**. Following this methodology it has been prepared the BDPA derivatives with bromine, cyano and acid groups at the 4-position of the phenyl ring.

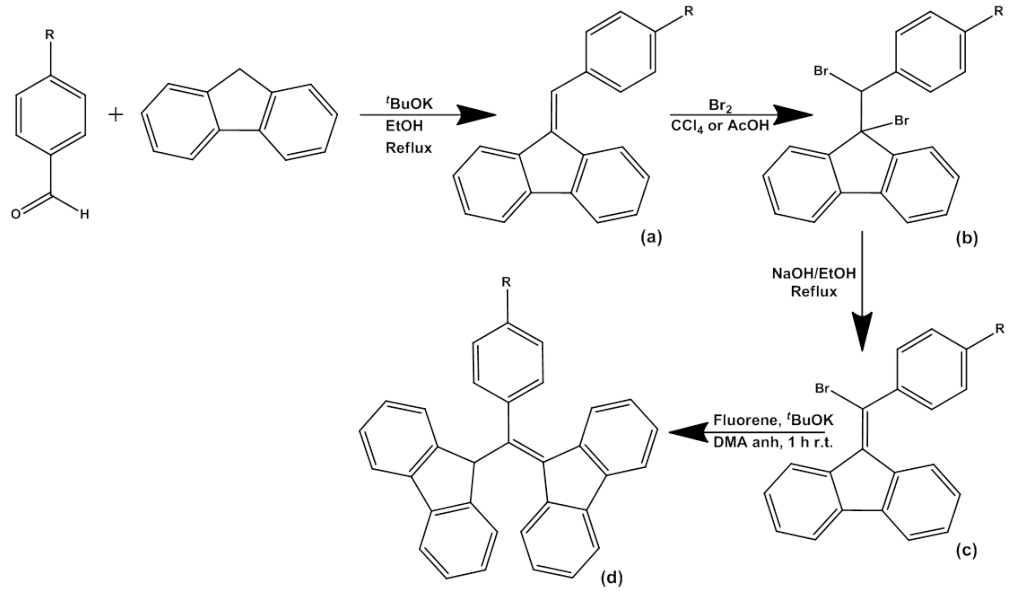

Scheme 3.9: Synthetic scheme of BDPA derivatives. R= Br, CN or COOH.

The first step of this synthesis generated the compounds of type (**a**). All of them were prepared by condensation of the anion of fluorene, generated with potassium *tert*-butoxide in ethanol, with the corresponding 4-substituted benzaldehyde under reflux overnight. They were purified by column chromatography and eventually by recrystalization obtaining good yields (**Table 3.1**).

The second step, the double bond bromination, consisted of the reaction between the corresponding compound type (**a**) in chloroform or acetic acid, with Br_2 under sonication. The resulting dibromide derivatives, compounds of type (**b**), were obtained in good yields with a very short time of reaction (**Table 3.1**). The sonication of the suspended type (**a**) compounds seems to be helpful for the reaction evolution.

In the third step of the synthesis, dibromides of type (**b**) were refluxed in ethanol in presence of sodium hydroxide with the purpose of eliminating hydrogen bromide and produce the conjugated acceptors type (**c**) (**Table 3.1**). It is important to take into account that for the cyano derivative the reaction time had to be shorter to avoid the possible hydrolysis of the cyano group; so in this case the reaction time was 15 minutes while for the other two compounds it was for an hour (**Chapter 8**, Experimental Details).

The last reaction of each conjugate acceptor of of type (**c**) with the fluorene anion, in the presence of anhydrous dimethylacetamide ($DMA_{anh.}$), yield a deep blue (acid and bromo derivatives) or green (cyano derivative) solution of the corresponding BDPA derivative carbanion. These intermediates were quenched with 2 M HCl and purified by column chromatography to give the functionalized BDPA derivatives compounds of type (**d**) (R= Br (**14**), CN (**19**) or COOH (**26**)) which were isolated as white/off-yellow powders that can be stored due to their high stability in air (**Table 3.1**).

Table 3.1: Yields of BDPA derivatives synthesis.

Final Compound	Step 1 (type **a**)	Step 2 (type **b**)	Step 3 (type **c**)	Step 4 (type **d**)
BDPA-Br (**14**)	90	99	95	97
BDPA-CN (**19**)	90	97	90	97
BDPA-COOH (**26**)	91	88	98	54

All the BDPA derivatives and precursors were characterized by NMR (**Figure 3.7**, as an example), IR-ATR and MALDI-TOF. Finally, the radical oxidation of the carbanion was be monitored by UV-Visible as in the PTM derivatives. Finally, the radical characterization was performed by EPR.

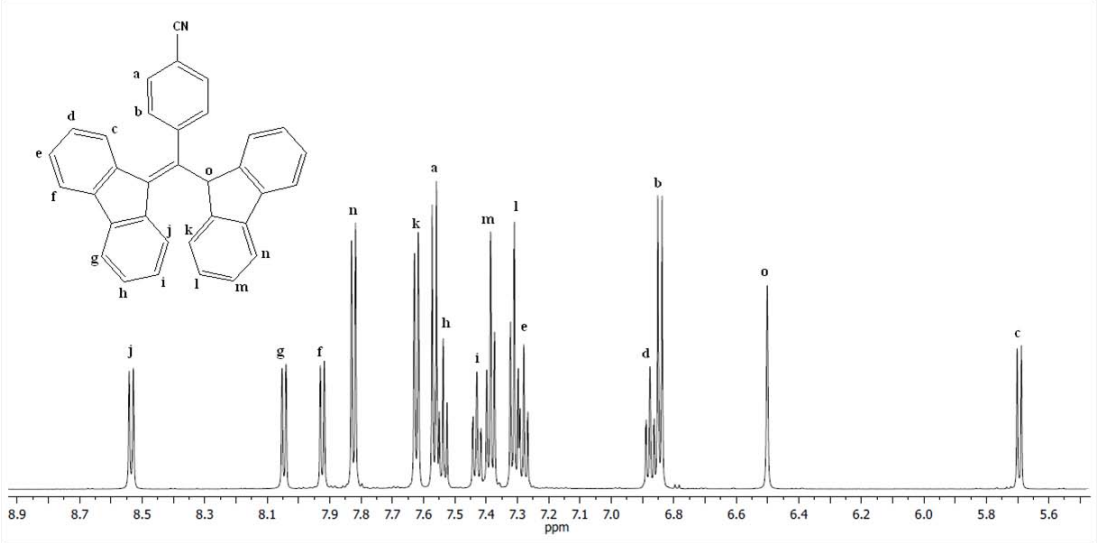

Figure 3.7: ^{1}H NMR of a BDPA derivative, BDPA-CN (**19**).

Derivatization of BDPA-Br (**14**), BDPA-CN (**19**) and BDPA-COOH (**26**)

With the resulting non-radical αH-BDPA derivatives and by means of different reactions to modify their functional groups, we prepared a family of different new BDPA radical derivatives. These radical derivatives were used directly for Dynamic Nuclear Polarization (DNP) studies (**Chapter 5**) or as a precursor for obtaining other BDPA derivatives including for the formation of biradicals (**Chapter 4**). The structures and synthetic paths to obtain these new compounds are summarized in **Scheme 3.10**.

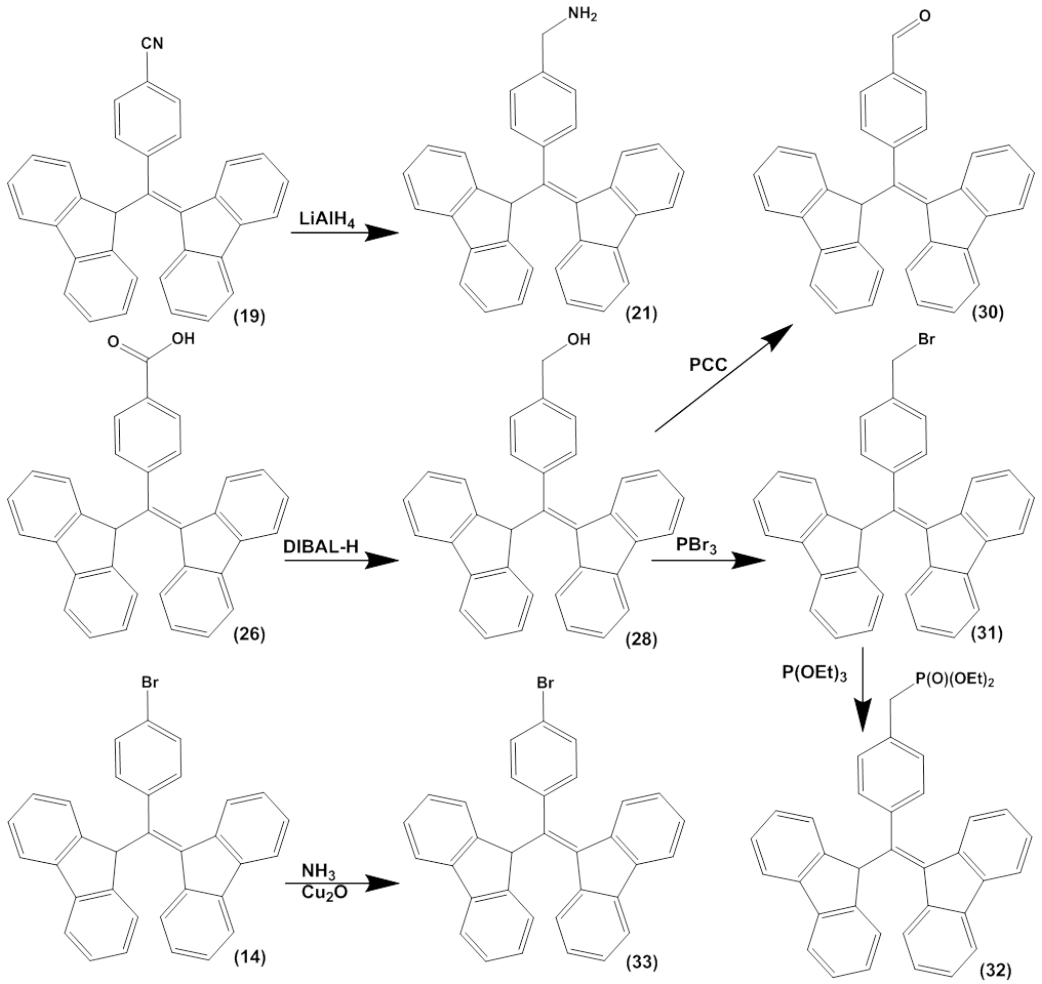

Scheme 3.10: Synthetic pathway for all αH-BDPA derivatives.

Starting from the cyano derivative of αH-BDPA (αH-BDPA-CN **19**) and by reduction with $LiAlH_4$ in anhydrous THF at low temperature, the benzylamino derivative **21** was isolated after treatment in acid media (**Scheme 3.11**), which appeared as a slightly red colored solid suggesting the presence of radical traces as confirmed later on by the EPR spectrum. Although the sample contained such radical traces, the NMR spectra could be registered without problems.

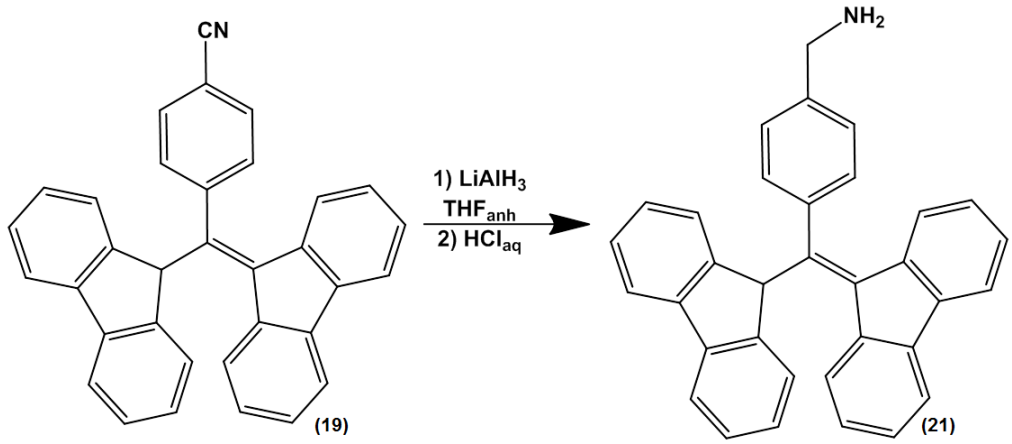

Scheme 3.11: Synthesis of αH-BDPACH$_2$NH$_2$ (αH-BAm-BDPA)(**21**).

The synthesis of the benzyl alcohol derivative **28** was carried out by reduction of BDPA-COOH (**26**) in anhydrous THF at 0 °C (**Scheme 3.12**). In this case, the use of DIBAL-H, as a reducing agent, allowed us obtaining the desired product throughout the generation of the corresponding anion in a very good yield (98%).

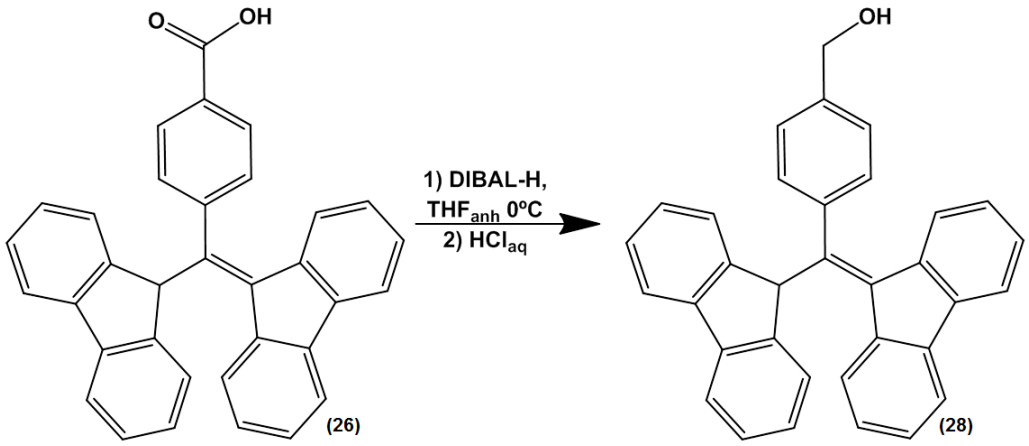

Scheme 3.12: Synthesis of αH-BDPACH$_2$OH (**28**).

The synthesis of the aldehyde derivative **30** (αH-BDPA-CHO) was attempted by reduction with DIBAL-H from the acid derivative **26**, but in all cases the obtained product was the alcohol derivative. After these results, the strategy for obtaining the aldehyde was changed to the oxidation of the alcohol derivative in presence of 1.5 equivalents of pyridinium chlorochromate (PCC) (**Scheme 3.13**). These conditions allowed us to isolate the desired compound **30** with a high yield (96%).

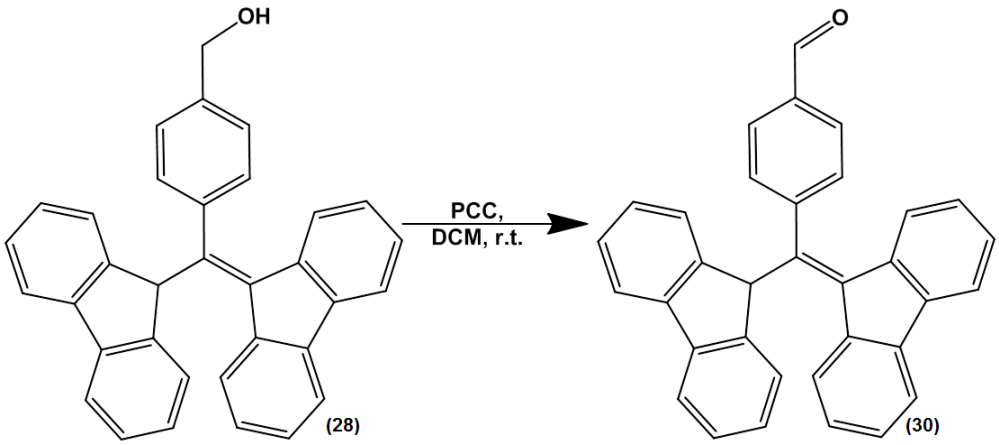

Scheme 3.13: Synthesis of αH-BDPA-CHO (**30**).

The benzyl bromine derivative **31** was synthesized by a classical nucleophilic substitution of the alcohol group of αH-BDPACH_2NH_2 (**28**) with PBr_3 (**Scheme 3.14**). The reaction was carried out in anhydrous dichlorometane. The addition of the PBr_3 was performed in an ice bath, but then, the mixture was warmed and controlled by TLC. The desired αH-BDPACH_2Br (**31**) was isolated as a yellow powder with a good yield (75%). The product, after its characterization was used for obtaining the phosphonate derivative **32** that it is the precursorfor several Wittig-type reactions.

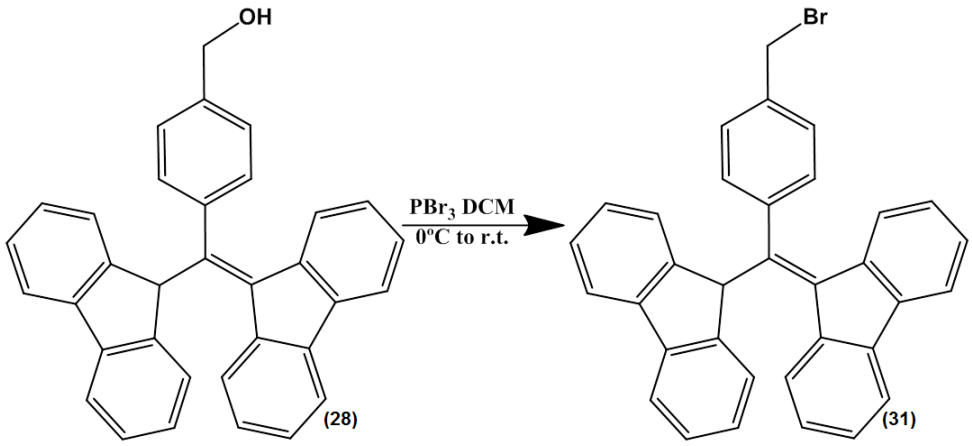

Scheme 3.14: Synthesis of αH-BDPACH_2Br (**31**).

With the purpose of obtaining the phosphonate derivative **32**, as in the αH-PTM derivative case, the αH-BDPACH_2Br derivative **31** was refluxed in $P(OEt)_3$ for four hours (**Scheme 3.15**) . The consumption of the starting material was monitored by TLC. After elimination of the excess of $P(OEt)_3$ in high vacuum and purification, the product was isolated as a brown powder with a yield of 90 %. No radical traces were detected in this compound.

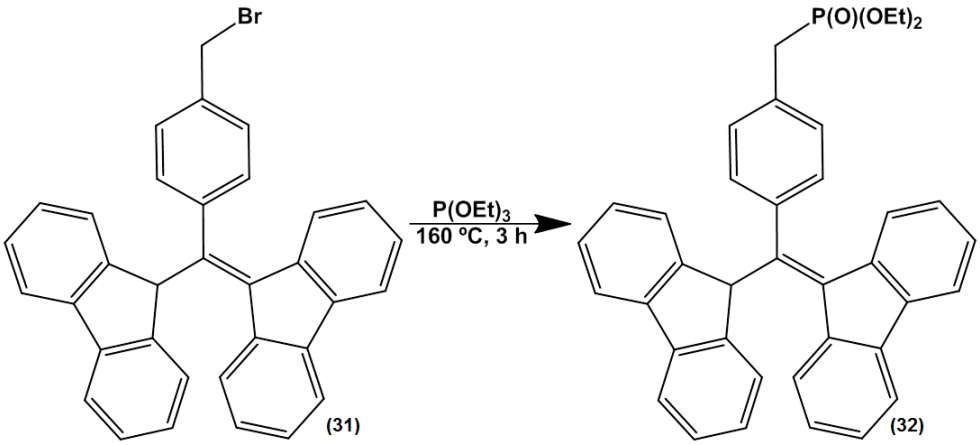

Scheme 3.15: Synthesis of phosphonate αH-BDPA derivative (**32**).

The preparation of αH-BDPA-NH_2 (**33**) (**Scheme 3.16**) was attempted by an amination reaction under copper oxide catalysis. For this reaction, αH-BDPA-Br (**14**) was added to a 1:1 mixture of water and N-methylpirrolidone (NMP) containing 5 % of the copper catalyst. The blue solution became a pink-white suspension after the addition of ammonia. The reaction was heated for two days at 90^0C but the desired product could not be isolated.

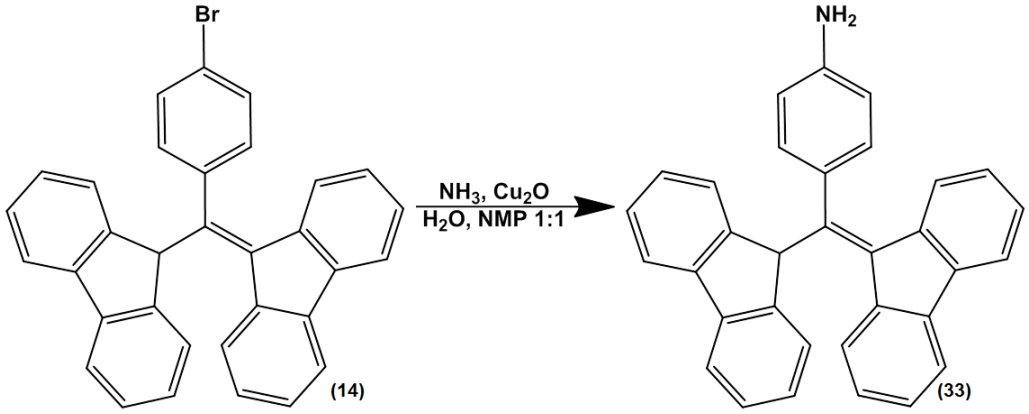

Scheme 3.16: Synthesis attempt of αH-BDPA-NH_2 (**33**).

Concerning the BDPA radicals generated from the αH-BDPA, some of them were prepared by treatment of the αH-BDPA with DBU (1,8-diazabicyclo[5.4.0]undec-7-ene) as a base in DCM and the subsequent anion oxidation of the resulting anion derivative to the radical with $AgNO_3$. The carbanion formation and its oxidation to radical were monitored by UV-Vis (**Figure 3.8**) due to the different absorbance of the BDPA carbanion that shows an absorption bands at around 600 nm and the radical at around 495 nm. Indeed, the anion formation was controlled by the appearance of the characteristic band at around 600 nm and the basic treatment was maintained until the stabilization

of its absorbance value. On the other hand, the radical formation was monitored by the reduction of the absorbace of this band until its complete extinction and the appearance and growing of the radical band at 495 nm. The BDPA anion use to be blue, in the case of electron-withdrawing cyano and aldehyde groups, the anion obtained was green. However, all radicals were found to exhibit the same red color as was expected from the electron density of the SOMO orbital, which is located over the fluorenyl rings, with a null perturbation of the substituted phenyl ring. [26,27]

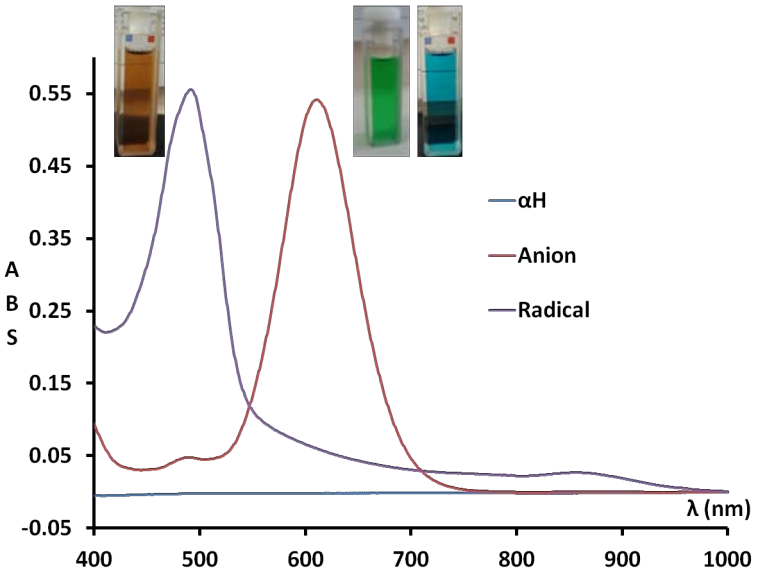

Figure 3.8: UV-Vis absorption spectra of BDPA carbanion (in red), BDPA radical (in purple) and αH BDPA (in blue). Inset, the different colors of compounds, radical (red) and carbanion (green or blue, depending on the substituent of the phenyl ring).

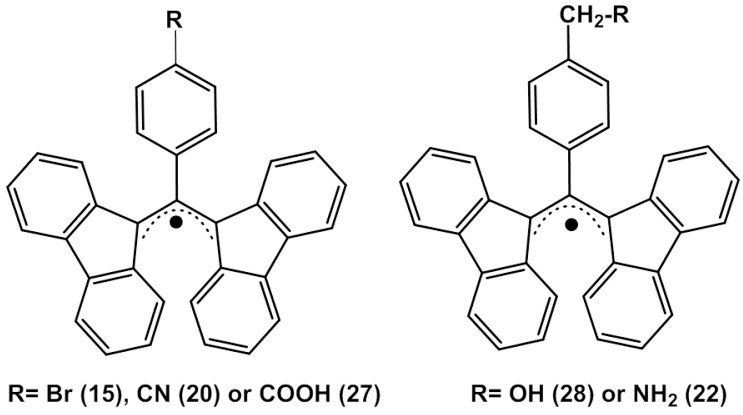

Scheme 3.17: Chemical structure of BDPA radical derivatives prepared.

The radical characterizations were carried out by EPR. In general, there were no big differences in the EPR spectra of the different BDPA derivatives since the delocalization

of the free electron in BDPA radicals takes place essentially over the fluorenyl rings. As an example, **Figure 3.9** shows the EPR in liquid solution of one BDPA radical, the benzyl alcohol BDPACH_2OH, **29**, in dichlorometane. The parameters obtained from the simulation of the spectrum were: g: 2.0024, and ΔH_{pp}: 0.31 G and the hyperfine splintings: a(4H): 1.988 G; a(4H): 1.827 G; a(4H): 0.539 G; a(4H): 0.365 G; a(2H): 0.065 G; and a(2H): 0.062 G. The EPR data for all the obtained BDPA radical derivatives can be found in **Chapter 8**, (see Experimental Details).

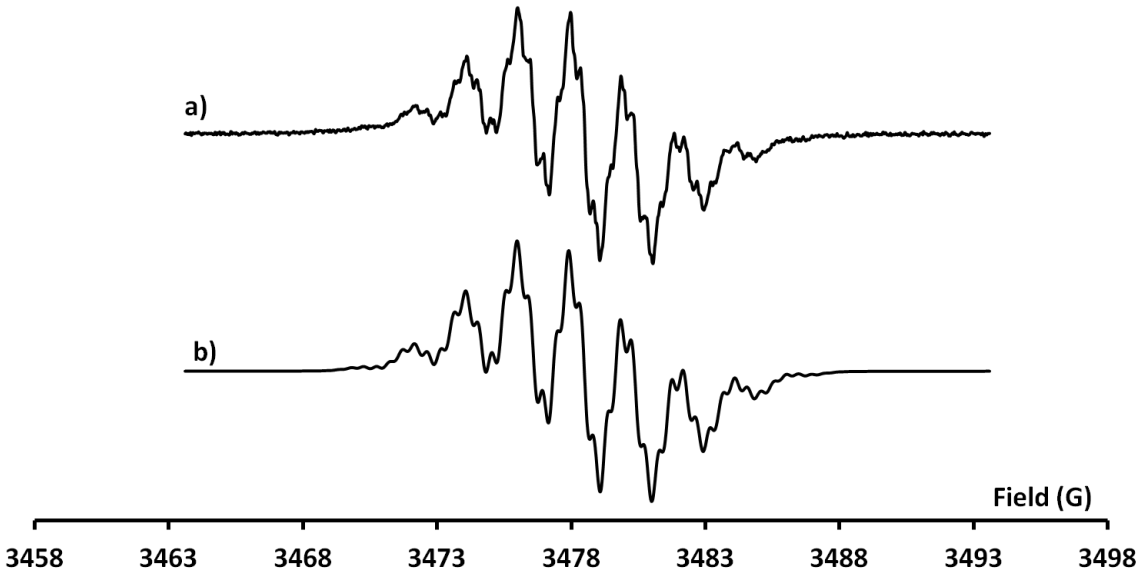

Figure 3.9: Liquid solution EPR of BDPA-CH_2OH radical (**29**) in DCM at 300 K, a) experimental and b) simulated.

The frozen solution EPR spectrum of BDPA-CH_2NH_2 radical is shown in **Figure 3.10a**. As in the PTM case, the compound presents a small anisotropy.

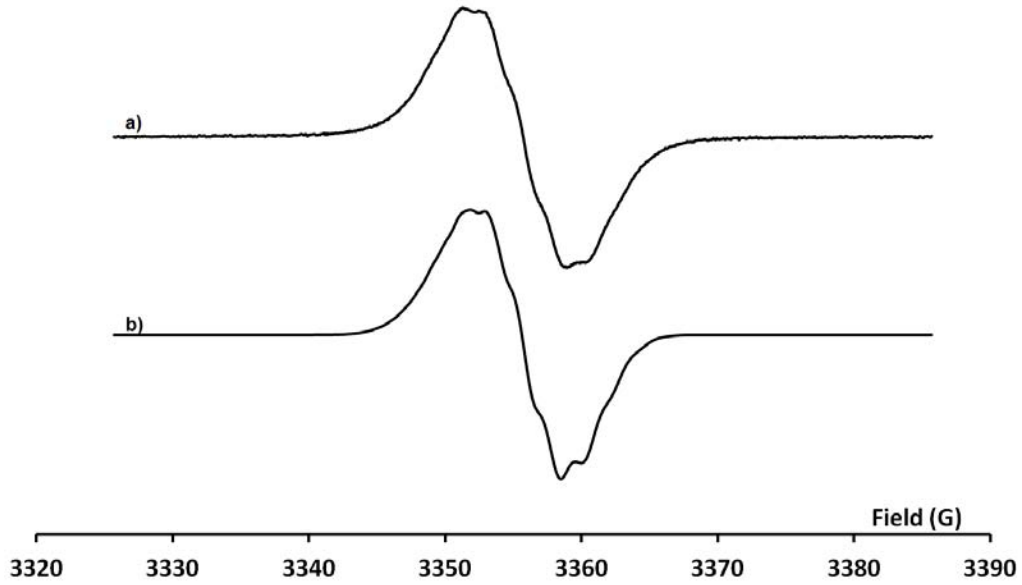

Figure 3.10: Frozen solution EPR spectra of BDPA-CH_2NH_2 radical (**22**) a) experimental and b) simulated in DCM at 120 K.

In the literature[28] can be found the parameters to perform the EPR simulation of the BDPA radicalin solid state. The parameters found in our simulation were g_{xx}: 2.0010; g_{yy}: 2.0026; and g_{zz}: 2.0048; and the hyperfine coupling constants $a(8H_a)$: a_{xx}: 1.85 G; a_{yy}: 1.85 G; a_{zz}: 2,0 G; $a(8H_b)$: a_{xx}: 0.45 G, a_{yy}: 0.45 G; a_{zz}: 0.90 G; and the ΔH_{pp}: 1G. The simulated spectrum with such parameters fits the experimental spectrum as can be seen in **Figure 3.10b**.

3.2.3 2,2,6,6-Tetramethylpiperidine 1-oxyl radical (TEMPO) derivatives

The general scheme for preparation of 2,2,6,6-tetramethylpiperidine radicals (**Scheme 3.18**) can be divided into two steps, the synthesis of the piperidine ring (by condensation of ketones and amonia) and the amine oxidation into the corresponding stable nitroxide 2,2,6,6,-tetramethylpiperidine-N-oxide radical (TEMPO) derivative. The α-methyl groups are crucial for the stabilization of this family of radicals. The most useful starting material for the preparation of TEMPO radicals is 2,2,6,6-tetramethylpiperidine-4-one. It can be prepared on a large scale from readily available materials although it is commercially available[29–33] at low cost. As can be found in the literature, the 2,2,6,6-tetramethylpiperidine-4-one is a versatile starting compound since it is susceptible to be converted in a great number of derivatives. As examples, their sodium borhydride reduction forms the 4-hydroxyl derivative[34] while an electrochemical reduction process enable its direct conversion into the 4-amino derivative.[35,36] The conversion of 2,2,6,6-tetramethylpiperidines to its corresponding nitroxide was first described by Lebedev *et al.*[37] The oxidation generally involves the use of hydrogen peroxide and a tungsten-based catalyst, such as sodium tungstate or phosphotungstic acid. This oxidation reaction tolerates the presence of a number of substituents on the piridine ring. The crystal structure of the radical indicates that the piperidine ring adopts a chair conformation with the exception of 4-oxo-TEMPO in which the piperidine ring adopts a boat conformation.[38,39]

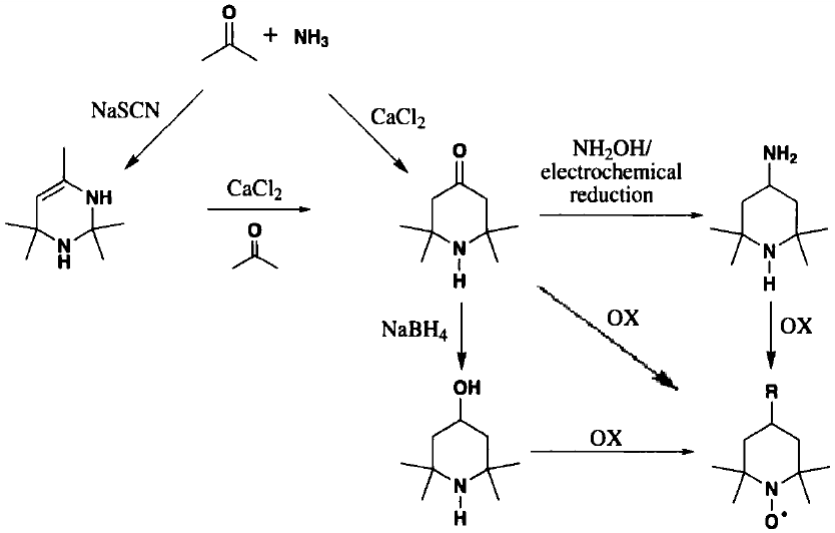

Scheme 3.18: Synthetic scheme of TEMPO derivatives.[40]

On the other hand, it is important to take into account that the 4-oxo and the 4-hydroxy derivatives could rearrange to a nitroso compound upon oxidation under basic conditions (**Scheme 3.19**).[41]

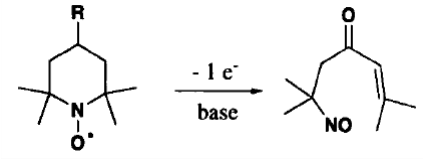

Scheme 3.19: Degradation of nitroxides.[40]

In the present work, we have used the commercially available 4-hydroxy-TEMPO (**34**), 4-amino-TEMPO (**35**) and 4-oxo-TEMPO (**36**) radicals. Moreover, the synthetic modification of 4-oxo-TEMPO allowed us to obtain the radical derivative 4-carboxy methylidene-TEMPO (**38**) through the methyl ester derivative **37** (**Figure 3.11**). TEMPO derivatives with a double bond in the 4-position show the boat conformation, as has been mentioned before, which produced a reduction in the linewith of their EPR lines. Moreover, these derivatives present a more rigid structure which can be advantageous for the synthesis of rigid or semirigid biradicals. In addition, nitroxides with narrow linewidths are essential for low-frequency EPR spectroscopy and *in vivo* EPR imaging.[42]

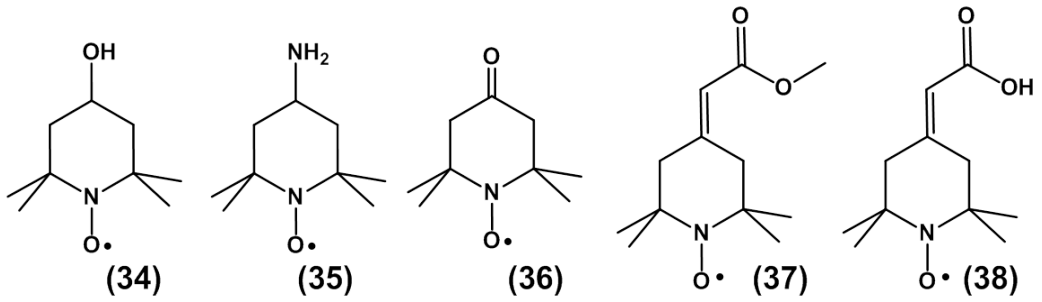

Figure 3.11: TEMPO derivatives employed in this work, a) 4-hydroxy-TEMPO **34**, b) 4-amino-TEMPO **35**, c) 4-oxo-TEMPO **36**, d) 4-(2-methoxycarbonylmethylidene)-TEMPO **37** and e) 4-carboxymethylidene-TEMPO **38**.

The reaction between 4-oxo-TEMPO (**36**) and methyl 2-(methylsilyl)acetate, through a Wittig-type reaction (**Scheme 3.20**), allowed us to incorporate at the 4-position an exocyclic double bond bearing a functional group (in this particular case, an ester group) that would allow us further synthetic modifications. The reaction was performed in anhydrous THF at -78 ^{0}C obtaining the desired product **37** with a high yield (75%) as an orange oil which eventually solidifies.

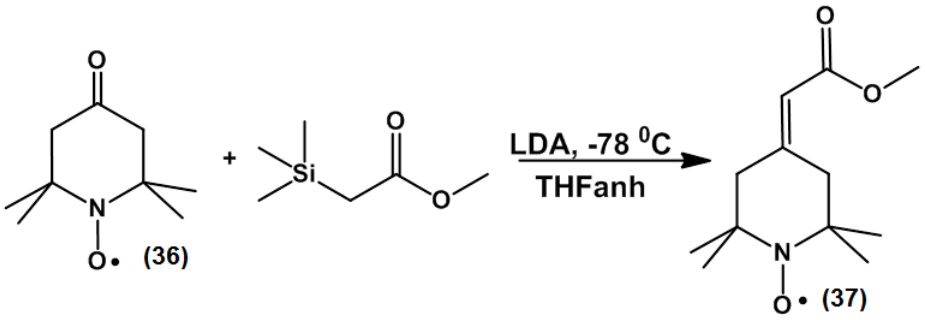

Scheme 3.20: Synthetic scheme of 4-(2-methoxycarbonylmethylidene)-TEMPO radical (**37**).

Moreover, the ester derivative **37** could be hydrolyzed to the corresponding acid product **38** by treatment with KOH in a mixture of MeOH/water in warm conditions (35-38 ^{0}C) for 6 hours (**Scheme 3.21**).

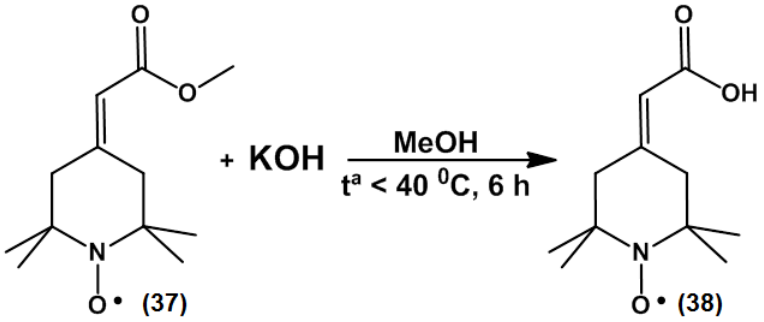

Scheme 3.21: Synthetic scheme of 4-carboxymethylidene-TEMPO (**38**).

Both radicals, **37** and **38**, were characterized by EPR. In all cases, the coupling of the electron with the nitrogen nucleus (I=1) generates a hyperfine splitting of three lines (m = 2nI+1), see **Figure 3.12**. Regarding the linewidth, as it was expected, the two monoradicals with the 4-position homosubstituted (**37** and **38**) showed a narrower linewidth (ΔH_{pp}: 0.86 G and 1.07 G, respectively) than a monoradical with an heterosubstitution, as for example 4-amino-TEMPO, ΔH_{pp}: 1.56 G. (**Figure 3.13** and **Table 3.2**).

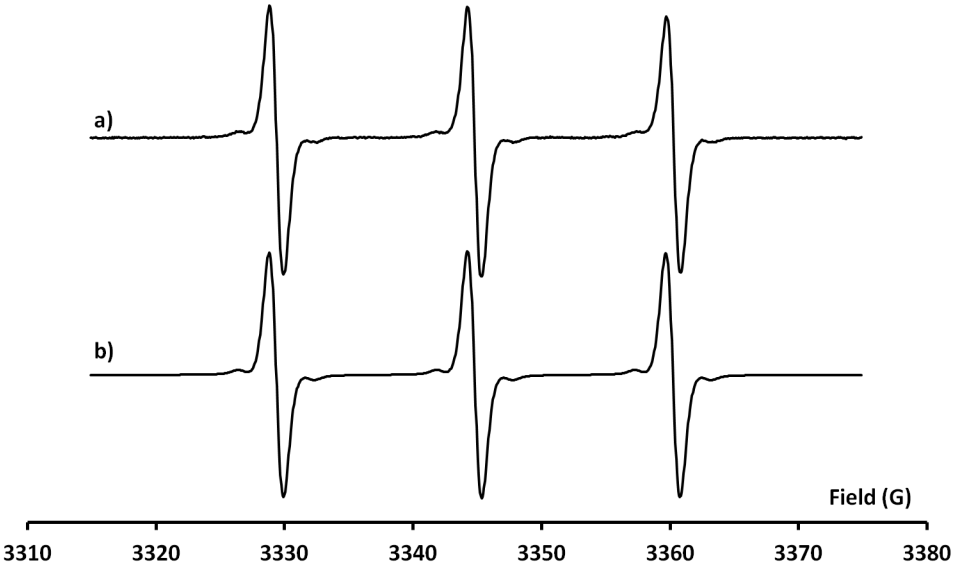

Figure 3.12: X-Band EPR spectrum of 4-carboxymethylidene-TEMPO (**38**) in DCM/Toluene 1/1, a) experimental and b) simulated.

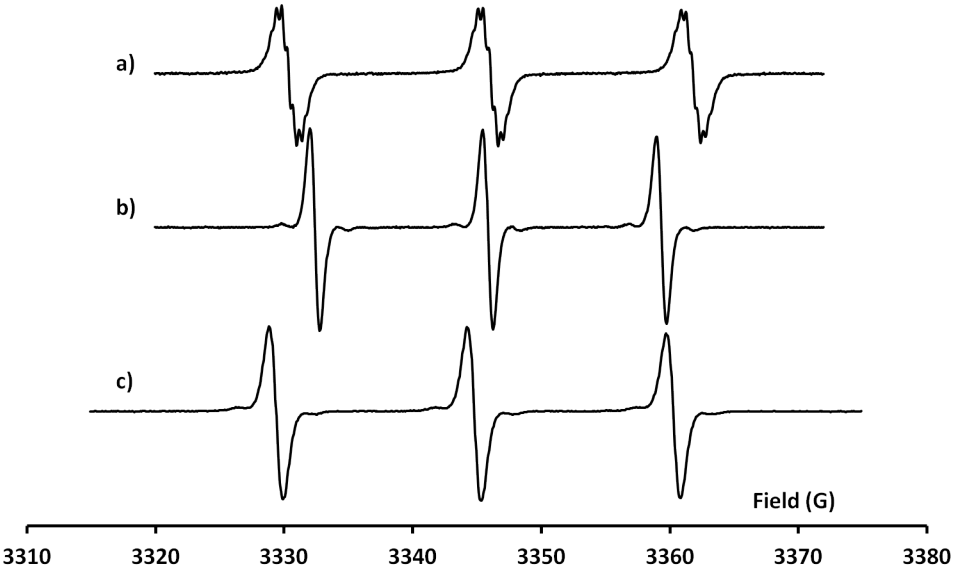

Figure 3.13: EPR spectra of a) 4-aminoTEMPO (**35**), b) 4-(2-methoxycarbonylmethylidene)-TEMPO (**37**) and c) 4-carboxymethylidene-TEMPO (**38**) in DCM/Toluene 1:1.

Lowering the temperature of the sample increases the viscosity of the solution producing a lowering of tumbling of the molecules. As the molecular tumbling correlation time increases, the extent of averaging of anisotropic features decreases and the spectrum approaches the signal of powder sample. In this context, the g factor is strongly

Table 3.2: EPR parametes for 4-aminoTEMPO, 4-(2-Methoxycarbonylmethylidene)-TEMPO and 4-carboxymethylidene-TEMPO.

Compound	g	a_N (G)	ΔH_{pp} (G)
4-aminoTEMPO (**35**)	2.0057	15.7	1.56
4-(2-Methoxycarbonylmethylidene)-TEMPO (**37**)	2.0058	15.5	0.86
4-carboxymethylidene-TEMPO (**38**)	2.0056	15.4	1.07

dependent on the molecular symmetry and its tensorial nature is manifested. For TEMPO radical, the sum of the three principal components of the g factor (g_{xx}, g_{yy} and g_{zz}) generate the final spectrum, as can be seen in **Figure 3.14**. As in the case of the g factor, the hyperfine coupling splitting at each of the principal axes is different, being the hyperfine coupling in Z 5-fold than in X or Y ones.

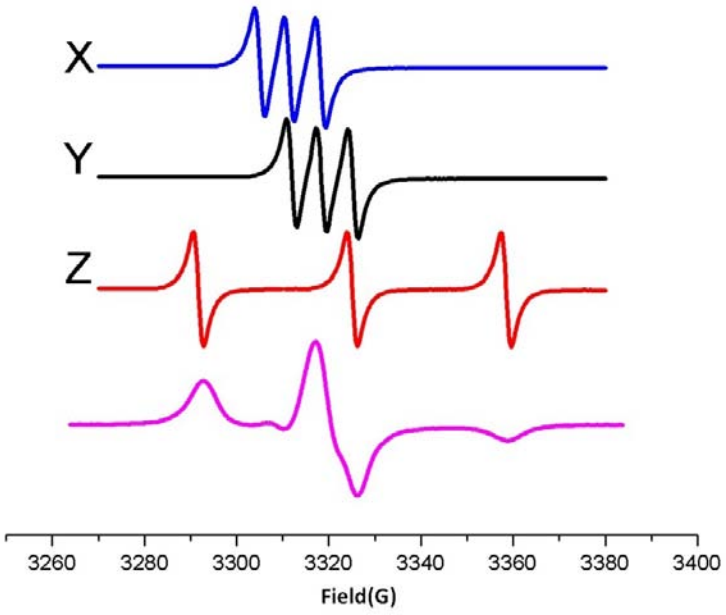

Figure 3.14: X-Band powder EPR of 4-aminoTEMPO (**35**). Spectra, from up to down, are the X, Y, Z components and the sum result.

The frozen solution EPR spectra of 4-amino-TEMPO (**35**) (experimental and simulated) are represented in **Figure 3.15**. This pattern is the typical one observed for all TEMPO monoradicals in frozen solution. The diagonal components of the g tensor can be clearly identified, being g_{xx}: 2.0091; g_{yy}: 2.0064; and g_{zz}: 2.0023. The hyperfine splitting constants are a_{xx}: 6.8 G; a_{yy}: 6.3 G; and a_{zz}: 35.6 G. Finally, the spectrum width of 71 G (7.1 mT) and ΔH_{pp}: 6.0 G, 5.5 G and 6.0 G, respectively for x, y and z components.

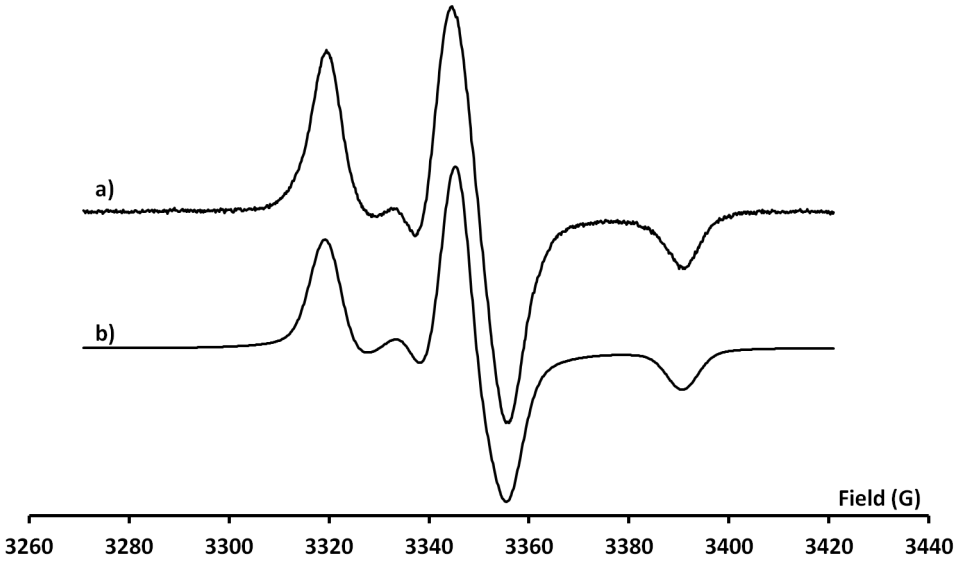

Figure 3.15: X-Band EPR frozen solution of 4-carboxymethylidene-TEMPO **38** a) experimental and b) simulated.

3.3 Conclusions

- The perchlorotriphenylmethyl (PTM) radical, functionalized with benzyl bromine **4** has been synthesized with good yield and high purity. Starting from it, the $PTMCH_2OH$ (**5**), PTM-CHO (**6**), $PTMCH_2NH_2$ (**8**) and the phosphonate (**9**) derivatives have been prepared in their αH forms.

- The 1,3-bis(diphenylene)-2-phenylallyl (BDPA) functionalized at the 4-position of the phenyl ring with a bromine, **14**, a cyano, **19**, and a acid, **26**, groups, have been synthesized with good yield and high purity. Starting from BDPA-CN (**19**) or BDPA-COOH (**26**) the $BDPACH_2NH_2$ (**21**), $BDPACH_2OH$ (**28**), BDPA-CHO (**30**), $BDPACH_2Br$ (**31**) and the phosphonate (**32**) derivatives have been prepared in their αH forms. The radical species do not show big differences in their EPR spectra characterization.

- From the modification of 4-oxo-TEMPO it has been generated the 4-carboxymethylidene-TEMPO (**38**), after the hydrolisys of 4-(2-methoxycarbonylmethylidene)-TEMPO (**37**). The EPR spectra of **37** and **38** radicals show narrower linewidth than those derivatives with different substituents at the 4-position.

Bibliography

[1] Walker R.W. *Symposium (International) on Combustion*, 22(1):p.883, **1989**.

[2] Yndall G.S., Cox R.A., Granier C., Lesclaux R., Moortgat G.K., Pilling M. J.M., Ravishankara A.R., and T.J. Wallington. *Journal of Geophysical Research: Atmospheres*, 106(D11):p.12157, **2001**.

[3] Halliwell B. Wiley-VCH Verlag GmbH and Co. KGaA, **2006**.

[4] Richard T. O. John Wiley and Sons, Inc., **2007**.

[5] Rawson J., Banister A., and Lavender I. *Adv. Heterocycl. Chem.*, 62:p.137, **1995**.

[6] Griller D. and Ingold K.U. *Acc. Chem. Res.*, 9(1):p.13, **1976**.

[7] Lomnicki S., Truong H., Vejerano E., and Dellinger B. *Environ. Sci. Technol.*, 42(13):p.4982, **2008**.

[8] Gomberg M. *J. Am. Chem. Soc.*, 22:p.757, **1900**.

[9] Golman K., Zandt R.I., Lerche M.and Pehrson R., and Ardenkjær-Larsen J.H. *J. Am. Chem. Soc.*, 66(22):p.10855, **2006**.

[10] Ballester M., Pascual I., Carreras C., and Vidal-Gancedo J. *J. Am. Chem. Soc.*, 116:p.4205, **1994**.

[11] Ballester M. *Pure Appl. Chem.*, 15:p.123, **1967**.

[12] Ballester M. *Adv. Phys. Org. Chem.*, 25:p.267, **1989**.

[13] Ballester M., Riera J. V., Castañer J., Badia C., and Monso J.M. *J. Am. Chem. Soc.*, 93:p.2215, **1971**.

[14] Horn M. and Mayr H. *J. Eur. Chem. A*, 16(25):p.7469, **2010**.

[15] Gyot A. and Kovache A. *Hebd. Seances Acad. Sci.*, 154:p.122, **1912**.

[16] Ballester M., Molinet C., and Castañer J. *J. Am. Chem. Soc.*, 82:p.4254, **1960**.

[17] Ballester M., Veciana J., Castaner J., Rovira C., and Armet O. *J. Org. Chem.*, 51(13):p.4272, **1986**.

[18] Sporer C., Ratera I., Ruiz-Molina D., Zhao Y., Vidal-Gancedo J., Wurst K., Jaitner P., Clays K., Persoons A., Rovira C., and Veciana J. *Angew. Chem. Int. Ed.*, 43:p.5266, **2004**.

[19] Armet O., Veciana J., Rovira C., RieraJ., Castañer J., Molins E., Rius J., Miravitlles C., Olivella S., and Brichfeus J. *J. Phys. Chem.*, 91:p.56080, **1987**.

[20] Koelsch C.F. *J. Am. Chem. Soc.*, 79:p.1165, **1957**.

[21] Kuhn R. and Neugebeauer F.A. *Monatsh. Chem.*, 95:p.3, **1964**.

[22] Dane E.L., Galia T.M., Debelouchina T., Griffin R.G., and Swager T.M. *Org. Lett.*, 11(9):p.1871, **2009**.

[23] Plater M.J., Kemp S., and Lattmann E. *J. Chem. Soc. Perkin Trans. 1*, page p.971, **2000**.

[24] Hiroyuki N., Naoki Y., Yukoh S., Ritsuko G., Takeshi M., and Eishun T. *J. Macromol. Sci., Part A*, 29(9):p.775, **1992**.

[25] Breslin D.T. and Fox M.A. *J. Phys. Chem.*, 97(50):p.13341, **1993**.

[26] Mullegger S., M.and Fattinger M. Rashidi, and Koch R. *J. Phys. Chem. C*, 116(42):p.22587, **2012**.

[27] Azuma N., T. Ozawa, and J. Yamauchi. *J. Chem. Soc., Perkin Trans. 2*, page p.203, **1994**.

[28] Bennati M., Farrar C.T., Bryant J.A., Inati S.J., Weis V., Gerfen G.J., riggs Gelasco P., Stubbe J., and Griffin R.G. *J. Magn. Reson.*, 138:p.232, **1999**.

[29] Francis F. *J. Chem. Soc.*, 3:p.2897, **1927**.

[30] Sosnovsky G. and Konieczny M. *Synth.*, page p.735, **1976**.

[31] Sosnovsky G. and Konieczny M. *Naturforsch.*, 32b:p.328, **1977**.

[32] Zhenkun M., Qingtao H., and J.M. Bobbitt. *J. Org. Chem.*, 58(18):p.4837, **1993**.

[33] Murayama K., Morimura S., Amakasu 0., Toda T., and Yamao E. *Chem. Abstr.*, 70:p.114968, **1970**.

[34] Lutz W.B., Lazarus S., and Meltzer R.I. *J. Org. Chem*, 27(5):p.1695, **1962**.

[35] Dagonneau M., Kagan E.S., Mikhailov V.I., Rozantsev E.G., and Sholle V. D. *Synth.*, 11:p.895, **1984**.

[36] Fioshin M.Y., Avrutskaya I.A.and Surov I.I., and Novikov V.T. *Collect. Czech. Chem. Commun.*, 52:p.182, **1987**.

[37] Levedev O.L. and Kazarnovskii S.N. *Chem. Abstr.*, 55:p.7792, **1961**.

[38] Atovmyan L. O., Golubev V.A., N.I. Golovina, and Klitskaya G.A. *Chem. Abstr.*, 82:p.163631, **1975**.

[39] Ciunik Z. *J. Mol. Struct.*, 412:p.27, **1997**.

[40] Merbouh N., Bobbitt J.M., and Brückner. *Org. Prep. Proced. Int.*, 36(1):p.1, **2004**.

[41] Moad G., , E. Rizardo, and Solomon D.H. *Tetrahedron Lett..*, 22:p.27, **1981**.

[42] Burks S.R., Makowsky M. A., Yaffe Z.A., Hoggle C., Tsai P., Muralidharan S., Bowman M.K., Kao J.P.Y., and Rosen G.M. *J. Org. Chem.*, 75:p.4737, **2010**.

Chapter 4

Diradicals

4.1 Introduction

In the present Chapter, it will be explored the synthesis and properties of diradicals, which are molecular species with two unpaired electrons occupying two degenerate molecular orbitals (MOs). There is a considerable contemporary interest in the preparation and properties of stable organic systems with two (or more) linked radicals, not only to explore their potential as bases for new magnetic materials (*e. g.* molecular magnets, switching devices, molecular wires) but also to prove the nature of the interactions between the unpaired electrons,[1–5] as well as to use them as polymerization initiators,[6] spin labels for structural investigation of biomolecules[7] or molecular probes for many types of studies.[8]

The magnitude and sign of the interspin coupling interaction (J) in exchange-coupled diradicals exert a crucial effect on the physicochemical properties of them. The spin-spin coupling interaction can be through bond and/or space[9] and its value vary by many orders of magnitude.[10] Several factors, such as the nature of the linker between the two radical moieties, the conformations, substituents and experimental conditions (*e.g.* temperature or solvent among others) control the magnitude of the exchange coupling in biradicals.[11] When a molecule presents two unpaired electrons in the same molecule, the term diradical or biradical refers to the molecule. According to the IUPAC Compendium of Chemical Terminology,[12] biradical is a technical term for molecules where the two electrons do not interact or the interacions are very weak or almost null.[12] In other words, the electron exchange interaction (J) between the two unpaired electrons is negligible or nearly negligible. When the magnitude of the interaction in a molecule with two unpaired electrons is large enough to produce two spin states, namely, singlet (S, S = 0, spin multiplicity = 1) and triplet (T, S = 1, spin multiplicity = 3), the molecular species with the two unpaired electrons is referred to as a diradical.[13]

We can classify the wide term of diradicals into homodiradicals (two identical rad-

icals) and heterodiradicals (two different radicals). If their units are of the same nature or different even if they come from the same family of radicals. The properties of diradicals come not only from the nature of the linked radicals but also from the radical-radical distance and the kind of bridge between them. As long as the bridge introduces flexibility or rigidity between the two radicals and allows or avoids the interaction between them, it can modify extremely their properties introducing dynamic intramolecular effects on their properties.

In this way, this Chapter has been divided into two sections devoted to the preparation and study of homodiradicals and heterodiradicals. The bridge used for the homodiradicals studied (TEMPO-TEMPO, PTM-PTM or BDPA-BDPA) has always been a double bond that introduces certain rigidity to the system. In particular, it has been studied the following heterodiradicals (PTM-BDPA, PTM-TEMPO and BDPA-TEMPO). On the contrary, the type of bridges used for linking the heterodiradicals have been either a double bond or a more flexible one like an ester or amide junction.

In the literature there have been reported many homodiradicals, especially those prepared with two TEMPO or two PTM units. However, heterodiradicals are not so common as homobiradicals. The use of this kind of systems in Dynamic Nuclear Polarization (DNP) has generated a great expectation and the synthesis and study of homo and or heterodiradicals have become an important field of research in the last years.

Indeed, the majority of the persistent diradicals described up to date have two similar (or identical) moieties such as bisnitroxides,[14] bisPTM[15,16] or bisnitronylnitroxides.[17] Other examples are bis-phenoxyl, bis-semiquinones or bis-hydrazyls.[18–26] A much smaller number of heterodiradicals have been reported until now[27] including phenoxy-nitroxide, semiquinone-nitroxide or hydrazyl-nitroxide diradicals.[28] The vast majority of the diradicals initially described have either a conjugated bridge[21] or a very flexible linker as the bis-nitroxides, studied by Falle and Luckhurst.[29] More recently, and thanks to the great interest to perform Dynamic Nuclear Polarization studies, the research in diradicals field has increased and several new diradical systems have been appeared, mostly homodiradicals[30,31] with rigid structures but a few heterodiradicals have also been reported.[32] Some examples of heterodiradicals that have been explored their potential application as polarizing agents are BDPA-TEMPO[33] or trityl-nitroxide compounds.[34,35]

4.1.1 Considerations about EPR spectra of diradicals

At a first glance, the EPR spectra of free monoradicals in solution under isotropic conditions provides information about the g-values and the hyperfine coupling constants. However, much more information can be obtained from the widths of the lines of spectra under non isotropic conditions. The linewidths of solution spectra often vary with the temperature and solvent. The relaxation mechanism responsible of this effect is

known to be the anisotropy in the g and a hyperfine tensors together with the Brownian motion that can average completely or partially the anisotropic contribution of such tensor.[36,37] A detailed linewidth analysis may result in the evaluation of data like the elements of the g tensor of the radical[38] or the rotational correlation time of the studied molecules. In more cases, the width of the hyperfine lines alternates,[39] a phenomenon caused by an out-of-phases modulation of the isotropic coupling constants.[40] Other processes that may be responsible of the modulation of the hyperfine splitting a includes rotational isomerism[40] and the formation and destruction of hydrogen bonds.[41]

In a diradical molecule there are more aspects to take into account. Thus, for homobiradicals like dinitroxides one can distinguish two different situations: when they have rigid structures and when they are flexible. In rigid structures, and depending on the bridge length and the type of conformations adopted, one can distinguish three different cases. In the absence of a significant isotropic spin exchange (J) value the biradical behaves as two independent single radicals and the electron paramagnetic resonance spectrum would consist of three lines separated by the coupling constant with the N nucleus a_N (the nitrogen hyperfine splitting), **Figure 4.1a**. However, if there is a strong exchange interaction J between the two electrons such that $|J| \gg |a_N|$ then the spectrum will consist of five lines separated by 1/2 a_N, **Figure 4.1b** because both electrons are coupled with the two N nuclei simultaneously.[42] When the J coupling is comparable to the hyperfine ^{14}N coupling constant of the nitroxide moiety the EPR spectrum exhibits a more complex nine-line pattern (**Figure 4.1c**).

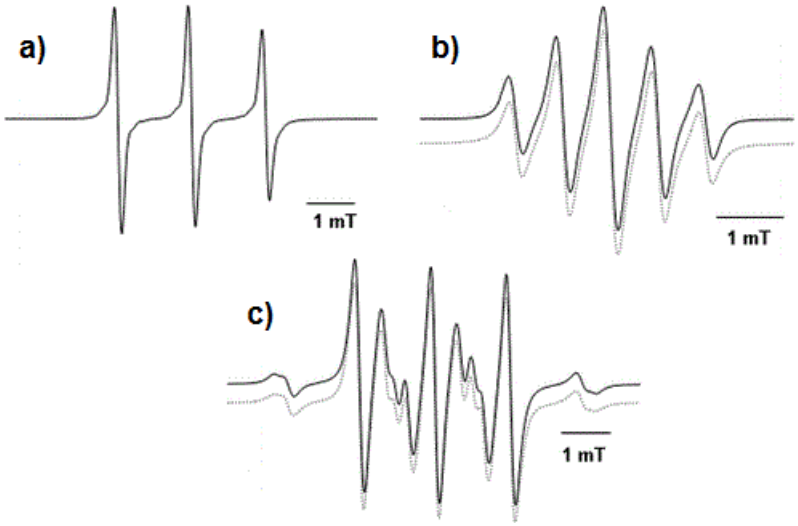

Figure 4.1: X band EPR spectra of dinitroxides with a) $|J| \ll |aJ_N|$, b) $|J| \gg |a_N|$ and c) $|J| \approx |a_N|$ (grey line: simulated spectra).[43]

On the other hand, in flexible diradicals the spin exchange J value critically depends on the frequency of collisions of the spin-bearing functional groups.[44–46] The

EPR spectra are thus affected by the temperature, viscosity and nature of the solvent. Moreover, in the flexible diradicals two limiting cases can be considered: 1) the conformations where the two nitroxide radicals are far away from each other, and hence $|J| \ll |a_N|$, the spectrum of the biradical is similar to that of two independent monoradicals exhibiting three lines separated by the hyperfine coupling constant a_N with relative intensities 1:1:1; 2) the conformations with the two nitroxides close to each other and therefore $|J| \gg |a_N|$, the spectrum consist on a five-line hyperfine pattern with 1/2 a_N separation and relative intensities of 1:2:3:2:1. Therefore, there are different rates of interconversion between these two different conformations depending mainly on the temperature. **Figure 4.2** illustrates this case. It can be observed that as the temperature is gradually lowered, the alternating 2^{nd} and 4^{th} lines broaden and disappear going from the $|J| \gg |a_N|$ to the $|J| \ll |a_N|$ limits. This thermally modulated intramolecular spin exchange interaction process can also be obtained by other phenomena like an out-of-phases modulation of the isotropic coupling constants, formation and destruction of hydrogen bonds, etc.

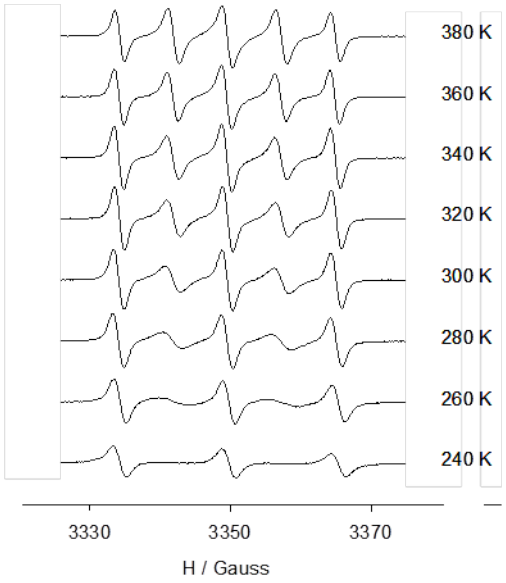

Figure 4.2: EPR spectra of a flexible dinitroxide at different temperatures.

On the other hand, heterobiradical systems can be perfectly illustrated with the following example, where a trityl (T) and a nitroxide (N) radicals are connected through bridge with different lengths. **Figure 4.3** shows the simulated EPR spectra of T-N diradicals as a function of J values. When the trityl and nitroxide moieties are far away from each other and uncoupled ($J = 0$), the superimposed trityl (a single line, T) and nitroxide signals (three lines, N with a_N= 17 G) can be observed. With the increase in J values but being still smaller than a_N (*i. e.*, J= 2-5 G), each line from trityl and nitroxide signals splits into doublet, affording eight lines in total. On the other hand, if J is comparable to a_N (*i. e.*, J= 10 and 25 G) the forbidden transitions

marked with a (*) appear besides the doublets. When J is moderately larger than a_N, a doublet pattern can be seen at the low-field part of the spectra (*i. e.*, J= 25-100 G). The separation of this doublet is inversely proportional to the J value. With a further increase of J value, this doublet merges into singlet line (J= 200 G), thus affording an EPR with a pattern separation of approximately 8.5 G (1/2 a_N). When J is very large (J= 1000 G), the EPR spectrum is almost symmetric with the same width and amplitude for the triplet.[34]

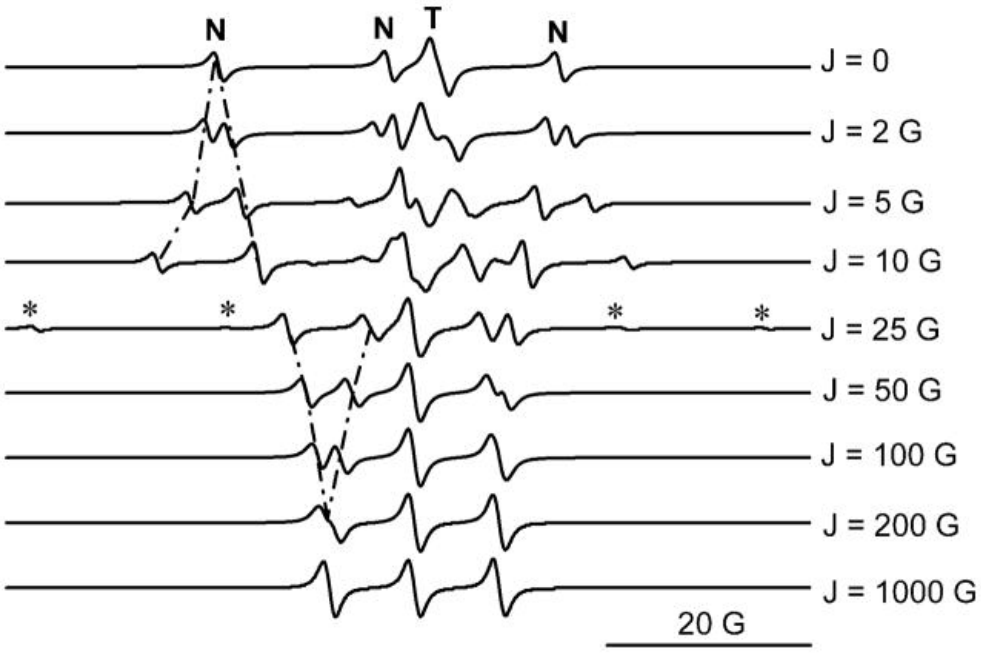

Figure 4.3: Simulated EPR spectra of trityl-nitroxide diradicals with various J values and a_N= 17 G . T and N indicate the trityl and nitroxide signals, respectively and (*) shows forbidden transitions of biradicals.[34]

4.2 Synthesis and study of homodiradicals

4.2.1 Carbon centered homodiradicals derived from PTM and BDPA

4.2.1.1 PTM=PTM diradical (40)

The first homodiradical (previously synthesized by a different pathway) synthesized in this Thesis was, PTM=PTM (**40**). It was obtained from the phosphonate **9** and the aldehyde **6** derivatives and consisted of two PTM units joined by a *E*-double bond. Its preparation was made by a Wittig-Horner-Emmons method (**Scheme 4.1**). This methodology implies a nucleoplilic addition of the stabilized carbanion of the phosphonate to a carbonyl carbon and subsequent elimination driven by a phosphorous-oxigen bond. It generates a *E*-double bond between the carbonyl carbon and the carbon directly bonded to the phosphorous atom.

In the present case, the synthesis of diradical PTM=PTM (**40**) (**Scheme 4.2**) was carried out by the reaction of the anion phosphonate derivative **9**, generated with ^{t}BuOK at $-78\,^{\circ}$C, with the corresponding aldehyde derivative **6**, both of them in α-H forms. The synthesis of both precursors were already described in Chapter 3. The distance between the two α carbons in diradical was estimated, by the Avogadro software, to be 12.5 Å.

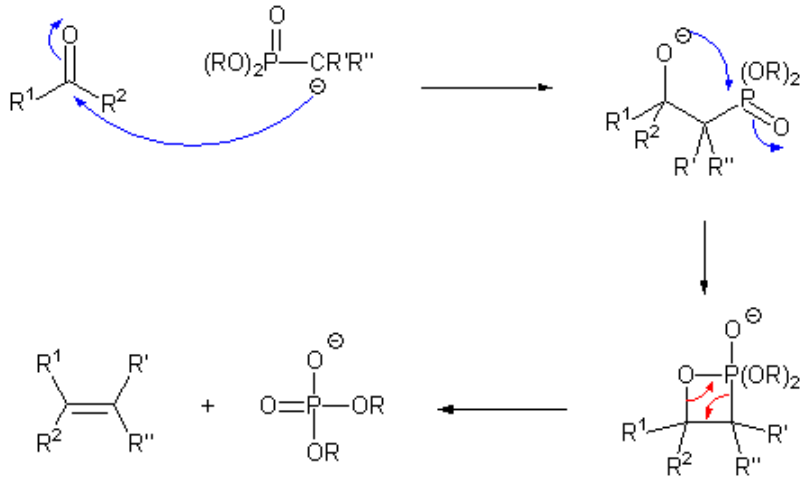

Scheme 4.1: Wittig-Horner-Emmons reaction mechanism.

After chromatographic purification, the *bis*αH form **39** was isolated with a poor yield (Y: 10%). This could be due to the big sizes of the two neighboring chlorines close to the carbonyl group that may hinder the approach of the anion. Nevertheless, the resulting αH derivative could be characterized by IR, ^{1}H NMR and MALDI-TOF. Finally, diradical (**40**) was obtained by deprotonation with NBu_4OH and subsequent oxidation with $AgNO_3$ (in ACN)and characterized *in situ* by EPR.

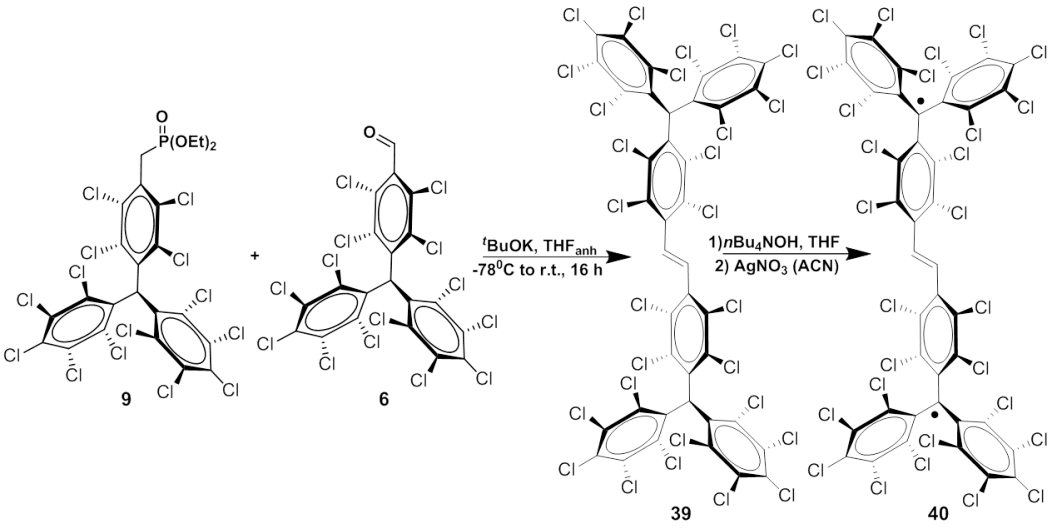

Scheme 4.2: Synthetic scheme for PTM=PTM homodiradical (**40**).

In **Figure 4.4a** it can be observed the EPR spectrum in THF at 300 K, which shows only one principal line. In addition, there are weak satellite lines which are originated from the hyperfine couplings of the unpaired electron with magnetically active ^{13}C nuclei in natural abundance at the α, *bridgehead* and *ortho* positions. From the simulation of the 300 K spectrum (**Figure 4.4b**) it could be obtained the ^{13}C hyperfine coupling constants: $a_{^{13}\mathrm{C}_\alpha}$, 14.4 G; $a_{^{13}\mathrm{C}_{\mathrm{bridge}}}$, 6.0 G; and $a_{^{13}\mathrm{C}_{\mathrm{ortho}}}$, 5.3 G; the linewidth, 1.0 G and the g value 2.0029.

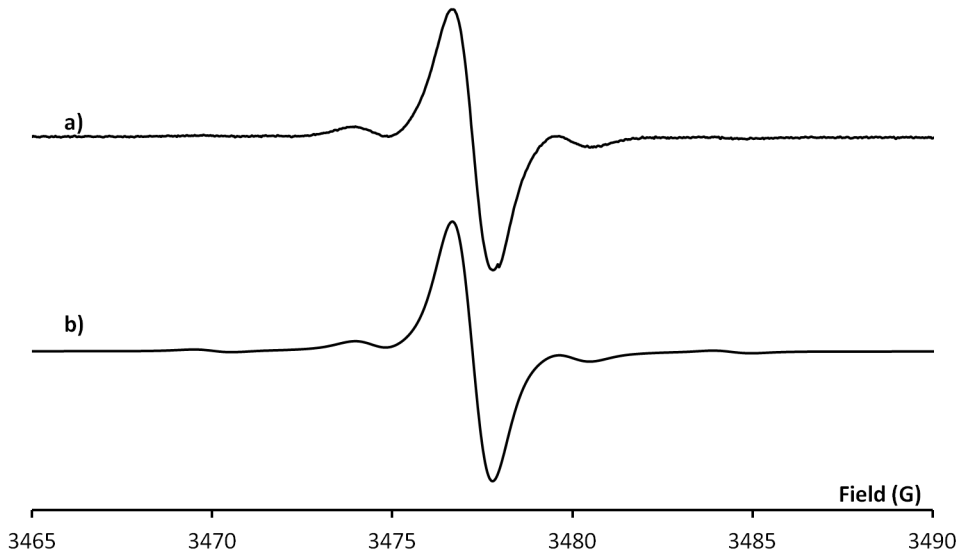

Figure 4.4: EPR spectrum of PTM=PTM diradical (**40**) at 300 K in THF. a) Experimental and b) simulated.

On the other hand, at 220 K (**Figure 4.5a**), as the linewidths of the EPR decreases

due to the lower temperature, it could be distinguished that the principal line consisted in three overlapped lines. From the simulation (**Figure 4.5b**) of the 220 K spectrum, it was obtained the coupling of the free electron with the ^{1}H nuclei of the etylenic unit a_H(2H); 0.52 G with ΔH_{pp}; 0.36 G.

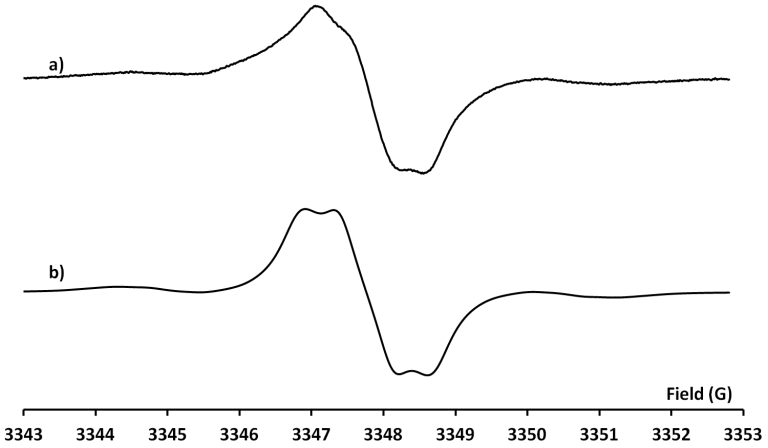

Figure 4.5: EPR spectrum of PTM=PTM (**40**) at 220 K in THF. a) Experimental and b) simulated.

From those data we can say: i) The two electrons are coupled with the 2 H of the double bond, and these 2 H seem to be equivalent due to the molecular symmetry. ii) The hyperfine coupling constants of the ^{13}C and ^{1}H are half of the values for the typical PTM monoradicals as well as the a_H of monoradical PTM with a double bond. This result suggests that the two unpaired electrons interact magnetically within the so-called "strong exchange limit", so that the exchange coupling constant J is much higher than a_H: $|J| \gg |a_H|$ and $|J'| \gg |a_{^{13}C}|$.

The EPR in frozen conditions(**Figure 4.6**) shows a typical single line corresponding to a frozen PTM radical with a 6.4 G width. As we obtained the diradical *in situ* and in diluted conditions, the EPR spectrum at half-field was impossible to record.

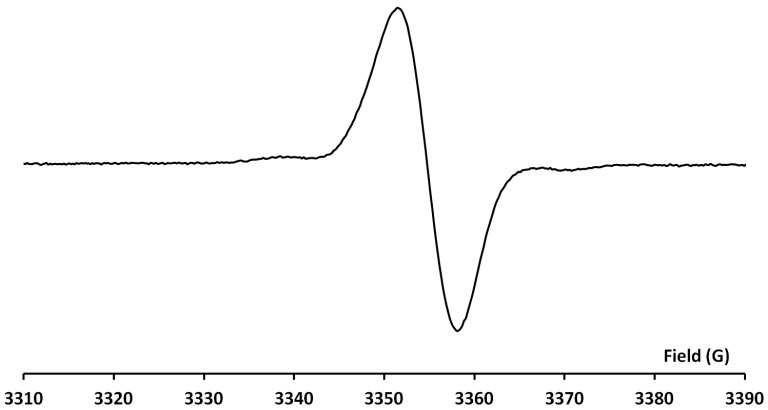

Figure 4.6: EPR spectrum of PTM=PTM (**40**) at 130 K in THF.

4.2.1.2 BDPA=BDPA biradical (42)

The homodiradical BDPA=BDPA (**42**), that joins two carbon centered BDPA moieties was prepared, as in the previous case, by a Wittig-Horner-Emmons reaction. The reaction involved, once again, a phosphonate, in this case the phosphonate derivative of BDPA **32** and the corresponding BDPA derivative modified in the 4-position of the phenyl ring with an aldehyde group, compound **30**. Following the same Wittig-Horner-Emmons mechanism (**Scheme 4.1**), the anion phosphonate derivative, in anhydrous THF, generated with ^{t}BuOK at $-78\,^\circ$C, attacked the aldehyde carbonyl. The mixture was kept at room temperature for 16 hours (**Scheme 4.3**) and after chromatographic purification, the hydrocarbon precursor of **41** was isolated as a red powder (Y: 44%) with radical traces and characterized by IR and MALDI-TOF. The *in situ* deprotonation with DBU and oxidation with $AgNO_3$ afforded the biradical **42** which was characterized by EPR (parameters g: 2.0026 , a_H(4H): 1.8 G, a_H(4H): 1.5 G, a_H(4H): 0.57 G, a_H(4H): 0.39 G, a_H(2H): 0.067 G, ΔH_{pp}: 0.25 G). The distance between the two carbons that joins the fluorenyl rings was estimated, by Avogadro software, to be 12.3 Å, a value very close to the previous diradical.

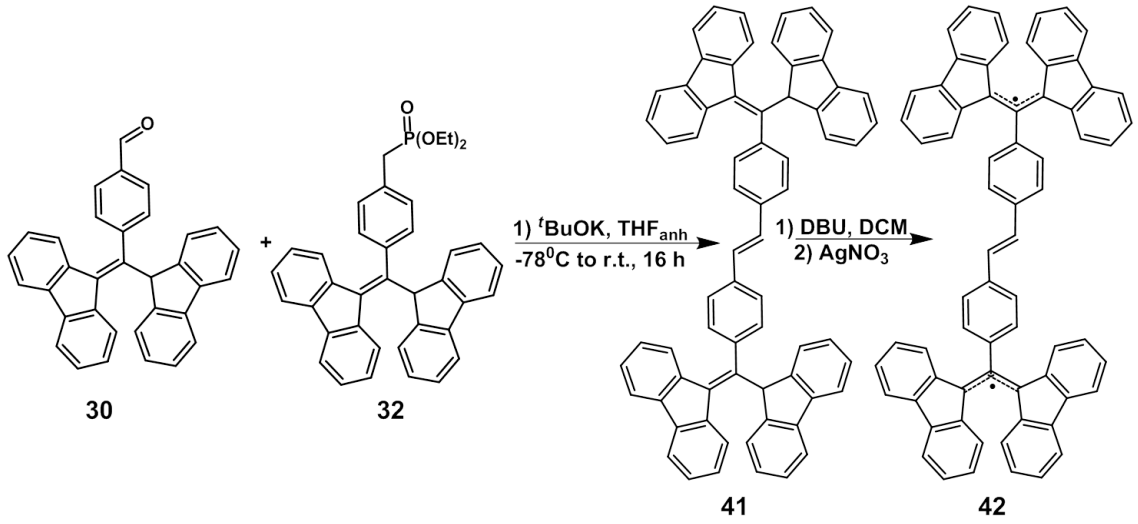

Scheme 4.3: Synthetic scheme for BDPA=BDPA homobiradical (**42**).

The EPR of the biradical **42**, at room temperature (**Figure 4.7**), shows the typical spectrum of a BDPA monoradical that consists of 9 principal lines with a complex hyperfine structure. The simulation of the EPR spectra gave the following parameters: g, 2.0026; a_H(4H), 1.8 G; a_H(4H), 1.5 G; a_H(4H), 0.57 G; a_H(4H), 0.39 G; a_H(2H), 0.067 G; and ΔH_{pp}, 0.25 G. Interestingly, the presence of the double bond in 4-position of the phenyl ring does not change the electronic distribution of the SOMO orbital as the parameters of **42** do not differ significantly from the BDPA monoradical. We can conclude that in this species the spin exchange interaction between both BDPA radical units is almost null being therefore a biradical. Consequently, the magnitude of J is

smaller than the hyperfine coupling constants *i.e.* $|J| \ll |a_{\mathrm{H}}|$ and $|J'| \ll |a_{^{13}\mathrm{C}}|$ and the spectrum is similar to that of two independent monoradicals.

Figure 4.7: EPR spectrum of BDPA=BDPA diradical (**42**) at 300 K in THF/benzene. a) Experimental and b) simulated.

The spectrum in frozen solution of the BDPA=BDPA biradical (**42**) has a total spectral width similar to that of a frozen BDPA monoradical ($\sim$ 5.3 G). This result suggests that the electron-electron dipolar interaction is very weak due to the large interadical separation of a 12.3 Å. As we obtained the biradical *in situ* and in diluted conditions, the EPR spectrum at half-field was impossible to record although it was not expected any EPR signal there.

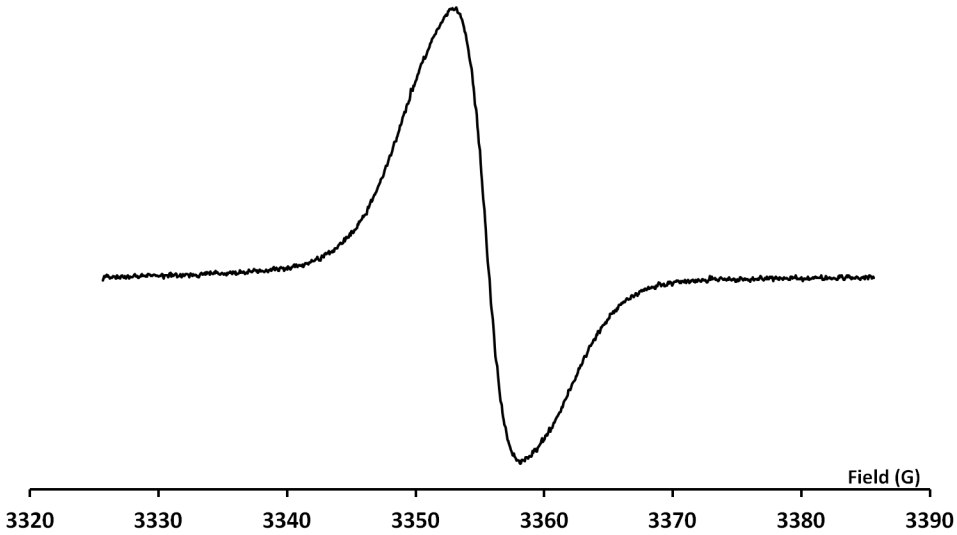

Figure 4.8: Frozen solution EPR spectrum of BDPA=BDPA biradical (**42**) in THF/benzene at 120 K.

4.2.2 Nitrogen centered homodiradicals derived from TEMPO

Nitroxide radicals are very common since many years. Since then they have been used in several applications. They are commercially available and show a high stability. The diradicals of this Section were prepared from two pathways. The first one was the use of the corresponding amine form to obtain the bisamine derivative by a McMurry reaction and then the oxidation of bisamine to the diradical, as in the case of TEMPO=TEMPO diradical **44**. The second pathway was by reaction of the radical acid derivative **38** prepared from the commercial 4-oxo-TEMPO **36** with 4-hydroxy-TEMPO **34** to yield the TEMPOesterTEMPO, **45** or with 4-amino-TEMPO **35** to afford the TEMPOamidoTEMPO diradical **46** that are also commercially available.

4.2.2.1 TEMPO=TEMPO diradical (44)

The synthesis of TEMPO=TEMPO diradical (**44**) was firstly attempted by a direct double bond formation in the 4-positions of two TEMPO units. Unfortunately, the direct reaction between two units of 4-oxo-TEMPO **36** did not allowed the isolation of **44**. This product was finally prepared in a two-step synthesis following the McMurry reaction (**Scheme 4.4**) using the amine derivative (**Scheme 4.5**) instead of the radical one.

The carbonyl coupling in a McMurry reaction takes place basically in two steps (**Scheme 4.4**): 1) reductive dimerization of the starting ketone using $TiCl_4$ as a reducting agent to form the carbon-carbon bond, and 2) deoxigenation of the 1,2-diolate intermediate with Zn to yield the alkene.

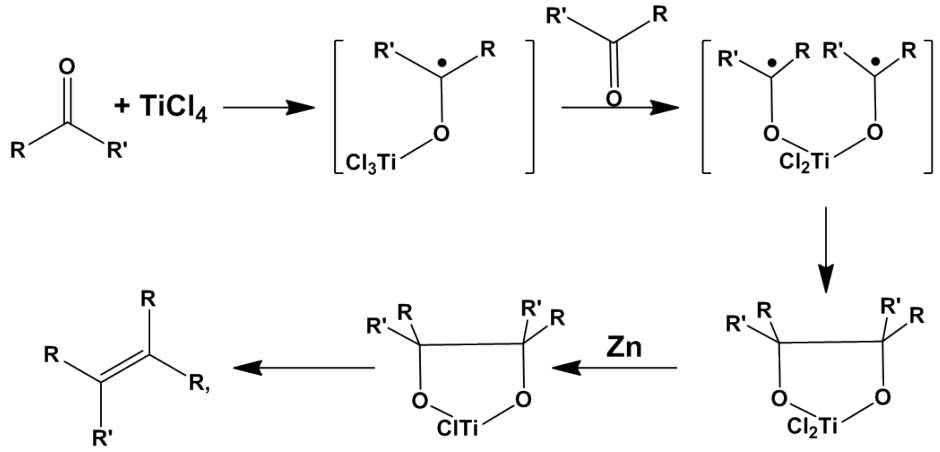

Scheme 4.4: Mechanism of McMurry reaction.

The first reaction is a pinacol reduction carried out with a low valence titanium derivative ($TiCl_4$), although it can also be used other metals. It is known that reducing metals are able to add an electron to a ketone or aldehyde carbonyl group, yielding an anion radical that dimerizes.[47,48] Then, pinacols are eliminated by refluxing the mixture, leading to the final double bond.

For the present case, the use of 2,2,6,6-tetramethyl-4-piperidone generated the desired exocyclic double bond (**Scheme 4.5**). The diamine product **43** was isolated, purified (Y: 87%), characterized and finally it was oxidized with *m*CPBA to generate the diradical **44**. The oxidation of the biamine **43** (**Scheme 4.5**) to the N-oxide biradical was carried out with *m*CPBA in dichloromethane for 2 hours, obtaining the desired diradical **44** after chromatographic purification (Y: 76%).[49] This diradical was characterized by IR, UV-Vis, MALDI-TOF and EPR.

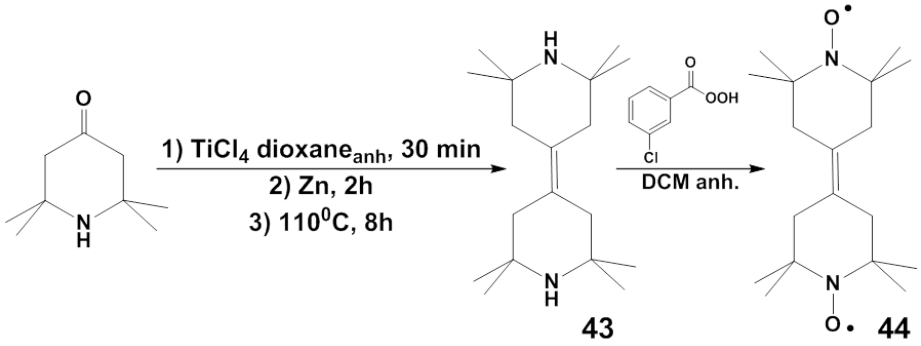

Scheme 4.5: Synthetic scheme for TEMPO=TEMPO diradical (**44**).

The EPR spectrum at room temperature of the diradical **44** showed five lines with a, g, 2.0058; ΔH_{pp}; 1.3-1.4 G, and a_N 7.7 G, which is half of the value of a TEMPO radical moiety. This implies a strong spin exchange interaction (J) between the two TEMPO radicals with $|J| \gg |a_N|$. The spectrum resulted to be strongly dependent of the temperature, since as the temperature is gradually lowered the alternate 2^{nd} and 4^{th} lines broaden and tend to disappear (**Figure 4.9**). As the system is rigid, the dynamics of the thermally modulated intramolecular spin-exchange process could be explained due to the rotations and conformational changes (chair and boat) between the two radical units, in terms of an out of phase modulation of the a_N coupling constants.[50–52]

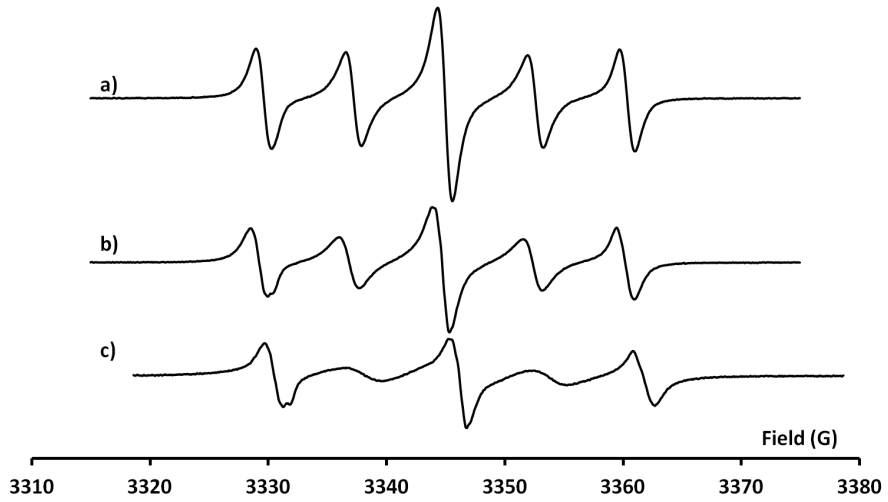

Figure 4.9: EPR spectra of TEMPO=TEMPO diradical (**44**) in DCM/toluene 1/1 at different temperatures: a) 300, b) 260 and c) 220 K.

At 120 K, the EPR spectrum of a frozen solution of the diradical (**Figure 4.10**) shows a clearly different spectrum than that of a frozen TEMPO monoradical (Chapter 3) due to the dipolar interaction between the two coupled electrons of the molecule. The central line corresponds to the presence of a monoradical-like TEMPO. The extracted parameters from the simulation were g_{xx}, 2.0050; g_{yy}, 2.0025; and g_{zz}, 2.0050; $a_{N_{xx}}$, 3.0 G; $a_{N_{yy}}$, 16.0 G; and $a_{N_{zz}}$, 5.0 G; $\Delta H_{pp_x}=\Delta H_{pp_y}=\Delta H_{pp_z}$, 5 G. On the other hand, a $Zero-Field\ Splitting$ parameter, D, of 61 G was obtained from the spectral simulation. This parameter allowed us to determine a radical-radical distance of 6.7 Å, using **Equation 4.1**,[53–56] that is in agreement with the estimated distance by the Avogadro software (6.9 Å).

$$D = \frac{3g^2\beta^2}{2r^3} \tag{4.1}$$

where g is the g-factor, β is the Bohr magneton and r is the distance among radicals.

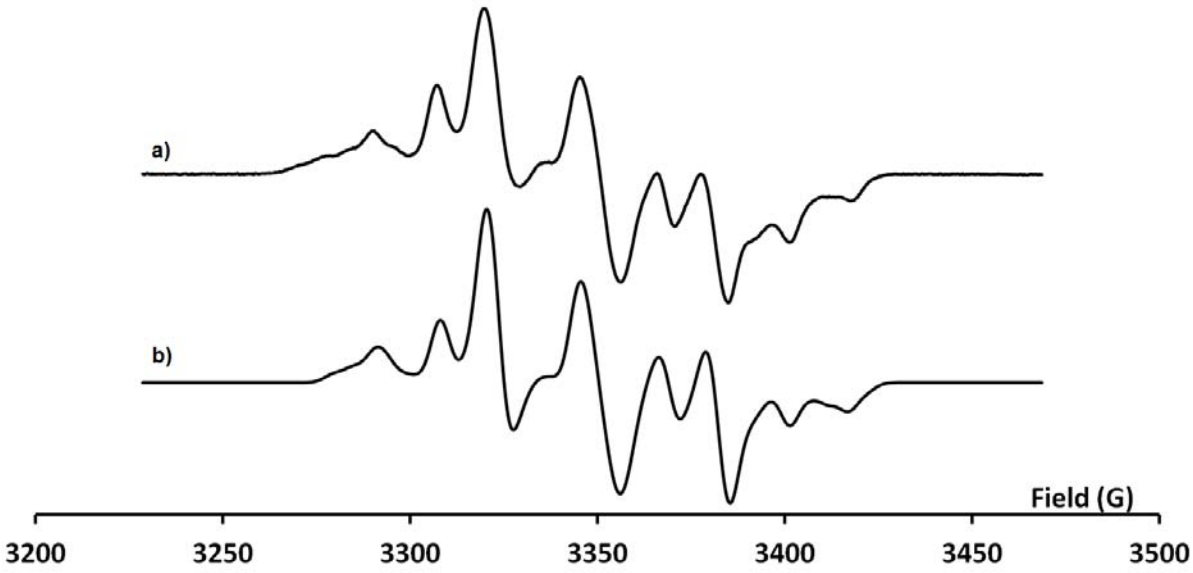

Figure 4.10: EPR spectrum of a frozen solution of TEMPO=TEMPO diradical **44** in DCM/toluene (1/1) at 120 K. a) Experimental and b) simulated. The simulation is the sum of the spectrum of diradical plus a frozen monoradical-like TEMPO.

At frozen conditions, a signal due to half-field $|\Delta m_s| = 2$ transition was also observed, which gives direct evidence of the presence of a thermally available triplet state (S=1), **Figure 4.11**.

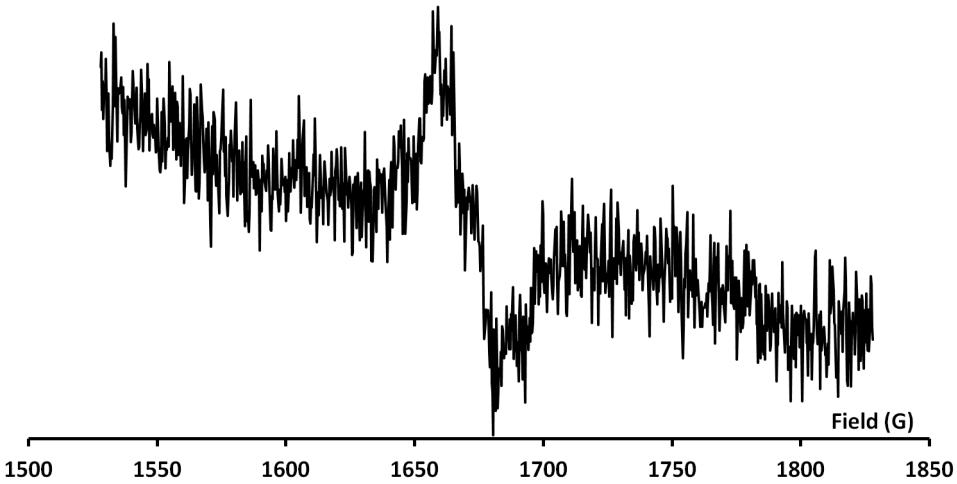

Figure 4.11: Half field EPR spectrum of a 10^{-3} M frozen solution of TEMPO=TEMPO diradical (**44**) in DCM/toluene (1:1) at 120 K.

4.2.2.2 TEMPOesterTEMPO diradical (45)

The synthesis of diradical TEMPOesterTEMPO (**45**) involves an esterification reaction between the commercial 4-hydroxy-TEMPO (**34**) and 4-carboxymethylidene-2,2,6,6,-tetramethyl-1-piperidyloxyl (**38**) using carbodiimides (**Scheme 4.6**).

The formation of an ester using a carbodiimide is straightforward, (**Scheme 4.6**) but with several side reactions that often complicates the synthesis. The acid **a** reacts with the carbodiimide to produce a key intermediate: the O-acylisourea **b**, which can be viewed as a carboxylic ester with an activated leaving group. The O-acylisourea will react with alcohols to give the desired ester **d** and urea **e**. The side reaction of the O-acylisourea **b** produces undesired products. Then, the O-acylisourea **b** can react with an additional carboxylic acid **a** to give the carboxylic anhydride **h**, which can react further to give the desired ester **d**. The main undesired reaction pathway involves the rearrangement of the O-acylisourea **b** to afford the stable N-acylurea **f**. The use of solvents with low-dielectric constants such as dichloromethane or chloroform can minimize this side reaction.

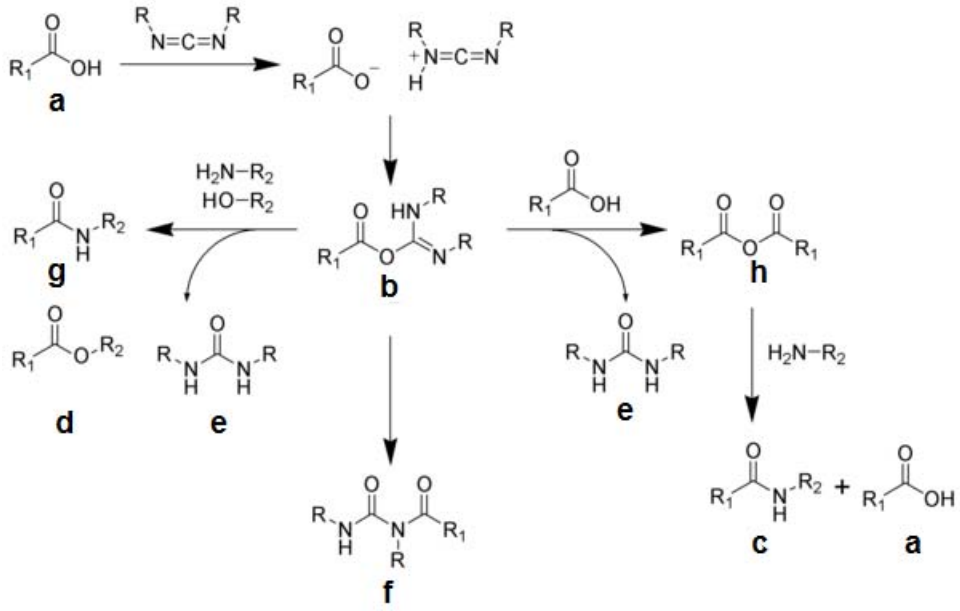

Scheme 4.6: Synthetic mechanism of an ester/amide synthesis with a carbodiimide.

The reaction between 4-hydroxy-TEMPO (**34**) and 4-carboxymethylidene-2,2,6,6,-tetramethyl-1-piperidyloxyl (**38**) was performed using 4-dimethylaminopyridine (DMAP) and N,N'-diciclohexilcarbodiimide (DCC)as a coupling agent in anhydrous THF under Ar atmosphere for 16 hours (**Scheme 4.7**). After chromatographic purification the TEMPOesterTEMPO diradical (**45**) (Y: 70%) was isolated as an orange powder which was characterized by IR, EPR and MALDI-TOF.

The distance between the two nitrogen atoms in the biradical was estimated with the Avogadro software to be 10.5 Å. It is important to remind here that this molecule

is less rigid than the diradical TEMPO=TEMPO (**44**) and the possible conformations that can adopt are the boat and chair conformations of the cyclohexane rings and also the rotation of the TEMPO unit that does not present the exocyclic double bond.

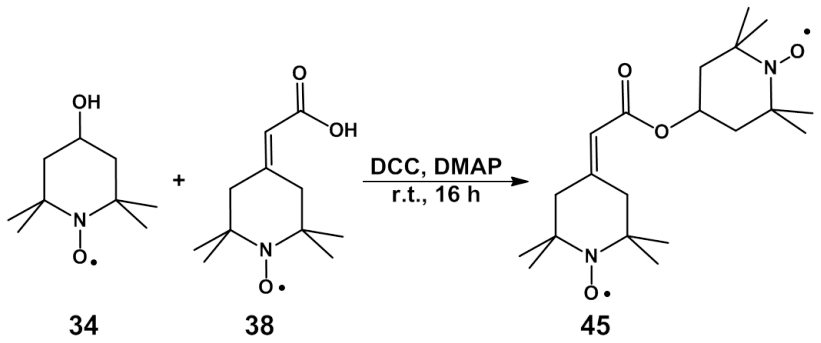

Scheme 4.7: Synthetic scheme for TEMPOesterTEMPO diradical (**45**).

The EPR of this longer diradical at 300 K showed three main lines, with a few weak additional lines between them (**Figure 4.12a**), which are seen better at lower temperatures (**Figure 4.12b-d**). This special pattern was observed in other bis-TEMPO diradicals[57] and is explained by the existence of some degree of exchange coupling between the two nitroxides, fulfilling the condition $|J| \approx |a_N|$. The spectra of **45** are not significantly dependent of the temperature.[50–52] The parameters extracted from the experimental spectrum at 300 K were g, 2.0067; a_N, 15.4 G; and ΔH_{pp}, 1.2-2.0 G.

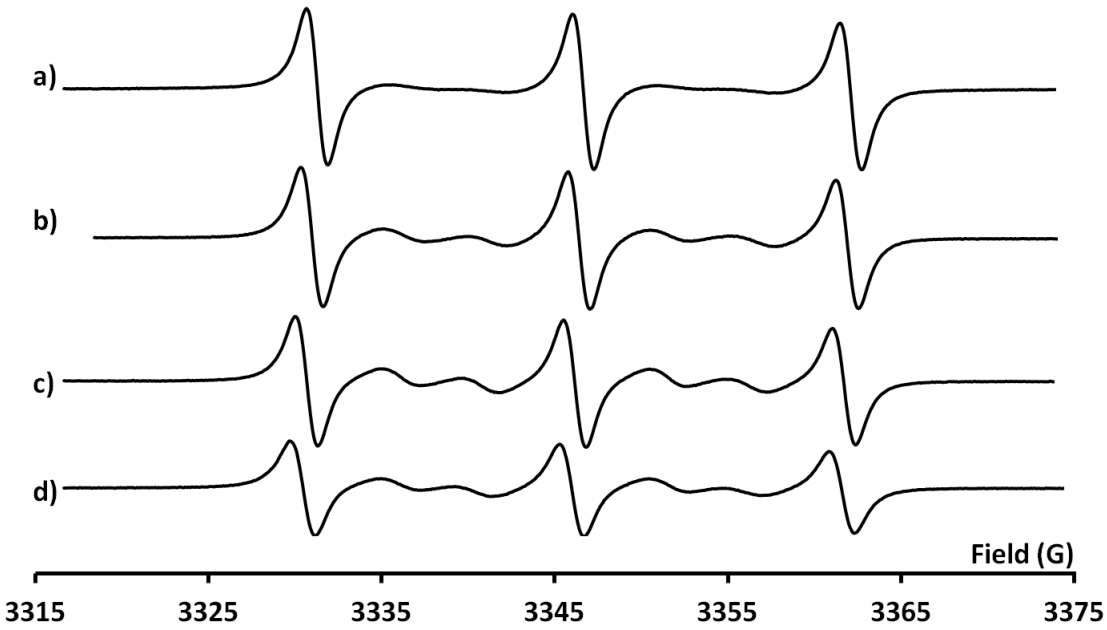

Figure 4.12: EPR spectra of the TEMPOesterTEMPO diradical (**45**) in DCM/toluene (1/1) at different temperatures: a) 300, b) 280 c) 260 and d) 240 K.

At 130 K the spectrum of a frozen EPR solution of TEMPOesterTEMPO diradical (**45**) (**Figure 4.13**) shows $Zero - Field\ Splitting$ (D) of 12 G which is much lower than for TEMPO=TEMPO diradical (**44**). This value allowed us to determine an intermolecular distance of 11.6 Å, with the **Equation 4.1** which is close to the estimated value with the Avogadro software (10.5 Å). The other extracted parameters from the simulation were g_{xx}: 2.0100; g_{yy}: 2.0064; and g_{zz}: 2.0022; the hyperfine coupling constant of $a_{N_{xx}}$: 6.5 G; $a_{N_{yy}}$: 6.3 G; and $a_{N_{zz}}$: 18.0 G; $\Delta H_{pp_{xx}}$=$\Delta H_{pp_{zz}}$: 6 G; $\Delta H_{pp_{yy}}$: 8 G. To simulate the experimental spectrum it was needed to add a small contribution of a frozen monoradical-like TEMPO.

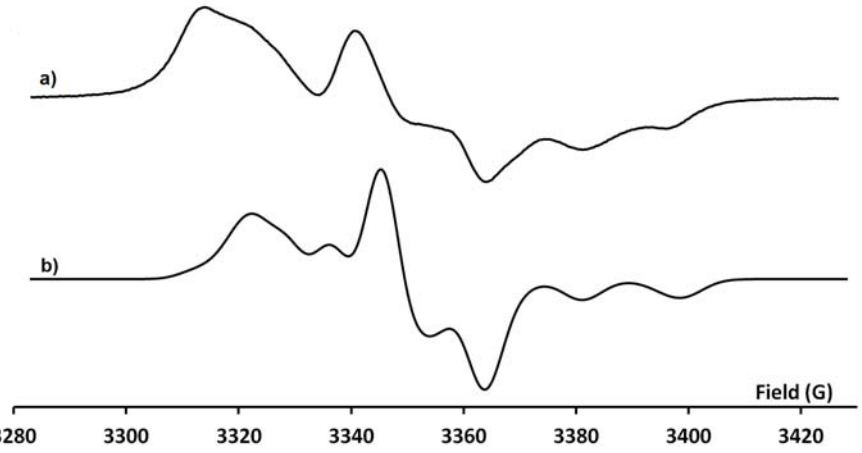

Figure 4.13: EPR spectra of 10^{-4} M frozen solution of TEMPOesterTEMPO (**45**) diradical in DCM/toluene (1:1) at 130 K. a) Experimental and b) simulated. The simulation spectrum is the sum of the spectrum of the diradical plus a little contribution of a frozen monoradical-like TEMPO.

The EPR spectrum recorded at half field (**Figure 4.14**) showed a very weak, almost non-existent $|\Delta m_s|$= 2 transition. The weak intensity of this forbidden transition is in agreement with the large separation of the two radical units. It must be inversely proportional to the radical-radical distance to the sixth power.[55]

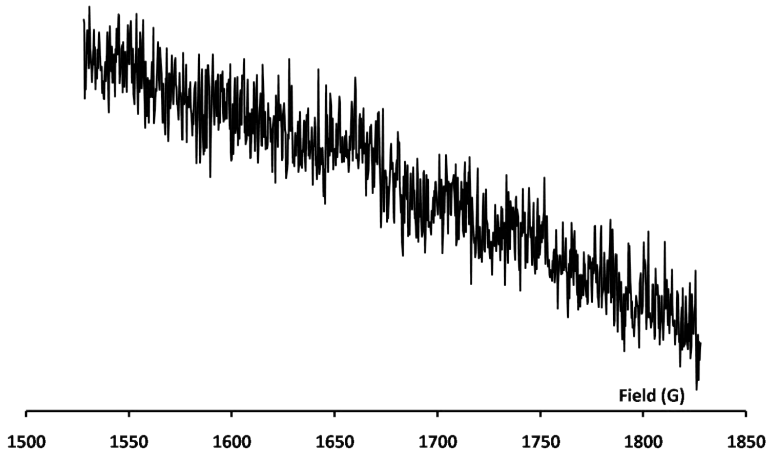

Figure 4.14: EPR spectrum of TEMPOesterTEMPO diradical (**45**) at half field in DCM/toluene (1/1), at 130 K.

4.2.2.3 TEMPOamidoTEMPO diradical (46)

The synthesis of the TEMPOamidoTEMPO diradical (**46**) involves an amidation reaction between the commercially available 4-amino-TEMPO (**35**) and 4-carboxymethylidene-2,2,6,6,-tetramethyl-1-piperidyloxyl (**38**). The reaction, as in the previous case, was performed using DMAP and DCC, as a coupling agent, in anhydrous THF under Ar atmosphere for 16 hours (**Scheme 4.8**). After chromatographic purification the diradical **46** (Y: 76%) was isolated as an orange pure powder which was characterized by IR, MALDI-TOF and EPR.

The distance between the two nitrogen atoms of biradical **46** was estimated by the Avogadro software to be 9.6 Å. It is important to remind that this molecule is also less rigid than the TEMPO=TEMPO diradical (**44**). The possible conformations that can adopt, as in the ester case are the boat and chair conformations of the cyclohexane rings and the rotation of the TEMPO unit from 4-amino-TEMPO moiety, as well as possible fluctuations of the sp^2 hybrid bond of the amide, that in this case is slower than in the ester case.

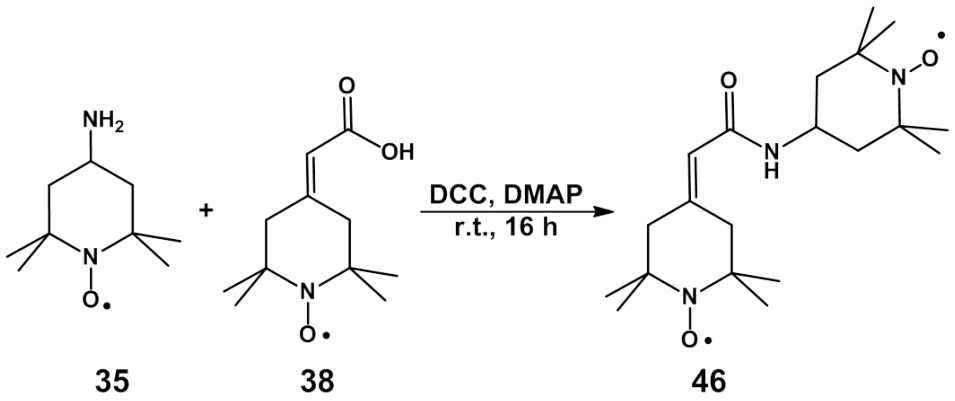

Scheme 4.8: Synthetic scheme for TEMPOamidoTEMPO diradical (**46**).

The EPR spectral pattern of this diradical (**Figure 4.15**) is the same than of the TEMPOesterTEMPO diradical (**45**) which, as said before, has a J coupling comparable to the hyperfine ^{14}N coupling of a TEMPO moiety ($|J| \approx |a_N|$). In fact, it has a nine-line EPR spectrum shown in **Figure 4.16**. However, in this case the additional lines are more intense than in TEMPOesterTEMPO diradical (**45**), which means that in this biradical the J value is somewhat higher, although in both cases are comparable to a_N. This is in good agreement with the lower distance between the two TEMPO moieties in compound **46** than in **45**. As can be observed in **Figure 4.15** the spectra are somewhat dependent of the temperature, which means that the value of J is temperature dependent too. This dynamic intramolecular spin exchange interaction can be explained by the interconversion of the different conformers of the compound. The parameters obtained at 300 K were: g: 2.0068; a_N: 15.4 G; and ΔH_{pp}: 1.2-1.5 G.

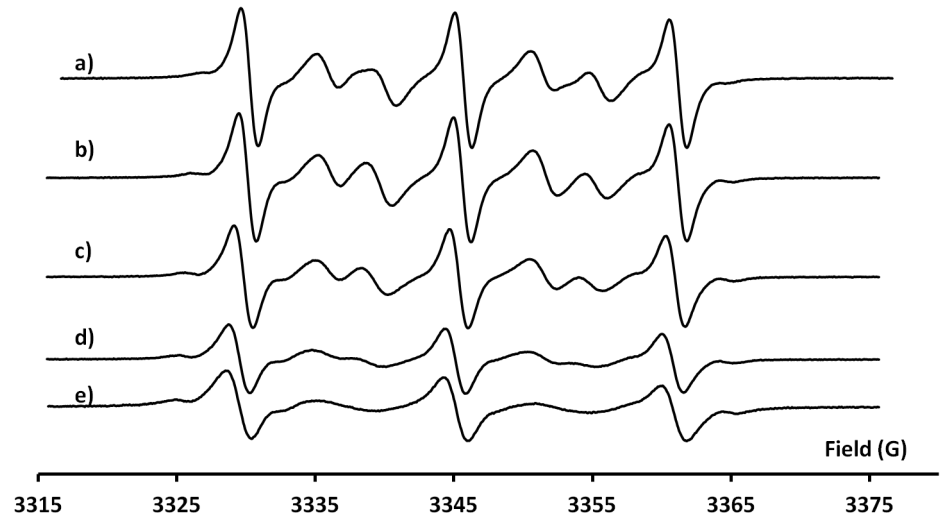

Figure 4.15: EPR spectra of TEMPOamidoTEMPO diradical (**46**) in DCM/toluene (1/1) at different temperature; a) 300, b) 280 c) 260 d) 240 and e) 220 K.

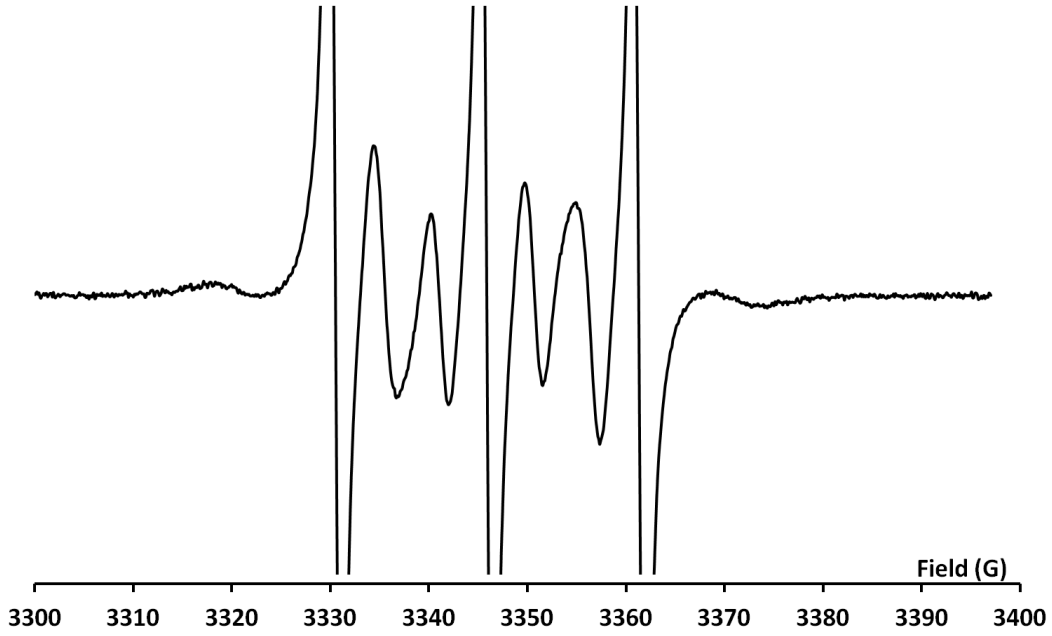

Figure 4.16: Expanded EPR spectrum of TEMPOamidoTEMPO diradical (**46**) in DCM/toluene (1/1) at 340 K.

At 130 K, the EPR spectrum of frozen solution (**Figure 4.17**) of the TEMPOamidoTEMPO diradical (**46**) shows similar spectral pattern than that of TEMPOesterTEMPO diradical (**45**). Thus, it shows a similar $Zero - Field\ Splitting$ (D) of 12 G indicating a similar distance, calculated with **Equation 4.1**, of 11.6 Å, which is a little bit higher than the estimated obtained with the Avogadro software (9.6 Å).

The rest of spectral parameters from the simulation were g_{xx}: 2.0100; g_{yy}: 2.0064; and g_{zz}: 2.0022; the hyperfine couplings were, $a_{N_{xx}}$: 6.5 G; $a_{N_{yy}}$: 6.3 G; and $a_{N_{zz}}$: 18.0 G; $\Delta H_{pp_x}=\Delta H_{pp_z}$: 6 G; and ΔH_{pp_y}: 8 G.

Figure 4.17: Experimental EPR spectra in DCM/toluene (1:1) at 130 K of a 10^{-3} M frozen solution of a) TEMPOesterTEMPO (**45**) and b) TEMPOamidoTEMPO (**46**) diradical.

The EPR spectrum of a frozen solution of **46** recorded at half field showed a very weak $|\Delta m_s|= 2$ transition (**Figure 4.14**) which, as in the ester biradical, is in agreement with the large radical-radical distance.

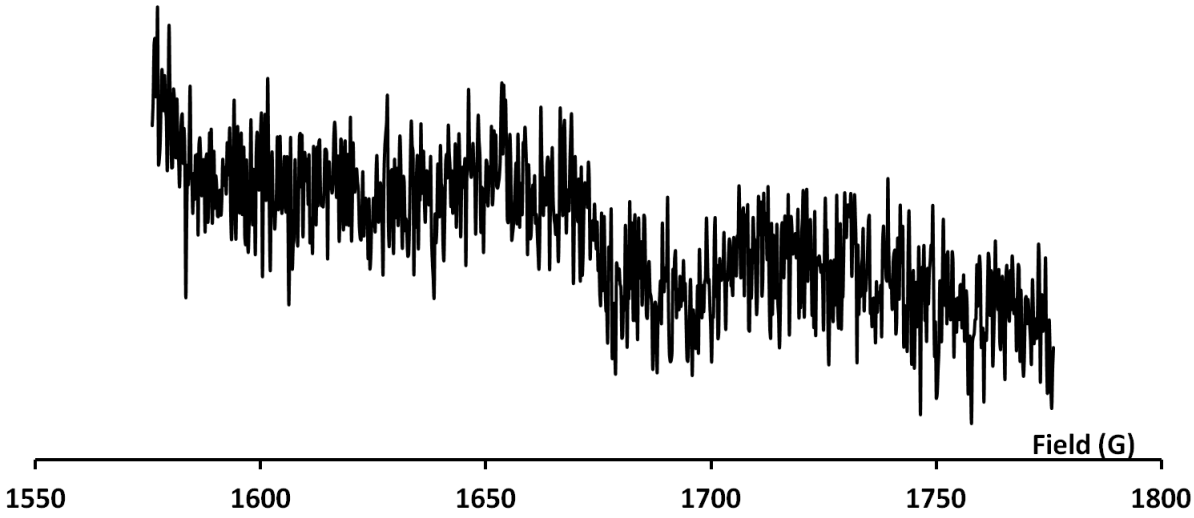

Figure 4.18: EPR spectrum of TEMPOamidoTEMPO diradical (**46**) in DCM/toluene (1/1) at half field, at 130 K.

4.3 Synthesis and study of heterodiradicals

4.3.1 Heterodiradical PTM=BDPA (48)

The heterodiradical containing two different carbon centered radicals prepared in this Thesis was synthesized by a Wittig-Horner-Emmons reaction (**Scheme 4.1**). The reaction involved the phosphonate derivative of PTM **9** and the corresponding aldehyde of BDPA **30**, both in their αH forms. The anion of the phosphonate derivative in anhydrous THF, generated with ^{t}BuOK at $-78\,^{\circ}$C, reacted with the aldehyde derivative of BDPA for 16 hours (**Scheme 4.9**). The final acid work up was enough for obtaining a compound with the αH form of PTM but the BDPA unit as radical. Therefore, it was isolated the monoradical **47** which was purified (Y: 61%) and characterized by IR, MALDI-TOF and EPR (**Figure 4.19**).

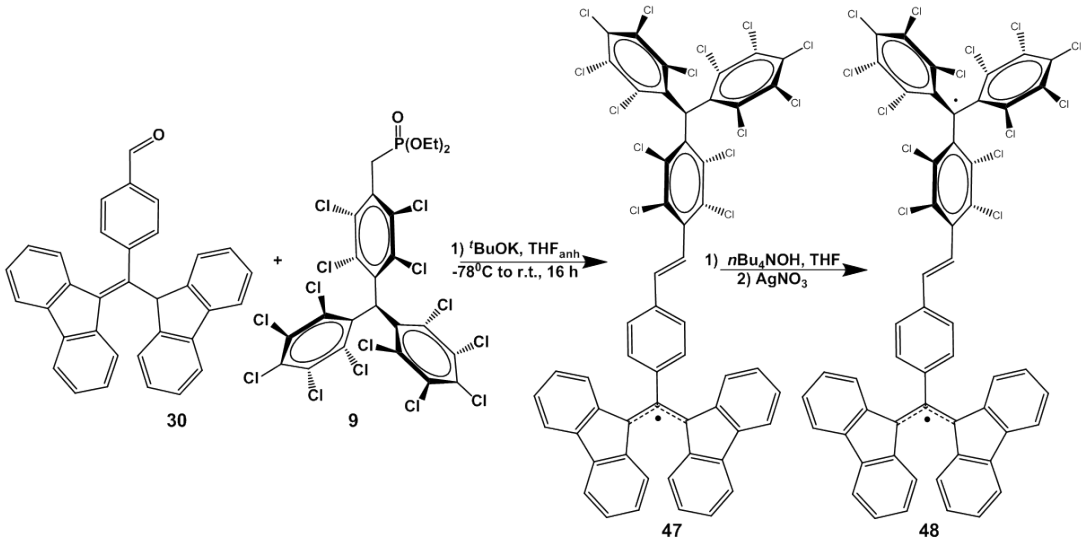

Scheme 4.9: Synthetic scheme for PTM=BDPA heterobiradical (**48**).

The EPR of the isolated monoradical αH-PTM=BDPA **47** was the typical of BDPA monoradicals, as can be seen in **Figure 4.19** with the following parameters g: 2.0023; a_{H}(4H): 1.99 G; a_{H}(4H): 1.86 G; a_{H}(4H): 0.48 G; a_{H}(4H): 0.37 G; a_{H}(2H): 0.073 G; and $\Delta \mathrm{H}_{\mathrm{pp}}$: 0.22 G.

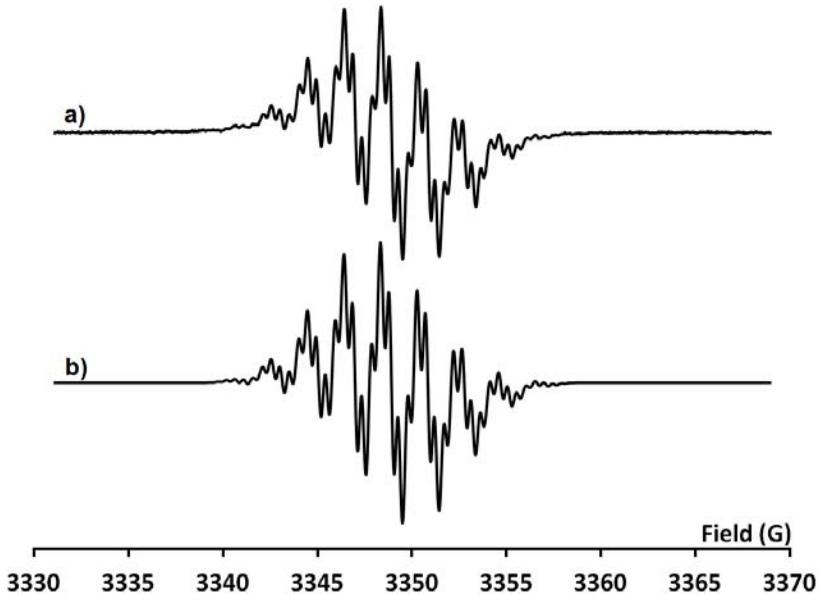

Figure 4.19: EPR spectrum of αH-PTM=BDPA (**47**) in THF/benzene at room temperature. a) Experimental and b) simulated.

After the isolation of this monoradical we proceeded to the *in situ* synthesis of the corresponding diradical. The treatment of a small amount of this monoradical in anhydrous THF/benzene (1/1) with nBu$_4$OH and then with $AgNO_3$ lead to the diradical **48**. It was characterized by EPR at room temperature. The EPR of **48** **Figure 4.20** is completely different than for monoradical **47** indicating the presence of an interaction between both radicals. The spectral parameters obtained by simulation were g: 2.0033; a_H(4H): 0.849 G; a_H(4H): 0.848 G; a_H(4H): 0.139 G; a_H(4H): 0.135G; a_H(2H): 2.220 G; a_H(2H): 2.219 G; and ΔH_{pp}: 0.1 G. In this case, the diradical fulfills the condition $|J| \gg |a_H|$ as there are a double number of lines with the hyperfine coupling constants half of the BDPA monoradical. It is thought that the interaction probably takes place through the chain due to the conjugation and the rigidity of the molecule.[58]

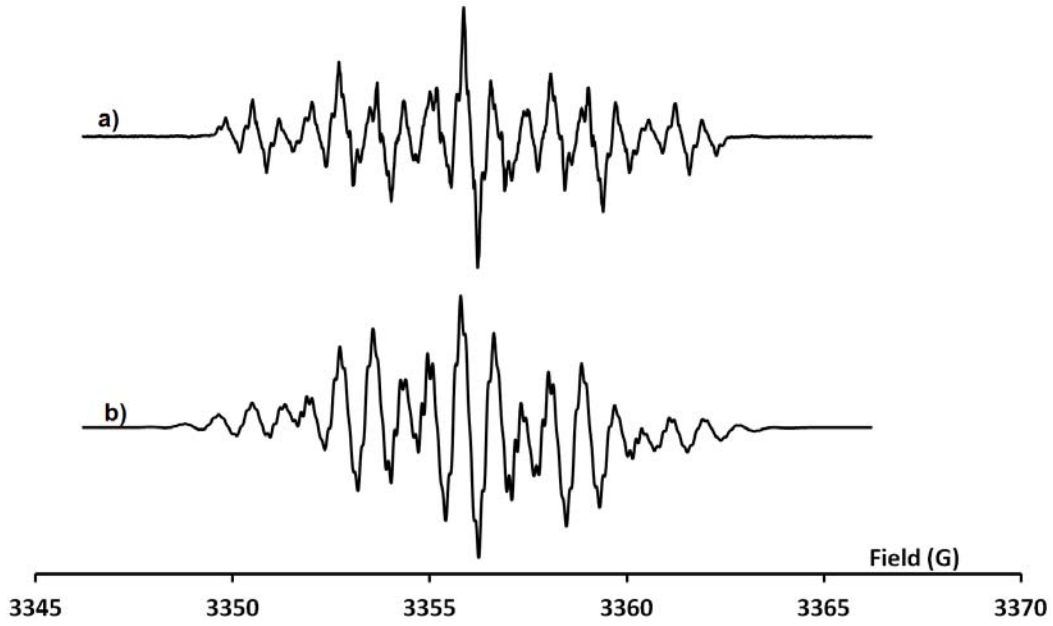

Figure 4.20: EPR spectrum of PTM=BDPA diradical (**48**) in THF/benzene at 300 K. a) experimental and b) simulated.

The distance between the αC of PTM and the carbon that joins the fluorenyl rings of BDPA in diradical **48** was estimated, by the Avogadro software, to be 12.6 Å.

4.3.2 Heterodiradicals derived from PTM and TEMPO

4.3.2.1 PTM=TEMPO diradical (49)

The first of the heterodiradicals synthesized, the PTM=TEMPO diradical (**49**), consisted of a PTM joined to a TEMPO by a double bond. It was also obtained by a Wittig-Horner-Emmons reaction (**Scheme 4.1**). The synthesis was carried out using as starting materials the phosphonate derivative **9** and the commercially available 4-oxo-TEMPO **36**. Following the Wittig-Horner-Emmons methodology, the anion phosphonate derivative of the PTM, generated with ^{t}BuOK at $-78\,^{\circ}$C in anhydrous THF, reacted with the ketone derivative of TEMPO **36** for 16 hours (**Scheme 4.10**). Finally, the oxidation of the PTM unit, generated the diradical **49** that was purified and characterized by IR, MALDI-TOF and EPR (Y: 82%).

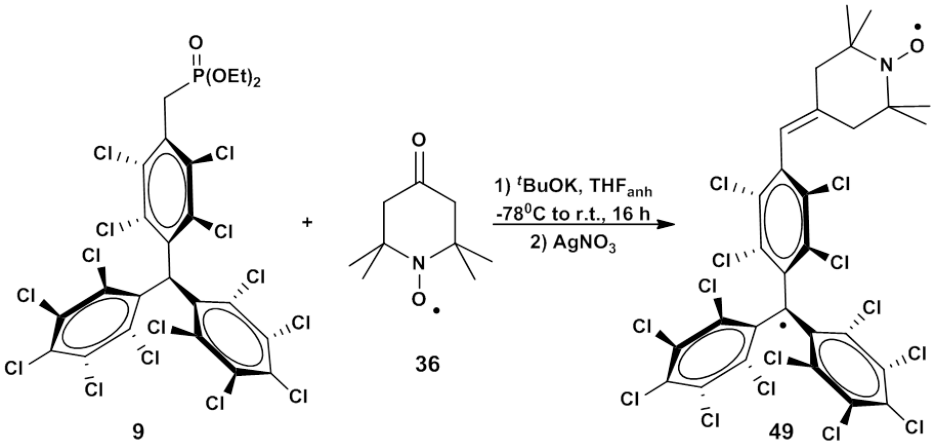

Scheme 4.10: Synthetic scheme for PTM=TEMPO diradical (**49**).

The EPR spectrum of the diradical **49** (**Figure 4.21 a**) at room temperature shows separate signals from the two radical subunits indicating that the exchange coupling J between them is not significant and belong to the biradical category. Thus, this biradical exhibits three narrow lines due to the coupling with N (a_{N}: 14.61 G) centered at a g-value of 2.0063 with a linewidth of 0.6 G; typical of a TEMPO radical with an exocyclic double bond in 4-position. The spectrum also shown a doublet of triplets due to a coupling with two different H nuclei ($\mathrm{a_H} = 7.89$ G and $\mathrm{a_H} = 1.24$ G) at a g-value of 2.0023 due to the PTM radical subunit. The simulated EPR spectrum (**Figure 4.21 b**) reproduces the experimental data with high accuracy.

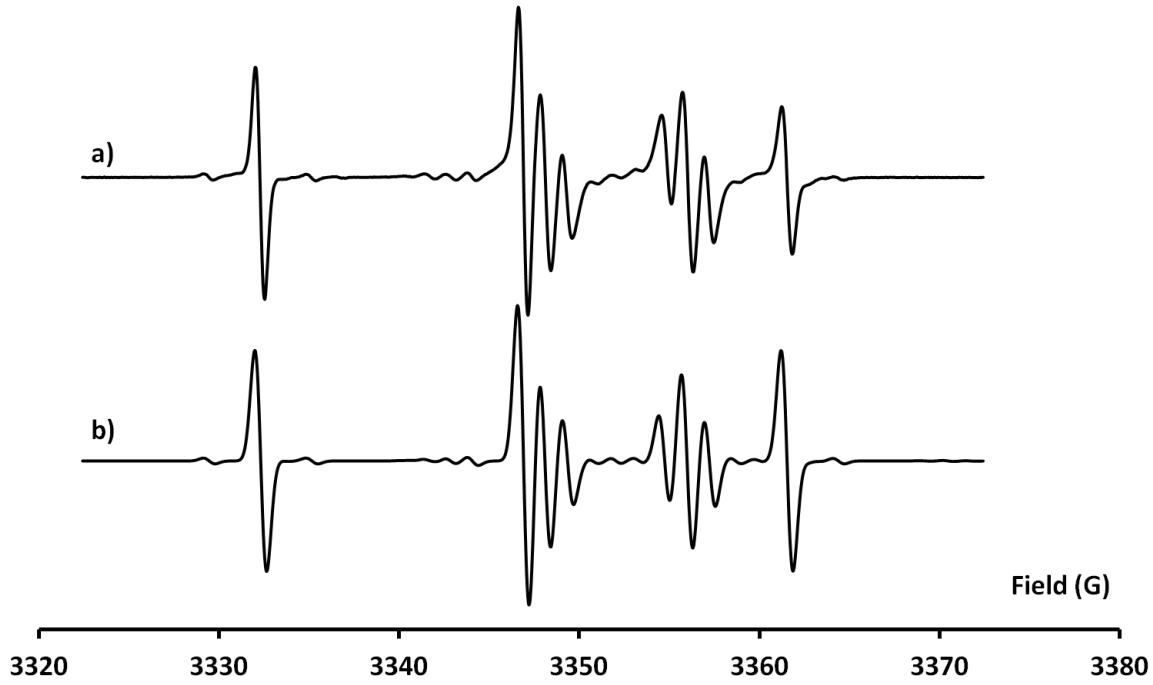

Figure 4.21: EPR spectra of PTM=TEMPO diradical (**49**) in DCM at 300 K. a) Experimental and b) simulated. The simulated spectrum is the sum of the TEMPO radical subunit and the PTM radical subunit.

In order to confirm the previous argumentation of the hyperfine coupling of diradical **49**, the monoradical **50** with only a PTM radical and TEMPE non-radical unit with the same linkage was prepared as a model compound. With this purpose, and following the same strategy than in the case of the biradical, the anion phosphonate derivative of the PTM, in anhydrous THF, reacted with 4-oxo-2,2,6,6-tetramethylpiperidine for 16 hours (**Scheme 4.11**). After the final oxidation of the PTM unit, the monoradical **50** was purified and characterized (Y: 70%) by IR, MALDI-TOF and EPR.

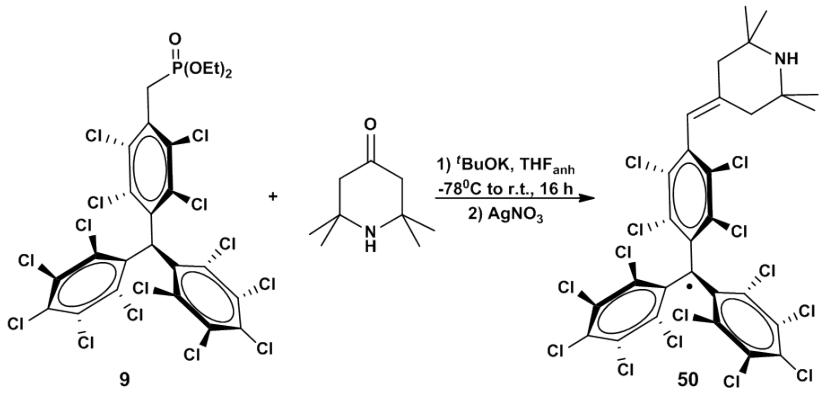

Scheme 4.11: Synthetic scheme for PTM=TEMPE monoradical (**50**).

The EPR spectrum of PTM=TEMPE monoradical **50** (**Figure 4.22**) at room temperature appears as a doublet of triplets at a g-value of 2.0027 with a linewidth of 0.9 G. The origin of such lines is the coupling of the unpaired electron with the methylenic proton ($a_{\mathrm{H}} = 6.94$ G) and with the two equivalent protons of the piperidine ring closest to the PTM subunit ($a_{\mathrm{H}} = 1.40$ G). Moreover, the EPR frozen solution shows two lines in contrast of the typical one from other PTM monoradicals (**Figure 4.23d**).

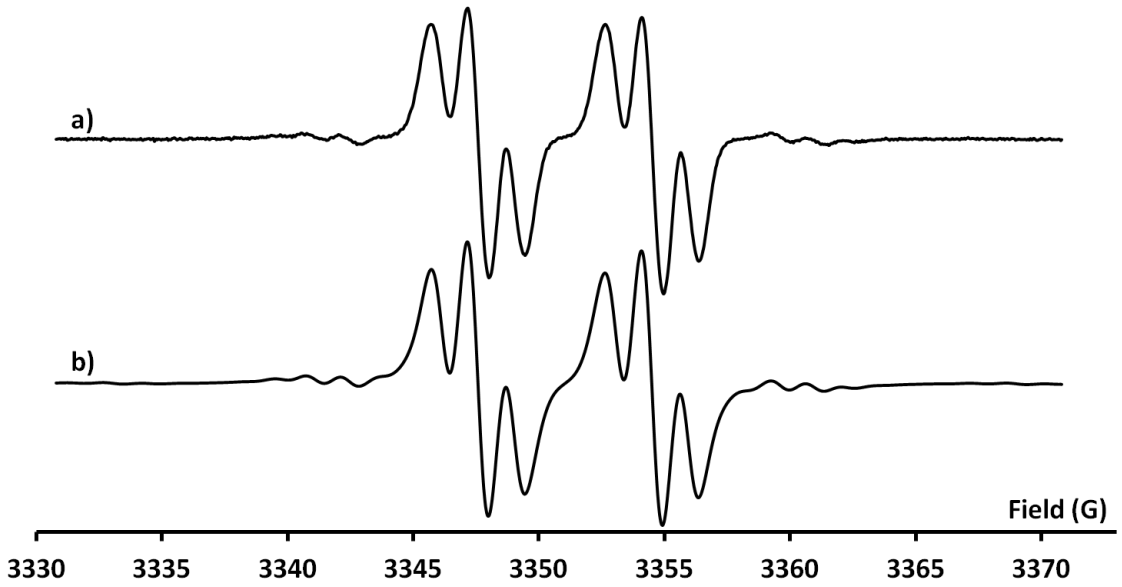

Figure 4.22: EPR spectra of PTM=TEMPE monoradical (**50**) in DCM at 300 K. a) Experimental and b) simulated.

The EPR spectrum of PTM=TEMPO biradical (**49**), in frozen solution (120 K) (**Figure 4.23a**) does not show resolved dipolar couplings. It can be well reproduced as the sum of the spectra of 4-oxo-TEMPO **36** and PTM=TEMPE monoradical **50** (**Figure 4.23b**), indicating that electron-electron dipolar interaction is very weak or null. The spectra did not show a $|\Delta \mathrm{m_s}| = 2$ transition at half field. Both results are in agreement with the fact that the Avogadro theoretical estimation of the distance between the α carbon of PTM and the oxygen of TEMPO is 9.4 Å.

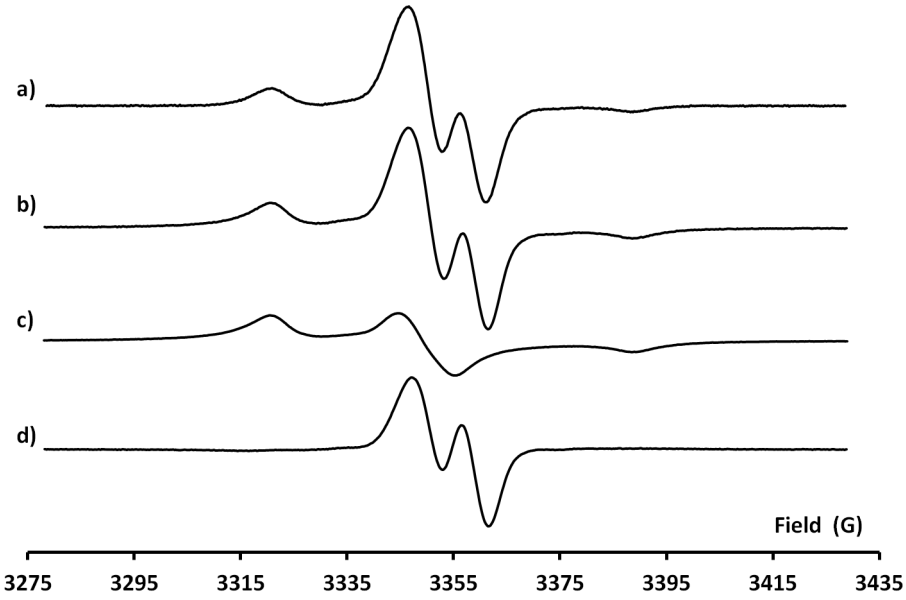

Figure 4.23: EPR spectra of a frozen solution of a) biradical PTM=TEMPO **49**; b) sum of 4-oxo-TEMPO **36** and monoradical PTM=TEMPE **50**; c) 4-oxo-TEMPO **36** and d) monoradical PTM=TEMPE **50**.

4.3.2.2 PTMesterTEMPO diradical (52)

The synthesis of the PTMesterTEMPO diradical **52** involves the esterification reaction between the benzyl alcohol derivative of αH-PTM (**5**) and 4-carboxymethylidene-2,2,6,6,-tetramethyl-1-piperidyloxyl (**38**); (**Scheme 4.12**). The first attempt to synthesize the diradical **52** was using the PTM derivative in the radical form **5r**. However, the desired product was not isolated. For this reason, it was used the PTM derivative in the αH form **5** and the compound **51** with the PTM subunit in αH form was obtained using DCC/DMAP, as in previous cases. Thus, the mixture of DMAP, 4-carboxymethylidene-2,2,6,6,-tetramethyl-1-piperidyloxyl **38** and DCC was stirred in anhydrous DCM and then, the αH-PTM derivative was added. The mixture, under Ar atmosphere, was stirred for 16 hours. After chromatographic purification a red powder was isolated (Y: 46%) that correspond to monoradical **51** with PTM in αH form.

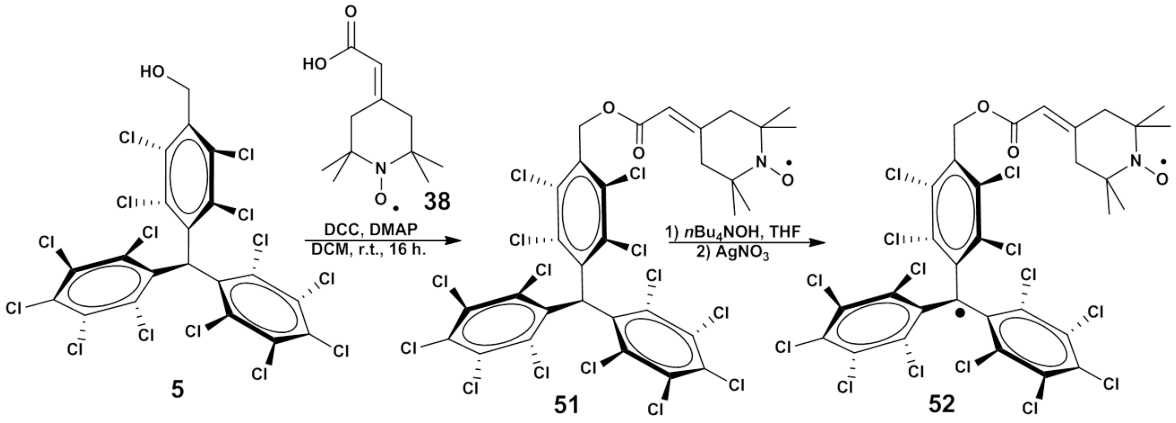

Scheme 4.12: Synthetic scheme for PTMesterTEMPO heterodiradical (**52**).

The formation of the diradical **52** from the monoradical **51** was attempted *in situ*, in different conditions. The use of tetrachloro-*p*-benzoquinone as an oxidant after the treatment of the monoradical **51** with Bu_4NOH in THF to obtain diradical **52** destroyed the TEMPO radical moiety as the EPR spectrum only presented the PTM line. However, the use of Bu_4NOH in THF followed by $AgNO_3$ produced the EPR spectrum of **Figure 4.28**, that is similar to those shown by diradicals with a similar structure. In the EPR spectrum at 300 K (**Figure 4.28a**) it can be observed simultaneously the typical lines of both radicals moieties, the three lines corresponding to the TEMPO radical unit (market as T_1, T_2 and T_3) with a_N: 15.2 G; $a_{^{13}C}$: 5.0 G at a g value of 2.0059 with ΔH_{pp}: 1.0 G, and a single line corresponding to the PTM radical moiety (marked as PTM in **Figure 4.28a**) at a g value of 2.0027 and with $\Delta H_{pp}$of 1.4 G. This spectrum pattern could correspond to the diradical with a conformation with $J \approx 0$ (conformer I). In addition to these lines, another three lines marked with an asterisk (*1, *2 and *3) in the EPR spectrum (**Figure 4.28a**) were obtained. Such lines showed three main features: i) the distance among such tree lines is half the value of the radical TEMPO hyperfine coupling constant (7.6 G), ii) the g value corresponds to the

mean value between the g value of a TEMPO unit and of a PTM radical unit (2.0043), and iii) their linewidths are like the PTM one (higher than the TEMPO linewidth). For these three reasons these extra lines should correspond to a stable conformer of diradical **52** in which the interaction between both radicals units fulfills the condition that the spin exchange interaction is higher than the hyperfine coupling constant a_N *i. e.* $|J| \gg |a_N|$. The fact that these three lines have not the same intensity, the first one (*1) is lower than the other two (*2 and *3) could be explained if in this conformation II the exchange has a very large value of J and the molecule shows a slow tumbling. Indeed, this spectrum is very similar to a spectrum in **Figure 4.3** with J= 200 G spectrum, not like to the last one with J= 1000 G. The conformation II of the biradical **52** has a value of J higher than the hyperfine coupling. This situation can be refereed as $|J| > |a_N|$ and the J= 1000 G case as $|J| \gg |a_N|$. The simulation of the spectrum (**Figure 4.28b**) was done as the superposition of the spectra of two conformers, the conformer I with $J \approx 0$ and the conformer II with a high J value. Therefore, the experimental spectrum (**Figure 4.28b**) can be explained by the sum of the two spectra: one corresponding to the conformer I, which is the responsible of lines T_1, T_2 and T_3 and the PTM line and another conformer II responsible of lines *1, *2 ans *3. Therefore, the presence of two conformers in solution for diradical **52** is in agreement with the theoretical estimation by the Avogadro software of the distance between the α carbon of PTM and the oxygen of TEMPO of 9.4 Å. Nevertheless, it is necessary to take into account that the molecule is not rigid and other conformations can show different distances between the radicals.

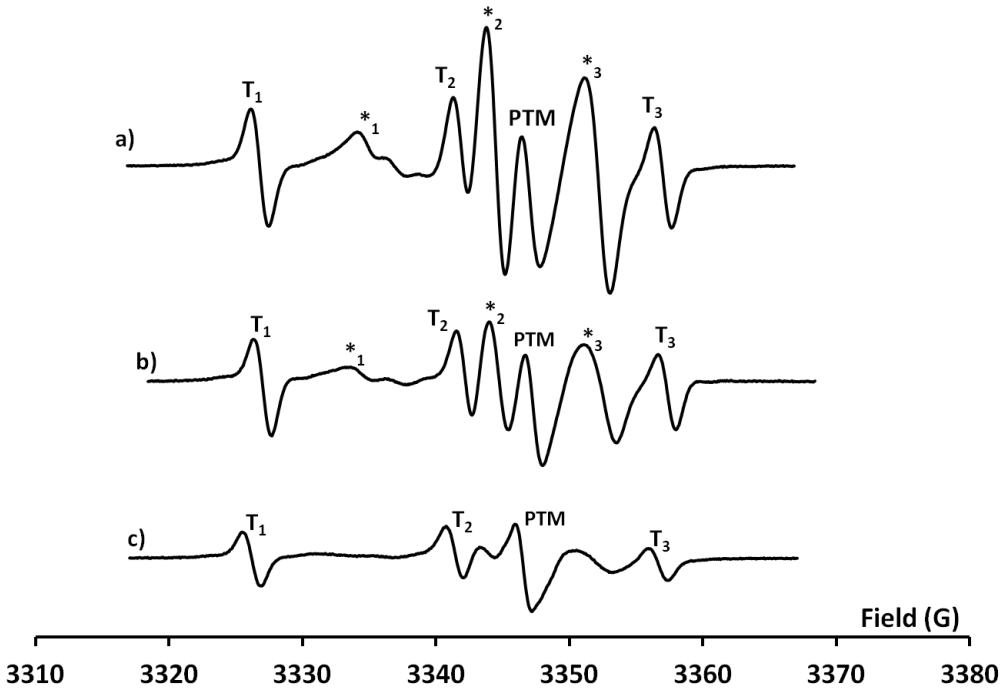

Figure 4.24: EPR spectrum of the PTMesterTEMPO diradical (**52**) in THF at different temperatures a) 300 K b) 260 K and c) 220 K.

As the temperature decreases (**Figure 4.24**) it can be observed different behavior in the EPR spectra of both conformers. While the spectrum of conformer II decreases its intensity and tends to disappear, the spectra of conformer I is maintained. When the temperature is increased again to 300 K, the shape and intensity of the spectra were completely recovered (**Figure 4.25**).

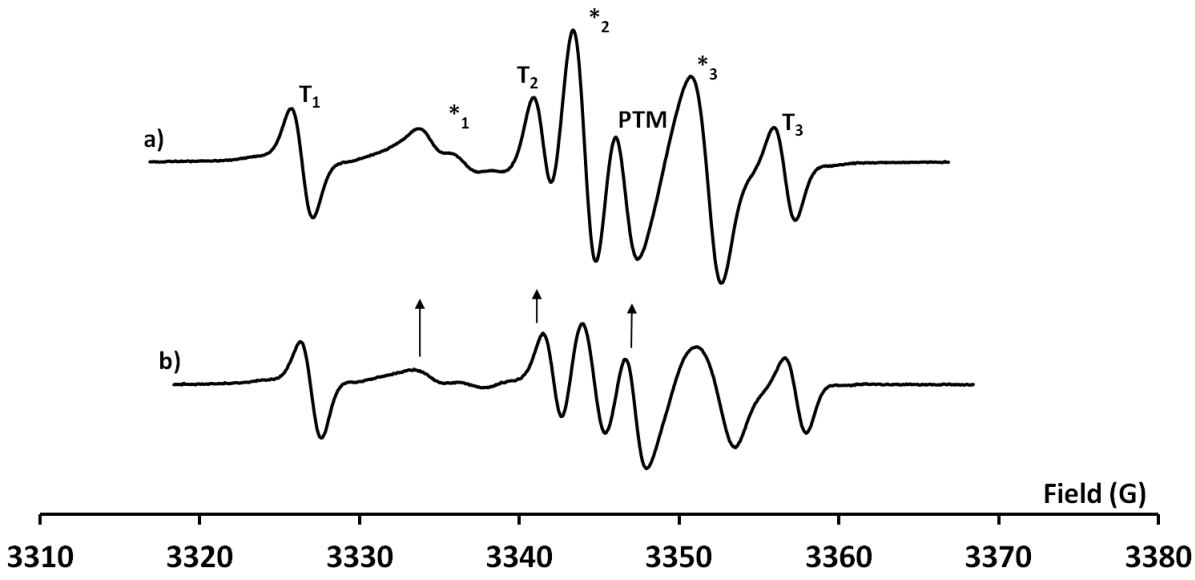

Figure 4.25: EPR spectrum of the PTMesterTEMPO diradical (**52**) in THF at different recovery temperatures a) 300 K b) b) 260 K.

The frozen spectra showed the superposition of a TEMPO and PTM moieties (**Figure 4.26**), and in this conditions it could be observed a very weak $|\Delta m_s|= 2$ transition at half field (**Figure 4.27**).

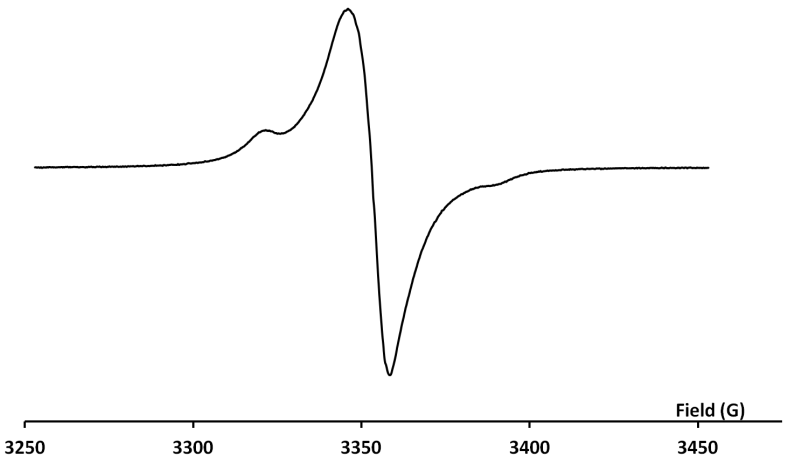

Figure 4.26: EPR spectrum of PTMesterTEMPO diradical (**52**) in DCM/toluene (1/1) at 130 K.

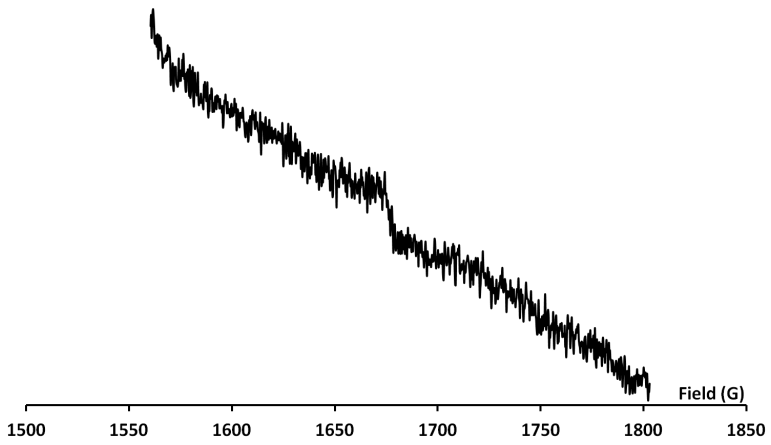

Figure 4.27: EPR spectrum of PTMesterTEMPO diradical (**52**) in DCM/toluene (1/1) at half field, at 130 K.

4.3.2.3 PTMamidoTEMPO diradical (54)

The synthesis of the PTMamidoTEMPO biradical (**52**) diradical involves the amidation reaction between the benzyl amino derivative of PTM **8** and 4-carboxymethylidene-2,2,6,6,-tetra methyl-1-piperidyloxyl (**38**) (**Scheme 4.13**). Once again, the molecule is not rigid and other conformations can show different distances between the radicals. The reaction, as in the previous case, was performed using DCC/DMAP. Thus, the mixture of DMAP, 4-carboxymethylidene-2,2,6,6,-tetramethyl-1-piperidyloxyl **38** and DCC was stirred in anhydrous DCM and then, the αH-PTM derivative **8** was added. The mixture, under Ar atmosphere, was stirred for 16 hours (**Scheme 4.13**). After chromatographic purification a orange pure product (Y: 89%) was isolated and characterized as the monoradical **53**, that contains the PTM subunit as αH form, by IR, MALDI-TOF and EPR.

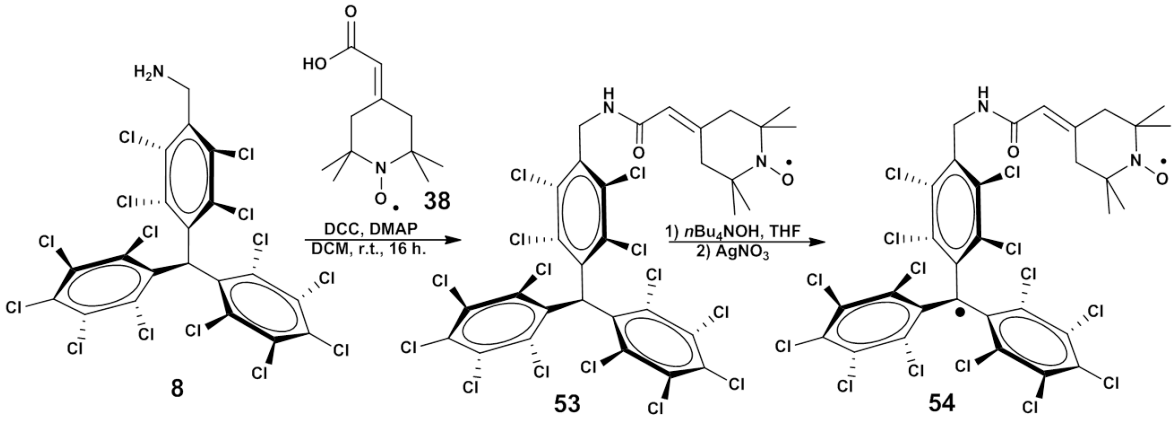

Scheme 4.13: Synthetic scheme for PTMamidoTEMPO diradical (**54**).

The formation of the diradical **54** from the monoradical **53** was tested *in situ*. The

use of Bu_4NOH in THF followed by $AgNO_3$ produced the EPR spectrum of **Figure 4.28a**) at 300 K in DCM/toluene (1:1). It shows the same pattern than in the ester case **52** and the same behaviour with temperature. Indeed, there are three lines corresponding to the TEMPO radical unit, (T_1, T_2 and T_3), a PTM line and another three lines (*1, *2 and *3). The values obtained from the simulation (**Figure 4.28b**) were: g_{TEMPO}: 2.0065; a_N: 15.2 G; and ΔH_{pp}: 0.9 G, g_{PTM}: 2.0041; ΔH_{pp}: 1.4 G, and the from the broader peaks, g: 2.0050, $a_{*1\text{-}*2}$=$a_{*2\text{-}*3}$: 7.7 G, ΔH_{pp}: 1.4 G. The three lines marked as *1, *2 and *3 follow the same pattern than in the ester case *i. e.* the "J= 200 G like spectrum" with three lines (from the coupling of the electron with the N of TEMPO unit, the PTM radical unit has not any nuclei to couple), with half of the value of the TEMPO hyperfine coupling, with an intermediate value of g (between TEMPO and PTM g values), with a linewidth like the PTM radical, and with the first line (*1) broader than the other two (*2 and *3). As in the PTMesterTEMPO, the simulation of the interaction spectrum (**Figure 4.28b**) was done in the $|J| \gg |a_N|$ condition as with our simulation software we cannot introduce the J value and hence the spectrum has three lines with the same intensity. Therefore, the final simulated spectrum is the sum of two simulated spectra: 1) the TEMPO spectrum (T_1, T_2 and T_3), and 2) the coupling of TEMPO with a second electron, from PTM subunit. As in the PTMesterTEMPO diradical (**52**), we performed the estimation with Avogadro software of the distance between the α carbon of PTM and the oxygen of TEMPO, obtaining, as in the ester biradical, a distance of 9.4 Å.

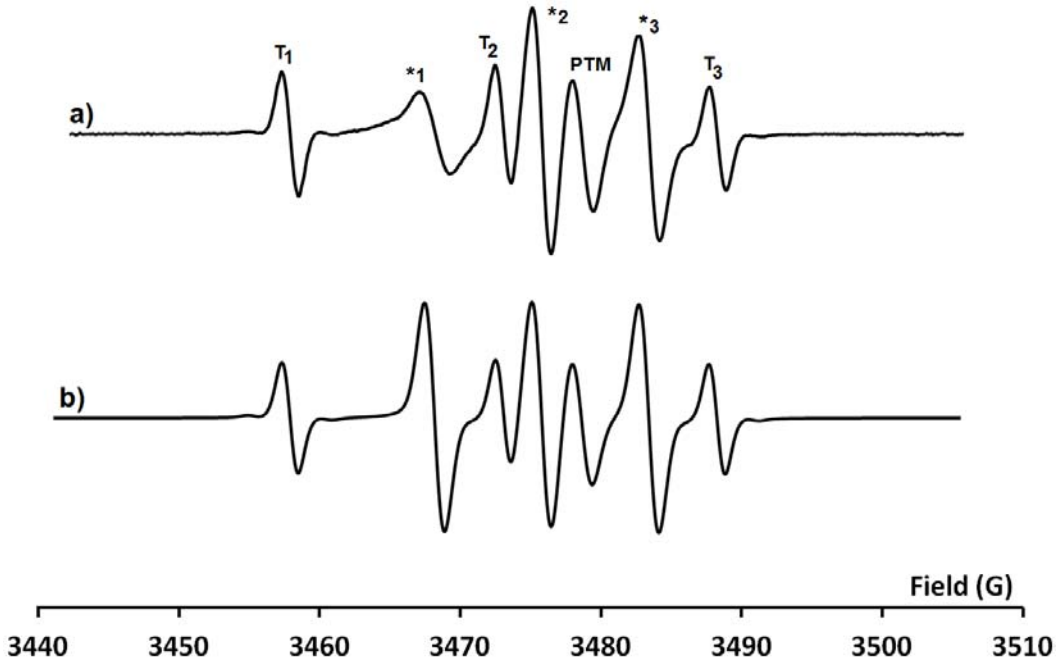

Figure 4.28: EPR spectrum of the PTMesterTEMPO diradical (**54**) in THF at 300 K: a) experimental and b) simulated. The simulated spectrum is the sum of two simulated spectra one corresponding to a conformer with $J \approx 0$ and another with $|J| \gg |a_N|$.

4.3.3 Heterodiradicals derived from BDPA and TEMPO

4.3.3.1 BDPA=TEMPO biradical (56)

The first heterobiradical derived from BDPA and TEMPO, obtained in this Thesis, the BDPA=TEMPO diradical (**56**), consists of a BDPA joined to TEMPO radical by a double bond. The synthesis was carried out using as starting materials the phosphonate derivative of αH-BDPA **32**, and the commercially available 4-oxo-TEMPO **36** (**Scheme 4.14**). Following the Wittig-Horner-Emmons methodology, the anion phosphonate derivative of BDPA unit, in anhydrous THF, that was generated with ^{t}BuOK at $-78\,^{\circ}$C, reacted whit the ketone derivative of TEMPO for 16 hours. After chromatografic purification, the monoradical **55** was isolated as a red powder which was purified and characterized by IR, MALDI-TOF and EPR (Y: 63%).

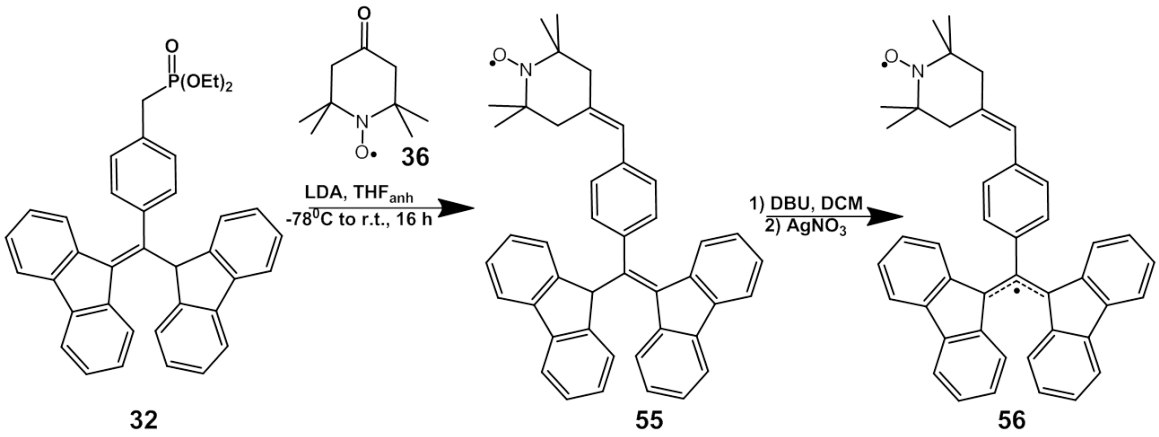

Scheme 4.14: Synthetic scheme for BDPA=TEMPO diradical (**56**).

After the final deprotonation and *in situ* oxidation, of the BDPA unit of monoradical **55** with DBU as a base followed by the treatment with $AgNO_3$ as an oxidant in DCM, the diradical **56** was obtained which was characterized by EPR. The EPR spectrum of this diradical (**Figure 4.29**) shows two different groups of lines, one group of three lines corresponding to the TEMPO radical unit (T_1, T_2 and T_3) at a g value of 2.0054 and with a_N: 14.8 G; $a_{^{13}C}$: 5.5 G; and ΔH_{pp}: 0.4 G, and another group corresponding to the BDPA radical moiety at a g value of 2.0020, and with a_H(4H): 1.92 G; a_H(4H): 1.91 G; a_H(4H): 0.41 G;a_H(4H): 0.37 G; and ΔH_{pp}: 0.5 G. Therefore, this spectrum indicates that exchange interaction between both radicals units is very weak or null, so it belongs to the biradical category as in the PTM=TEMPO **49** case, with $|J| \ll |a_N|$.

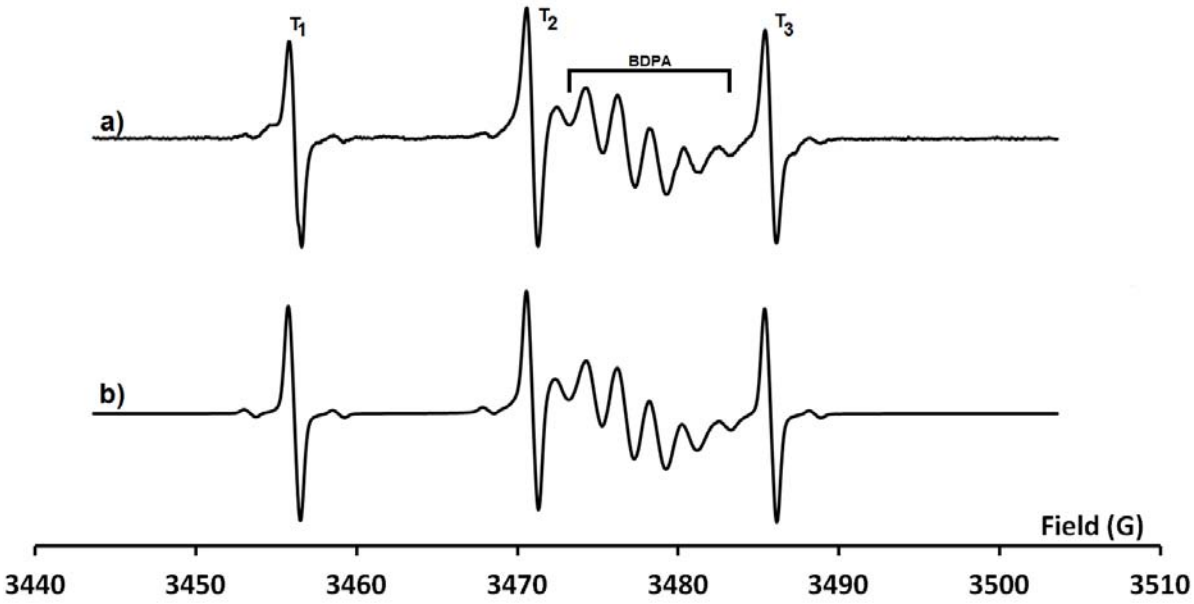

Figure 4.29: EPR spectrum of BDPA=TEMPO diradical (**56**) in DCM/benzene at 300 K. a) Experimental and b) simulated. The simulated spectrum is the sum of the spectra of two independent radical units of TEMPO and BDPA.

The frozen spectra showed the superposition of a TEMPO and BDPA moieties (**Figure 4.30**). The $|\Delta m_s|= 2$ transition at half field was not observed as the radical moieties do not interact magnetically. The Avogadro estimation of the distance between the carbon that joins the fluorenyl rings of BDPA in the biradical and the oxygen of TEMPO radical of 10.2 Å, that corresponds to the shortest (by bond) distance between these radicals without modifying their entities.

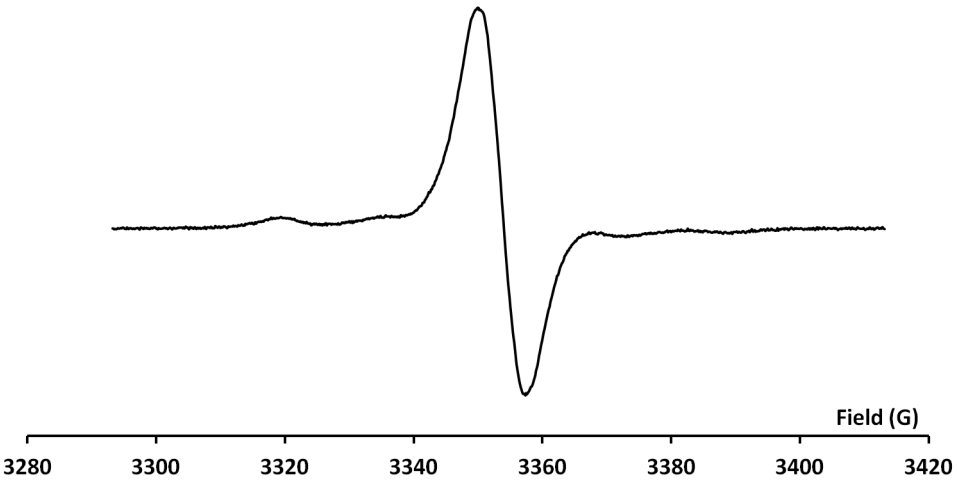

Figure 4.30: EPR spectrum of a frozen solution of BDPA=TEMPO diradical **56** in DCM/toluene (1/1) at 130 K.

4.3.3.2 BDPAesterTEMPO diradical (58)

The synthesis of the diradical BDPAesterTEMPO (**58**) involved the esterification reaction between the benzyl alcohol derivative of BDPA, BA-BDPA (**28**), and 4-carboxymethylidene-2,2,6,6,-tetramethyl-1-piperidyloxyl (**38**) (**Scheme 4.15**). The reaction, as in previous cases, was performed using the DCC/DMAP. Thus, the mixture of DMAP, 4-carboxymethylidene-2,2,6,6,-tetramethyl-1-piperidyloxyl (**38**) and DCC was stirred in anhydrous DCM and then the BDPA derivative **28** was added. They were stirred, under Ar atmosphere for 16 hours. After chromatographic purification the monoradical **57**, an orange pure product (Y: 46%), was isolated and was characterized by IR, MALDI-TOF and EPR.

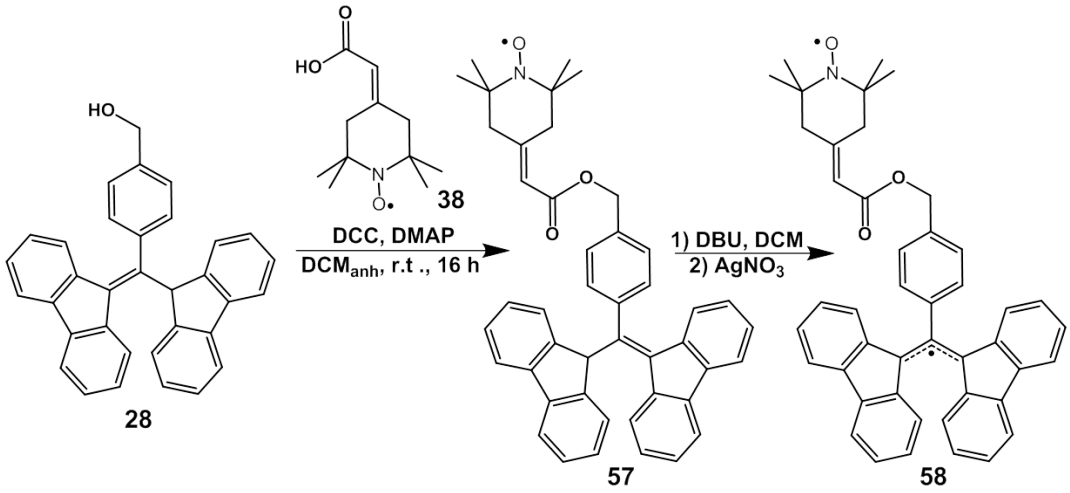

Scheme 4.15: Synthetic scheme for BDPAesterTEMPO diradical (**58**).

The treatment of monoradical **57** with DBU followed by $AgNO_3$ lead to the diradical **58**. The EPR spectrum of diradical **58** (**Figure 4.31a**) shows the same pattern than the PTMesterTEMPO diradical (**52**) and PTMamidoTEMPO diradical (**54**) but the contribution of BDPA is not clearly seen as far as its signal is at the same position of *2. Thus, there is a contribution from the TEMPO unit (three lines marked as T_1, T_2 and T_3 in **Figure 4.31a** at a g value 2.0065; with a_N: 15.1 G; $a_{^{13}C}$: 5.0 G; and ΔH_{pp}: 1.0 G) and another contribution of three broad lines marked as *1, *2 and *3. Such three lines apparently show a hyperfine coupling constant half a value of a TEMPO unit; *i. e* a_N of 7.74 G. However, there are two main differences with respect the spectra of diradicals **52** and **54**: i) the intensity of the three lines is the same and ii) the linewidth of each line is higher (ΔH_{pp}: 3.2 G). The first feature can be explained because in this diradical the interaction between both radicals is in the limit case where $|J| \gg |a_N|$, *i. e.* in the "J= 1000 G spectrum-like" of **Figure 4.3**. Thus, the $|J|$ value in this case is somewhat higher than in PTMesterTEMPO (**52**) and PTMamidoTEMPO (**54**). The reason why the linewidth is broader than in PTMesterTEMPO (**52**) and PTMamidoTEMPO (**54**) cases is because in this case BDPA has 16 hydrogen atoms

that the electron can couple with, and, as their hyperfine coupling constants are half of the value of a monoradical one, we loose resolution appearing the signal as a broader line. The data obtained from the simulation of this contribution (**Figure 4.31b**) shows the 1/2 a_H of BDPA and 1/2 a_N of TEMPO at an intermediated g value (g: 2.0049, a_H(4H): 1.0 G, a_H(4H): 0.92 G, a_H(4H): 0.23 G, a_H(4H): 0.36 G, a_N: 7.74 G, ΔH_{pp}: 0.4 G).

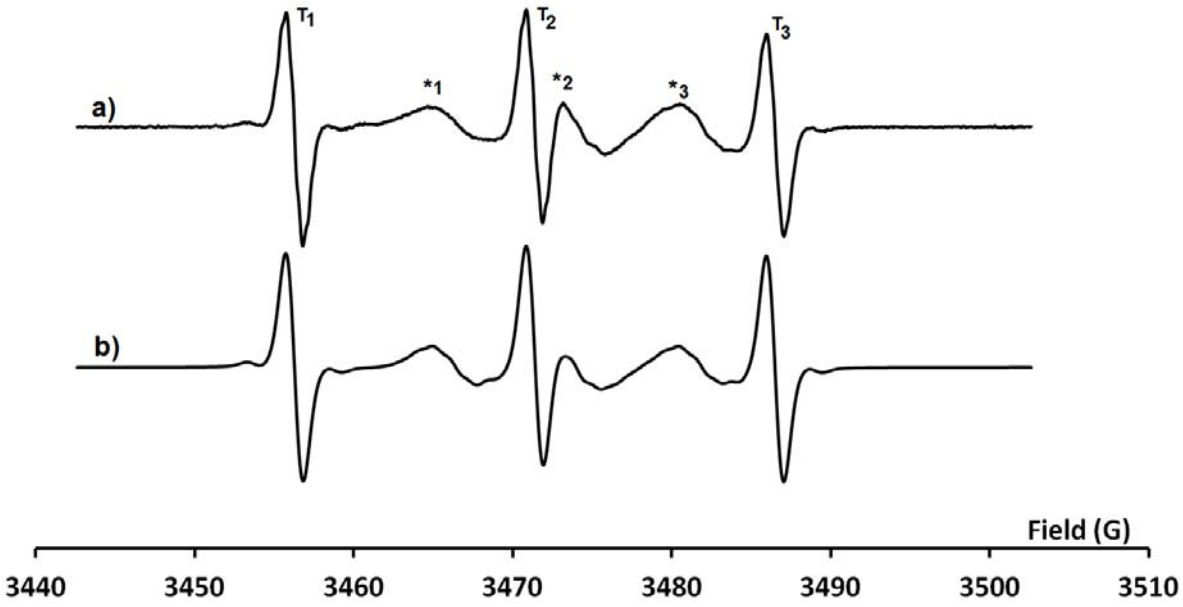

Figure 4.31: EPR spectrum of the BDPAesterTEMPO diradical (**58**) in THF/benzene at 300 K. a) Experimental and b) simulated.

The frozen spectrum, as in BDPA=TEMPO biradical (**56**), showed the superposition of a TEMPO and BDPA moieties spectra (**Figure 4.32**). However, the EPR spectrum at $|\Delta m_s|= 2$ showed a very weak transition which is in agreement with the weak interaction between radical moieties (**Figure 4.33**). The theoretical estimation of the distance between the carbon that joins the fluorenyl rings of BDPA in the biradical and the oxygen of TEMPO radical with Avogadro software was a distance of 13.9 Å.

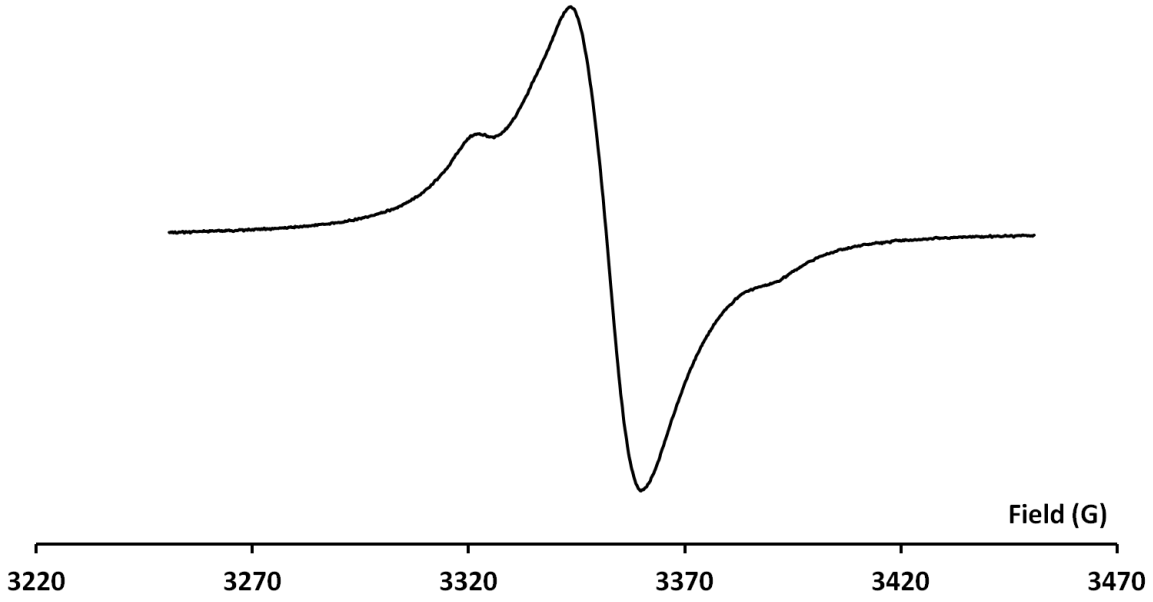

Figure 4.32: EPR spectrum of a frozen solution of BDPAesterTEMPO diradical **58** in DCM/toluene (1/1) at 130 K.

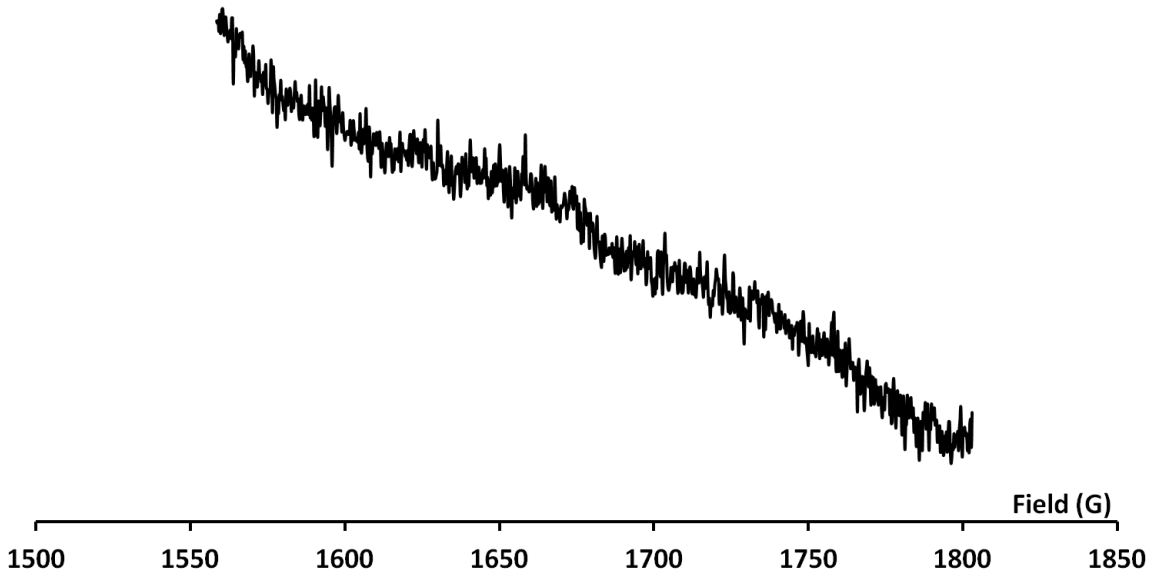

Figure 4.33: EPR spectrum of BDPAesterTEMPO diradical **58** in DCM/toluene (1/1) at 130 K, at half field.

4.3.3.3 BDPAamidoTEMPO diradical (60)

The synthesis of the diradical BDPAamidoTEMPO (**60**) involves the amidation reaction between the benzyl amino derivative of BDPA BAm-BDPA (**21**) and 4-carboxymethylidene-2,2,6,6,-tetramethyl-1-piperidyloxyl (**38**), (**Scheme 4.16**). The reaction,

as in previous cases, was performed using DCC/DMAP. The mixture of DMAP, 4-carboxymethylidene-2,2,6,6,-tetramethyl-1-piperidyl-oxyl and DCC was stirred in anhydrous DCM and then, the BDPA derivative was added stirring under Ar atmosphere for 16 hours. After a chromatographic purification a red product was isolated (Y: 89%) that was characterized by IR, MALDI-TOF and EPR. The final deprotonation of monoradical **59** and oxidation of the BDPA subunit (with DBU followed by $AgNO_3$), allowed the obtaining of diradical **60**.

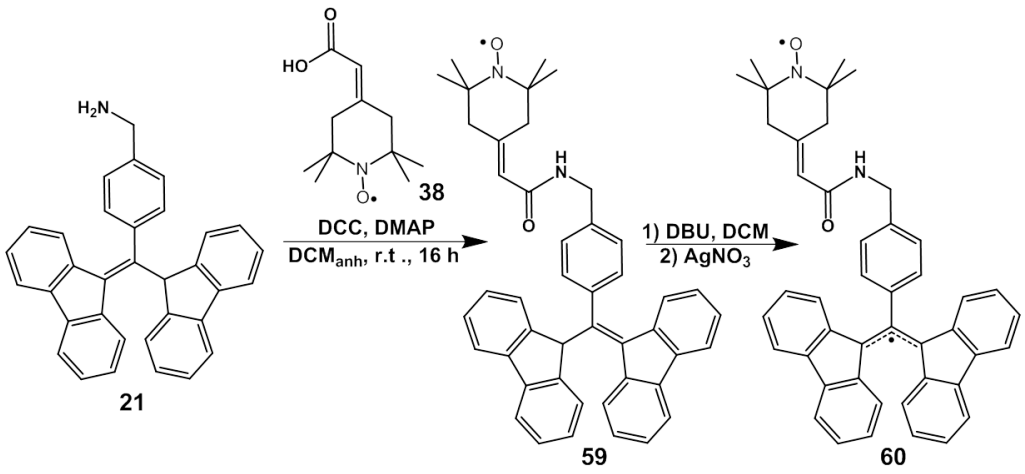

Scheme 4.16: Synthetic scheme for the BDPAamidoTEMPO diradical (**60**).

The EPR spectrum obtained for diradical **60** at 300 K has the same pattern than the one obtained for biradical **58**. Thus, it shows three lines marked as T_1, T_2 and T_3 in **Figure 4.34a**, at a g value 2.0065; with a_N: 15.46 G; $a_{^{13}C}$: 5.0 G; $a_{H_{(CH_3)}}$: 0.29 G; and ΔH_{pp}: 0.24 G from the TEMPO moiety and another three lines marked as *1, *2 and *3 in **Figure 4.34a**. The contribution of BDPA is not clearly seen as far as its signal is in the same g value of *2. As in the previous case, this spectrum consist also of three lines with a hyperfine coupling constant half the value of the TEMPO a_N (8.0 G) and with a total linewidth of 3.3 G. The three broad lines can be explained, as in the previous case, as $|J| \gg |a_N|$, *i. e.* as the "J= 1000 G spectrum-like" of **Figure 4.3**. The data obtained from the simulation (**Figure 4.34b**) shows the 1/2 a_H of BDPA and 1/2 a_N of TEMPO at an intermediate g value (g: 2.0049, a_H(4H): 1.0 G, a_H(4H): 0.9 G, a_H(4H): 0.0.4 G, a_H(4H): 0.2 G, a_N: 8.0 G, ΔH_{pp}: 0.5 G).

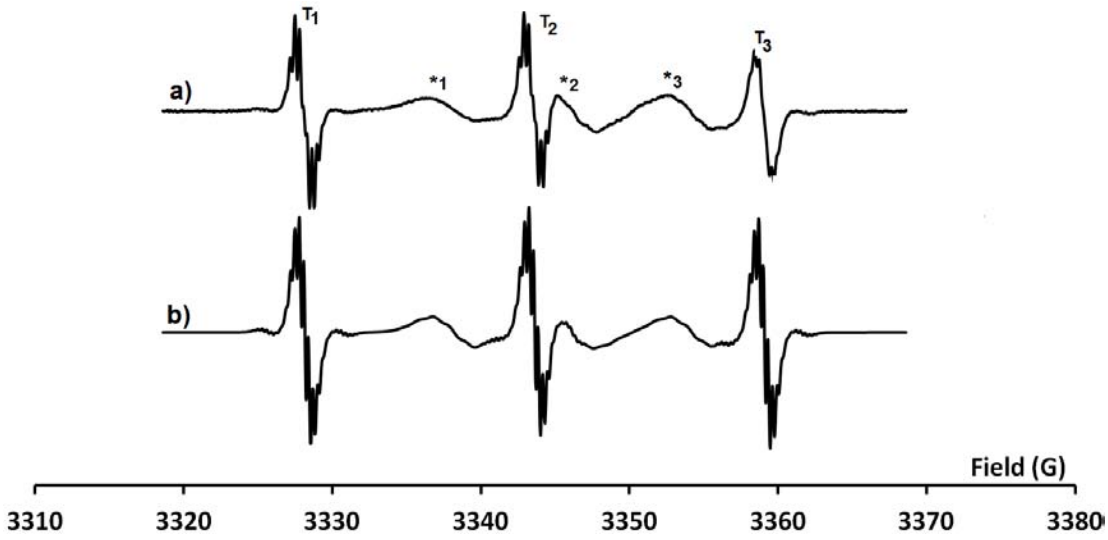

Figure 4.34: EPR spectrum of the BDPAamidoTEMPO diradical (**60**) in THF/benzene at 300 K. a) Experimental and b) simulated.

The frozen spectrum, as in BDPAesterTEMPO biradical (**58**), showed the superposition of a TEMPO and BDPA moieties spectra. The EPR spectrum at $|\Delta m_s|= 2$ as well showed a very weak transition which is in agreement with the weak interaction between radical moieties. The Avogadro theoretical calculation estimates a distance between the carbon that joins the fluorenyl rings of BDPA in the biradical and the oxygen of TEMPO radical of 11.9 Å.

4.4 Conclusions

A series of twelve bi and diradicals were synthesized and characterized. Five of them were homodiradicals and seven heterodiradicals. From their EPR study, we observed different degrees of exchange interactions between the two radical units in each diradical. In particular we can mention:

- Homodiradicals:

Diradical PTM=PTM (**40**) shows a high intramolecular exchange interaction.

Biradical BDPA=BDPA (**42**) behaves as two independent monoradicals that do not interact between them, thus, $|J| \ll |a_{\mathrm{H}}|$.

TEMPO based homodiradicals like TEMPO=TEMPO (**44**), TEMPOesterTEMPO (**45**) and TEMPOamidoTEMPO (**46**) show different distances between radicals and/or different rigidity which influence the exchange interactions. Thus, TEMPO=TEMPO diradical (**44**) shows $|J| \gg |a_{\mathrm{N}}|$ which is modulated decreasing the temperature while diradicals TEMPOesterTEMPO (**45**) and TEMPOamidoTEMPO (**46**) show analogous spectra characteristics with $|J| \approx |a_{\mathrm{N}}|$.

- Heterodiradicals:

The seven heterodiradicals obtained can be classified in three families: PTM-BDPA heterodiradical, PTM-TEMPO heterodiradicals, and BDPA-TEMPO heterodiradicals.

PTM=BDPA diradical **48** contains two carbon centered radicals. It shows high exchange interaction between radicals $|J| \gg |a_{\mathrm{H}}|$.

The PTM-TEMPO and BDPA-TEMPO families contain three diradicals each one with some similarities. Thus, the rigid biradicals PTM=TEMPO (**49**) and BDPA=TEMPO (**56**) behave as two independent monoradicals without interaction between them, thus, $|J| \ll |a_{\mathrm{H}}|$.However, the less rigid biradicals PTMesterTEMPO (**52**), PTMamidoTEMPO (**54**) and those of the BDPA family, BDPAesterTEMPO (**58**), and BDPAamidoTEMPO (**60**) show similar behaviors. There is the contribution of TEMPO and PTM moieties while the contribution of BDPA is not clearly seen. Moreover, three additional lines of high exchange interaction between radical units. In **52** and **54** $|J| > |a_{\mathrm{N}}|$ and in **58** and **60** the value of J is even higher: $|J| \gg |a_{\mathrm{N}}|$.

Bibliography

[1] Forrester A.R. *Organic Chemistry of stable Free Radicals*. Academic Press, London, **1968**.

[2] Catala L. and Turek P. *J. Chim. Phys.*, 96:p.1551, **1999**.

[3] Frank N.L., Clerac R., Sutter J.P., Daro N., Kahn O., Coulon C., Green M.T., Golhen S., and Ouahab L. *J. Am.Chem. Soc.*, 122:p.2053, **2000**.

[4] Ziessel R., Ulrich G., Lawson R.C., and Echegoyen L. *J. Mater. Chem.*, 9:p.1435, **1999**.

[5] Hamachi K., Matsuda K., Itoh T., and Iwamura H. *Bull. Chem. Soc. Jpn.*, 71:p.2937, **1998**.

[6] Kaim A., Pietrasik K., and Stoklosa T. *Eur. Polym.*, 46:p.519, **2010**.

[7] Yang Z.Y., Liu Y.P., Borbat P., Zweier J.L., Freed J.H., and Hubell W.L. *J. Am. Chem. Soc.*, 134:p.9950, **2012**.

[8] Roshchupkina G.I., Bobko A.A., Bratasz A., Reznikov V.A., Kuppusamy P., and Khramtsov V.V. *Free Radical Biol. Med.*, 45:p.312, **2008**.

[9] Rajca A., Mukherjee S., Pink M., and Rajca S. *J. Am. Chem. Soc.*, 128:p.13497, **2006**.

[10] Rajca A., Olankitwanit A., and Rajca S. *J. Am. Chem. Soc.*, 133:p.4750, **2011**.

[11] Forbes M.D.E., Dukes K.E., Avdievich N.I., Harbron E.J., and DeSimone J.M.J. *J.Phys.. Chem. A*, 110:p.1767, **2006**.

[12] IUPAC. *Compendium of Chemical Terminology, release 2.3.2; International Union of Pure and Applied Chemistry (IUPAC).* p.168, Wiley-Interscience, Research Triangle Park, NC, **2012**.

[13] IUPAC. *Compendium of Chemical Terminology, release 2.3.2; International Union of Pure and Applied Chemistry (IUPAC).* p.427, Wiley-Interscience, Research Triangle Park, NC, **2012**.

[14] Song C., Hu K.-N., Joo C.-G., Swager T.M., and Griffin R.G. *J. Am. Chem. Soc.*, 128:p.11385, **2006**.

[15] Lloveras V., Vidal-Gancedo J., DuarteT., Nierergarten J.-F., Novoa J.J., Ventosa N., Veciana J., and Rovira C. *J. Am. Chem. Soc.*, 15:p.5818, **2011**.

[16] Bonvoisin J., Launay J.-P., Rovira C., and Veciana J. *Angew. Chem. Int. Ed.*, 33:p.2106, **1994**.

[17] Coulaud E., Hagebaum-Reignier D., Siri D., Tordo P., and Ferré N. *Phys. Chem. Chem. Phys.*, 14:p.5504, **2012**.

[18] Borden W.T. *Diradicals.* Jonh Wiley & Sons, New York, **1982**.

[19] Kozaki M., Nakamura S., Sato K., Takui T., and Okada K. *Mol. Cryst. Liq. Cryst.*, 334:p.131, **1999**.

[20] Briere R., Dupeyre R.M., Lemaire H., Morat C., and Rassat A. *Bull. Chem. Soc. Fr.*, page p.3290, **1965**.

[21] Catala L., Turek P., Moigne J., Cian A., and Kyritsakas N. *Tetrahedron Lett.*, 41:p.1015, **2000**.

[22] Iwamura H. and Koga N. *Acc. Chem. Res.*, 26:p.346, **1993**.

[23] Izuoka A., Hiraishi M., Abe T., and Sugawara T. *J. Am.Chem. Soc.*, 122:p.3234, **2000**.

[24] Tanaka M., Matsuda K., Ioth T., and Iwamura H. *J. Am.Chem. Soc.*, 120:p.7168, **1998**.

[25] Liao Y., Lahti P., Weber R.T., and Barr D.P. *J. Org.Chem.*, 64:p.5176, **1999**.

[26] Shultz D.A. and Boal A.K. *Mol. Cryst. Liq. Cryst.*, 272:p.75, **1995**.

[27] Ishiguro K., Ozaki M., Sekine N., and Sawaki Y. *J. Am. Chem. Soc.*, 119:p.3625, **1997**.

[28] Ionita P., Whitwood A.C., and Gilbert B.C. *J. Chem. Soc. Perkin Trans.*, 2:p.1453, **2001**.

[29] Falle H.R. and Luckhurts G.R. *Mol. Phys.*, 11:p.49, **1966**.

[30] Zagdoun A., Casano G., Ouai O., Schwarzwälder M., Rossini A.J., Aussenac F., Yulikov M., Jeschke G., Copéret C., Lesage a., Tordo P., and Emsley L. *J. Am. Chem. Soc.*, 135:p.12790, **2013**.

[31] Macholl S., Jóhannesson H., and Ardenkjær-Larsen J.H. *Phys. Chem. Chem. Phys.*, 12:p.5804, **2010**.

[32] Muñoz-Gómez J.-L., Marín-Montesinos I., Lloveras V., Pons M., Vidal-Gancedo J., and Veciana J. *Org. Lett.*, 16:p.5402, **2014**.

[33] Dane E.L., Maly T., Debelouchina G.T., Griffin R. T., and Swager T.M. *Org. Lett.*, 11(9):p.1871, **2009**.

[34] Liu Y., Villamena F.A., Rockenbauer A., Song Y., and Zweier J.L. *J. Am. Chem. Soc.*, 135:p.2350, **2013**.

[35] Liu Y., Villamena F.A., Song Y., Sun J., Rockenbauer A., and Zweier J.L. *J. Org. Chem.*, 75:p.7796, **2010**.

[36] Kivelson D. *J. Che. Phys.*, 33:p.1094, **1960**.

[37] McLachlan A.D. *Proc. Roy. Soc. A*, 280:p.271, **1964**.

[38] Carrington A., Hudson A., and Luckhurst G.R. *Proc. Roy. Soc. A*, 284:p.582, **1965**.

[39] Carrington A. *Mol. Phys.*, 5:p.425, **1962**.

[40] Freed J.H. ahd Fraenkel G.K. *J. Chem. Phys.*, 41:p.699, **1964**.

[41] Bolton J.R., Carrington A., and Todd P.F. *Mol. Phys.*, 6:p.169, **1963**.

[42] Slichter C.P. *Phys. Rev.*, 99:p.479, **1955**.

[43] Ysacco C., Rizzato E., Virolleaud M.-A., Haroui H., Rockenbauer A., Le Moigne F., Siri D., Ouai O., Griffin R.R., and Tordo P. *Phys. Chem. Chem. Phys.*, 12:p.5841, **2010**.

[44] Molin J.N., Salikhov K.M., and Zamaraev K.I. *Spin Exchange*. Springer, Berlin, **1980**.

[45] Luckhurst G.R. *Mol. Phys.*, 30:p.543, **1966**.

[46] Parmon V.N. and Zhidomirov G.M. *Mol. Phys.*, 27:p.367, **1974**.

[47] McMurry J.E. *Chem. Rev.*, 89:p.1513, **1989**.

[48] Fitting R. *Liebigs Ann. Chem.*, 110:p.23, **1859**.

[49] Iwazaki K. *Process for producting organic compounds having nitroxide free radical.* US 6271382 B1, **2001**.

[50] Luckhurst G.R. *Molecular Physics*, 10(6):543, **1966**.

[51] Lemaire H. *J. Chem. Phys.*, 64:p.559, **1967**.

[52] Parmon V.N., Kokorin I., Zhidomirov G.M., and Zamaraev K.I. *Molecular Physics*, 26(6):p.1565, **1973**.

[53] Weil J.A., Bolton J.R., and Wertz J.E. *Electron Paramagnetic Resonance.* Jonh Wiley & sons, Canada, **1994**.

[54] Frank Neese. *Calculation of NMR and EPR Parameters. Theory and Applications.* Wiley-VCH, Weinheim, **2004**.

[55] Eaton S.S., More M.M., Sawant B.M., and Eaton G.R. *J. Am. Chem. Soc.*, 105:p.6560, **1983**.

[56] Akita T. and Kobayashi K. *Tetrahedron*, 52(20):p.6893, **1996**.

[57] Dane E.L., Corzilius B., Rizzato E., Stocker P., Maly T., Smith A.A., Griffin R.G., Ouai O., Tordo P., and Swager T.M. *J. Org. Chem.*, 77:p.1789, **2012**.

[58] Rodríguez González S., Nieto-Ortega B., González Cano R.C., Lloveras V., Novoa J.J., Mota F., Vidal-Gancedo J., Rovira C., Veciana J., Corro E., Taravillo M., Baonza V.G., López Navarrete J.T., and Casado J. *J. Chem. Phys.*, 140:p.164903, **2014**.

Chapter 5

Dynamic Nuclear Polarization

5.1 Introduction

Over the past few decades, many techniques for studying molecular structures have been developed such as X-ray crystallography[1] or nuclear magnetic resonance Spectroscopy (NMS).[2] In particular, Nuclear Magnetic Resonance (NMR), is an important analytical technique that has achieved a widespread use for the identification and characterization of molecules of interest in chemistry and biochemistry. Moreover, magnetic resonance imaging (MRI), based on NMR phenomena, is one of the best non invasive clinical imaging methods used nowadays in medicine.[3]

One of the main limitation of NMR is its intrinsic low sensitivity. The NMR signal is proportional to the nuclear polarization, P, which is governed by the Boltzmann distribution (**Equation 5.1**) of nuclear spins at the Zeeman energy levels[4] which provides a very small population difference between different spin states (N $\downarrow$ and N $\uparrow$) at room temperature and with achievable magnetic fields.

$$\frac{\mathrm{N}\uparrow}{\mathrm{N}\downarrow} = e^{-\Delta E/\kappa \mathrm{T}} \tag{5.1}$$

where ΔE is the energy difference between the two states, κ is the Boltzmann constant and T is the temperature in Kelvin.

In order to overcome this intrinsic limitation some instrumental improvements have appeared in the last few decades, such as the development of cryogenically cooled probes[5] and the availability of superconducting magnets that yields higher magnetic fields.[6] Moreover, several methods to enhance the nuclear polarization have been also developed which are in constant expansion. Among them the most extended ones are optical pumping,[7,8] the *para*-hydrogen induced polarization (PHIP) and the dynamic nuclear polarization (DNP).[9,10] All these methods create a hyperpolarization in nuclear spin systems. In a hyperpolarized spin system the normal distribution of populations has been disturbed creating an excess of populations in one of the energetic levels, thus

boosting the net magnetization of the system. Dynamic nuclear polarization (DNP) has emerged as one of the most general and effective methods for nuclear hyperpolarization consisting in a process by which the high spin Boltzmann polarization, typically derived from a bath of free radical electrons presented in the sample, is transferred to a nuclear spins bath to the sample to be hyperpolarized. As a result, the population difference between the nuclear energy levels of the nuclei of interest is enhanced (**Figure 5.1**). This process takes place by microwave irradiation of the sample at low temperature, at the electron paramagnetic resonance (EPR) frequency of the free radical, producing a dramatic enhanced NMR signal which improve its sensitivity.

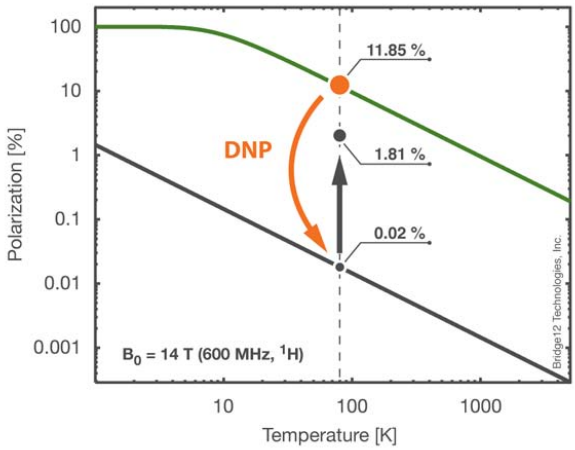

Figure 5.1: Temperature dependence of the electron (green) and nuclear spin (black) reservoir polarization at a given external field strength of 14 T, corresponding to a ^{1}H nuclear Larmor frequency of 600 MHz. Image adapted from web site: www.bridge12.com/learn/dynamic-nuclear-polarization-dnp-nmr.

In the last decades it has been developed a new methodology, named fast dissolution DNP, for obtaining strongly polarized nuclear spins in solution.[11] This method uses a low temperature and a high magnetic field to strongly polarize nuclear spins in solid state, normally from a frozen solution. After that, the solid samples are subsequently dissolved rapidly in a suitable hot solvent to create a solution of molecules with hyperpolarized nuclear spins. The resulting hyperpolarized liquid sample is then transferred to a high resolution NMR spectrometer, where the enhanced NMR signal can be acquired, or may be used as an agent for *in vivo* magnetic resonance imaging (MRI). The production of hyperpolarized molecular imaging agents has sparked a great enthusiasm in the MRI community due to its potential application as a clinically viable method for assessing *in vivo* metabolites enabling to generate maps of some hyperpolarized metabolites inside the body.[12]

Generally, ^{13}C nuclei directly attached protons are not feasible candidates for dissolution-DNP due to its short relaxation time (T_1). Most ^{13}C DNP substrates studied use to

have carbonyl moieties, including carboxylic acids, ketones, esters, and amides. Among compounds with carbonyl group, the carboxylic acids are very attractive because they are: 1) abundant endogenous molecules, 2) typically water-soluble, 3) often amenable to ^{13}C enrichment, 4) have longer T_1's, and (5) are involved directly in or positioned near sites of biochemical routes modifications. The last feature is critical, as most hyperpolarized magnetic resonance (HP MR) strategies rely on chemical shift to observe *in vitro* and *in vivo* reactions. The most popular molecule to date for hyperpolarization studies is [1-^{13}C]pyru-vic acid, although other common metabolites are also under study,[15,16] such as [1,4-^{13}C]diethyl-succinate or [1-^{13}C]fumarate, to study of tricarboxylic acid (TCA) cycle and its metabolite products. The dicarbonyl structure of pyruvic acid (seen in other DNP substrates, e.g., dehydroascorbic acid or benzoylformic acid) has a carboxylic acid at the 1-position and a ketone at the 2-position, and both sites can be easily ^{13}C-enriched for metabolic studies. Moreover, [1-^{13}C] pyruvate has a long T_1 at clinically relevant field strengths (60 s at 3 T).

Hyperpolarazing (HP) ^{13}C agents can be divided into three categories according their discrete utilities: 1) endogenous molecules, modified only by an ^{13}C or ^{2}H enrichment, 2) environmental sensors, and 3) molecules that interrogate and expand the reach of DNP-NMR, as an imaging technique. HP [1-^{13}C] pyruvate and [1,4-$^{13}C_2$] fumarate are examples of probes in the first category, used to follow basic biochemical routes with many potential applications in oncologic imaging.[12] For this set of HP agents, the principal question is what the data reveals about flux through metabolic pathways, and how this information might help us better understand and treat diseases. The second category of DNP agents may be non-endogenous and include [2-^{13}C] benzoylformic acid and [^{13}C,D_3]-*p*-anisidine, used to detect reactive oxygen species, ^{13}C HCO_3^- used to interrogate pH and salicylic acid, to detect hydrophobic binding *in vitro*.[13] These agents may also be applied to biological studies, but the emphasis here is detecting chemical environment, usually by a reaction based mechanism. The third category of DNP ^{13}C probes includes those that are critical in advance and understanding of DNP-NMR technology. For example, [2,3-$^{13}C_2$] diacetyl has been used to study spin polarization in the singlet state, allowing retention of a HP signal beyond that dictated by T_1.[14]

Since the enhanced NMR signal is created in solid state and at different magnetic field, B_0, it cannot be regenerated once the molecular probe has been dissolved and will disappear according with the liquid state longitudinal relaxation time (T_1). This time dependence limits and governs the selection of molecular probes. So, T_1 needs to be long enough for the survival of the signal along the handling time of the sample. Long liquid state T_1 values have been found for ^{13}C carbons in small molecules that have no direct attached protons, *i. e.* carbonyl, carboxyl and certain quaternary carbons. Moreover, all the hyperpolarized dissolutions show a significant reduction in T_1 related to those samples which do not contain the paramagnetic compound used to achieve the hyperpolarization. Therefore, the possibility of eliminating the paramagnetic species in

the transfer process would be useful. This is specially important in biological samples not only for avoiding the presence in the injected sample but also for the longer retention of the polarization.

Implementation of DNP experiments requires that high frequency microwave instrumentation and probes are interfaced to conventional NMR spectrometers. Glassy solvents, particularly those that form a glass regardless of the cooling rate, are required to ensure an homogeneous dispersion of the polarizing agent into the frozen solid solution. In addition, successful DNP experiments require non perturbing paramagnetic polarization agents that could be added to the sample. The design and synthesis of new radicals and biradicals has been the main subject of **Chapters 3** and **4** of this Thesis. In the present Chapter we will describe the DNP experiments developed in order to evaluate the viability of those radicals and biradicals as polarizing agents for DNP.

From the point of view of the paramagnetic species, there are three main spectroscopic parameters that have to be taken into account in order to choose one or other paramagnetic species to polarize a specific nucleus:

- Homogeneous electron paramagnetic resonance linewidth (δ) can be defined as base-to-base distance of the EPR lineshape. The narrowest linewidth are found for C-centered radicals, such as trityl radicals or BDPA derivatives. On the other side, nitroxides show the broadest linewidth due to the large coupling constant between the electron and the nitrogen nuclei (**Figure 5.2**).[17]

- Spectral breadth (Δ), which will be determined by the homogeneous and the inhomogeneous breadths depending on the presence of fluctuations. The homogeneous broadened system can be fitted by a Lorentzian function, while the inhomogeneous can be fitted by a Gausian one.

- Larmor frequency of the paramagnetic species (ω_S), which is the frequency at which the EPR tansition takes place.

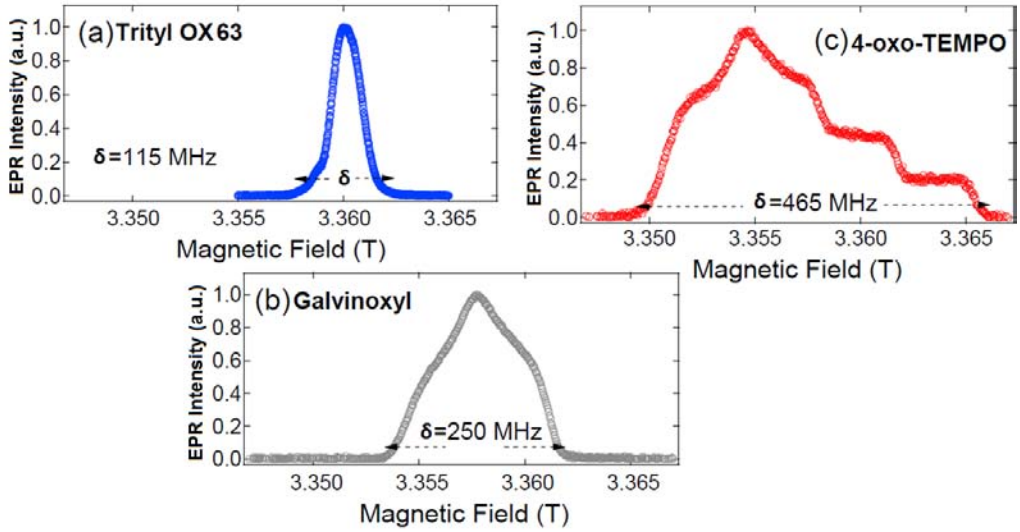

Figure 5.2: W EPR band spectra of a) trityl OX63 (**61**) [15 mM in 1:1 glycerol:water], b) galvinoxyl [40 mM in 1:1 ethyl acetate:chloroform], and c) 4-oxo-TEMPO [15 mM in 1:1 glycerol:water] at 100 K.[17]

In addition of these spectroscopic parameters of the paramagnetic species, it is also necessary to take into account the characteristics of the target nucleus to be polarized. In this sense, the Larmor frequency of the nuclei of interest (ω_{0I}) and its gyromagnetic factor (γ_I) are two of the most important parameters to take into account.

The efficiency of a DNP experiment is defined by the enhancement ratio (ε), that relates the signal obtained for a nucleus with and without a DNP experiment. The maximum theoretical enhancement is given by the ratio of the giromagnetic factors, γ_S/γ_I, of the electron and the nucleus, respectively. The experimental enhancement (**Equation 5.2**) is determined by the ratio of NMR signal integrals of the hyperpolarized sample solution ($I_{Hp.}$) and the thermal one ($I_{Th.}$). As it is necessary to perform more than one scan in the thermal case to obtain a good signal-to-noise relation, the expression must be multiplied by the square root of the number of scans (N) performed in the thermal experiment.

$$\varepsilon = \frac{I_{\text{Hp.}}}{I_{\text{Th.}}}\sqrt{N} \tag{5.2}$$

Depending on the experimental conditions, the DNP of nuclear spin in solid state can occur through three different mechanisms, known as: a) Solid effect (SE), b) Cross effect (CE) and/or c) Thermal mixing (TM):

Solid effect (**SE**) is a two spin process (**Figure 5.3**) that governs the polarization process that occurs when $\omega_{0I} > \Delta, \delta$. This process requires radicals with narrow EPR linewidths such as trityl or BDPA radicals. The frequency dependence of the enhancement profile for those radicals shows a minimum and maximum when the irra-

diation frequency is $\omega_{0S} \pm \omega_{0I}$, leading a zero-quantum or double-quantum transitions, where forbidden electron-nuclear flip-flops are excited leading to a negative or positive enhancement. Since the solid effect mechanism involves forbidden transitions, the enhancements scale as ω_0^{-2} and are, therefore, attenuated at high magnetic fields. [18]

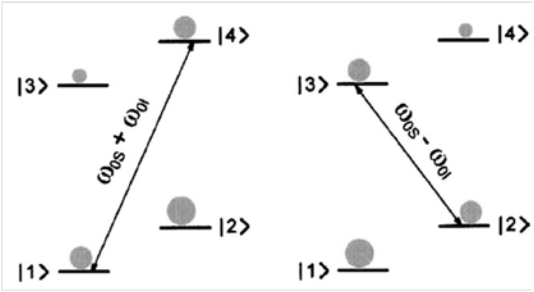

Figure 5.3: Saturation of the forbidden zero-quantum (left) and double-quantum transitions (right) leads to negative and positive enhancements through the SE. [19]

Cross-effect (**CE**) is a three-spin process (**Figure 5.4**) operative for diradicals as HP agents. It requires that the inhomogeneous breadth (Δ) of the EPR spectrum has to be larger than the nuclear Larmor frequency ω_{0I} ($\Delta > \omega_{0I}$) and the homogeneous width must satisfy the condition $\delta < \omega_{0I}$. To accomplish this condition there are two molecular orientations, resulting in two effective EPR resonance frequencies, separated by the correct frequency. The mechanism has been shown to yield high efficient transfer at high-fields. It relies on the fact that the resonance frequencies of two electrons, ω_{0S1} and ω_{0S2}, in the EPR spectrum satisfy the condition ω_{0S1} - $\omega_{0S2} = \omega_{0I}$ and as such the enhancements scale as ω_0^{-1}. Furthermore, it works well with a set of radicals. Assuming that dipole-dipole couplings exist among the two electrons and the nucleus, THz irradiation near either ω_{0S1} or ω_{0S2} flips one of the electrons up, and then there is a subsequent three spin cross relaxation process with the energy difference between the two electron spins going into polarizing the nuclear spin. The efficiency of CE depends on two spatial factors, the distance between the two electron spins, which determines the electron-electron dipolar coupling and the relative orientation of the two radicals, which determines, *via* the *g*-anisotropy tensor, the frequency separation ω_{0S1} - ω_{0S2}.

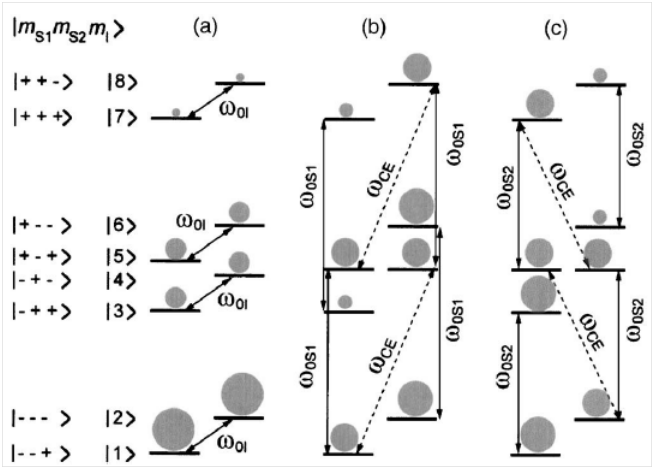

Figure 5.4: Population distribution at thermal equilibrium for a general spin system (a). Saturation of the allowed EPR transitions for one of the dipolar coupled electrons (ω_{0S1}) leads to negative enhancement (b). Saturation of the transition corresponding to the second electron (ω_{0S2}) leads to positive enhancement (c).[19]

Thermal mixing (**TM**) involves an homogeneously broadened EPR linewidth arising from multiple dipolar coupled electrons. In the TM mechanism, the condition $\delta > \omega_{0I}$ must be satisfied. This condition implies that at high magnetic fields the concentration of the polarizing agent must be high. TM effect is usually treated from a thermodynamic point of view, based on the concept of spin temperature. The electron-nuclear spin system can be described as a set of three interacting baths, each one characterized by a spin temperature: the electron Zeeman system (EZS), the electron dipolar system (EDS) and the nuclear Zeeman system (NZS). Off resonance irradiation of the allowed EPR transition results in a large polarization gradient across the EPR linewidth, which is equivalent to cooling the EDS. This bath is in thermal contact with the NZS, which is also cooled in an energy-conserving three spin electron-electron-nuclear exchange process, leading to an DNP enhancement. The TM mechanism can be direct (the enhancement is caused by the direct coupling between the NZS and the EDS) or indirect, when both allowed and forbidden transitions are included. However, compared to CE, the TM effect is less efficient and results in a smaller enhancements.

Finally is worth to mention that the largest signal enhancements observed in experiments are those when the thermal mixing or cross-effect mechanisms are operative.

5.2 Fast dissolution-DNP experiments

From a practical point of view it is important to describe here a typical DNP experiment with a radical which requires to perform a few different steps that are summarized as follows:

- Sample preparation. To perform a DNP experiment it is necessary an accurate preparation of the sample and in this sense some variables have to be taken into account. In a first place, if the analyte to polarize is liquid, the miscibility with the paramagnetic radical has to be tested. Moreover, if they are miscible, they have to form a glassy solid solution at low temperature (1.4 K). This is the most suitable sample but when the analyte is solid or it is not miscible with the paramagnetic radical, an extra compound called glassing agent must be added. The glassing agent must solubilize both the analyte and paramagnetic radical and it must form also a glassy solid solution at low temperatures.

- Determination of the optimal frequency of irradiation. The prepared sample is introduced inside the DNP equipment and frozen to around 1.4 K. After that, it is irradiated at different frequencies and the nuclear spin polarization is recorded as a function of the pumping microwave frequency (ω_m), **Figure 5.5** to obtain the so-called ^{13}C microwave DNP spectrum. Finally the frequency obtained taken to hyperpolarize the ^{13}C nuclei.

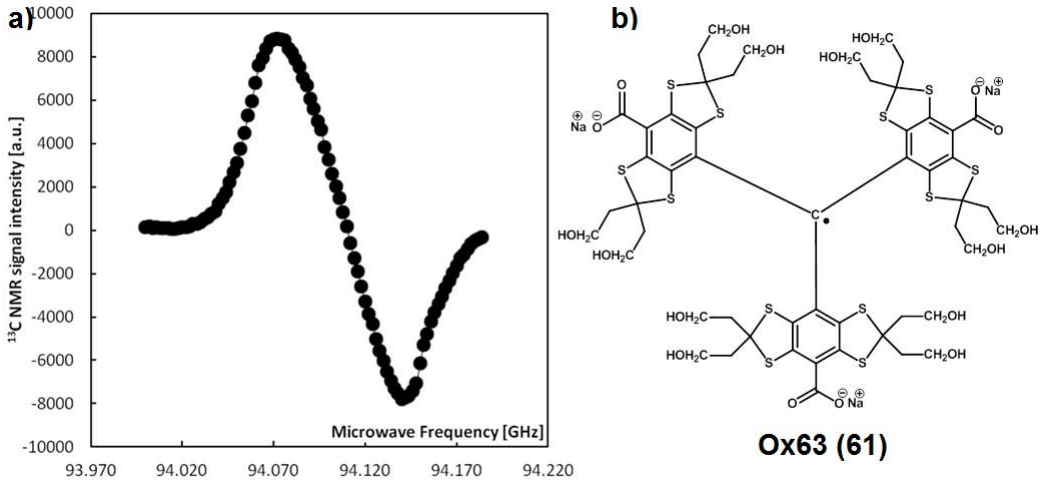

Figure 5.5: a) Typical result of the nuclear spin polarization as a function of the pumping microwave frequency (ω_m) for [1-^{13}C]pyruvic acid doped with 15 mM of OX63 (**61**) radical at 3.35 T and 1.4 K b) Chemical structure of OX63 radical (**61**).

- Determination of the optimal concentration. Once the optimal frequency of irradiation is determined, aliquotes of the same volume and with different radical concentrations are polarized to find the optimal concentration. The polarization

build-up curves are then recorded. The optimal concentartion is that providing a larger saturation value in the shortest time. **Figure 5.6**.

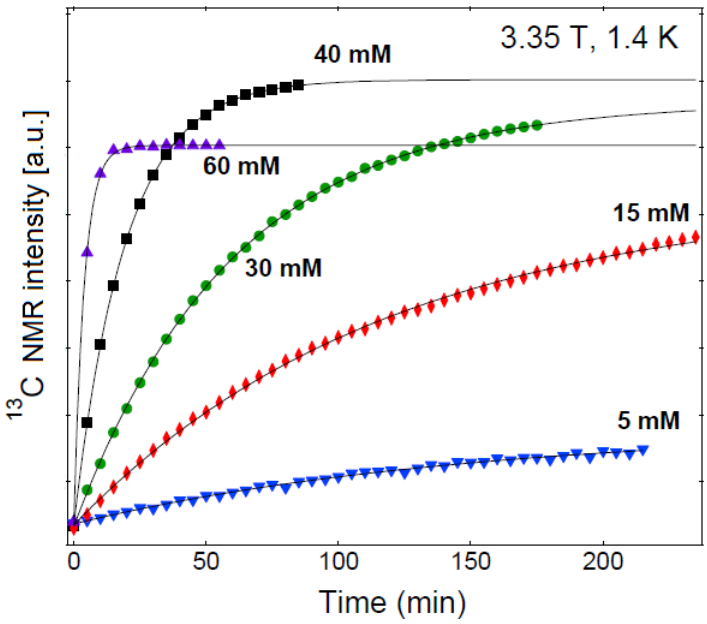

Figure 5.6: ^{13}C polarizarion build-up curve of BDPA radical **10** at different concentrations. All the polarized samples have the same sample volume.[20]

- Fast dissolution (for fast dissolution experiments). In this step, the hyperpolarized solid samples, at around 1.4 K, are dissolved in a suitable hot solvent and transferred to the NMR spectrometer in a very short time, in order to avoid the lost of polarization of the molecule by the longitudinal relaxation time T_1. In this step are important both the solvent which dissolves the analyte and the transference time.

- Data acquisition. The last step can be performed with different pulse sequences in order to obtain different information. On one hand, to determine the enhancement (ε) ratio the NMR pulse is usually 90^0 (**Figure 5.7a**), and all the information is recorded in one scan. On the other hand, if the longitudinal relaxation time (T_1) is the information required, a sequence of scans with smaller angle has to be performed (**Figure 5.7b** and **c**).

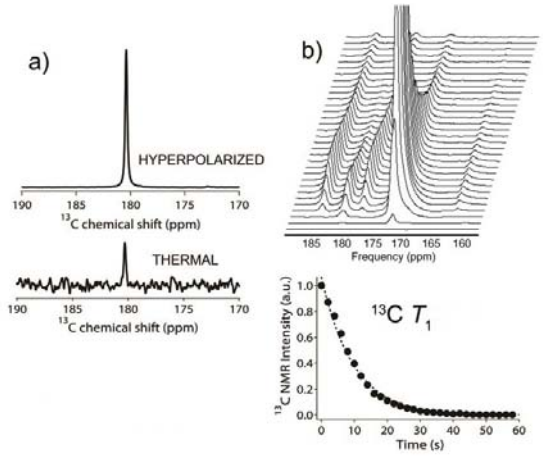

Figure 5.7: a) Top: ^{13}C hyperpolarized spectrum with 1 scan at θ= 90^0. Bottom: thermal equilibrium spectrum of the same sample with 32 scans at θ= 30^0 b) TOP: Stacked plot of spectra from a dynamic study in which spectra were acquired every 1 s. Bottom: Plot of the signal decay with time.

Considerable efforts have been deployed to reduce the polarization losses during sample transfer prior to infusion. This is of particular interest in the context of *in vivo* metabolic imaging where more than 60 s may be required between the dissolution and the injection. To limit the loss of polarization, the use of radical scavengers,[21] the storage of hyperpolarized longitudinal polarization in the form of long lived states (LLS)[22] or the elimination of the paramagnetic compound has been the most successful approach.[20] Whatever method is chosen for extending the live times of hyperpolarization, in many cases the mere presence of proton spins in the molecule may impose a severe erosion of the hyperpolarized sample. Nuclear spin-lattice relaxation driven by intramolecular dipolar interaction, in particular between an hyperpolarized ^{13}C spin and ^{1}H spins, even when they are at two or more bonds of distance, may offer efficient relaxation pathways.

5.2.1 Fast dissolution Dynamic Nuclear Polarization of mono-radicals

The Hypersense DNP equipment is commercially available from Oxford Instruments and can provide DNP polarization of different nuclei samples. It is a highly complex instrument, which requires routine checks and attention to detail.

An Hypersense equipment is built on a modified 3.35 T vertical bore Oxford magnet. It has a 94 GHz, 100 mW controllable power microwave source. Inside the bore of the magnet there is a cryogenic chamber (VTI, variable temperature insert) that contains the sample during the polarization process which is maintained at 1.4 K using a mixture of vacuum cooling and a liquid helium bath.

All the fast dissolution experiments performed in this Thesis were carried out with

this equipment in collaboration with the "Servei de Ressonància Magnètica" (SeRMN) of UAB and Dr Teo Parella with the technical support of Dr. Eva Monteagudo or in Parc Cientific of UB with the technical support of Dr. Ildefonso Marin and Prof. Miquel Pons. Concerning the DNP experiments performed at the UAB, due the possibility of performing DNP-MRI experiments, the polarizations were performed with [1-^{13}C]pyruvic acid as a target of polarization that is liquid at room temperature. Additionally, it generates a glass working temperature of 1.4 K, so if the paramagnetic radical is soluble in it, it is possible to perform experiments without extra glassy agents. On the other hand, in the experiments performed at the Parc Cientific of UB the target of polarization was [2-^{13}C]acetone.

5.2.1.1 BDPA-CN (20) radical

Due to the insolubility of the BDPA-CN radical **20** in neat [1-^{13}C]pyruvic acid, the samples were prepared as is described in the literature[20] for the commercially available BDPA (**10**) radical using sulfolane as a cosolvent. Thus, the radical was completely dissolved in sulfolane and, once it was dissolved, the same amount of [1-^{13}C]pyruvic acid was added. 3.54 mg of BDPA-CN radical **20** were dissolved in 100 μl of sulfolane and once the radical was completely dissolved, 100 μl of [1-^{13}C]pyruvic acid were added, obtaining a final 40 mM concentration of the radical in the mixture.

The microwave spectrum was acquired with 100 μl of the previously prepared solution which was frozen at 1.4 K at the pressure of 3 mbar. The frequency was scanned from 93.950 GHz to 94.250 GHz with steps of 5 MHz during 300 s in each step in order to obtain the microwave spectrum and determine the polarization peaks, and the optimum frequency of irradiation for the DNP experiments. It can be seen (**Figure 5.8a**) from the microwave spectrum that the positive polarization peak is located at 94.080 GHz and the negative one at 94.120 GHz. The frequency of work was determined as the positive peak polarization, P(+) = 94.080 GHz; the separation between the polarization peaks (|P(+) - P(-)|= 94080 - 94120) was of 40 MHz. This value is close to that of the non functionalized BDPA (50 MHz).[23] So this radical fulfill the requirements to polarize ^{13}C nuclei by the thermal mixing mechanism, as commercial BDPA does.[20]

The polarization build-up curve (**Figure 5.8b**) was performed with a 30 μl aliquote of the frozen sample irradiating at the optimal frequency of 94.080 GHz. The sample was introduced in the DNP equipment, and before the acquisition started, the sample remained inside the helium cavity until the pressure and the temperature became stable at 3.2 mbar and 1.4 K. Data were acquired every 1 minute and the total time of polarization, until saturation, was 90 minutes.

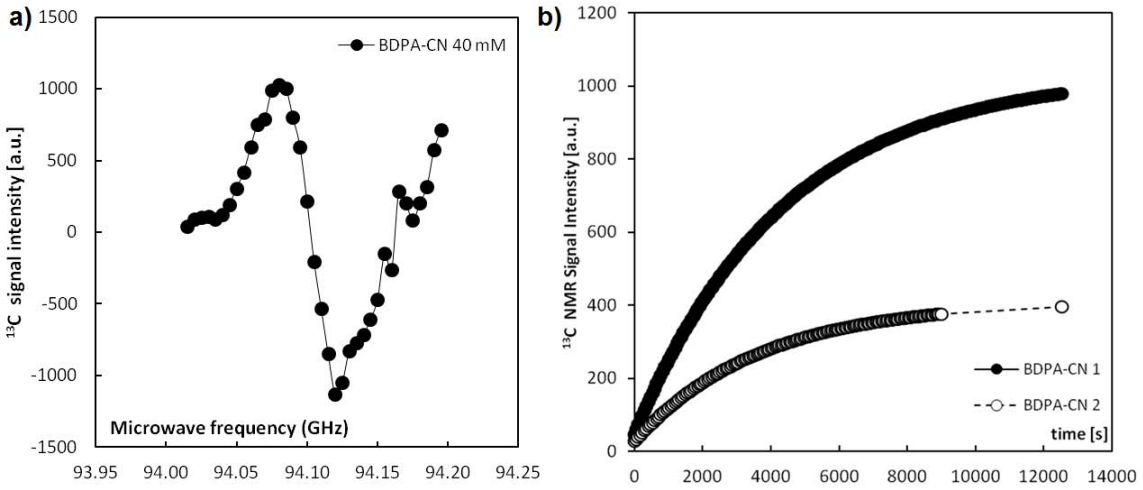

Figure 5.8: a) ^{13}C microwave spectrum of 100 μl of a 1:1 (v/v) [1-^{13}C]pyruvic acid:sulfolane doped with 40 mM BDPA-CN **20** at 3.35 T and 1.4 K. b)^{13}C polarization build-up curves of 30 μl 1:1 (v/v) [1-^{13}C]pyruvic acid:sulfolane doped with 40 mM BDPA-CN **20**, freshly prepared (black circles) and after been stored for 2 hours at -20°Cin the freezer (white circles).

As can be observed in **Figure 5.8b**, the ^{13}C polarization changes with time even if the sample was stored in the freezer at -20°C. Thus, after 2 hours in the freezer the saturation value of the polarization build-up curve was less than the half value of a freshly prepared one. It was checked if a the decomposition of the radical could be the origin of this behaviour, since it was reported that the best stability of BDPA radicals is obtained in presence of benzene or in poor hydrogenated solvents[24]. Moreover, the commercial BDPA (**10**) is complexed with benzene. For this reason we repeated the experiments with an equimolar quantity of radical and benzene.

A new sample of BDPA-CN radical **20** was prepared dissolving of 3.54 mg of the radical in 100 μl of sulfolane and 80 mM in benzene. Once the radical was completely dissolved, 100 μl of [1-^{13}C]pyruvic acid were added, obtaining a final solution radical concentration of 40 mM. As in the previous sample, the polarization build-up curve was performed with an aliquote of 30 μl irradiating the frozen sample at 1.4 K at the same frequency (94.080 GHz). The sample remained inside the helium cavity until the pressure and the temperature became stable (3.2 mbar and 1. 4 K). Data were acquired every 1 minute and the total time of polarization, until saturation, was 90 minutes. The data obtained by the build-up curves were similar to those obtained in the previous case with BDPA-CN alone. Thus, it seemed that the BDPA cyano derivative is not good enough to be used as a polarizing agent of [1-^{13}C]pyruvic acid.

5.2.1.2 BDPA-CH_2OH (BA-BDPA) (29) radical

The benzyl alcohol derivative of the BDPA radical, the radical BDPA-CH_2OH (**29**), is soluble in neat [1-^{13}C]pyruvic acid, allowing us to prepare samples of this radical in pure [1-^{13}C]pyruvic acid in presence of an equimolar quantity of benzene. Concerning

the acquisition of the ^{13}C microwave DNP spectrum, a 100 μl sample of [1-^{13}C]pyruvic acid doped with 40 mM of BA-BDPA (**29**) and benzene were prepared.

The microwave DNP spectrum (**Figure 5.9a**) obtained with an aliquote of 50 μl showed the positive polarization peak at 94.087 GHz and the negative one at 94.117 GHz. The frequency of work was determined as the positive peak polarization, P(+) = 94.087 GHz. The separation between both polarization peaks (|P(+) - P(-)|= 94087 - 94117) was 30 MHz, which is narrower compared to that of the BDPA (**10**) (50 MHz) and the cyano derivative radical BDPA-CN (**20**) (40 MHz). With the purpose of determining the optimum concentration of the radical **29** in [1-^{13}C]pyruvic acid, samples with concentration of 20, 40, 60 and 80 mM were prepared as described previously. Each of them were polarized at the optimal frequency of 94.087 GHz until the saturation was achieved(**Figure 5.9b**). As the build-up time constant (t_c) changes with the concentration, the time needed to saturate each concentration is different, being the solutions with higher concentrations, associated to pure thermal mixing mechanism, those with the lower values of build-up time constants (**Figure 5.10**).

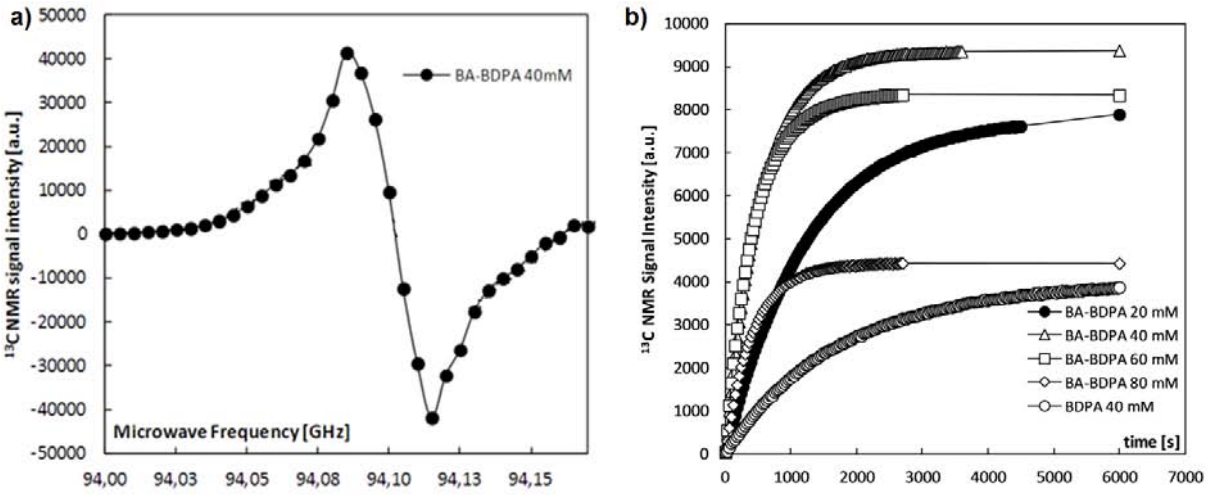

Figure 5.9: a) ^{13}C microwave DNP spectrum of 50 μl [1-^{13}C]pyruvic acid doped with 40 mM of radical **29** at 3.35 T and 1.4 K. b) ^{13}C polarization build-up curves of 20 μl of [1-^{13}C]pyruvic acid doped with different concentrations of radical **29**, and compared with 20 μl 1:1 (v/v) [1-^{13}C]pyruvic acid:sulfolane doped with the radical BDPA (**10**) at its optimal concentration (40 mM).

The best results were obtained with samples doped with a 40 mM concentration of the radical **29**, both with respect the solid state polarization value at saturation and the time of polarization (**Figure 5.9b**).

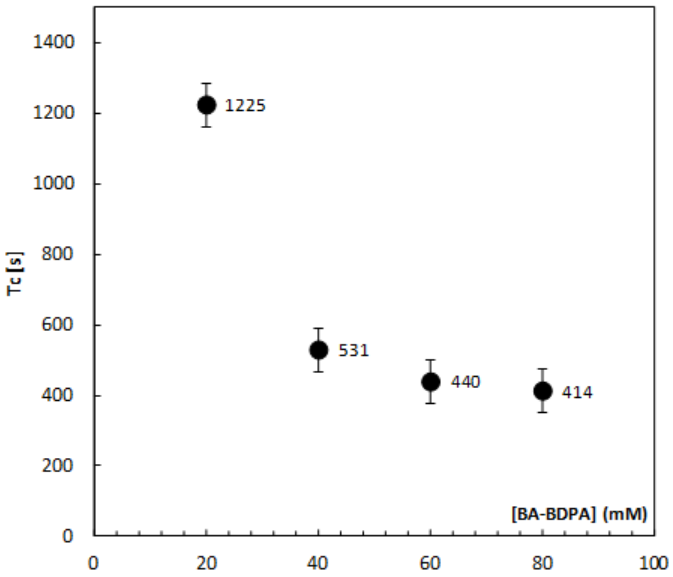

Figure 5.10: Build-up time constants (t_c) versus concentration of the radical **29**.

As already mentioned, the presence of the radical together with the polarized molecule can decrease the polarization and generate some toxicity for *in vivo* experiments. For this reason a *in-line* filtration to eliminate the radical from the [1-^{13}C]pyruvic acid once it has been hyperpolarized and diluted via water where the radical **29** is completely insoluble. The filtration was integrated to the transfer process from the DNP polarizer to the NMR spectrometer using a homemade filter (**Figure 5.11a**) with a plastic syringe filled with cotton and a pressure adapter in each extreme. This filter was connected to the DNP equipment and the other side to the NMR spectrometer. As can be seen in **Figure 5.11b** by the color, the filter retains the radical.

Figure 5.11: Filter used in the transfer process from the DNP to the NMR system to remove the radical from the hyperpolarized solution. a) Filter without using and b) filter after the transfer process. The orange color of the retained radical can be seen at the beginning of the filter.

After the polarization step, the samples were quickly dissolved in a solution of

Na_2EDTA in hot water and automatically transferred to a 600 MHz *Bruker* NMR spectrometer through the homemade *in-line* filtration system (8 s of transference, 2 s of stabilization and 500 μs of measurement time). This filtration system completely removed the radical from the hyperpolarized solution down to 10^{-7} M, as confirmed by UV-Vis and EPR, since there was no signals in the UV-Vis and in the EPR spectra of the filtered hyperpolarized solutions. In addition, this process could reduce the loss of hyperpolarization by relaxation that implies the presence of paramagnetics centers in the hyperpolarized solutions.[11] With these experiments it could be determined the enhancement ratio in liquid state of the hyperpolarized solutions using for the data acquisition 1 scan with a flip angle $\theta = 90^0$, for the hyperpolarized sample, and 32 scan with a flip angle $\theta = 30^0$ for the thermal one. The hyperpolarized sample was maintained 15 minutes outside the magnet to ensure the hyperpolarization was lost in order to employ it to calculate the thermal one. With the purpose of comparing with other radicals commonly used as polarizing agents, the same experiment was performed for [1-^{13}C]pyruvic acid:sulfolane (1:1) doped with 40 mM of BDPA radical**10**, and for [1-^{13}C]pyruvic acid doped with 15 mM of OX63 radical (**61**), using the previously represented optimal concentrations. The results are summarized in (**Figure 5.12**).

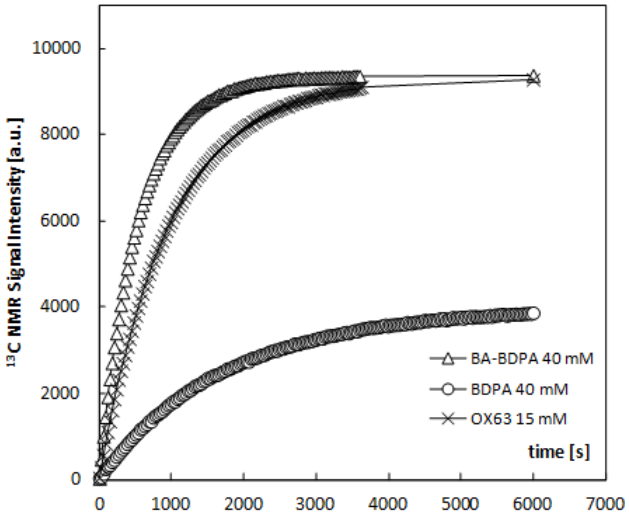

Figure 5.12: ^{13}C polarization build-up curves of 20 μl [1-^{13}C]pyruvic acid doped with 40 mM of radical **29** (open triangles), 20 μl 1:1 (v/v) [1-^{13}C]pyruvic acid:sulfolane doped with 40 mM of BDPA radical **10** (open circles) and 20 μl [1-^{13}C]pyruvic acid doped with 15 mM of OX63 radical (**61**) (crosses) at 3.35 T and 1.4 K. It should be noticed that the quantity of [1-^{13}C]pyruvic acid in BDPA sample is half of the others because its formulation.

Table 5.1: Liquid-state NMR enhancement ratio measured 10 s after dissolution of [1-^{13}C]pyruvic acid samples doped with different concentrations of radical **29**. BDPA radical **10** and OX63 radical(**61**).

Radical conc. (mM)	Hyperpolarized compound	Dissolution solvent	Liquid-state enhancement (ε)
BA-BDPA 20 mM	[1-^{13}C]pyruvic acid	water	2191
BA-BDPA 40 mM	[1-^{13}C]pyruvic acid	water	2886
BA-BDPA 60 mM	[1-^{13}C]pyruvic acid	water	2726
BA-BDPA 80 mM	[1-^{13}C]pyruvic acid	water	1387
BDPA 40 mM	[1-^{13}C]pyruvic acid	water	2454
OX63 15 mM	[1-^{13}C]pyruvic acid	water	2658

As can be observed in **Figure 5.12** BA-BDPA radical (**29**) and OX63 radical (**61**) showed similar polarization level in solid state. However a slightly higher polarization was obtained for the sample doped with 40 mM of BA-BDPA (**29**) radical in liquid state (**Table 5.1**). This result could be explained by the presence of the OX63 (**61**) radical in the solution. The presence of the paramagnetic OX63 (**61**) in the final dissolution could reduce the relaxation time (T_1) of the hyperpolarized species and consequently the final polarization level, obtaining less polarization in practice. From these experiments we may conclude that the relative easy and fast elimination of the radical **29** together with the similar hyperpolarization level makes this radical an excellent candidate for *in vivo* experiments where pyruvic acid is the target compound to be hyperpolarized.

5.2.1.3 BDPA-CH_2NH_2 (BAm-BDPA) (22) radical

The benzyl amino derivative of BDPA radical (BAm-BDPA) **22** is also soluble in neat [1-^{13}C]pyruvic acid, as BA-BDPA **29**. The sample formulation was performed as in the previous case. The acquisition of the ^{13}C microwave DNP spectrum was performed with a sample of 50 μl of [1-^{13}C]pyruvic acid doped with 40 mM of radical **22** and an equimolar quantity of benzene. An aliquote of 50 μl was used to perform the experiments. The microwave DNP spectrum showed (**Figure 5.13a**) a positive polarization peak at 94.080 GHz and a negative one at 94.125 GHz. The separation between both polarization peaks (|P(+) - P(-)|= 94080 - 94125) was 45 MHz. This value is between non functionalized BDPA radical **10** (50 MHz) and the cyano derivative radical BDPA-CN **20** (40 MHz). The frequency of work was determined as the positive peak polarization of P(+) = 94.080 GHz;

Samples of 20, 40, 60 and 80 mM were prepared to determine the optimal concentration of the radical **22** for DNP experiments. The samples were prepared by dissolution of the appropriate quantity of the radical in [1-^{13}C]pyruvic acid, adding an equimolar quantity of benzene. A 20 μl sample of each concentration was polarized at the optimal frequency of 94.080 GHz until saturation (**Figure 5.13b**). As the build-up time con-

stant (t_c) changes with the concentration, the time needed to saturate the samples of different concentration was quite different, being lower at higher concentrations which is associated to pure thermal mixing mechanism (**Figure 5.14a**). In particular, the polarization time needed for a sample doped with 80 mM of radical is reduced with respect to another doped with a 60 mM concentration however, a similar polarization level in solid state. Therefore, with this radical, the best results were obtained with samples doped with 60-80 mM concentration. It is worth mentioning that the polarization time needed to polarize [1-^{13}C]pyruvic acid for radical **22** is much less than with OX63 (**61**), BDPA (**10**) and BA-BDPA (**29**) radicals, being the build-up time constant also inferior (**Figure 5.14b**). It is a very important point to notice that the polarization of [1-^{13}C]pyruvic is very fast with radical **22**, opening the possibility to perform experiments with shorter times reducing the consume of liquid helium.

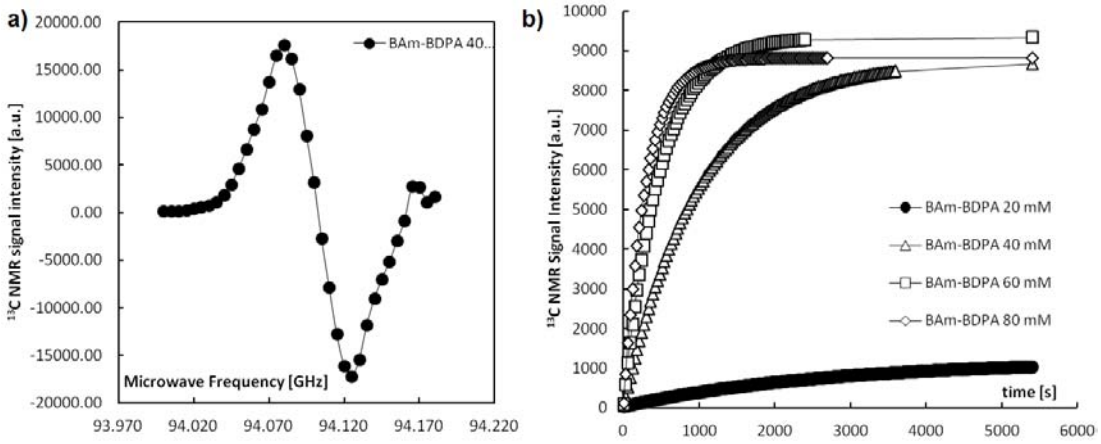

Figure 5.13: a) ^{13}C microwave DNP spectrum of 50 μl [1-^{13}C]pyruvic acid doped with 40 mM radical **22** at 3.35 T and 1.4 K. b)^{13}C polarization build-up curves of 20 μl [1-^{13}C]pyruvic acid doped with different concentrations of radical **22**.

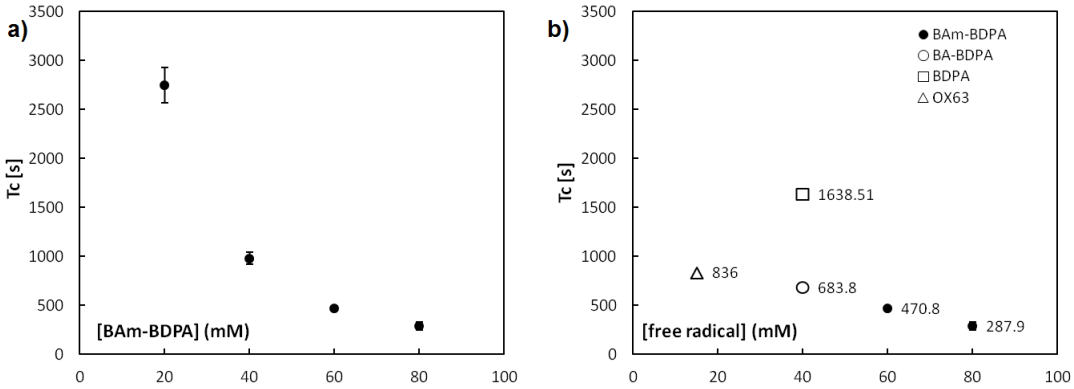

Figure 5.14: a) Build-up time constants (t_c) *versus* concentration of radical **22**, b) Comparison of build-up time constant (t_c) of OX63 radical (**61**), BA-BDPA (**29**) and BA-BDPA radical (**22**), performed at optimal concentration in [1-^{13}C]pyruvic acid. BDPA **10** includes sulfolane in a 1:1 ratio.

With the purpose of eliminating the radical by filtration in the transfer process, the home made filter (**Figure 5.11a**) was used, as in BA-BDPA **29** experiments. Unfortunately, the formation of the salt between the amine of BAm-BDPA **22** and the acid group of [1-^{13}C]pyruvic acid produced the radical amonium salt, soluble in the transfer solvent. For this reason, the transfer conditions were modified. Therefore, the transference was performed directly without filtering and with a reduction in transference time (6 s of transference, 2 s of stabilization and 500 μs of measurement time).

It was thought in the possibility of removing the radical species from the sample using a phosphate buffer as transfer dissolution. It increases the pH of the transfer dissolution and the radical could be retained by filtration (**Figure 5.15b**). Therefore, the *in vivo* transfer conditions could allow the radical elimination. However, the filtration was achieved in an *out line* mode.

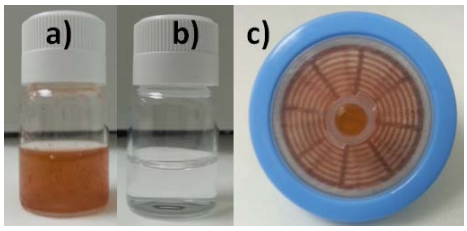

Figure 5.15: a) 80 mM sample in 4 ml of phosphate buffer without filtering, b) the same sample after filtration through a 0.2 μm filter. c) The orange color of the retained radical can be seen on the filter.

After polarization, all samples were fast dissolved in a solution of and automatically transferred to the 600 MHz *Bruker* NMR spectrometer. The enhancement ratio in liquid state of the hyperpolarized solution was determined using 1 scan with a flip angle $\theta = 90^0$, for both the hyperpolarized sample and for the thermal one. To calculate

the thermal one, the hyperpolarized sample was maintained 15 minutes outside the magnet to ensure the hyperpolarization loss of the sample. For comparing, similar experiments were performed with and using the following solutions: [1-^{13}C]pyruvic acid doped with40 mM of BA-BDPA **29**, [1-^{13}C]pyruvic acid:sulfolane (1:1) doped with 40 mM of BDPA **10**, and for [1-^{13}C]pyruvic acid doped with 15 mM of OX63 (**Figure 5.16**).

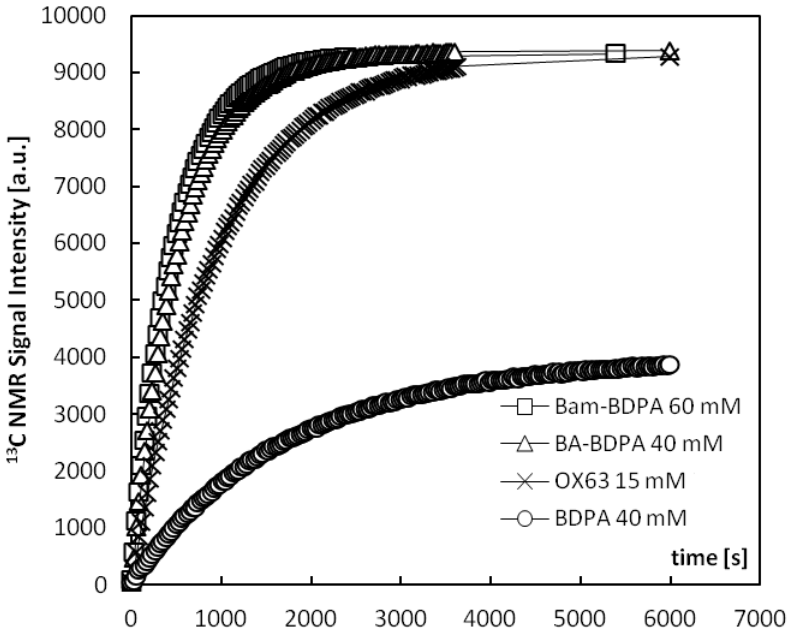

Figure 5.16: ^{13}C polarization build-up curves at 3.35 T and 1.4 K of 20 μl [1-^{13}C]pyruvic acid doped with 60 mM of BAm-BDPA **22** (squares, 24.7 mg), 20 μl of[1-^{13}C]pyruvic acid doped with 40 mM BA-BDPA **29** (triangles, 23.9 mg), 20 μl [1-^{13}C]pyruvic acid doped with 15 mM OX63 (**61**) (crosses, 26.1 mg) and 20 μl 1:1 (v/v) [1-^{13}C]pyruvic acid:sulfolane doped with 40 mM BDPA **10** (circles, 25.2 mg) at 3.35 T and 1.4 K. It should be noticed that the quantity of [1-^{13}C]pyruvic acid in the sample with BDPA is half of the others because of its formulation.

Table 5.2: Liquid-state NMR enhancement ratio measured 8.5 s after the dissolution in a Na_2EDTA in hot water of [1-^{13}C]pyruvic acid samples doped with different concentrations of radical **22**. BA-BDPA **29**, BDPA **10** and OX63 (**61**) radicals were also measured in their optimal conditions, for comparison.

Radical conc. (mM)	Polarization time (s)	Liquid-state enhancement (ε)	%^{13}C pol after diss.
BAm-BDPA 20 mM	5400	872	1.1
BAm-BDPA 40 mM	3600	7109	8.7
BAm-BDPA 60 mM	1800	9358	11.4
BAm-BDPA 80 mM	1200	6623	8.1
BA-BDPA 40 mM	3600	9807	12.0
OX63 15 mM	3600	12369	15.1
BDPA 40 mM	5400	11583	14.1

As it is observed in **Figure 5.16**, the polarization levels that can be reached in solid state for a solution with 80 mM BAm-BDPA **22** and OX63 radical (**61**) are similar but the polarization time required to reach the saturation level is three times higher for OX63 radical (**61**). Thus, the use of radical **22** is advantageous since it reduces the time of the experiment and the consume of helium. Nevertheless, the use of radical (**22**) as polarizing agent shows a disadvantage with respect to radical OX63 since the liquid state enhancement ratio and the %^{13}C polarization (**Table 5.2**) are partially lost for BAm-BDPA **22**. It could be attributed to the high concentration of paramagnetic species in the dissolution samples which reduces the relaxation time leading to a reduction in the expected enhancement.[11] Moreover, the radical salt form of the pyruvate makes faster the relaxation.[25] However, the use as a transfer solvent, of a phosphate buffer, allowed us to eliminate the BAm-BDPA (**22**) by filtration in a *out line* mode. Nevertheless, the elimination of BAm-BDPA **22** in the transfer process could improve the percentage of ^{13}C polarization of the filtered solutions.

5.2.2 Fast dissolution Dynamic Nuclear Polarization of diradicals

As already mentioned the *Cross-Effect* is one of the mechanisms for which a large signal enhancement is expected. The ideal CE polarizing agent would be a biradical with an EPR spectrum consisting of two sharp lines separated by the Larmor frequency of the nuclei to be polarized, ω_{0I}. However, at high magnetic fields (> 5 T), where contemporary NMR experiments are performed, only a few known radicals exhibit narrow line spectra. Among them, one can mention trityl radicals and BDPA radicals derivatives, which have similar isotropic g-values. Consequently, if a trityl or a BDPA radical unit is responsible of one of the lines in the EPR spectrum of a diradical as polarizing agent, to satisfy the CE matching mechanism condition it is necessary to

introduce another radical unit with a line separated from the first by a value of, ω_{0I}. There are no known stable radicals that provide a narrow line and meet this condition. However, TEMPO derivatives have a broad line with significant spectral density at a frequency separation matching ω_{0I}.

To overcome this limitation it has recently been proposed that mixed biradicals based on trityl radical[19,26,27] and nitroxide radicals are potentially the best biradical candidates to attain the maximal DNP enhancement by CE because two reasons. First the EPR frequency separation between the nitroxide g_{yy} component and the isotropic g value of trityl radicals matches the ω_{0I} for ^{13}C nuclei and second both radicals show optimal relaxation times which allow simultaneous microwave saturation and polarization turnover. The moderately weak coupling interactions in which J is typically smaller than the ^{14}N hyperfine splitting in the case of nitroxide biradicals[28] does not perturb the EPR frequency matching between the two spins which is a requisite for a maximal enhancement.

Most of the reported biradicals are based up to now on two homogeneous radical moieties rather than mixed radicals, although some examples of OX63 or BDPA joined to TEMPO unit have been reported during the last years.[29,30] Such results provided out the interest in preparing and studying as polarizing agents, new biradicals made with trityl or BDPA and with nitroxide moieties, like those prepared in Chapter 4.

5.2.2.1 PTM=TEMPO (49) diradical

Diradical PTM=TEMPO (**49**) was tested as a dissolution-DNP polarizing agent using [2-^{13}C]acetone as the target of polarization in a matrix of sulfolane, as a glassing agent.[31] The sample preparation was performed as follows, *i. e.* TM=TEMPO diradical (**49**) was dissolved in a sulfolane:[2-^{13}C]acetone (1:1) (v/v) mixture to yield a 120 mM solution. Solutions with concentration of of 5, 10, 40, 60 and 90 mM of diradical **49** were prepared from the 120 mM solution by dilution in order to determine the optimal concentration for DNP experiments.

With the purpose of determining the optimal frequency of polarization, a DNP microwave spectrum of 100 μl a of sulfolane:[2-^{13}C]acetone (1:1) doped with 90 mM of diradical **49** was used. It can be seen from the resulting microwave DNP spectrum (**Figure 5.17a**) that the positive polarization peak is located at 94.067 GHz, while the negative one appears with a very weak intensity at around 94.220 GHz. The broad polarization band with a width of 150 MHz indicated an operative polarization mechanism different from a pure SE. Due to the high concentration of biradical, a thermal mixing polarization mechanism might be the dominant one. The frequency of work was determined as the positive peak polarization of P(+) = 94.067 GHz.

In order to determine the optimal concentration of diradical **49** samples with different concentrations (5, 10, 40, 60, 90 and 120 mM) were polarized at the optimal frequency of 94.067 GHz at 3.35 T and 1.4 K (**Figure 5.17b**). The best polarization level is achieved with a 90 mM concentration of the diradical.

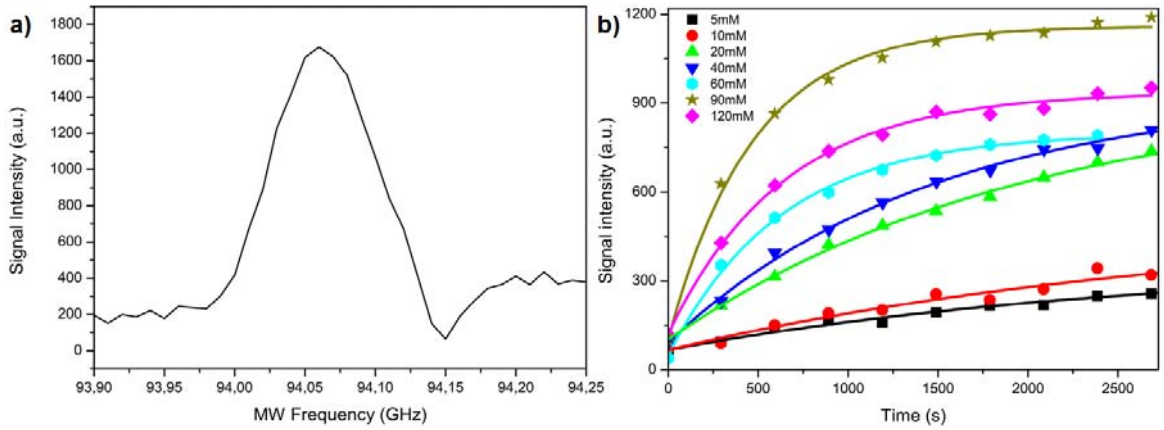

Figure 5.17: a) ^{13}C microwave DNP spectrum of 100 μl sulfolane:[2-^{13}C]acetone 1:1 doped with 90 mM of diradical **49** at 3.35 T and 1.4 K. b)^{13}C polarization build-up curves made at different concentrations of diradical **49**.

As can be observed in the plot of the build-up time constants (t_c) *vs* concentrations (**Figure 5.18**), it seems there is a change in the polarization mechanism with the concentration, being the dominant one, at the optimal concentration of the diradical, the thermal mixing mechanism .

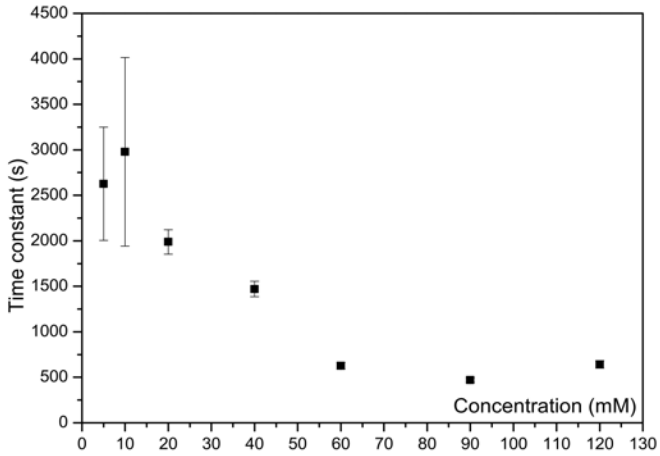

Figure 5.18: Build-up time constant (t_c) *versus* concentration of diradical (**49**).

To compare the hyperpolarization achieved with the biradical **49** with the one obtained with the gold standard radical, the OX63 (**61**), a 100 μl solution of sulfolane:[2-^{13}C]acetone 1:1, doped with 90 mM of biradical **49**, and a 100 μl solution of sulfolane:d^6-DMSO 1:1 doped with 15 mM of OX63 radical (**61**) were polarized. As can be observed in **Figure 5.19**, the solid state polarization obtained for the diradical was higher than that obtained with the radical OX63 (**61**).

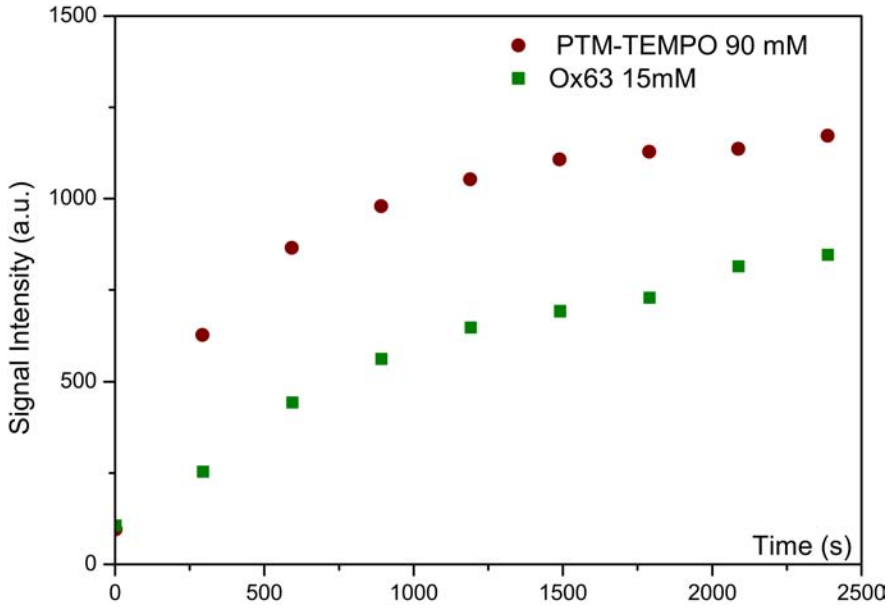

Figure 5.19: ^{13}C polarization build-up curves of 100 μl sulfolane:[2-^{13}C]acetone (1:1) doped with 90 mM of biradical **49** (brown) and 100 μl d^6-DMSO:[2-^{13}C]acetone (1:1) doped with 15 mM of radical OX63 (**61**) (green) at 3.35 T and 1.4 K.

Due to the promising results obtained in solid state, fast dissolution experiments were performed in order to determine the liquid state enhancements achieved by DNP with the diradical **49** and OX63. This was made by transferring the dissolution sample, in hot methanol to a Varian Inova 500 MHz NMR spectrometer obtaining the corresponding NMR spectra (**Figure 5.20**) using 2 s for the stabilization, 1.25 s for the transference and 0.5 s for the acquisition.

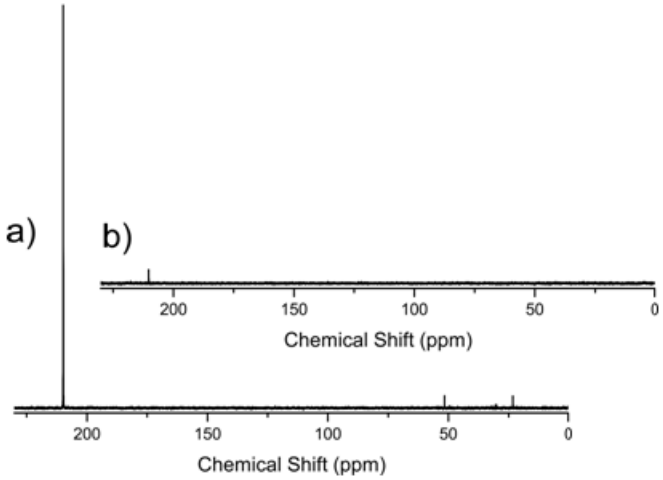

Figure 5.20: a) ^{13}C NMR spectrum of [2-^{13}C]acetone hyperpolarized with with diradical **49** with θ= 15° and 1 scan at 3.35 T and 1.4 K and b) ^{13}C NMR spectrum NMR spectrum of [2-^{13}C]acetone hyperpolarized with 15 mM of OX63 (**61**) with θ= 35° and 1 scan.

Regarding the enhancement calculation, since the pulse sequence is different in thermal than in hyperpolarized samples, the calculation was performed using **Equation 5.3**, where $(S/N)_{hp}$ and $(S/N)_{th}$ are the signal-to-noise ratios of the hyperpolarized and thermal spectra, respectively. $Sin(\theta_{hp})$ and $Sin(\theta_{th})$ are the flip angle of the hyperpolarized and the thermal spectra, respectively and C_{hp} and C_{th} are the concentrations after the dissolution of [2-^{13}C]acetone in methanol for the hyperpolarized and the thermal sample, respectively, and nt_{hp} and nt_{th} are the number of transients in the hyperpolarized and thermal spectra, respectively.

$$\varepsilon = \frac{(S/N)_{hp}}{(S/N)_{th}} \times \frac{Sin(\theta_{hp})}{Sin(\theta_{th})} \times \frac{C_{hp}}{C_{th}} \times \sqrt{nt_{th}/nt_{hp}} \tag{5.3}$$

The obtained enhancements were 1522 for **49** and 100 for the diradical and for OX63 (**61**) radical, respectively. The difference of the enhancements in liquid state is much higher than in the solid state. This result could be explained as the loss of polarization is attenuated in the case of the diradical, due to the formation of aggregates in the dissolution solvent while the radical OX63 (**61**) is completely soluble. Thus, the final effective concentration of paramagnetic centers is smaller for the diradical than for the radical OX63 (**61**).

To evaluate the effect of the diradical **49**, a monoradical, PTM=TEMPE (**50**), with the same molecular structure than the diradical but with only the C-centered radical was studied as polarizing agent of [2-^{13}C]acetone. In addition, it was also evaluated as polarizing agent with radicals 4-oxo-TEMPO and a physical mixture of the monoradicals 4-oxo-TEMPO and PTM=TEMPE. Solutions of sulfolane:[2-^{13}C]acetone (1:1) doped with 90 mM radical **50**, 4-oxo-TEMPO and the mixture of 90 mM of 4-oxo-TEMPO and 90 mM of PTM=TEMPE were prepared and samples of 100 μl of all of them were used for the acquisition of the microwave DNP spectrum (**Figure 5.21a**). As can be observed, the intensity of the polarization peaks are substantially smaller for all samples with respect that obtained with diradical **49**. Moreover, they could not be improved by increasing the concentration.

To compare the polarization in solid state, an aliquote of 100 μl of the previous solutions of sulfolane:[2-^{13}C]acetone (1:1) doped with 90 mM radical **50**, 4-oxo-TEMPO and a mixture of 90 mM of 4-oxo-TEMPO and PTM=TEMPE were polarized, obtaining a low level of polarization (**Figure 5.21b**). From these experiments it can be concluded that neither 4-oxo-TEMPO nor the physical mixture generates the same polarization level obtained with the diradical concluding that exists a dipolar coupling between the two radical centers at the working temperature that allows a faster relaxation of the one of radicals centers by the flip-flop coupling between them.

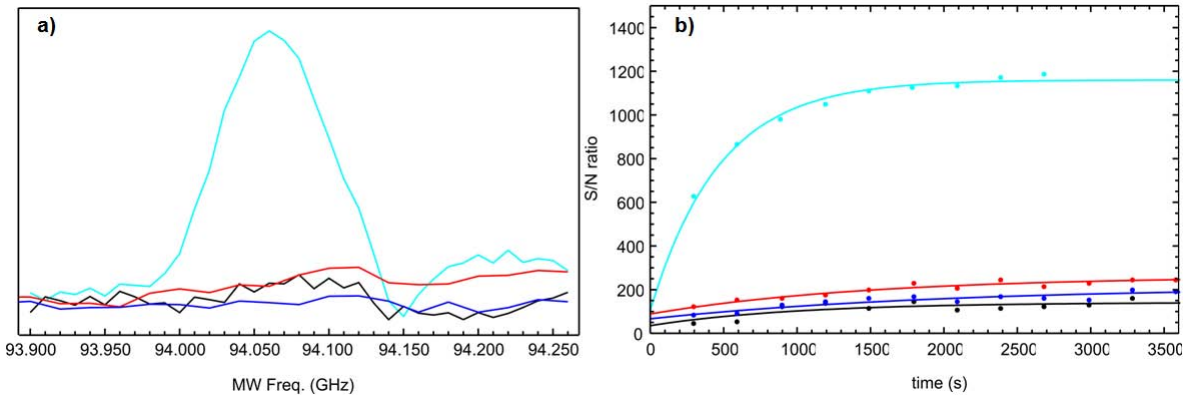

Figure 5.21: a) ^{13}C microwave DNP spectra of 100 μl sulfolane:[2-^{13}C]acetone (1:1) doped with 90 mM of diradical **49** (blue), monoradical PTM=TEMPE (**50**) (black), 4-oxo-TEMPO (**36**) (red) and a mixture of PTM=TEMPE (90 mM) and 4-oxo-TEMPO (90 mM) (dark blue) at 3.35 T and 1.4 K. b)^{13}C polarization build-up curves of 100 μl of sulfolane:[2-^{13}C]acetone (1:1) doped with 90 mM of diradical **49** (blue), monoradical PTM=TEMPE (**50**) (black), 4-oxo-TEMPO (**36**) (red) and a mixture of PTM=TEMPO (90 mM) and 4-oxo-TEMPO (90 mM) (dark blue) at 3.35 T and 1.4 K.

5.2.2.2 BDPAesterTEMPO (58) diradical

Diradical BDPAesterTEMPO (**58**) was also tested as a polarizing agent using as the target of polarization [2-^{13}C]acetone in a matrix of sulfolane as a glassing agent. The sample preparation was performed from a 120 mM stock solution of the diradical prepared in a mixture of sulfolane:[2-^{13}C]acetone 1:1 (v/v). Solutions with concentrations of 5, 10, 20, 30, 40, 60 and 90 mM of diradical **58** were prepared by dissolution of the stock solution in order to determine the optimal concentration of the DNP experiments.

To determine the optimal frequency of polarization, a microwave DNP spectrum with 100 μl of sulfolane:[2-^{13}C]acetone (1:1) doped with 18 mM of diradical **58** was used. It can be seen (**Figure 5.22**) from this spectrum that the positive polarization peak is located at 94.090 GHz, while the negative one was not observed due to the broad positive peak with a width of 220 MHz. The broad peak could reflect a polarization transfer mechanism involving more than one electronic spin. In this case, and due to the relatively low concentration of diradical, the most probable mechanism should be the *Cross-Effect* and the frequency of work was determined as the positive peak polarization of P(+) = 94.090 GHz.

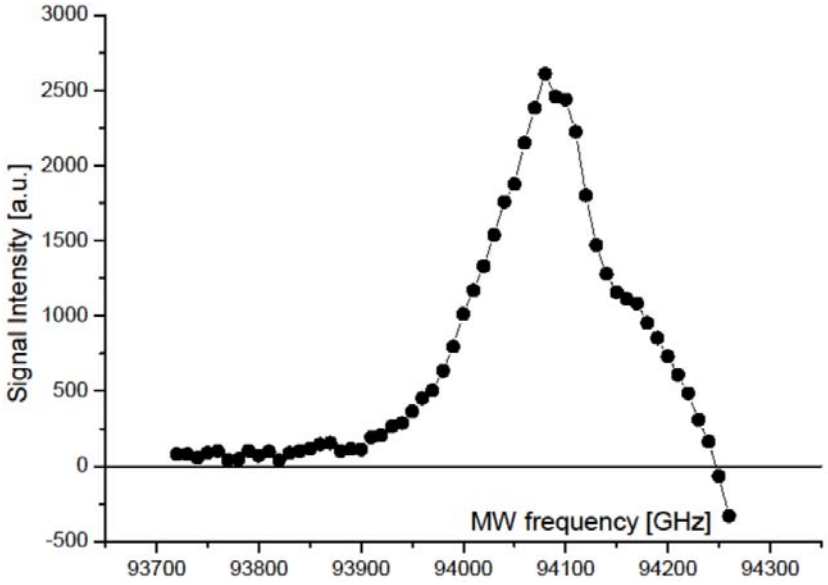

Figure 5.22: ^{13}C microwave spectrum of 100 μl sulfolane:[2-^{13}C]acetone 1:1 doped with 18 mM BDPAesterTEMPO (**58**) at 3.35 T and 1.4 K.

To determine the optimal concentration of BDPAesterTEMPO diradical (**58**) in sulfolane:[2-^{13}C]acetone 1:1 (v/v) for DNP experiments, samples with different concentrations (5, 10, 20, 30, 40, 60, 90 and 120 mM) were polarized at the optimal frequency of 94.110 GHz at 3.35 T and 1.4 K for 1.5 hours (**Figure 5.23**).

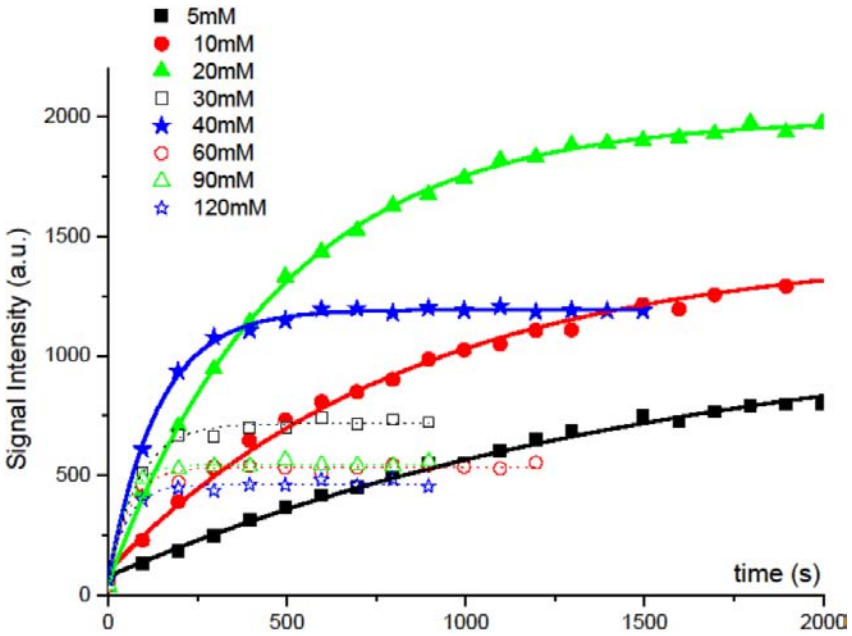

Figure 5.23: ^{13}C polarization build-up curves of 100 μl samples doped with different concentrations of BDPAesterTEMPO diradical (**58**) sulfolane:[2-^{13}C]acetone (1:1).

The optimal concentration found for the BDPAesterTEMPO diradical (**58**) was 20 mM. This is also clearly shown in the plot of the time constants *versus* concentration (**Figure 5.24**). The operative mechanism for the lower concentrations (5, 10 and 20 mM) probably corresponds to a *cross-effect* mechanism, while that operative at larger concentrations (30 to 120 mM) is the *thermal mixing* one due to the high concentration.

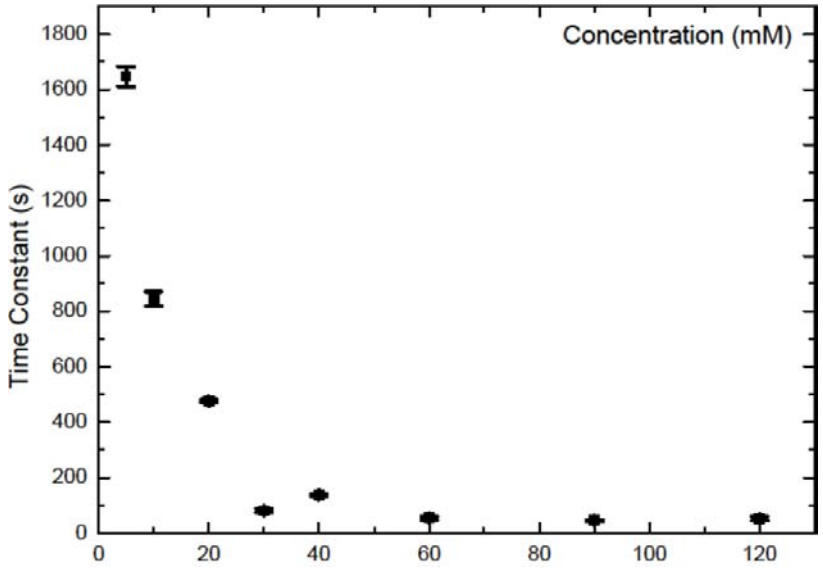

Figure 5.24: Build-up time constants *versus* concentration of BDPAesterTEMPO diradical (**58**).

With the objective of comparing the diradical BDPAesterTEMPO (**58**) and the gold standard radical OX63 (**61**), 100 μl solution of sulfolane:[2-^{13}C]acetone (1:1) doped with 20 mM and 40 mM of diradical **58**, 90 mM of PTM=TEMPO diradical (**49**) and a 100 μl solution of d^6-DMSO:[2-^{13}C]acetone (1:1) doped with 15 mM OX63 (**61**) were polarized. As can be observed in **Figure 5.25**, the solid state polarization obtained for diradical BDPAesterTEMPO (**58**) is very much higher than the obtained with the diradical **49** and radical OX63 (**61**) at their optimal concentrations.

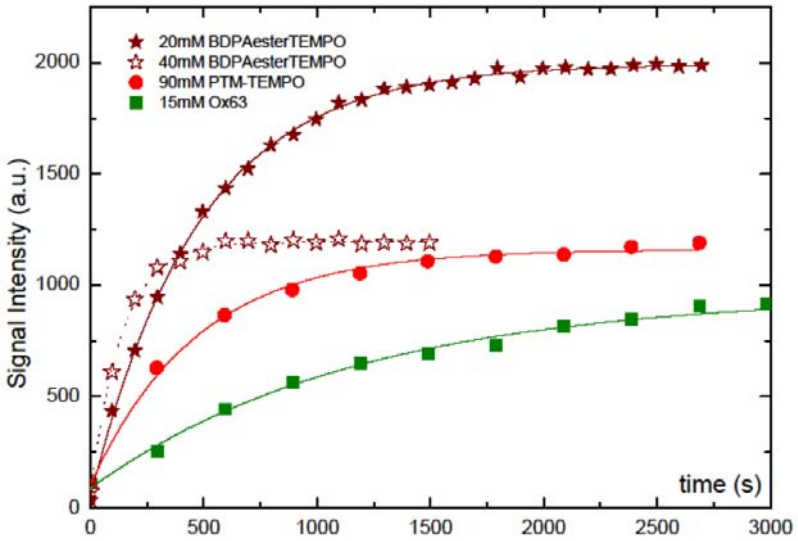

Figure 5.25: ^{13}C polarization build-up curves at 3.35 T and 1.4 K of 100 μl of sulfolane:[2-^{13}C]acetone (1:1) doped with 2o mM (close stars) and 40 mM (open stars) of BDPAesterTEMPO (**58**); 100 μl of sulfolane:[2-^{13}C]acetone (1:1) doped with 90 mM of PTM=TEMPO diradical (**49**) (red), and 100 μl d^6-DMSO:[2-^{13}C]acetone (1:1) doped with 15 mM OX63 (**61**) (green).

From **Figure 5.25** can be conclude that the best polarization level in solid state was achieved with the 20 mM solution of BDPAesterTEMPO (**58**), with a very big difference with respect to diradical **49** and OX63.

5.2.2.3 BDPAamidoTEMPO (60) diradical

As for the previous diradicals, the target of polarization with BDPAamidoTEMPO (**60**) diradical was [2-^{13}C]acetone in a matrix of sulfolane as a glassing agent. The sample preparation was performed by dissolution from a 100 mM stock solution of diradical **60** in a 1:1 (v/v) mixture sulfolane:[2-^{13}C]acetone, obtaining solutions with 1, 5, 13.3, 18, 20, 30, 40, 60 and 80 mM concentrations of the diradical

With the purpose of determining the optimal frequency of polarization, a microwave DNP spectrum of 100 μl of sulfolane:[2-^{13}C]acetone 1:1 doped with 18 mM of BDPAamidoTEMPO diradical (**60**) was used. It can be seen (**Figure 5.26**) from the microwave spectrum that the positive polarization peak is located at 94.110 GHz while a very

weak negative one appears at around 94.240 GHz. The broad polarization bands with a width of 140-150 MHz could reflect a polarization transfer mechanism that involves more than one electronic spin. In this case, and due to the relatively low concentration of diradical, the most probable mechanism should be the *cross-effect* one. The frequency of work was determined as the positive peak polarization of P(+) = 94.110 GHz.

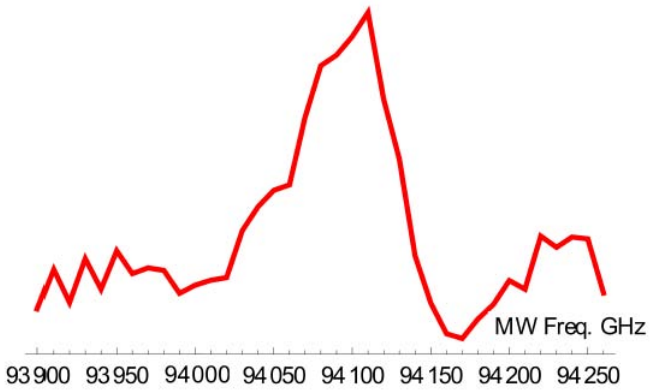

Figure 5.26: ^{13}C microwave DNP spectrum at 3.35 T and 1.4 K of 100 μl sulfolane:[2-^{13}C]acetone 1:1 doped with 18 mM of BDPAamidoTEMPO diradical (**60**).

In order to determine the optimal concentration of BDPAamidoTEMPO diradical **60** as polarizing agent, samples of different concentrations (1, 5, 13.3, 18, 20, 30, 40, 60, 80 and 100 mM) in sulfolane:[2-^{13}C]acetone 1:1 (v/v) were polarized at the optimal frequency of 94.110 GHz at 3.35 T and 1.4 K for 1.5 hours (**Figure 5.27**).

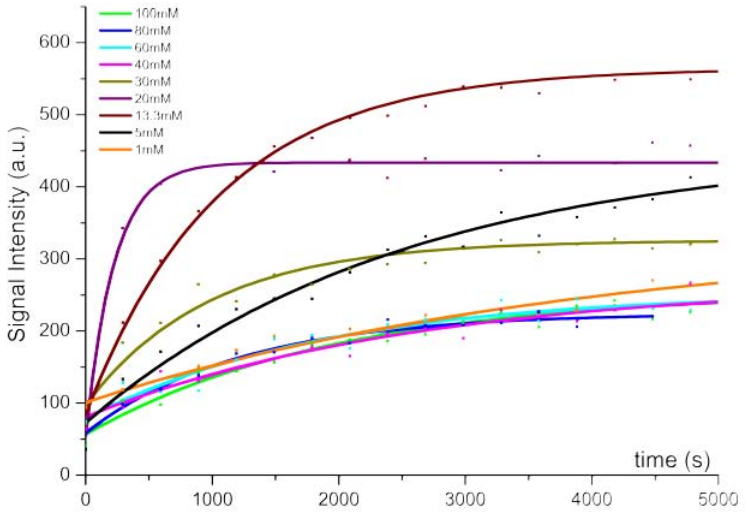

Figure 5.27: ^{13}C polarization build-up curves of 100 μl samples sulfolane:[2-^{13}C]acetone 1:1 doped with different concentrations of BDPAamidoTEMPO (**60**).

The optimal concentration for BDPAamidoTEMPO diradical (**60**) as polarizer was

13.3 mM which it is also clearly shown in the plot of the time constants *versus* concentration (**Figure 5.28**), where two minima are observed. The first minimum probably corresponds to a *cross-effect* mechanism, while the second one is probably dominated by *thermal mixing* due to the high concentration.

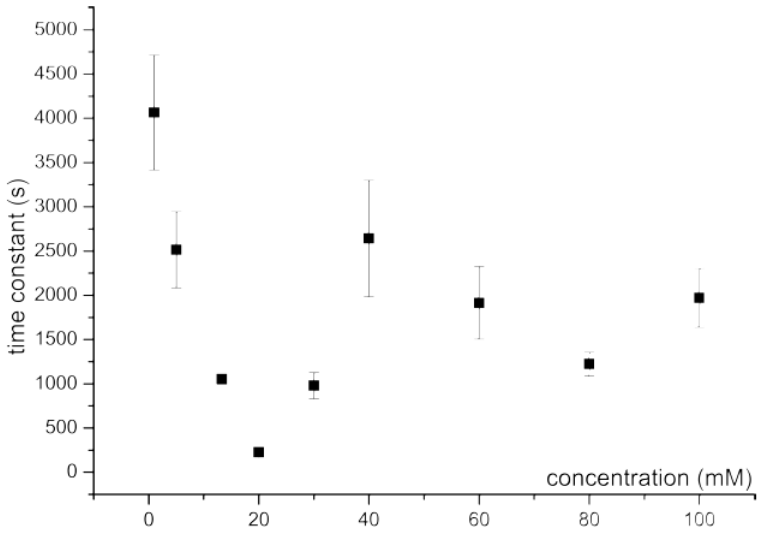

Figure 5.28: Build-up time constants *versus* concentration of BDPAamidoTEMPO diradical (**60**).

With the objective of comparing the efficiency of diradical BDPAamidoTEMPO (**60**) with radical OX63 (**61**), a 100 μl dissolution of sulfolane:[2-^{13}C]acetone (1:1) doped with 13.3 mM of diradical **60** and a 100 μl dissolution of d^6-DMSO:[2-^{13}C]acetone (1:1) doped with 15 mM OX63 (**61**), were polarized. As can be observed in **Figure 5.29**, the solid state polarization obtained for OX63 (**61**) was very much higher than the obtained with the diradical **60**.

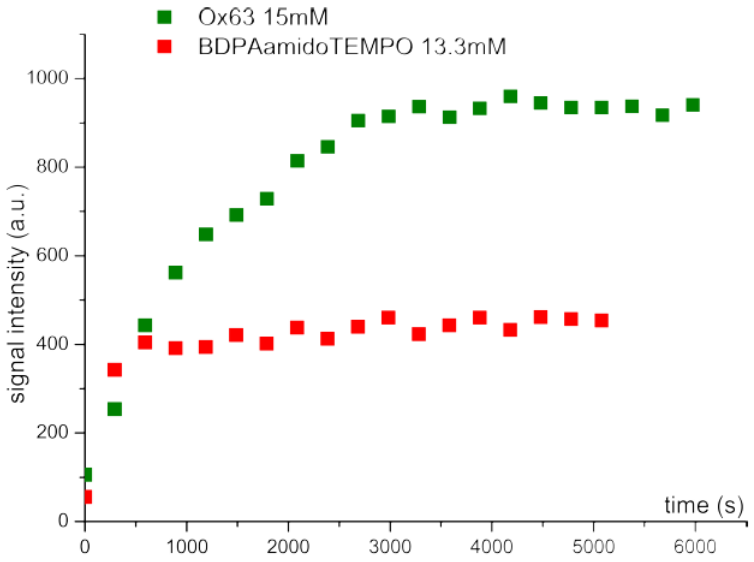

Figure 5.29: ^{13}C polarization build-up curves at 3.35 T and 1.4 K of 100 μl sulfolane:[2-^{13}C]acetone (1:1) doped with 13.3 mM of BDPAamidoTEMPO (**60**) (red) and 100 μl d^6-DMSO:[2-^{13}C]acetone (1:1) doped with 15 mM OX63 (**61**) (green).

5.3 MAS-Dynamic Nuclear Polarization

Magic Angle Spinning Nuclear Magnetic Resonance (MAS-NMR) is a standard technique used to improve the spectral resolution of powder samples, which has advantages for determination of properties of solid molecules as well as for determining protein structures. As in the conventional NMR, in MAS-NMR the low sensitivity, due to the thermal Boltzmann distribution of Zeeman populations, is a very limiting factor for practical applications. This makes hard for NMR users to study, for instance, surface properties or short living chemical intermediates that may appear in chemical reactions or during biological reactions. NMR is witnessing a breakthrough that can partially overcome these limitations via DNP at high magnetic fields. MAS-DNP at high magnetic fields has become possible through the work of Griffin and coworkers,[32] who introduced the use of gyrotrons as high frequency and high power microwave sources. The significant signal enhancements achieved with gyrotrons during MAS-DNP experiments have allowed the study of various biological systems including membranes and proteins[33,34] or the study of surface properties in material science.[35]

Exchange-coupled TEMPO diradicals have found applications as polarizing agents in solid-state dynamic nuclear polarization, but heterodiradicals start to be checked with the same purpose.[29,36] In general all these diradical systems show spin-spin exchange couplings that can be either through a bond or through the space between the two radical moieties,[37] Several factors, such as the nature of the linker between the two spin centers, the conformation, the substituents, and the environment (e.g. temperature, solvent, etc.), control the magnitude of the exchange coupling in diradicals that may vary several orders of magnitude.[38–40].

The success of diradicals as polarizing agents in solid state DNP is primarily attributed to the uniformly short distance between the two unpaired electrons in this kind of molecules, which guarantees that unpaired electrons are somewhat coupled to at least at one other electron. Initially, the EPR transition of one electron when is irradiated and nuclear polarization is generated in a subsequent three transition flip-flop process. Therefore, the $cross\text{-}effect$ is optimized when there is an enough strong dipolar coupling between them and the electron Larmor frequencies approximates the nuclear Larmor frequency (**Equation 5.4**). These requirements can be fulfilled more easily within a diradical than with dispersed monoradicals.[41]

$$\omega_{0S1} - \omega_{0S2} \approx \pm\omega_{0I} \tag{5.4}$$

In MAS-DNP experiments it has been generally assumed that the polarization process is similar to the static case. However, recent experimental results, such as the dependence of MAS-DNP enhancement on spinning frequency, [11] indicates that a better understanding of the MAS-DNP process is estill needed. There is controversial with respect to the origin of the spinning frequency dependence.[42–44]

In the past few years DNP-enhanced solid-state NMR spectroscopy under magic angle spinning (MAS) conditions has made great progress, and DNP signal enhancement factors of up to approximately 50 and up to around 100 have been reported working

at 9.4 T, 263 GHz and 100 K.[47] Earlier studies of a series of diradicals based on two TEMPO radicals as polarizing agents in high-field DNP experiments suggested that a conformation in which the two g_{zz} (or g_{yy}) tensor axes of the TEMPO moieties have a dihedral angle of 90^0 and have a weak exchange coupling should exhibit improved performance as a result of the efficient frequency matching.[48,49] Based on these precedents we wanted to study the effect of the distance between the unpaired electrons by using the three TEMPO diradicals prepared in this Thesis which show different distances between radical centers. Moreover, the different radical interaction and the different rigidity may affect the DNP enhancements.

5.3.1 MAS-Dynamic Nuclear Polarization experiments

All the MAS-DNP NMR experiments reported in this Thesis were performed in an ADVANCE Bruker 9.4 T spectrometer for MAS-DNP equipped with a gyrotron generating a continuous wave at the NMR laboratory of Prof. G. Bodenhausen (EPFL, Switzerland) with the assistance of Dr. Pérez-Linde. The μwave irradiation was transmitted through a corrugated wave guide to a triple resonance ^{1}H/X/Y MAS probe with 3.2 mm rotors.[45,46] NMR spectra with μwave irradiation "on" or "off" were acquired at a temperature of 100 K, which was stabilized using a BioSpin MAS cooling system. The one dimensional (1D) cross-polarization magic angle spinning (CP-MAS) ^{1}H $\rightarrow^{13}$C and ^{1}H $\rightarrow^{15}$N experiments were performed in the ADVANCE Bruker 9.4 T spectrometer for DNP-MAS.

5.3.1.1 TEMPO=TEMPO (44) diradical

TEMPO=TEMPO (**44**) was the diradical with the shortest distance between the two TEMPO moieties (6.9 Å). The EPR shows a large dipolar interaction with a half-field transition. The sample for MAS-DNP experiments was prepared by dissolution of diradical **44** in 60 μl of ^{6}d-DMSO and, after its complete dissolution, 34 μl of D_2O and 6 μl of H_2O were added until obtaining a solution with a 20mM concentration of diradical in the final DNP juice mixture. The solution was then stirred to be homogenized and 30 μl of sample were put in a 3.2 mm diameter sapphire rotor which was introduced in the NMR equipment and finally it was spun and frozen to 100 K. All the ^{1}H NMR spectra, with and without microwave irradiation (**Figure 5.30**), were recorded with a spinning rate of 8 KHz in order to plot the field dependence of the ^{1}H enhancement. Finally, several experiments were made in order to determine the optimal spinning frequency, the optimal microwave source power and the optimal concentration for the hyperpolarization of ^{1}H nuclei of water.

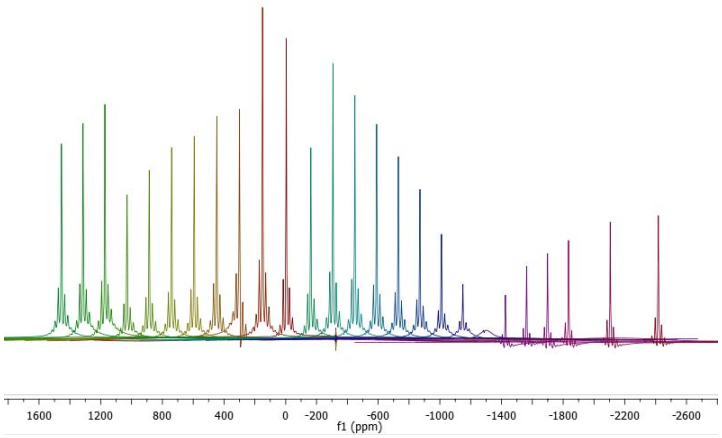

Figure 5.30: ^{1}H NMR of H_2O recorded at different magnetic fields with a 30 μl of a mixture of ^{6}d-DMSO/D_2O/H_2O (60/34/6) doped with 20 mM TEMPO=TEMPO diradical (**44**) at 9.4 T and 100 K.

The study of the field dependence of the ^{1}H enhancement of H_2O (**Figure 5.31a**) shows only a weak enhancement. This is related with the fact that a strong dipolar coupling with the diradical reduces the maximal possible enhancement. On the other hand, the maximal enhancement obtained was close to 7 when the spinning frequency was adjusted to 4 KHz (**Figure 5.31b**), being the concentration used of 20 mM. As can be seen in this figure, the increase of spinning frequency reduces the enhancement. The same result was obtained by decreasing the diradical concentration to 10 mM which yield an enhancement of 3. Unfortunately, the increase of concentration could not be studied due to the insolubility of the diradical at higher concentrations in the DNP juice. The microwave source reduction also produced the same result, since a reduction from 20 GHz to 15 GHz decreases the enhancement from 7 to 0.

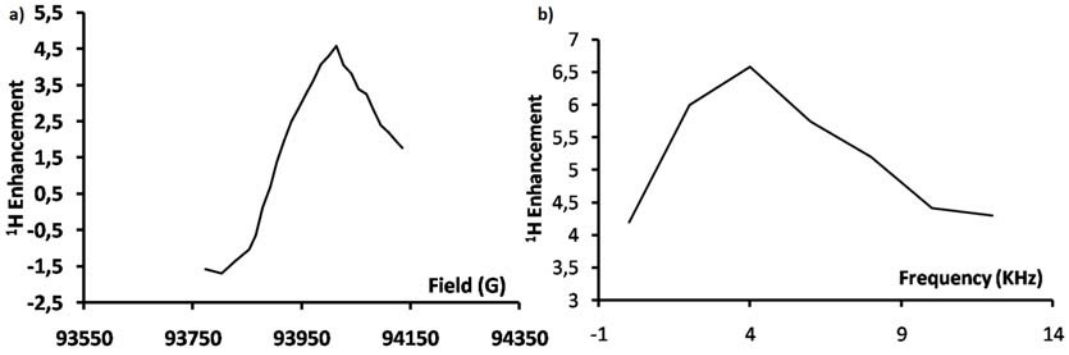

Figure 5.31: a) Field dependence of the ^{1}H enhancement (in a 3.2 mm ø rotor) of a 30 μl of a mixture of ^{6}d-DMSO/D_2O/H_2O (60/34/6) doped with 20 mM TEMPO=TEMPO diradical (**44**) at 9.4 T and 100 K with a spinning rate of 8 KHz. b) ^{1}H Enhancement *versus* spinning frequency of the rotor at 9.4 T and 100 K.

These results show that diradical **44** produces only low enhancements, allowing

to conclude that the TEMPO=TEMPO diradical **44**, which exhibits a strong dipolar coupling between TEMPO units, is not useful for its use as a solid-state polarizing agent in the tested conditions.

5.3.1.2 TEMPOesterTEMPO (45) diradical

The TEMPOesterTEMPO diradical (**45**) which shows the longest distance between the two TEMPO moieties (10.5 Å) among the synthesized diradicals based on TEMPO units was also studied as polarizing agent for MAS-DNP. This diradical shows some degree of dipolar interaction but without appreciable half field transition.

Initially, we also performed a study of the field dependence of the ^{1}H enhancement of H_2O (**Figure 5.32a**). As expected, the enhancement obtained in this case was higher than with the TEMPO=TEMPO diradical (**44**) due to the larger interadical distance. On the other hand, the enhancement obtained when the spinning frequency was adjusted to 8 KHz, with a concentration of 20 mM was close to 21. As can be seen in **Figure 5.32b**, the change in the spinning frequency increased the enhancement to 23 on reducing the spinning frequency to 6. By decreasing the diradical concentration to 10 mM the enhancement decreases down to 19. Unfortunately, a further increase of concentration could not be studied, as in the previous diradical **44**, as a consequence of the insolubility of the diradical **45** in the media. The reduction in the value of the microwave source produced the same result, since a reduction from 25 GHz to 20 GHz decreased the enhancement from 26 to 17.

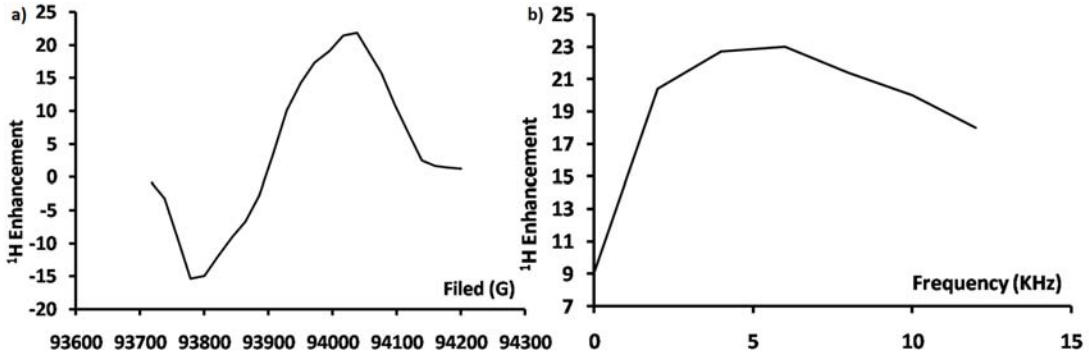

Figure 5.32: a) ^{1}H enhancement *versus* magnetic field of 30 μl of a mixtureof ^{6}d-DMSO/D_2O/H_2O (60/34/6) doped with 20 mM TEMPOesterTEMPO diradical (**45**) at 9.4 T and 100 K with a spinning rate of 8 KHz. b) ^{1}H Enhancement *versus* spinning frequency of the rotor at 9.4 T and 100 K.

5.3.1.3 TEMPOamidoTEMPO (46) diradical

The TEMPOamidoTEMPO diradical (**46**) shows the same two units than diradical **45**, but in this case, the link is an amide bond instead of an ester one. The distance between TEMPO moieties (9.6 Å) is somewhat shorter than in the ester structure. In accordance with this fact, the EPR shows some degree of dipolar interaction and a weak half-field transition. The first experiment performed with this diradical consisted of the study of the field dependence of the ^{1}H enhancement of H_2O (**Figure 5.33a**). As expected, the enhancement obtained in this case was higher than in the TEMPO=TEMPO diradical (**44**) since it was close to 25, when the spinning frequency was 8 KHz at a concentration of 20 mM. As can be seen in **Figure 5.33b**, the change in spinning frequency increase the enhancement to 26 on reducing the spinning frequency to 6 KHz, as in the previous case. The reduction of the diradical concentration to 10 mM also reduced the enhancement down to 22, as in the other cases. Fortunately influence of the increase of concentration could be studied for this diradical up to 30 mM due to tis larger solubility in the media. The obtained enhancements were similar ($\varepsilon = 22$) to the previous concentration but the relaxation time (T_1) was reduced from 2.5 to 1.7 s. The study of the reduction in the power of the microwave source produced the same result, as in the other cases since the reduction of the power from 25 GHz to 20 GHz decreased the enhancement from 26 to 24.

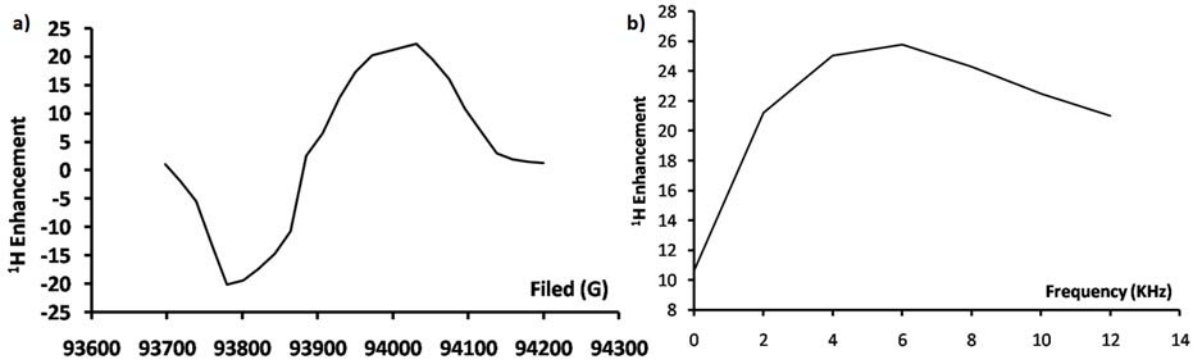

Figure 5.33: a) ^{1}H enhancement *versus* field of 30 μl of a mixture of ^{6}d-DMSO/D_2O/H_2O (60/34/6) doped with 20 mM TEMPOamidoTEMPO diradical (**46**) at 9.4 T and 100 K with an spinning rate of 8 KHz. b) ^{1}H Enhancement *versus* frequency spinning of the rotor at 9.4 T and 100 K

After the study of the three diradicals, we can conclude that the best diradical as a polarizing agent for MAS-DNP, in the studied conditions, was the TEMPOamidoTEMPO diradical (**46**). Thus, we performed cross polarization studies only with this diradical at the optimized conditions described above using a target molecule, like L-Proline or Vancomicine, to be hyperpolarized.

5.3.2 Cross Polarization experiments

Cross Polarization (CP)[50] is a double resonance technique that it is carried out using a second radio-frequency (rf) source, B_2, apart from the rf transmitter B_1 used for the detection of the spectrum. This technique enables to increase the sensitivity of non proton nuclei by transferring the hyperpolarization of ^{1}H nucleus to other nuclei (for instance ^{13}C). Thus, in our experiments the molecule to be detected contains ^{13}C or ^{15}N nuclei mixed with abundant nuclei with the active nuclei (^{1}H from H_2O) that yields a large signal. As in other DNP experiments, the polarization takes place by irradiating the sample with microwave sources at the EPR frequency of diradical at low temperature. The resulting electron polarization is transferred to the ^{1}H neighbors obtaining hyperpolarized ^{1}H nuclei that, with the double resonance, is finally transferred to the ^{13}C nuclei.

5.3.2.1 Hyperpolarization of L-Proline-$^{13}C_5$,^{15}N

To 100 μl of a mixture of ^{6}d-DMSO/D_2O/H_2O (60/34/6) containing 30 mM of TEMPOamidoTEMPO (**46**) and 0.1 M of the labeled proline was prepared. A sample of 30 μl of this solution was introduced in a sapphire 3.2 diameter rotor and frozen to 100 K. The T_1(^{1}H) relaxation time and DNP build-up curves were measured with a saturation recovery and the data was fitted to a mono-exponential function, yielding a value of τ=1.38 s. The enhancement was measured by comparing the ^{13}C NMR response using CP from ^{1}H to ^{13}C. ^{1}H-^{13}C cross polarization spectrum of proline required 62.5 KHz during the contact time when the spinning was set at 6 KHz. The contact time was set to 2500 μs, with a 100 KHz flip angles for the 90^0 pulse. The enhancement obtained for ^{13}C nuclei was 26 with respect the experiment without a microwave irradiation (**Figure 5.34**).

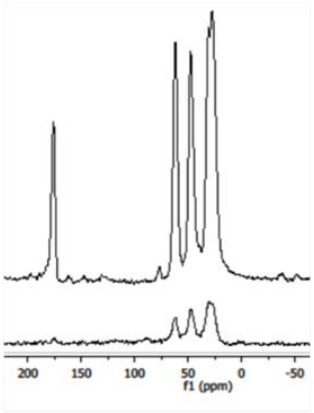

Figure 5.34: ^{13}C CP-MAS spectra of 0.1 M ^{13}C labeled L-proline solution in a mixture of ^{6}d-DMSO/D_2O/H_2O (60/34/6) doped with 30 mM TEMPOamidoTEMPO diradical (**46**) with (top) and without (bottom) microwave irradiation at 10 KHz MAS and 100 K.

5.3.2.2 Hyperpolarization of Vancomicine

A 100 μl of a mixture of ^{6}d-DMSO/D_2O/H_2O 60/34/6 containing 30 mM of TEMPOamidoTEMPO (**46**) and 0.1 M of vancomicine without isotope enrichment.[51] A sample of 30 μl of this mixture was introduced in a sapphire 3.2 diameter rotor and frozen to 100 K. The $T_1(^1H)$ relaxation time and DNP build-up curves were measured with saturation recovery and the data was fitted to a mono-exponential function, yielding a value of τ=0.9 s. The enhancement was measured by comparing the ^{13}C NMR response using CP from ^{1}H to ^{13}C. ^{1}H-^{13}C cross polarization spectrum of vancomicine required 71 KHz during the contact time when the spinning was set at 10 KHz. The contact time was set to 2000 μs, with a 100 KHz flip angles for the 90^0 pulse. The enhancement obtained in ^{13}C was 19 with respect the experiment without microwave irradiation (**Figure 5.35**).

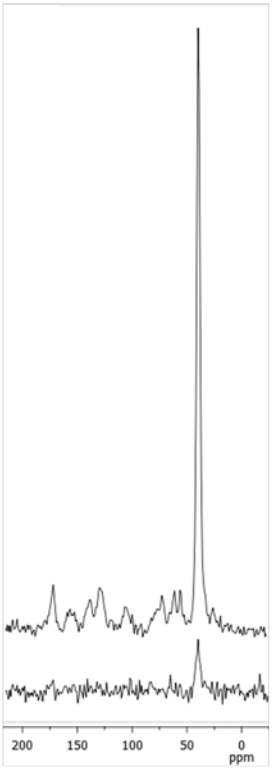

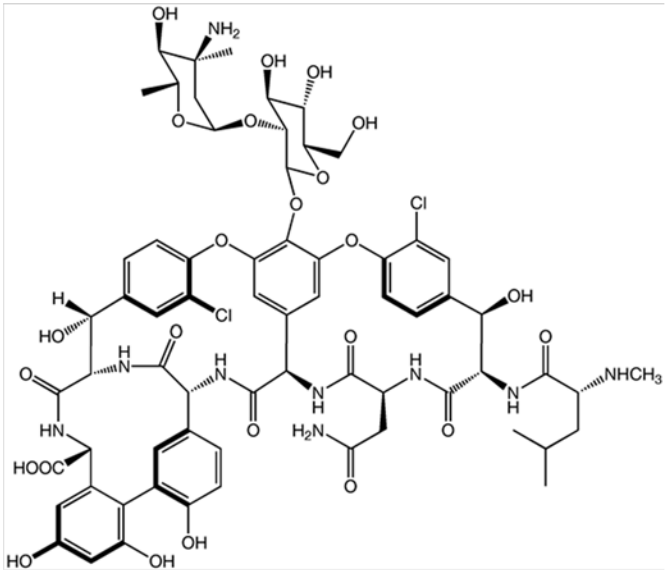

Figure 5.35: Left) ^{13}C CP-MAS spectra of 0.1 M vancomicine solution in a mixture of ^{6}d-DMSO/D_2O/H_2O (60/34/6) doped with 30 mM TEMPOamidoTEMPO (**46**) with (top) and without (bottom) microwave irradiation at 10 KHz MAS and 100 K. Right) Chemical structure of vancomicine.

With the above *CP* studies we can conclude that the diradical **46** is a quite efficient polarizing agent for MAS-DNP experiments.

5.4 Conclusions

- Monoradicals BDPA-CN (**20**), BA-BDPA (**29**) and BAm-BDPA (**22**) were tested as polarizing agents in fast dissolution-DNP with [1-^{13}C]pyruvic acid. The possibility of eliminating the glassing agent was successfully achieved for BA-BDPA (**29**) and BAm-BDPA (**22**). Moreover, it has been designed an *in-line* filtration system that allows the elimination of insoluble radicals in the transfer process.

- The polarization levels achieved with the monoradicals BA-BDPA (**29**) and BA-BDPA (**29**) in solid state were similar to OX63 (**61**). With the filtration system, the BA-BDPA (**29**) samples are free of radicals when water is used as transfer solvent whereas it is needed a phosphate buffer to obtain the same result with BAm-BDPA (**22**) and hence the loose of hyperpolarization is slower and good levels of polarization are achieved.

- Diradicals PTM=TEMPO (**49**), BDPAesterTEMPO (**58**) and BDPAamidoTEMPO (**60**) were tested as polarizing agents with [2-^{13}C]acetone. The results obtained indicates that PTM=TEMPO diradical (**49**), that shows less radical interaction between the units, generates a better polarization of [2-^{13}C]acetone in solid state than BDPAamidoTEMPO (**60**) or OX63 (**61**). On the other hand, BDPAesterTEMPO (**58**) showed the best [2-^{13}C]acetone polarization among tested systems.

- Diradicals TEMPO=TEMPO (**44**), TEMPOesterTEMPO (**45**) and TEMPOamidoTEMPO (**46**) were studied as polarizing agents of ^{1}H in MAS-DNP. TEMPO=TEMPO (**44**) was not a good polarizing agent while **45** and **46** showed a similar enhancements, being a little bit better the diradical**46**). This diradical was also tested in cross polarization experiments in order to polarize ^{13}C of labeled proline and vancomicine in natural abundance obtaining quite promising results.

Bibliography

[1] Abola E., Kuhn P., Earnest T., and Stevens R.C. *Nat. Struc. Biol.*, 7:p.973, **2000**.

[2] Claritge T. *High-resolution NMR techniques in organic chemistry*. Elsevier Science, **2008**.

[3] Kurhanewicz J., Vigneron D.B., Brindle K., Chekmenev E.Y., Deberardinis R.J., Green G.G., Riz R.R., Ross D.B., and Warren W.S. *Neoplasia*, 13:p.81, **2018**.

[4] Abragam A. *Principles of Nuclear Magnetism*. Oxford University Press, **1961**.

[5] kovacs H. and Moskau D.and Spraul M. *Prog. Nucl. Magn. Reson. Spectrosc.*, 46:p.131, **2005**.

[6] Fu R., Brey W.W., Shetty K., Gorkov P., Saha S., Long J.R., Grant S.C., Chekmenev E.Y., Hu J., Gan Z., Sharma M., Zhang F., Logan T.M., Brschweller R., Edison A., Blue A., Dixon I.R., Markiewicz W.D., and Cross T.A. *J. Magn. Reson.*, 177(1):p.1, **2005**.

[7] Colegrobe F., Schearer L., and Walters G. *Phys. Rev.*, 132:p.2561, **1963**.

[8] Kauczor H.-U.and Surkau R. and Roberts T. *Eur. Radiol.*, 8:p.820, **1988**.

[9] Abragam A.and Goldman M. *Reports on Progr. Phys.*, 41(3):p.395, **1978**.

[10] Sze K.H., Wu Q., Tse H., and Zhu. G. *Dynamic Nuclear Polarization: New Methodology and Applications*. Springer Berlin Heidelberg, **2012**.

[11] Ardenkjær-Larsen J.H., Fridlund B., Gram A., Hansson G., Hansson L., Lerche M.H., Servin R., Thaning M.l, and Golman K. *PNAS*, 100(183):p.10158, **2003**.

[12] Nelson S.J., Kurhanewicz J., Vigneron D.B., Larson P.E., Harzstark A.L., Ferrone M., van Criekinge M., Chang J.W., Bok R., Park I., Reed G., Carvajal L., Smal E.J., Munster P., Weinberg V.K., Ardenkjær-Larsen J.H., ChenA. P., Hurd R. E., Odegardstuen L.I., Robb F.J., Tropp J., and Murray J.A. *Sci. Transl. Med.*, 5:p.198ra108, **2013**.

[13] Lippert A.R., keshari K.R., Kurhanewicz J., and Chang C.J. *J.Am. Chem. Soc.*, 133:p.3776, **2011**.

[14] Warren W.S., Jenista E., Branca R.T., and Chen X. *Science*, 323:p.1711, **2009**.

[15] Billingsley K.L., Josan S., Park J.M., Tee S.S., Spielman-Sun E., Hur R., Mayer D., and Spielman D. *NMR Biomed.*, 27(3):p.356, **2014**.

[16] Kohler S.J., Yen Y., Wolber J., Chen A.P., Albers M.J., Bok R., Zhang V., Tropp J., Nelson S., Vigneron D.B., Kurhanewicz J., and Hurd R.E. *Magn. Reson. Med.*, 58(1):p.65, **2007**.

[17] Lumata L., Merritt M.E., Malloy C.R., Sherry A.D., Tol J., Song L., and Kovacs Z. *J. Magn. Reson.*, 227(0):p.14, **2013**.

[18] Nanni E.A., Barnes A.B., Griffin R.G., and Temkin R.J. *Terahertz Science and Technology, IEEE Transactions on*, 1(1):p.145, **2011**.

[19] Maly T., Debelouchina G.T., Bajaj V.S., Hu K.-N., Joo C.-G., MakJurkauskas M.L., Sirigiri J.R., van der Wel P. C.A., Herzfeld J., Temkin R.J., and R.G. Griffin. *J. Chem. Phys.*, 128(5):p.052211, **2008**.

[20] Lumata L., Ratnakar S.J., Jindal A., Merritt M., Comment A., Malloy C., Sherry A.D., and Kovacs Z. *Chem. Eur. J.*, 17(39):p.10825, **2011**.

[21] Miville P., Ahuja P., Sarkar R., Jannin S., Vasos P.R., Gerber-Lemaire S., Mishkovsky M., Comment A., Gruetter R., Ouari O., Tordo P., and Bodenhausen G. *Angew. Chem. Int. Ed.*, 49(35):p.6182, **2010**.

[22] Carravetta M., Johannessen O.G., and Levitt M.H. *Phys. Rev. Lett.*, 92(15):p.153003, **2004**.

[23] Lumata L., Merritt M.E., Malloy C.R., Sherry A.D., and Kovacs Z. *J. Phys. Chem. A*, 116(21):p.5129, **2012**.

[24] Breslin D.T. and Fox M.A. *J. Phys. Chem.*, 97(50):p.13341, **1993**.

[25] Bordes B., Coletta F., Ferrarini A., Gottardi F., and Nordio P.L. *Chem. Phys.*, 231:p.51, **1998**.

[26] K.-N. Hu, Bajaj V.S., Rosay M., and R.G. Griffin. *J. Chem. Phys.*, 126(4):p.044512, **2007**.

[27] Hu K.-N. *Solid State Nucl. Magn. Reson.*, 40(2):p.31, **2011**.

[28] K.-N. Hu, Debelouchina G.T., Smith A.A., and Griffin R.G. *J. Chem. Phys.*, 134(12):p.125105, **2011**.

[29] Liu Y., F.A. Villamena, Rockenbauer A., Song Y., and Zweier J.L. *J. Am. Chem. Soc.*, 135(6):p.2350, **2013**.

[30] Dane E. L., Maly T., Debelouchina G.T., R.G. Griffin, and Swager T.M. *Org. Lett.*, 11(9):p.1871, **2009**.

[31] Muñoz-Gómez J.-L., Marín-Montesinos I., Lloveras V., Pons M., Vidal-Gancedo J., and Veciana J. *Org. Lett.*, 16:p.5402, **2014**.

[32] Becerra L.R., Gerfen G.J., Temkin R.J., Singel D.J., and Griffin R.G. *Phys.Rev. Lett.*, 71(21):p.3561, **1993**.

[33] AkbeyU., Franks W.T., Linden A., Lange S., Griffin R.G., van Rossum B.-J., and Oschkinat H. *Angew. Chem., Int. Ed. Engl.*, 49(42):p.7803, **2010**.

[34] Linden A., Lange S., Franks W.T., Akbey U., Specker E., van Rossum B.-J., and Oschkinat H. *J. Am. Chem. Soc.*, 133(48):p.19266, **2011**.

[35] Rossini A.J., Zagdoun A., Lelli M., Gajan D., Rascón F., Rosay M., Maas W.E., Copéret C., Lesage A., and Emsley L. *Phys.Rev. Lett.*, 71(21):p.3561, **1993**.

[36] Macholl S., Johannesson H., and J.H. Ardenkjær-Larsen. *J. Chem. Phys.*, 12:p.5804, **2010**.

[37] Rajca A., Mukherjee S., Pink M., and Rajca S. *J. Am. Chem. Soc.*, 128(41):p.13497, **2006**.

[38] Rajca A., Olankitwanit A., and Rajca S. *J. Am. Chem. Soc.*, 133(13):p.4750, **2011**.

[39] Shultz D.A., Fico R.M., Lee H., Kampf J.W., Kirschbaum K., Pinkerton A.A., and Boyle P.D. *J. Am. Chem. Soc.*, 125(50):p.15426, **2003**.

[40] Shultz D.A., Boal A.K., and Farmer GT. *J. Am. Chem. Soc.*, 119(16):p.3846, **1997**.

[41] Matsuki Y., Maly T., Ouari O., Karoui H., F. LeMoigne, Rizzato E., Lyubenova S., Herzfeld J., Prisner T., Tordo P., and Griffin R.G. *Angew. Chem. Int. Ed.*, 48(27):p.4996, **2009**.

[42] Mentink-Vigier F., Akbey U., Hovav Y., Vega S., Oschkinat H., and Feintuch A. *J. Magn. Reson.*, 224:p.13, **2012**.

[43] Mentink-Vigier F., Akbey U., Hovav Y., Vega S., Oschkinat H., and Feintuch A. *J. Magn. Reson.*, 224(0):p.13, **2012**.

[44] Rosay M., Tometich L., Pawsey S., and Bader R. *Phys. Chem. Chem.*, 12(22):p.5850, **2010**.

[45] Song C., Hu K.-N., Joo C.-G., Swager T.M., and Griffin R.G. *J. Am. Chem. Soc.*, 128:p.11385, **2006**.

[46] Woskov P.P., Bajaj V.S., Hornstein M.K., Temkin R.J., and Griffin R.G. *IEEE Trans. Microwave Theory Tech.*, 53:p.1863, **2005**.

[47] Song C., Hu K.-N., Swager T.M., and Griffin R.G. *J. Am. Chem. Soc.*, 128:p.11385, **2006**.

[48] Hu K.-N., Song C., Yu H.-H., Swager T.M., and Griffin R.G. *J. Chem. Phys.*, 128(5):p.052302, **2008**.

[49] Ysacco C., Rizzato E., Virolleaud M.-A., Karoui H., Rockenbauer A., Le Moigne F., Siri D., Ouari O., Griffin R.G., and Tordo P. *Phys. Chem. Chem. Phys.*, 12:p.5841, **2010**.

[50] Hartmann S.R. and Hahn E.L. *Phys. Rev.*, 128(5):p.2042, **1962**.

[51] Pearce C.M. and Williams D.H. *J. Chem. Soc. Perkin Trans. 2*, page p.153, **1995**.

Chapter 6

Polyradical systems

6.1 Introduction

6.1.1 Dendrimers

The development of nanomaterials, based on nanometer size particles, is one of the major challenges for this century. Nanosized molecules are also attracting a considerable attention, and a particular emphasis is put on the special class of polymers known as dendrimers (tree-like molecules). Over the past few decades much interest has been developed in this group of macromolecules having either an organic, supramolecular, or coordination nature.

Dendrimers are a hyperbranched class of polymers of structurally controlled macromolecules with well defined sizes, shapes and even chemical properties. Dendrimers usually have a globular appearance since they have a symmetrical structure that starts from the central core followed by an exponentially increasing number of repeating units that end at the terminal groups.[1] The globular shape with a regular and highly symmetrical structure of this macromolecules offers a wide range of unusual physical and chemical properties mainly due to the presence of internal cavities (guest-host system). In addition, a defined number of functional end groups per molecule, in contrast to common linear polymers, enables a full control over many of the molecular design parameters at the single molecular level.

Dendrimers have three different structural domains (**Figure 6.1**): a central *core* which can be either a single atom or a group of atoms[2] having at least two identical functional groups. *Branches*, that emerge from the core and are constituted of repetitive units having at least one branch junction and whose repetition is organized in a spherical progression giving the different generations of the dendrimer. Finally, *terminal functional groups*, located at the exterior of the dendrimers, which play an important role in their properties.

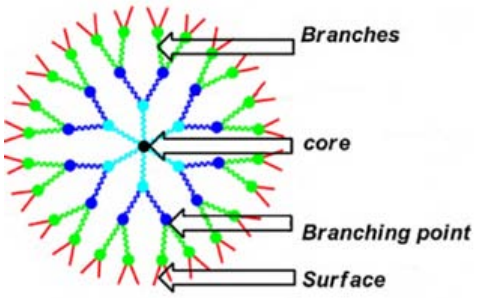

Figure 6.1: Description of the main components of dendrimers.

The synthesis of highly controlled dendrimer architectures has increased in importance due to the rising demand for special polymers that posses novel properties. There are two main methodologies for the synthesis of dendrimers.[3]

- The convergent method (**Figure 6.2a**), in which the dendrimers are built from smaller groups of molecules called dendrons which, as a final step, react with a multifunctional core in order to generate the corresponding dendrimer generation.
- The divergent method (**Figure 6.2b**) that builds up the dendrimer step by step from a multifunctional core which extends outwards through a series of consecutive reactions.

Each method presents advantages and disadvantages. Thus, dendrimers built up by the convergent method are easier to purify than those synthesized by the divergent method. However, the size of dendrimers built by the convergent approach is usually smaller due to the steric effect of the dendron size in the final coupling step with the core.

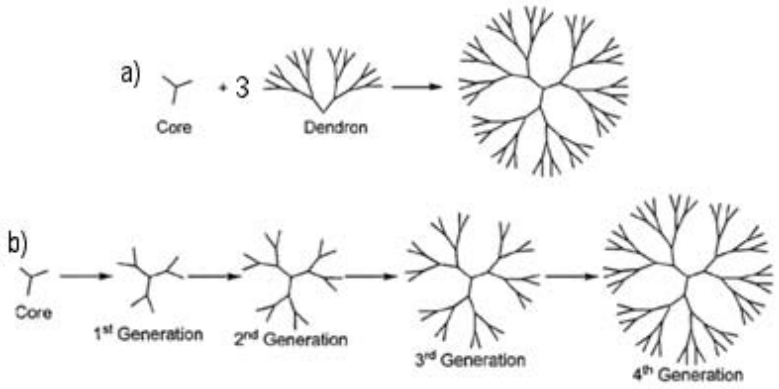

Figure 6.2: Synthesis of dendrimers by a) convergent and b) divergent methods.

The first dendrimers were prepared by the divergent strategy by Vögel[4] and co-workers in 1978. Since then, some researchers have been working with this approach with dif-

ferent atomic cores such as germanium[2] or silicon[5] atom cores using alkenylation followed by hydrogermilations/ hydrosilations to generate the corresponding dendrimers. Other examples are organic cores such as aromatic rings[6], amines[7] *e. g.* PAMAM dendrimers (builded up by a Michael addition followed by amidation), or cores based on phosphorous[8] built by a nucleophilic substitution of chlorine leading phosphodiester compounds followed by an hydrazone bond. In 1990 a convergent synthesis approach was introduced by Fréchet and coworkers with the synthesis of polyether dendrimers, based on 3,5-dihydroxybenzyl alcohol as a monomer.[3] Another example of convergent synthesis are phenylacetilene dendrimers reported by Moore and coworkers.[9]

Nowadays, most of the efforts in this field are mainly directed towards the development of dendrimer applications rather than for dendrimer design. Dendrimers are a very attractive field of research in areas such as nanomedicine,[21] cavity studies (host-guest), in chelate chemistry,[20] nanomedicine,[21] or the use of radical dendrimers[16–19], PAMAM modified with nitroxide radicals for the study of interactions between peptides, and phosphorous dendrimers for monocite activation.[22] The use of dendrimers in nanoscience for surface modifications has also been reported by Caminade' s group[23–25] for the preparation of biochips. These are just a few examples of dendrimer applications in a wide range of areas of research.

6.1.1.1 Dendrimer characterization techniques

As dendrimers belong to both the molecular world (for their step by step controlled synthesis), and to the polymer one (because of their repetitive structure made of monomers) they benefit from the analytical techniques of both worlds. *Nuclear Magnetic Resonance* (NMR) is certainly the most widely used technique in routine analysis for dendrimer characterizations. Rutine NMR analysis are specially useful during the step by step synthesis of dendrimers, even up to high generations, because they afford information about the chemical transformations that undergo by the end groups. ^{1}H and ^{13}C NMR are the most used ones even though ^{31}P NMR is specially useful in phosphorous containing dendrimers.[10–13] The *infra-red* (IR) technique is mainly used for the routine analysis of the chemical transformations occurring at the surface of dendrimers, such as the disappearance of aldehydes or the formation of characteristic bonds as amides or esters.[14] Due to their mass limitations, classical *Mass Spectometry* techniques such as, chemical ionization or fast atom bombardment (FAB), can be used only for characterization of small dendrimers, whose mass are < 3000 D.[3] For higher molecular weights, techniques developed for the characterization of proteins and polymers have to be applied. Indeed, ElectroSpray Ionization (ESI) can be used for dendrimers able to form stable multicharged species. The only technique useful for theorically unlimited masses is Matrix Assisted Laser Desorption Ionization Time of Flight (MALDI-TOF).[15] However, the supposed mildness of this technique is questionable for dendrimers absorbing light at the wavelength of the laser used for desorption. Techniques for polymer characterization like *Size Exclusion Chromatography* are also useful for dendrimer characterization since allows the separation of molecules according to size and the different generations

of dendrimer.

6.1.2 Radical dendrimers

Combination of the globular well-defined structure, low polydispersity and nanoscopic dimensions of dendrimers with the functional properties of radicals is one of the focal points of current research in dendritic molecules.[26–29] The architecture of radical dendrimers may give rise to new properties as, for example, molecular recognition, catalysis, and molecule-based electronics and optics. Functional radicals can also be introduced at the core of the dendrimer,[17] as pendant groups at the dendrimer surface,[16] or as noncovalently bonded encapsulated guests.[30]

An increasing number of dendrimers are being functionalized with stable organic radicals or redox active groups, aiming at materials with a wide variety of functional properties. So, high-spin molecules formed by organic radicals incorporated into a π-conjugated hyperbranched topology have been studied with the aim of obtaining organic magnetic materials.[31] In these kinds of radical dendrimers, dendritic branching is used to ensure a more robust intramolecular spin alignment that those obtained with linear or classically branched structures. The electrical conductivity of poly(amido amine) dendrimers with naphthalene diimide anion-radical as end groups, forming π-dimers or π-stacks, has been reported.[31] Redox active end groups, such as tetrathiafulvene and ferrocene, have also been attached at the periphery of dendrimers, as pendant groups. In these cases, multielectron oxidations to the corresponding cations can be accomplished.[32]

The interaction between pendant functional groups at the exterior of the dendritic surface and their dynamic behavior is of fundamental importance for understanding the magnetic properties of dendrimers. Magnetic interactions between neighboring radicals, not only in radical dendrimers, but also in radical polymers, gold nanoparticles or other supramolecular species, determine the most important properties of these compounds in different applications, like conducting systems, batteries, contrast agents for MRI, nanomagnetic materials, etc. In analogy to their linear macromolecular counterparts, the dynamic behavior of radical pendant groups and their mutual interactions can be probed using electron paramagnetic resonance (EPR) spectroscopy when the functional groups are stable radicals.[33] In the NANOMOL group we are developing this type of new molecules and their study by EPR with the same purpose as well as for studying their behavior in new applications,[18,19] such as, for example, contrast agents for MRI. Nowadays, radical dendrimers, in particular those water soluble, are a good option to be explored as contrast agents in order to avoid the gadolinium chelates currently used. To be a good candidate for MRI, the molecule has to have a large magnetic moment and null toxicity.

This Chapter is focused on the preparation of dendrimers, modification of their surface and functionalization with radicals of different families with the purpose of

obtaining polyradical dendrimers with magnetic properties for applications in Material Science and Nanomedicine.

For the functionalization of dendrimers with radicals we choose the family of phosphorous dendrimers having a phosphazene ring as a core, branched also with phosphorous atoms with aldehydes as terminal groups. The reason to use such dendrimers was the possibility to prepare a complete series of generations with high uniformity and low number of defects. Those phosphorous dendrimers ended with aldehyde groups offer the possibility to use several kind of reactions enabling to bond radical units with a great variety of linkers.

The aldehyde end groups of dendrimers can be modified, in mild conditions, with phosphonates by a Wittig reaction (**Scheme 6.1a**) to obtain vinyl derivatives, with hydrazines to form the corresponding hydrazones (**Scheme 6.1b**), with amines to form the imine derivatives (**Scheme 6.1c**), with organometallic derivatives to generate terciary alcohols (**Scheme 6.1e**) and with malonic acid to introduce a carboxilic acid group (**Scheme 6.1d**), among other possibilities.

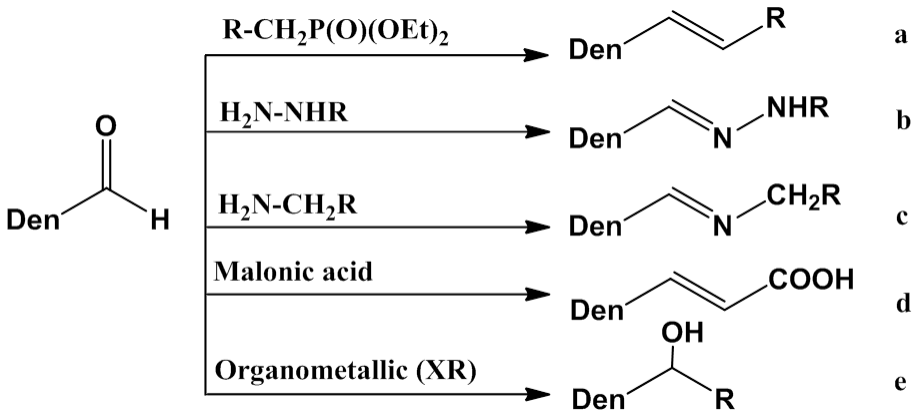

Scheme 6.1: Description of possible reactions on terminal aldehyde of dendrimers.

As radical units of dendrimers we choose PTM radicals since the magnetic properties of this radical unit arranged in such molecules have never been explored before. We also choose TEMPO and PROXYL radicals units as terminal radical units since the resulting polyradical dendrimers could be soluble in water and useful as contrast agents in MRI technique.

6.2 Phosphorous Dendrimers

As already mentioned, we choose the phosphorous dendrimers described in **Scheme 6.2** as precursor of radical dendrimers. For their preparation we followed the methodology previously described by the group of Caminade and coworkers.[34]
The synthesis of such phosphorous dendrimers involved two main synthetic steps. Starting from hexachlorocyclotriphosphazene (**62**) and by reaction with *p*-hydroxybenzaldehyde in basic media (Cs_2CO_3), the core of the zero generation, Gc_0 (**63**) was obtained. In a second step this product reacted with dichlorophosphonomethylhydrazide (**64**) to obtain the next dendrimer generation ending in chlorine atoms, (Gc_1 **65**). This two steps were repited since obtaining the desired generation. So, **65** was reacted with *p*-hydroxybenzaldehyde under the same conditions as before to obtain the next generation ending with aldehyde group Gc_1' (**66**), and so on with the following generations Gc_2 (**67**), Gc_2' (**68**), Gc_3 (**69**) and Gc_3' (**70**)(**Scheme 6.2**).

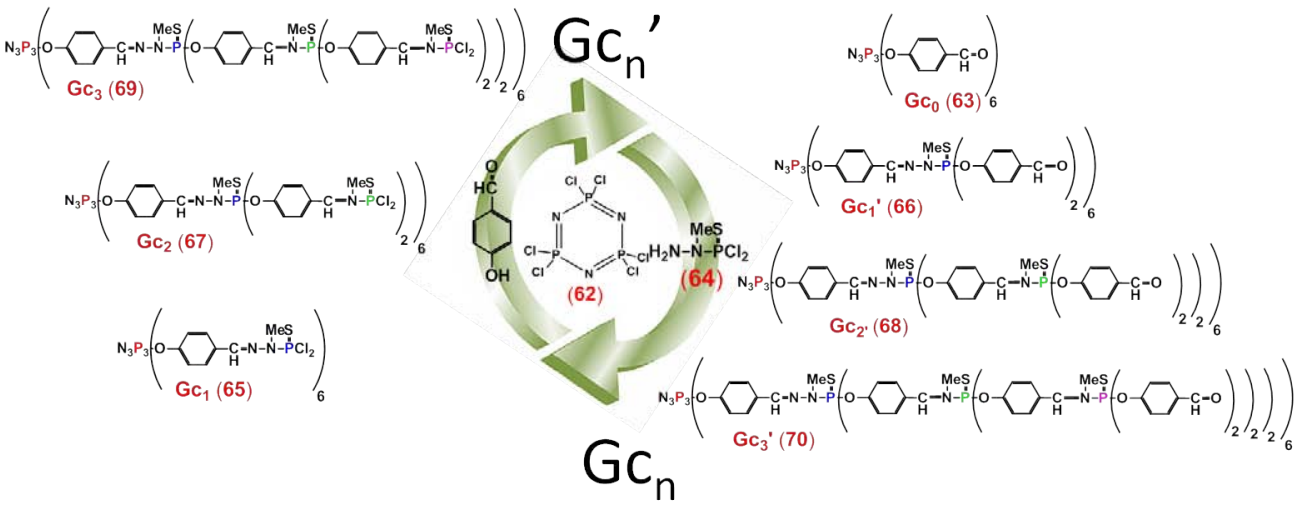

Scheme 6.2: Description of the synthesis of different generations (Gc_n and Gc_n') of phosphorous containing dendrimers.

^{31}P NMR spectroscopy has been shown to be an extraordinary useful tool for following the synthetic growth of phosphorous containing dendrimers and controlling the progress of all reactions performed either in the internal layers or on the surface. Indeed, each generation gives a different chemical shift (**Figure 6.3**), and substitution reactions on the surface generally result in a shielding or deshielding effect of the P signal. Moreover, the purity of the product can be easily checked by ^{31}P NMR spectroscopy because it can be detected any signal corresponding to the presence of a subproduct due to degradation.

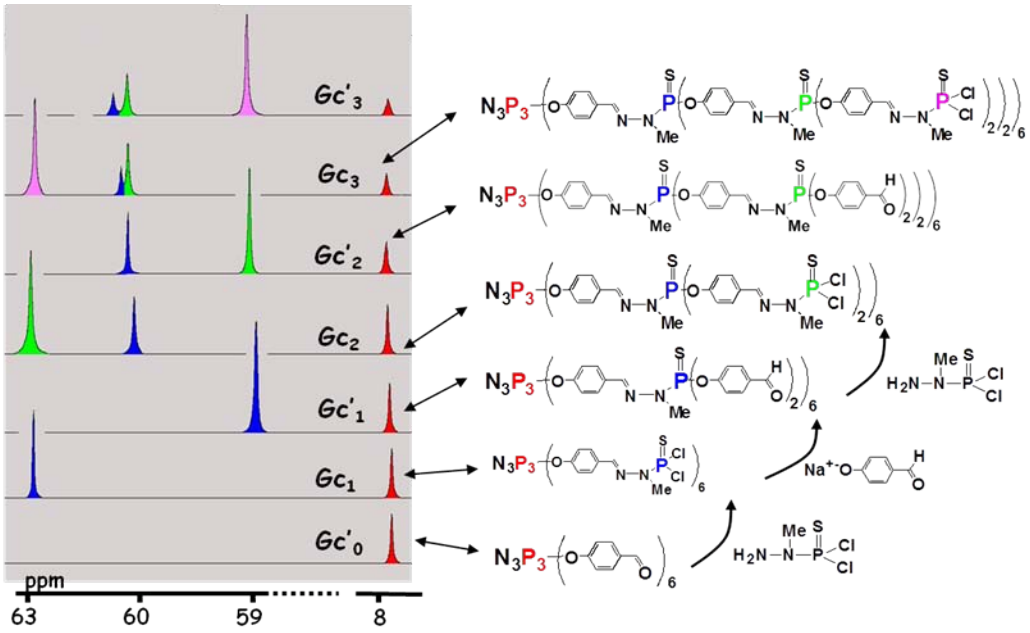

Figure 6.3: Example of NMR signals for each phosphorous dendrimer generation.

The synthesis of the phosphorous containing dendrimers were initially carried out under the same conditions described in the literature,[34] but then we performed some modifications that improved the yields. Thus, the synthesis of Gc_0 (**63**) was performed with different amounts of aldehyde using always a double amount of Cs_2CO_3 as a base, controlling the ratio of hexachlorocyclotriphosphazene (**62**)/solvent, the temperature and time of reaction. **Table 6.1** shows the different conditions assayed. The best results were obtained starting at 0 °C for 10 minutes and then at room temperature 4h 50 minutes, giving **63** as a white powder with a 97 % yield (entry 3, **Table 6.1**).

Table 6.1: Experiments to afford Gc_0 (**63**).

Entry	Aldehyde (eq.)	Cs_2CO_3 (eq.)	THF (ml/ g core)	T (^{0}C)	time (h)	Product	Gc_0 Yield (%)
1	7	14	60	room	18	Not pure	-
2	9	18	60	room	18	Not pure	-
3	8	16	40	0 to room	5	Pure	97

The preparation of dichlorophosphonomethylhydrazide (**64**) is a crucial step as it is repeatedly used in each generation and it is extremely sensitive to water. This reaction was carried out at −60 °C in chloroform/N_2 bath to avoid the formation of subproducts. Two equivalents of methylhydrazine in anhydrous $CHCl_3$ were used in this reaction, since one acts as a reagent and the other as a base. Its addition has to be done slowly to avoid an increase of temperature. It is extremely important to fix

the temperature between −60 °C and −50 °C because below −60 °C the reaction mixture is frozen and above −50 °C appear sideproducts of polysubstitution as detected by ^{31}P NMR. The prepared dichlorophosphonomethylhydrazide (**64**) solution in anhydrous $CHCl_3$ was stored in the fridge and directly used in the synthesis of each generation.

The first generation ending with chlorine atoms Gc_1 (**65**) was a very sensitive compound due to the presence of the unstable chlorine-phosphorous bonds. Because of that, the conditions were strictly anhydrous. In **Table 2** we sum up the different conditions used for the synthesis of **65**. The best results were achieved with 7.5 eq. of dichlorophosphonomethylhydrazide (**64**) at 0 °C for 1 hour and then 17 hours more at room temperature (entry 3, **Table 6.2**) yielding **65** with a 98%.

Table 6.2: Experiments to afford Gc_1 (**65**).

Entry	Hidrazide (eq.)	THF (ml/ g Gc_0)	T (^{0}C)	time (h)	Gc_1 Yield (%)
1	7	15	room	18	-
2	7	20	room	18	-
3	7.5	12	0 to room	18	98

The first generation ending with aldehyde group, Gc_1' (**66**) was also a very sensitive reaction, due to the presence of the unstable chlorine-phosphorous bonds. In **Table 6.3** we sum up the different conditions used. The best results were achieved with 16 eq. of *p*-hydroxybenzaldehyde at 0 °C for 30 minutes and 18 hours at room temperature (entry 4, **Table 6.3**) yielding **66** with a 97%.

Table 6.3: Experiments to afford Gc_1' (**66**).

Entry	Aldehyde (eq.)	Cs_2CO_3 (eq.)	THF (ml/ g Gc_1)	T (^{0}C)	time (h)	Product	Gc_1' Yield (%)
1	12.5	24	80	room	18	Not pure	-
2	15	24	50	room	18	Not pure	-
3	18	24	40	room	18	Not pure	-
4	16	32	11	0 to room	18	Pure	97

The second dendrimer generation ending with chlorine atoms, Gc_2 (**67**), was also a very sensitive compound due to the presence of 24 chlorine-phosphorous bonds. In this reaction, the precipitation with pentane was a very important step, as the water traces degradates the product. So, we had to use freshly distilled pentane over P_2O_5 under N_2. The best results were achieved with 15 eq. of dichlorophosphonomethylhydrazide (**64**) at 0 °C for 30 minutes and 3.5 hours more at room temperature (entry 3, **Table 6.4**) yielding **67** with a 99%.

Table 6.4: Experiments to afford Gc_2 (**67**).

Entry	Hidrazide (eq.)	THF (ml/ g Gc_1')	T (^{0}C)	time (h)	Product	Gc_2 Yield (%)
1	12.6	25	room	18	Not pure	-
2	15	20	room	18	Not pure	-
3	15	20	0 to room	4	Pure	99

The second dendrimer generation ending with aldehyde group Gc_2' (**68**) was obtained with good purity and yield under two different experimental conditions (entries 2 and 3, **Table 6.5**). The low volume of solvent makes the last one the best conditions for carrying out the reaction (entry 3, **Table 6.5**).

Table 6.5: Experiments to afford Gc_2' (**68**).

Entry	Aldehyde (eq.)	Cs_2CO_3 (eq.)	THF (ml/ g Gc_2)	T (^{0}C)	time (h)	Product	Gc_2' Yield (%)
1	32	64	50	room	4	Not pure	-
2	32	64	25	0 to room	4	Pure	97
3	32	64	16	0 to room	4	Pure	97

The third dendrimer generation ending with chlorine atoms Gc_3 (**69**) was obtained after having done some tests with anhydrous atmosphere and molecular sieves (**Table 6.6**) in order to eliminate completely the generated water. It was an extremely sensitive compound as well, due to the presence of 48 chlorine-phosphorous bonds. After some failed attempts, the Gc_3 generation was obtained with 30 eq. of dichlorophosphonomethylhydrazide (**64**) at 0 °C for 30 minutes and then 3.5 hours more at room temperature (entry 4, **Table 6.6**) with a 99 % yield. In this particular case we avoided to dry completely the product and the solvent of the reacting mixture was removed until half the initial volume and then freshly distilled anhydrous pentane was added to precipitate Gc_3.

Table 6.6: Experiments to afford Gc_3 (**69**).

Entry	Hidrazide (eq.)	THF (ml/ g Gc_2)	T (^{0}C)	time (h)	Product	Gc_3 Yield (%)
1	30	10	0 to room	4	Degraded	-
2	26.4	20	0 to room	4	Degraded	-
3	26.4	20/ Molecular sleeves	0 to room	4	No product	-
4	30	40	0 to room	4	Pure	99

The third generation ending with aldehyde group Gc_3' (**70**) was obtained using the experimental conditions optimized for Gc_2' (**68**); *i. e*, 1.33 eq. of *p*-hydroxybenzaldehyde

per each chlorine, twice the amount of base than aldehyde and similar solvent ratio (16 ml/g Gc_3). The product was isolated as a white powder with a high yield (93%).

All dendrimer generations were characterized by IR, MALDI-TOF and NMR (^{1}H and ^{31}P).

Since we were interested in obtaining water soluble dendrimers for applications as contrast agents for MRI, we decided to convert aldehyde terminal group of phosphorous dendrimers **63** and **66** into acid group. For that we used a Knoevenagel[24,35–37] reaction (**Scheme 6.3**).

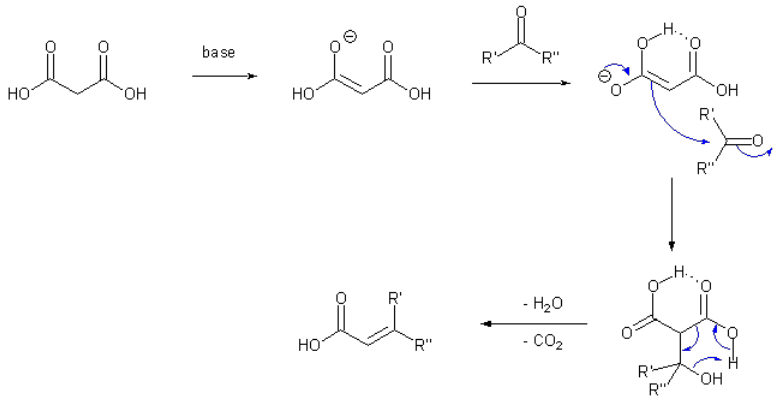

Scheme 6.3: Knoevenagel reaction mechanism.

Following the contribution reported in literature,[24] it was performed the modification of Gc_0 (**63**) and Gc_1' (**66**) treating both dendrimers with an excess of malonic acid and piperidine (**Scheme 6.4**). The resulting mixtures were then dissolved, under Ar atmosphere, in anhydrous pyridine and heated to 95°C for 4 hours. After that, the mixture was heated to reflux in order to induce the decarboxilation and to afford the desired acid dendrimers Gc_0COOH (**71**) and Gc_1COOH (**72**) with quantitative yields which were characterized by IR, MALDI-TOF and NMR (^{1}H and ^{31}P). **Table 6.7** summarizes the experimental conditions for each generation. For more details see Chapter 8 (Experimental details).

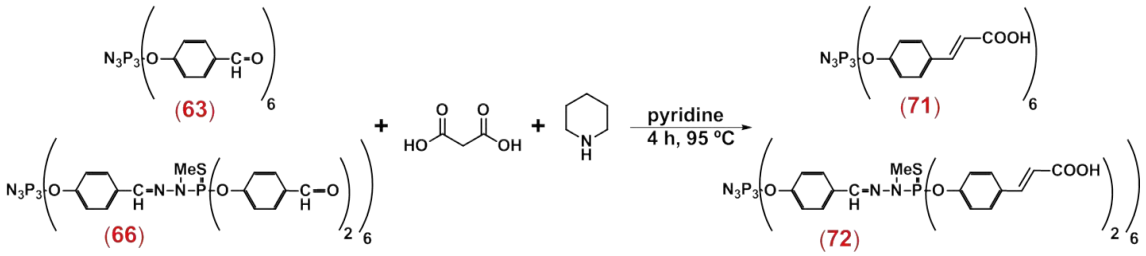

Scheme 6.4: Synthesis of dendrimers **71** and **72** ended with acid group using malonic acid.

Table 6.7: Experimental conditions to afford dendrimers Gc_0COOH (**71**) and Gc_1COOH (**72**).

Compound	Dendrimer	Malonic acid (eq)	Piperidine (eq)	Pyridine (ml)	Yield (%)
Gc_0COOH (**71**)	Gc_0	7.5	1.5	3	99
Gc_1COOH (**72**)	Gc_1'	7.5	1.5	9	99

The resulting dendrimers were found to be insoluble in some organic solvents and soluble in basic water solutions, as expected. In fact, Gc_0COOH is soluble in water at low concentrations whereas the larger generation Gc_1COOH is insoluble. Due to this reason we did not synthesize larger generations of acid dendrimers as long as our interest was focused on water soluble compounds.

6.3 Polyadical dendrimers

6.3.1 Dendrimers with terminal PTM radicals

Synthesis

Several PTM radical derivatives have been used to explore their magnetic properties as monoradicals, biradicals or triradicals. However, the magnetic properties have never been explored in polyradicals. For such a reason we decided to synthesize a complete family of dendrimers with terminal PTM radical units.

The synthesis of such dendrimers involves the chemical modification of the surface of dendrimers ending with aldehyde group by a Wittig-Horner-Emmons reaction with the phosphonate derivative of PTM **9**.[38] This selective reaction involves the formation of a double bond (**Scheme 6.1a**) with *E* conformation between the carbon atom of aldehyde group and the carbon atom to the phosphonate derivative.

The preparation of PTM dendrimers was performed in such a way for the four generations following the one pot reaction described in **Scheme 6.5** using the experimental conditions summarized in **Table 6.8**. Thus, in a Schlenk a mixture of an excess of diethyl 4-[bis(2,3,4,5,6-pentachlorophenyl)methyl]-2,3,5,6-tetrachlorobenzyl phosphonate (**9**) and potassium *tert*-butoxide were dissolved in anhydrous THF, under Ar atmosphere. The mixture, has a purple color of the PTM anion, was stirred for 10 minutes with the purpose of forming the phosphonium salt. After that, 1 equivalent of the generation of dendrimer (Gc_0 (**63**) or Gc_x' , where x= 1 (**66**), 2 (**68**) or 3 (**70**)) was added dissolved in anhydrous THF. The resulting mixture was then stirred until no aldehyde was detected following the reaction by IR-ATR and NMR. Once the reaction was finished, the oxidation of the PTM anion units to the PTM radical was performed using an excess of $AgNO_3$ in ACN. The conversion of $Gc_x(PTM^-)_y$ to $Gc_x(PTM^\bullet)_y$ in presence of $AgNO_3$ as oxidant, was monitored by UV-Vis by the disappearance of the 520 nm band (corresponding to its HOMO-LUMO transition) and the appearance of the band at 385 nm (corresponding to the transition from SOMO (Singly Occupied Molecular Orbital) to LUMO, of more energy).

During some preliminary test it was observed that a long exposition to $AgNO_3$ of the reaction mixture generated a very polar impurity, as detected by thin layer chromatography. For this reason, it was tried to reduce the time of exposition of dendrimers to silver nitrate in order to avoid any degradation. In all cases, 10-12 minutes of $AgNO_3$ exposure were enough to get the quantitative formation of the radical (see **Figure 6.4**). The oxidation was performed in homogeneous media ($AgNO_3$ dissolved in ACN) but it also procedeed completely under heterogeneous media with similar duration.

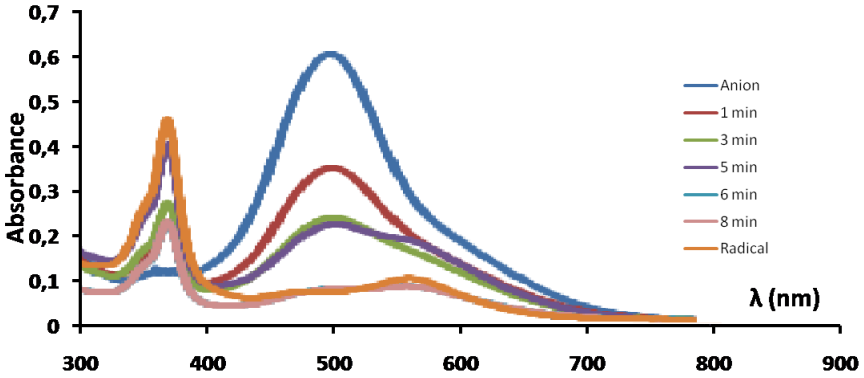

Figure 6.4: Example, of the conversion of $Gc_0(PTM^-)_6$ into $Gc_0(PTM^\bullet)_6$ *vs* time (min), using $AgNO_3$ as oxidant agent, followed by UV-Vis.

After the complete oxidation of the PTM anion units, the reaction mixture was filtered in order to eliminate the solid silver formed in the reaction and the excess of $AgNO_3$. Finally, the solvent was removed under vacuum and the products purified by column chromatography on Bio-Beads^{TM}gel (size exclusion chromatography) with THF (HPLC grade) as eluent obtaining the pure products as brown-green powders which were characterized by NMR, CV, EPR and MALDI-TOF.

Table 6.8: Experimental conditions to obtain PTM dendrimers **73**, **74**, **75** and **76**.

Compound	Dendrimer	^{t}BuOK (eq)	PTM (**9**) (eq)	$THF_{anh.}$ (ml)	time (h)	$AgNO_3$ (eq)	Yield (%)
$Gc_0(PTM^\bullet)_6$ (**73**)	Gc_0	14	7.2	5	18	8+8	38
$Gc_1(PTM^\bullet)_{12}$ (**74**)	Gc_1'	31	14.4	5	18	16+16	55
$Gc_2(PTM^\bullet)_{24}$ (**75**)	Gc_2'	57.6	28.8	5	18	28.8+28.8	40
$Gc_3(PTM^\bullet)_{48}$ (**76**)	Gc_3'	115.6	57.6	5	48	60+60	35

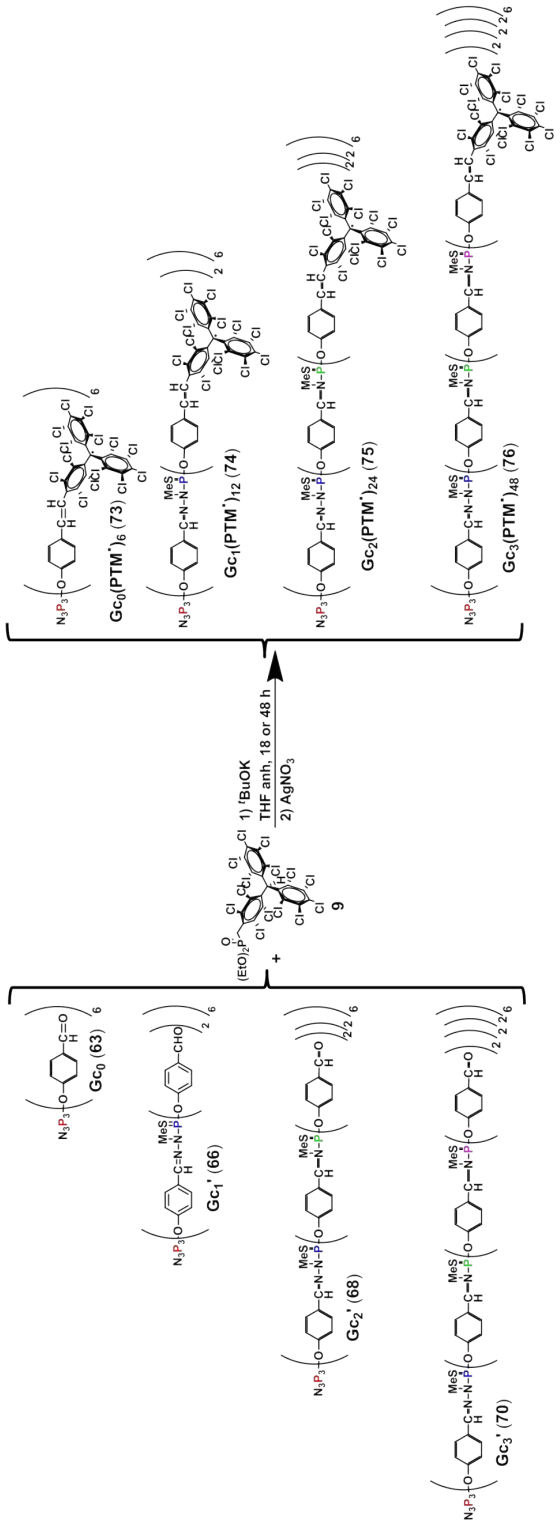

Scheme 6.5: One pot synthesis of the PTM radical dendrimers $Gc_0(PTM^{\bullet})_6$ (**73**), $Gc_1(PTM^{\bullet})_{12}$ (**74**), $Gc_2(PTM^{\bullet})_{24}$ (**75**) and $Gc_3(PTM^{\bullet})_{48}$ (**76**).

Electrochemical characterization

The electroactivity of PTM dendrimers allowed us to characterize the electrochemical properties of PTM radical dendrimers from the smallest ($Gc_0(PTM^{\bullet})_6$ (**73**)) to the largest generation ($Gc_3(PTM^{\bullet})_{48}$ (**76**)) by cyclic voltamperometry (CV).[40] CVs were performed using a platinum wire as auxiliary electrode, a graphite as working electrode, and a silver wire as the reference electrode. The electrolyte employed in all analysis were freshly prepared solutions of 20 mM $n\mathrm{BuN_4}^{+}\mathrm{PF_6}^{-}$ in anhydrous THF, previously degassed with argon. Ferrocene was used as an internal standard reference which in these conditions shows a reversible oxidation process at $E_{\frac{1}{2}} = 0.57$ V (see the ferrocene redox process in **Equation 6.1**). For further information about cyclic voltametry, see Annex C.

$$[Fe(C_5H_5)_2] \rightleftharpoons [Fe(C_5H_5)_2]^{+} + e^{-} \tag{6.1}$$

Voltamperograms of PTM dendrimers **73**, **74**, **75** and **76** (**Figure 6.5**) showed a quasi-reversible with an cathodic peak (E_{cp}) that corresponds to the transition of $Gc_n(PTM^{\bullet})_y$ to $Gc_n(PTM^{-})_y$) and a anodic peak (E_{ap}) that returns $Gc_n(PTM^{-})_y$ to $Gc_n(PTM^{\bullet})_y$. The CVs were carried out at different scan rates. All PTM radical dendrimers showed to be stable and reversible after ten cycles of reduction-oxidation process. As an example, in **Figure 6.6** it is shown the voltamogram of the first generation **74**.

The voltamperogram of the smallest generation, $Gc_0(PTM^{\bullet})_6$ (**73**), shows the most defined catodic and anodic peaks. However, in larger generations the voltamperogram waves are broader and with some shoulders, as shown in **Figure 6.7**. As can be seen in **Figure 6.5** there is a shift in the half-wave position, $E_{\frac{1}{2}}$, of the dendrimer being more negative on increasing the generation. This shift can be attributed to the increasing difficulty of forming the anions, when the number of radical units increase, due to the electrostatic repulsion among the neighboring anions already formed on the dendrimer surface. $Gc_3(PTM^{\bullet})_{48}$ (**76**) shows a cyclic voltametry too broad to extract the potential values with enough accuracy exhibiting a shoulder (**Figure 6.5**). The electrochemical data are summarized in **Table 6.9**.

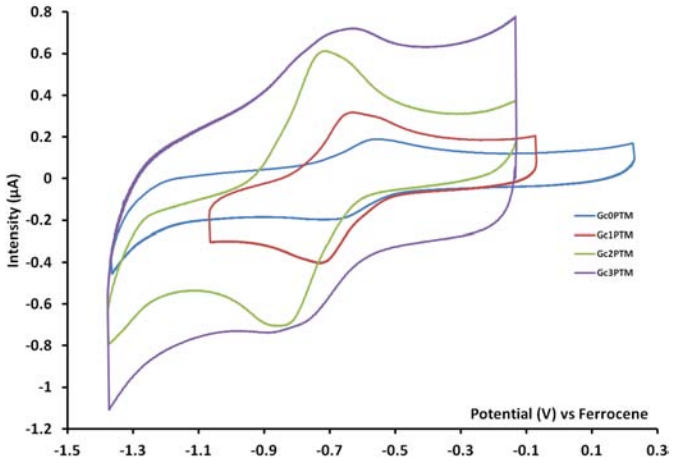

Figure 6.5: Voltamperograms of $Gc_0(PTM^{\bullet})_6$ **73**) in blue; $Gc_1(PTM^{\bullet})_{12}$ **74** in red; $Gc_2(PTM^{\bullet})_{24}$ **75** in green; and $Gc_3(PTM^{\bullet})_{48}$ **76** in purple. All of them with scan rate of 0.2 V/s.

Table 6.9: Experimental data extracted from **73**, **74**, and **75** PTM dendrimers voltamperograms.

Entry	E_{ap} (V)	E_{cp} (V)	$E_{\frac{1}{2}}$ [a] (V)
$Gc_0(PTM^{\bullet})_6$ (**73**)	-0.58	-0.66	-0.62
$Gc_1(PTM^{\bullet})_{12}$ (**74**)	-0.65	-0.73	-0.69
$Gc_2(PTM^{\bullet})_{24}$ (**75**)	-0.73	-0.85	-0.79

[a]Error for the wave potential of the third generation dendrimer are larger because the wave are to broad.

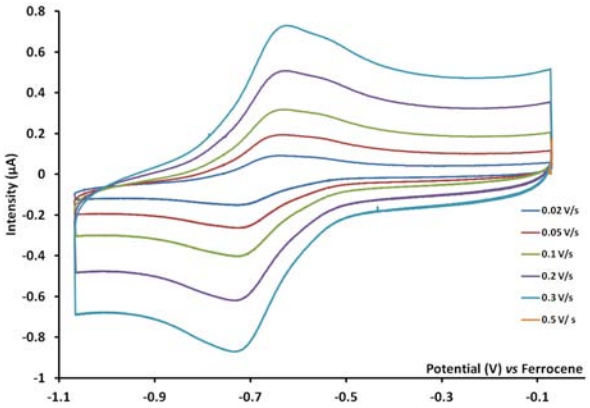

Figure 6.6: Voltamperogram of $Gc_1(PTM^{\bullet})_{12}$ (**74**) at different scan rates.

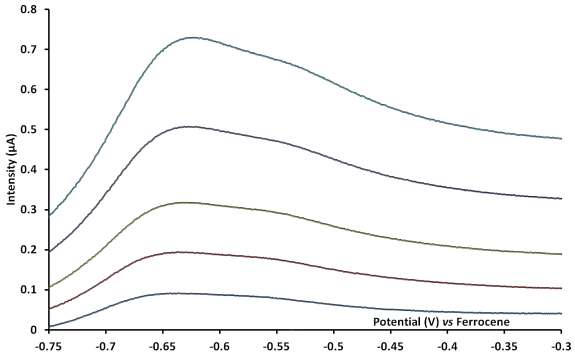

Figure 6.7: Scan rate dependence of the current of $Gc_1(PTM^{\bullet})_{12}$ (**74**).

Magnetic characterization

The study of the magnetic properties of dendrimers was carried out by magnetometry using a SQUID (Superconducting Quantum Interference Device) with an external magnetic field of 5 T in the temperature range of 2 and 300 K. The plots of χ_mT (cm^{-3}·K·mol^{-1}) *vs* temperature (K) for radical dendrimers $Gc_0(PTM^{\bullet})_6$ (**73**) and $Gc_1(PTM^{\bullet})_{12}$ (**74**) (**Figure 6.8**), shows that both compounds follow the Curie-Weiss law with weak antiferromagnetic interactions among PTM radicals units at low temperatures (below *c. a.* 40 k). In addition, such plots at high temperature gave χ_mT values of 2.23 and 4.46 cm^{-3}·K·mol^{-1} for **73** and **74**, respectively. These values allowed us to calculate with **Equation 6.2** the number of radical units on their surface that behave magnetically independent at high temperature. These values are in total agreement with the theoretically value expected of 6 and 12 radical units/dendrimer.

$$\chi T = \frac{n}{8} g^2 s(s+1) = 0.375n \tag{6.2}$$

where g is the Landé factor or g factor of free electron (g=2.0023193) and s is the total moment of the free electron (s=1/2), and n the number of free electrons. The result for one free electron is χ_mT=0.375.

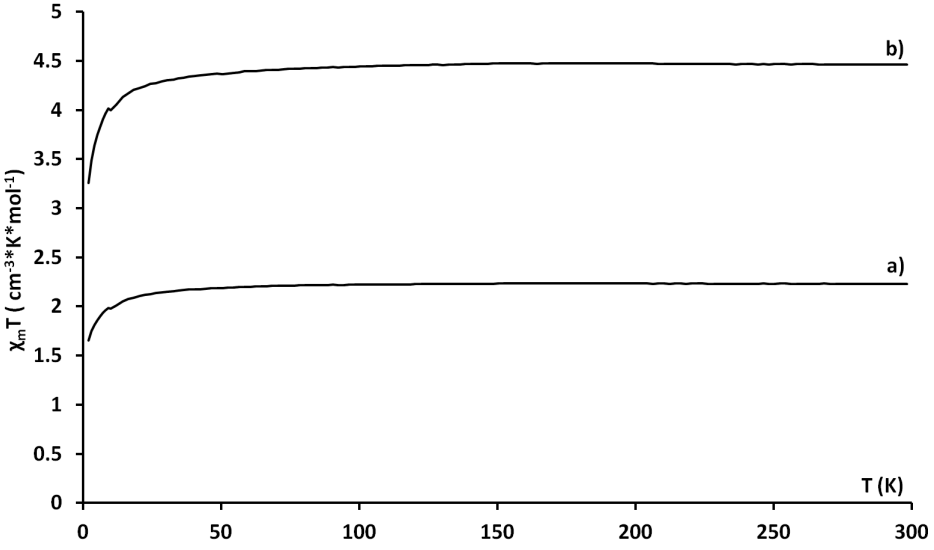

Figure 6.8: χ_mT vs T plots of dendrimers $Gc_0(PTM^{\bullet})_6$ (**73**) and b) $Gc_1(PTM^{\bullet})_{12}$ (**74**).

The magnetic characterization with SQUID magnetometry for the larger dendrimers was not performed due to the small amount of samples obtained and the high number of PTMs units on each dendrimer surface that generate big errors in the calculation of number of electrons per dendrimer.

Electron Paramagnetic Resonance (EPR) characterization

Before performing the characterization of the obtained series of dendrimers by EPR, it was though to obtain a monoradical as a model radical structurally similar to the terminal radical in the dendrimers. The synthesis of monoradical **78** (**Scheme 6.6**) consisted of three steps. Firstly, the protection of the hydroxyl group of *p*-hydroxybenzaldehyde with benzyl bromide using NaH as a base and TBAI to afford compound **77**. The second step, as in radical dendrimer synthesis, consisted of one pot reaction with two steps. In the first step the aldehyde of **78** is bond to PTM phosphonate (**9**) which was followed by the oxidation to the radical with $AgNO_3$. The monoradical **78** was obtained as a brown solid with a 78 % yield and it was characterized by IR, MALDI-TOF and EPR.

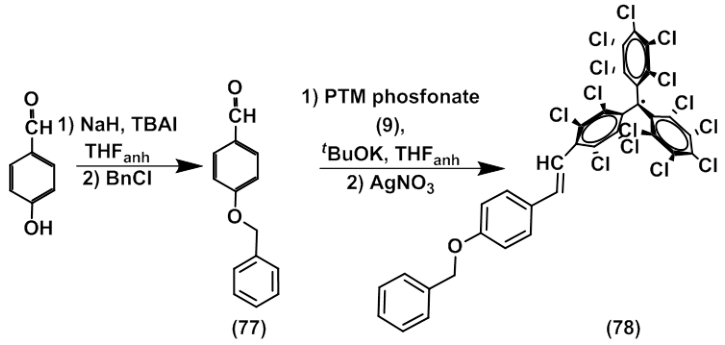

Scheme 6.6: Synthetic scheme for monoradical BnOPhCH=CHPTM$^\bullet$ (**78**).

The EPR spectra of all dendritic generations $Gc_0(PTM^\bullet)_6$ (**73**), $Gc_1(PTM^\bullet)_{12}$ (**74**), $Gc_2(PTM^\bullet)_{24}$ (**75**), $Gc_3(PTM^\bullet)_{48}$ (**76**), as well as of monoradical **78**, were recorded under the same isotropic conditions in solution ($3.5 \cdot 10^{-4}$ M) of each compound in toluene:dichloromethane 1:1 at room temperature. In these conditions, both g and hyperfine coupling constants (a) are averaged and therefore, the spectra are symmetric. The EPR spectra of monoradical **78** and polyradicals $Gc_0(PTM^\bullet)_6$, $Gc_1(PTM^\bullet)_{12}$, $Gc_2(PTM^\bullet)_{24}$, and $Gc_3(PTM^\bullet)_{48}$ are described in **Figure 6.10** and **Table 6.10** summarizes the experimental EPR parameters obtained from their respective spectra.

The EPR spectrum of monoradical **78** (**Figure 6.10a**) shows the two typical lines of a PTM monoradical with an ethylenic moiety due to the coupling of the unpaired electron with one H_a nuclei (**Figure 6.9**).

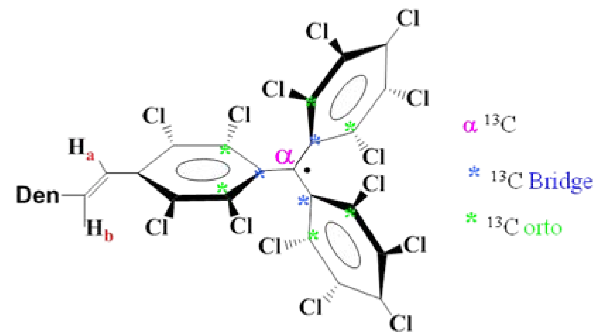

Figure 6.9: Atoms of a PTM derivative which interact with the unpaired electron.

The EPR spectrum of $Gc_0(PTM^{\bullet})_6$ (**73**) (**Figure 6.10b**) was similar to that of the monoradical but with a lower resolution due to the contribution of two main dendritic effects: 1) radical units are anchored on the dendrimer surface, so their tumbling are lower than in the free radical, and 2) the magnetic dipolar-dipolar interactions are favored because the proximity of radical units, which broaden the lines. In the case of $Gc_1(PTM^{\bullet})_{12}$ (**74**) and $Gc_2(PTM^{\bullet})_{24}$ (**75**) with 12 and 24 PTM radicals instead of 6, their interradical distance are closer, and the signal of the dendrimer wider so the dendrimer effects are stronger and consequently the EPR lines are overlaped and they appear as a one broad center line (**Figure 6.10c** and **d**). The EPR spectrum of the third generation exhibits more lines at higher fields that could be explained by the presence of unhomogeneous defects in the larger dendritic generation.

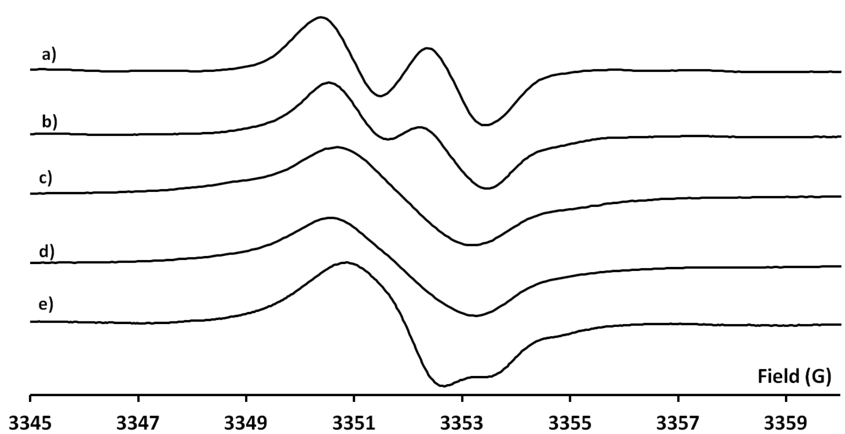

Figure 6.10: EPR spectra in solution under isotropic conditions of a) monoradical (**78**) and polyradicals b) $Gc_0(PTM^{\bullet})_6$ (**73**), c) $Gc_1(PTM^{\bullet})_{12}$ (**74**), d) $Gc_2(PTM^{\bullet})_{24}$ (**75**) and e) $Gc_3(PTM^{\bullet})_{48}$ (**76**). The intensities are normalized.

Table 6.10: Experimental EPR parameters of EPR spectra of mono and poly radicals **78**, **73**, **74**, **75** and **76**.

	g	a_H (G)	$a_{C_{orto}}$ (G)	$a_{C_{bridge}}$ (G)	a_{C_α} (G)	ΔH_{pp} (G)	ΔH_{sp}[d] (G)
BnOPhCH=CHPTM$^\bullet$ (**78**)[a]	2.0030	1.92	10.20	12.45	29.20	1.1	3.1
$Gc_0(PTM^\bullet)_6$ (**73**)[b][c]	2.0034	1.65	10	12	29	1.3	3.0
$Gc_1(PTM^\bullet)_{12}$ (**74**)[b][c]	2.0034	-	-	-	-	-	2.7
$Gc_2(PTM^\bullet)_{24}$ (**75**)[b][c]	2.0034	-	-	-	-	-	2.7
$Gc_3(PTM^\bullet)_{48}$ (**76**)[b][c]	2.0028	-	-	-	-	-	2.7

[a]Parameters obtained by simulation of the EPR spectra. [b] Parameters directly obtained from the experimental EPR spectrum. [c] Coupling constants with nuclei are not observed because the large linewidth of the larger generations. [d] EPR total spectrum width.

If the temperature is decreased at 200 K (**Figure 6.12**), the spectra are a little bit more resolved since the linewidth decreases. The principal pattern is dominated by two lines (a_H = 1.9 G) but not well resolved due to other transitions could take place such as $a_H/2$ or $a_H/3$ in lesser extension. It is worth mentioning that at this temperature the spectrum of the third generation $Gc_3(PTM^\bullet)_{48}$ shows a symmetrical pattern of three overlapped lines instead of the asymmetric one observed at 300 K. If the temperature is increased, the spectra obtained at higher temperatures is recovered. This process is reproducible for some cycles. Therefore, we can say that the process governing this change in the spectra with temperature is reversible.

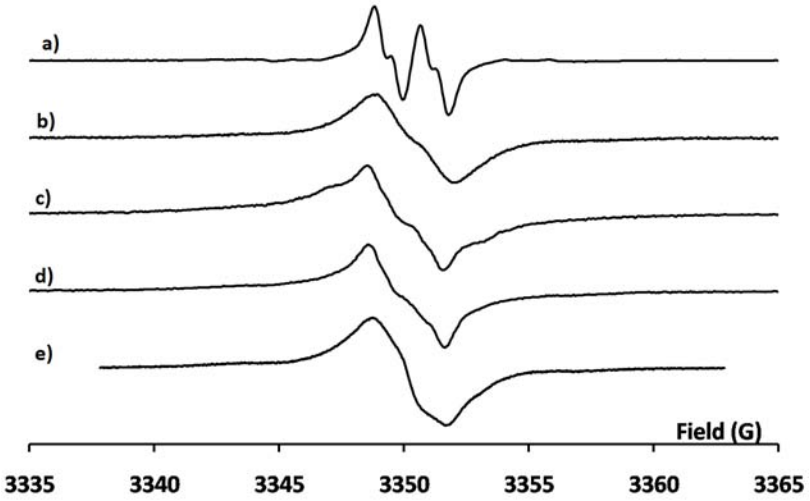

Figure 6.11: EPR spectra of a) monoradical (**78**) and polyradicals b) $Gc_0(PTM^\bullet)_6$ (**73**), c) $Gc_1(PTM^\bullet)_{12}$ (**74**), d) $Gc_2(PTM^\bullet)_{24}$ (**75**) and e) $Gc_3(PTM^\bullet)_{48}$ (**76**). All of them at $3.5 \cdot 10^{-4}$ M in toluene:dichloromethane 1:1 at 200 K.

Under frozen conditions at 120 K (**Figure 6.12**) it was observed similar spectra among dendrimer generations but it can be appreciated that when the generation increases the total width of the spectra decreases somewhat: 7.0, 6.7, 6.4 and 6.3 G from $Gc_0(PTM^{\bullet})_6$ to $Gc_3(PTM^{\bullet})_{48}$, respectively. This could probably be explained by the fact that at higher generations the radical ensembles will become larger, more compact and therefore more uniform. The tighter packing is expected to produce stronger spin exchange effects, leading to a narrower, Lorentzian lines. In addition, we can also observe the dipolar coupling in all the generations at this temperature (**Figure 6.13**). The D zero splitting value obtained for all of them is very similar, between 50.7 and 51.5 G.

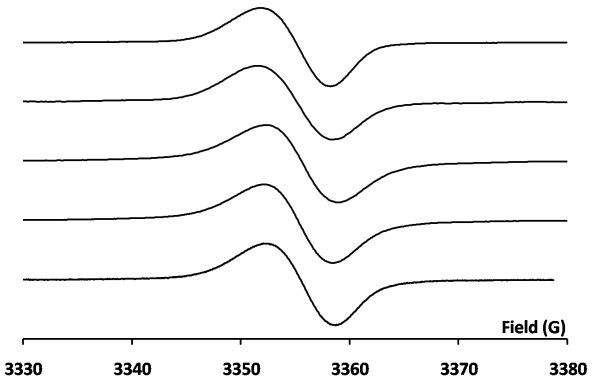

Figure 6.12: EPR spectra of a) monoradical (**78**) and polyradicals b) $Gc_0(PTM^{\bullet})_6$ (**73**), c) $Gc_1(PTM^{\bullet})_{12}$ (**74**), d) $Gc_2(PTM^{\bullet})_{24}$ (**75**) and e) $Gc_3(PTM^{\bullet})_{48}$ (**76**). All of them at $3.5 \cdot 10^{-4}$ M in toluene:dichloromethane 1:1 at 120 K.

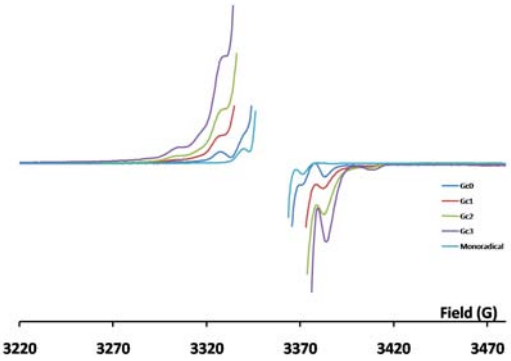

Figure 6.13: EPR expansion spectra of a) monoradical (**78**) and polyradicals b) $Gc_0(PTM^{\bullet})_6$ (**73**), c) $Gc_1(PTM^{\bullet})_{12}$ (**74**), d) $Gc_2(PTM^{\bullet})_{24}$ (**75**) and e) $Gc_3(PTM^{\bullet})_{48}$ (**76**). All of them at $3.5 \cdot 10^{-4}$ M in toluene:dichloromethane 1:1 at 120 K.

Under the previous conditions at 120 K it was observed a $|\Delta m_s| = 2$ transition at half field in all generations (**Figure 6.14**). This result gave a direct evidence of the presence of thermally accessible high-spin states for all generations. Interestingly, the intensity of these signals increase from the zero generation to the first one but from first to second the increase is smaller. Therefore, from the second to the third generations there is a little decrease. This could be explained by the fact that compound $Gc_3(PTM^{\bullet})_{48}$ probably has some solvent inside its cavities and hence the molarity calculation is not accurate.

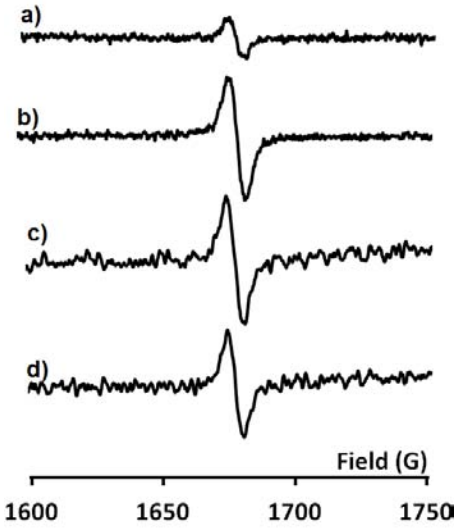

Figure 6.14: EPR spectra at half field of frozen solution of a) $Gc_0(PTM^{\bullet})_6$ (**73**), b) $Gc_1(PTM^{\bullet})_{12}$ (**74**), c) $Gc_2(PTM^{\bullet})_{24}$ (**75**) and d) $Gc_3(PTM^{\bullet})_{48}$ (**76**). All of them at $3.5 \cdot 10^{-4}$ M in toluene:dichloromethane 1:1.

As a main conclusion we can say that it is possible to obtain dendrimers of different generations and sizes which have PTM radical at their surface that exhibit a large degree of homogeneity, especially for the lower generations up to the second one. The through-space magnetic interactions among the terminal PTM radical units are weak but enough to be observed. The lack of water solubility of all generations of these dendrimer family of polyradicals made that we gave up its use as contrast agents for MRI.

6.3.2 Dendrimers with terminal TEMPO radicals

In order to use use of radical dendrimers for biological applications, and in particular as contrast agents in MRI, it is necessary to synthesize water soluble radical dendrimers. For this reason, it was thought to synthesize dendrimers with TEMPO radical unit because they are polar groups and might lead to water-soluble dendrimers. For their preparation we started with the dendrimers ended with acid groups, like Gc_0COOH (**71**) and Gc_1COOH (**72**), and then obtain the radical dendrimers by the coupling with 4-amino-TEMPO (**35**) generating amido groups between the starting dendrimer and the TEMPO radical.

The synthesis of TEMPO radical dendrimers (**79**) and (**80**) that present 6 and 12 radical units at their surfaces, respectively, was performed following the peptide strategy of amino acid couplings (**Scheme 6.7**). Thus, a mixture of the dendrimer **71** or (**72**) and DCC was dissolved in anhydrous DCM, under Argon atmosphere. Later the formation of the active intermediate between the carbodiimide and the acid group of dendrimers, the 4-amino-TEMPO radical was added to the mixture generating the desired products with yields of 54% and 68 %, respectively and diciclohexylurea as a subproduct.

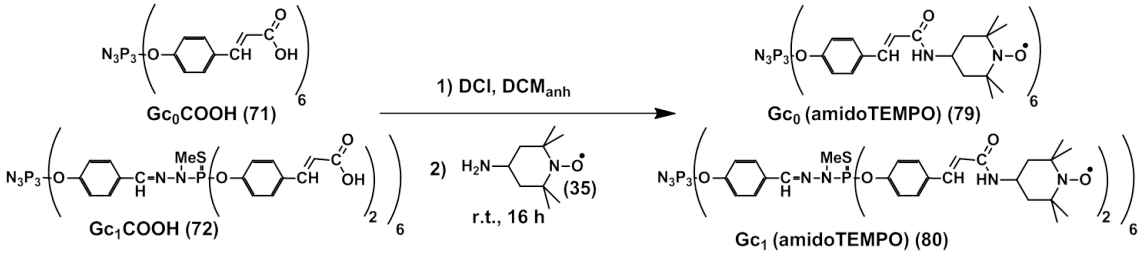

Scheme 6.7: Synthesis of TEMPO radical dendrimers (**79**) and (**80**).

Dendrimers fuctionalized with TEMPO radicals at the surface were characterized by IR, MALDI-TOF and EPR. Gc_0amidoTEMPO (**79**) was soluble in DMSO and quite soluble in water, but the Gc_1amidoTEMPO dendrimer (**80**) was hardly soluble in DMSO and quite insoluble in water. In spite of that, it could possible be registered their EPR in this solvent. As can be seen in **Figure 6.15**, neither Gc_0amidoTEMPO nor Gc_1amidoTEMPO showed exchange interactions among radicals in water, thus, $|J| \ll |a_N|$. **Table 6.11** summarizes these EPR parameters extracted from the EPR spectra.

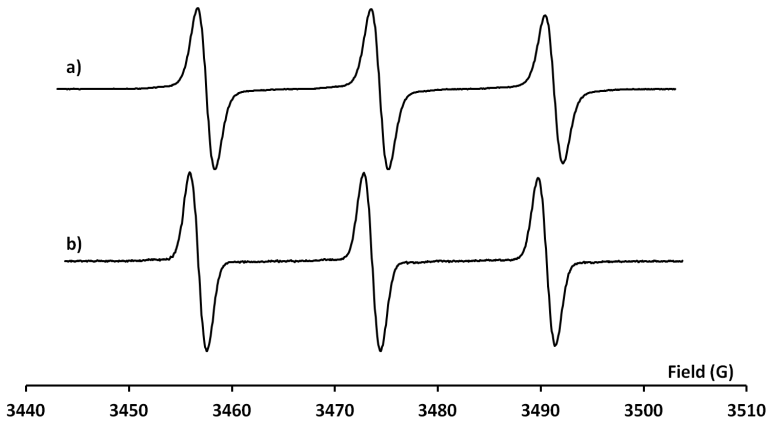

Figure 6.15: EPR spectra in water at 300 K of a) Gc_0amidoTEMPO (**79**) and b) Gc_0amidoTEMPO (**80**).

Table 6.11: Experimental EPR parameters for Gc_0amidoTEMPO (**79**) and Gc_1amidoTEMPO (**80**).

Compound	g	a_N (G)	ΔH_{pp} (G)
Gc_0amidoTEMPO (**79**)	2.0055	16.9	1.7
Gc_1amidoTEMPO (**80**)	2.0056	16.9	1.7

As already mentioned and unlike what was expected increasing the dendrimer generation the solubility in water decreases. So the Gc_1amido-TEMPO (**80**) is less water soluble than Gc_0amidoTEMPO (**79**). Consequently the poor water solubility of such dendrimer limited their possible application as contrast agents in MRI. Therefore, we had to change the strategy and introduce a polar charged group together with the radical one at the dendrimer surface that would help to increase the water solubility. On the other hand, it was decided to change the TEMPO radical by the PROXYL radical to improve the relaxivity since it is well, known that the relaxivity of PROXYL is higher than TEMPO.

6.3.3 Dendrimers with terminal PROXYL radicals

To obtain polar radical dendrimers it was decided to change the strategy. We decided to include on the radical dendrimer a polar charged group that could improve the water solubility. For this approach, and as we need three functional groups (one to bond the dendrimer, another to bond the radical and the third to introduce the polar charged group) we chose amino acids as linkers. It was decided to use the lateral functional group as dendrimer linker, the α-amino group to bond the radical, and the α-acid group as a polar anion group. The negative charged dendrimers cannot interact with nucleic acid if, for example, *in vivo* experiments are performed (**Scheme 6.8**).

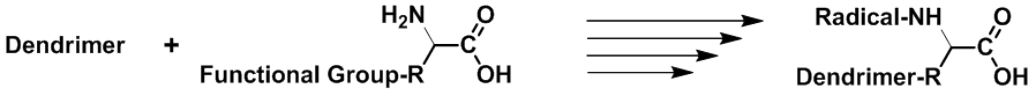

Scheme 6.8: Synthetic scheme to afford polar radical dendrimers.

As a radical, it was choose the 3-carboxy-PROXYL radical (**81**), and as a funcional α-amino acid, a flexible one as the Lysine (**82**) and a more rigid one as Tyrosine, (**83**). Their structures can be seen in **Figure 6.16**.

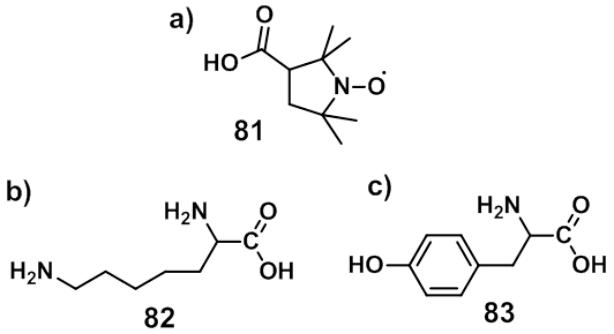

Figure 6.16: Structures of a) 3-carboxy-PROXYL (**81**) b) Lysine (**82**), and c) Tyrosine (**83**).

6.3.3.1 Lysine-PROXYL dendrimers

In order prepare such polar radical dendrimers, it was necessary to perform some synthetic steps. For lysine dendrimers these steps were the radical coupling to the protected lysine, the deprotection of the ϵ-amino of the lateral chain of lysine, followed by the dendrimer coupling with the ϵ-amino group of lysine and, finally, the α-acid deprotection to obtain the radical dendrimer (**Scheme 6.9**).

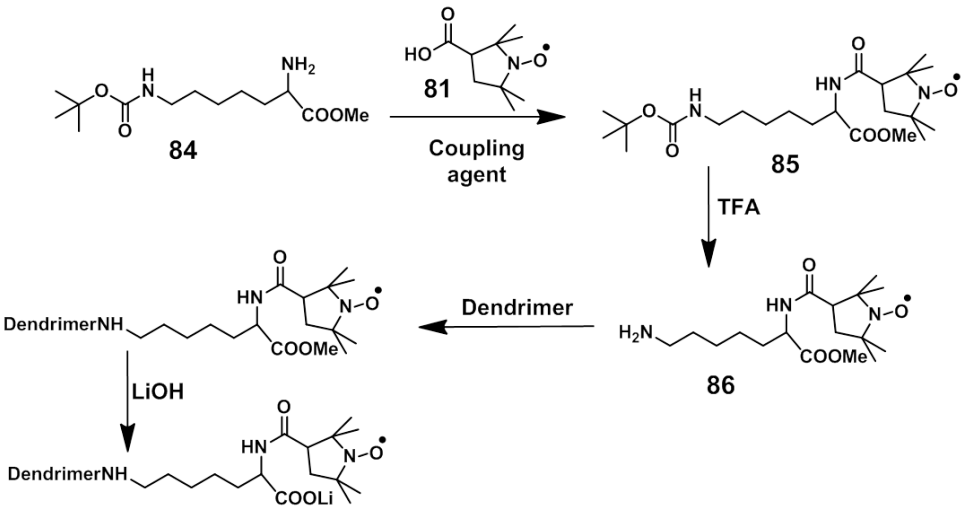

Scheme 6.9: Synthetic path to obtain lysine dendrimers.

Indeed, the first synthetic step consisted of the coupling of 3-carboxy-PROXYL radical (**81**) with the protected Lysine (H-Lys(BOC)OMe **84** (**Scheme 6.10**). The reaction was carried out under typical peptide synthetics conditions. Different coupling agents were tested to perform the reaction under mild conditions and with high yields. As in general procedure,[41] the coupling agent forms a highly active intermediate with the acid, providing a labile group (the characteristics of this labile group changes when the coupling agent is changed). Then, the nucleophilic species, in our case the amino group of the amino acid, attacks the active carbonyl group giving the final product. **Table 6.12** summarizes the tested coupling agents and the experimental conditions used. All the reactions were performed in anhydrous dichloromethane at room temperature and were kept under stirring for 16 hours. Finally, the best conditions were obtained with HATU, as a coupling agent. The isolated product was characterized by IR, MALDI-TOF and EPR. . The EPR (parameters: g: 2.0054, a_N: 14.7 G and ΔH_{pp}. 1.0) is very similar to that of **81**.

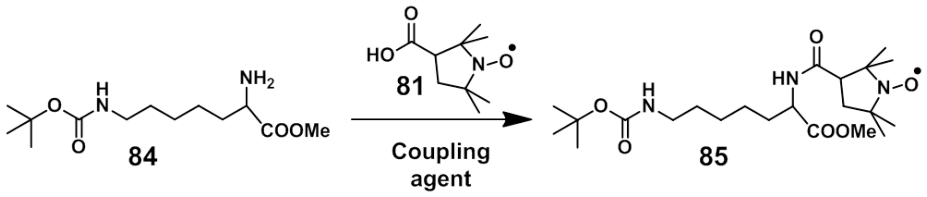

Scheme 6.10: Functionalization of commercial H-Lys(BOC)-OMe (**84**) with 3-carboxy-PROXYL radical (**81**) to obtain the H-Lys(BOC)-OMe radical(**85**).

Table 6.12: Experimental conditions assayed to afford PROXYL-Lys(BOC)-OMe radical (**85**).

Coupling agent	Base	Yield (%)
DCC	-	44
DCC	Et_3N	40
DCC	KOH	26
HOBt	DIEA	-
DCC+HOBt	DIEA	-
DCI	DIEA	21
HaBt	DIEA	5
HATU	DIEA	81

Once PROXYL-Lys(BOC)-OMe radical (**85**) was obtained with high yield and purity, the next step was to deprotect selectively the BOC group without deprotecting of the acid group (**Scheme 6.11**). The reaction was performed in anhydrous dichloromethaneadding trifluoroacetic acic (TFA) at 0 °C and then, keeping the reaction during 6 hours at room temperature. After testing the deprotection with TFA in mild conditions (stoichiometric quantities of acid or 2.5 eq), the deprotection was obtained using the conditions found in the literature[42] (20 eq of TFA). **Table 6.13** summarizes the experimental conditions assayed. The isolated product was characterized by IR, MALDI-TOF and EPR. The EPR spectrum (parameters: g: 2.0054, a_N: 14.7 G and ΔH_{pp}. 1.0) does not differ from the protected radical.

Scheme 6.11: Selective BOC deprotection of the PROXYL-Lys(BOC)-OMe radical (**85**) to obtain PROXYL-Lys-OMe (**86**).

Table 6.13: Experimental conditions tested to deprotect the PROXYL-Lys(BOC)-OMe radical (**85**).

TFA (eq)	Temperature (°C)	Yield (%)
1	0	-
1	0 to r.t.	-
2.5	0 to r.t.	-
20	0 to r.t.	99

PROXYL-Lys-OMe (**86**) presents the ϵ-amino group deprotected able to react with end-chloro dendrimers. On the other hand, the α-amino is functionalized with the radical and the α-acid,protected as a methyl ester, that will provide the polar group.

The reaction between primary ϵ-amine from Lysine and dendrimers (**Scheme 6.12**) could produce undesired subproducts of polysubstitution of the amine group, obtaining secondary, tertiary or even amonium salts that can be attributed to the higher reactivity of secondary amine than the primary ones. Similar reactions of dendrimers with amines are described in the literature.[43]

As the reaction involves radicals, the typical ^{31}P NMR growth control of the reaction cannot be used for determining the end of the reaction. Therefore, thin layer chromatography and IR were used to control it. Moreover, EPR was employed to evaluate the interaction among radicals in the dendrimers surface.

Since PROXYL-Lys-OMe radical (**86**) have a primary amine group, it was reacted with hexachlorocyclotriphosphacene (**62**) and Gc_1 (**65**) to obtain the products PROXYL-Lys(Gc_0)-OMe (**87**) and PROXYL-Lys(Gc_1)-OMe (**88**), respectively. The experimental conditions used were the same than those used for the dendrimer growth; *i. e.* cesium carbonate in anhydrous THF which gave a low yield (36%) for PROXYL-Lys(Gc_0)-OMe (**87**) and a higher yield for PROXYL-Lys(Gc_1)-OMe (**88**), 85%. Both radical dendrimers were characterized by IR, MALDI-TOF and EPR.

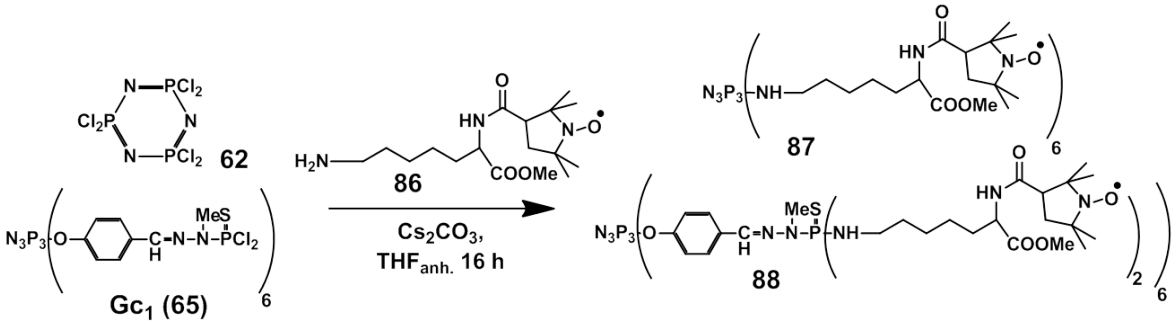

Scheme 6.12: Synthesis of PROXYL-Lys(Gc_0)-OMe (**87**) and PROXYL-Lys(Gc_1)-OMe (**88**).

The EPR spectra of radical dendrimers PROXYL-Lys(Gc_0)-OMe (**87**) (**Figure 6.17b**) and PROXYL-Lys(Gc_1)-OMe (**88**) (**Figure 6.17c**) show three well resolved lines, typical of the PROXYL radical monomer (**Figure 6.17a**) that in each PROXYL moiety corresponds to the coupling of the unpaired electron with the nitrogen (I = 1). The spectra are symmetric and the lines do not show any splitting indicating that all radical moieties has the same environment. It also indicates that there is no exchange interactions among radical substituents ($|J| \ll |a_N|$). Furthermore, focusing in the third spectral line (high field line) it is possible to see a small decrease in its intensity in comparison with first and second spectral lines. Such decrease is smaller in the zero generation than in the first generation dendrimer. This result is attributed to the restricted mobility of the radicals group on the dendrimer surfaces. EPR parameters of radical dendrimers **87** and **88** summarized in **Table 6.14**.

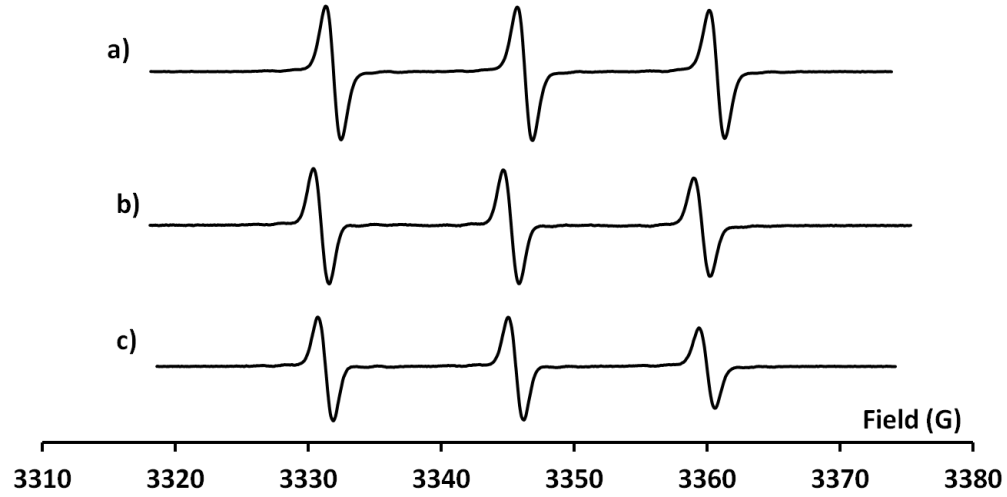

Figure 6.17: EPR spectra of: a) 3-caboxy-PROXYL (**81**) in DCM. b) PROXYL-Lys(Gc_0)-OMe (**87**) and c) PROXYL-Lys(Gc_1)-OMe (**88**), both in THF.

Finally, the last synthetic step consisted of the deprotection of the α-acid group of the previously synthesized PROXYL-Lys(Gc_x)-OMe. The ester group was hydrolyzed using LiOH in THF/H_2O (1/1) (**Scheme 6.13**) for 16 hours yielding the radical dendrimers **89** and **90** with quantitative yields (which were characterized by IR, MALDI-TOF and EPR. Both radical dendrimers show good water solubility as was expected.

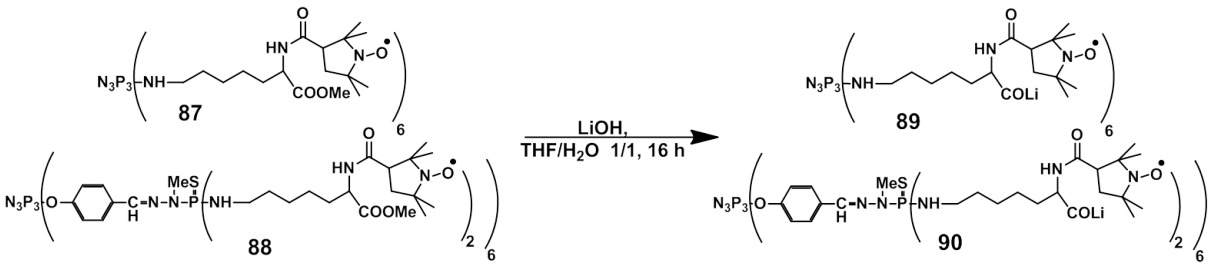

Scheme 6.13: Deprotection of PROXYL-Lys(Gc_x)-OMe dendrimers **87** and **88** to obtain PROXYL-Lys(Gc_0)-OLi (**89**) and PROXYL-Lys(Gc_1)-OLi (**90**).

The EPR spectra of the deprotected radical dendrimers **89** and **90**, performed in water, also show the three well resolved line pattern (**Figure 6.18**), without exhibiting any appreciable interaction among them. **Table 6.14** summarizes the experimental EPR parameters.

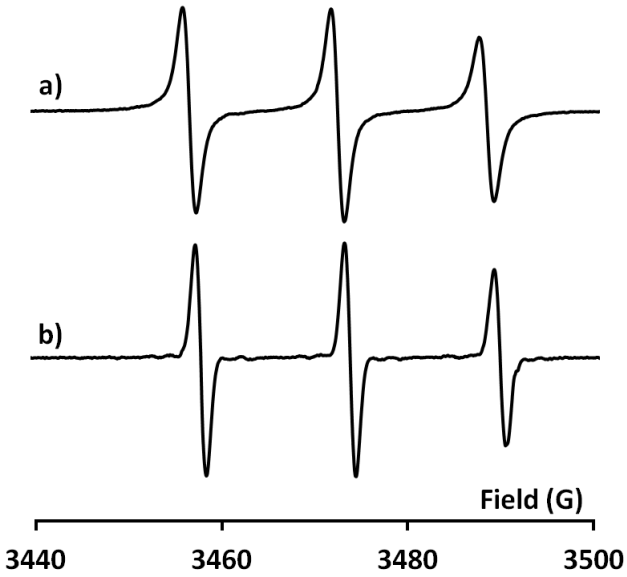

Figure 6.18: EPR spectra of a) PROXYL-Lys(Gc_0)-OLi (**89**) and b) PROXYL-Lys(Gc_1)-OLi (**90**), both in water.

Table 6.14: EPR parameters for 3-carboxy-PROXYL (**81**), PROXYL-LysGc_xOMe dendrimers **87** and **88**, and PROXYL-LysGc_xOLi **89** and **90** dendrimers.

Compound	g	a_N (G)	ΔH_{pp} (G)
3-Carboxy-PROXYL[a] (**81**)	2.0054	14.4	1.23
PROXYL-LysGc_0OMe[b] (**87**)	2.0055	14.3	1.10
PROXYL-LysGc_1OMe[b] (**88**)	2.0059	14.3	1.14
PROXYL-LysGc_0OLi[c] (**89**)	2.0058	16.0	1.44
PROXYL-LysGc_1OLi[c] (**90**)	2.0051	16.1	1.20

[a]In DCM. [b] In THF. [c] In H_2O.

As a main conclusion we can said that the obtained flexible radical dendrimers **80** and **81** were sinthesized without any significant presence of defects and they showed the desired water solubility. Moreover, they do not show a significant magnetic interaction among radicals.

6.3.3.2 Tyrosine-PROXYL dendrimers

In order to test the rigidity of the chain in the properties of radical dendrimers, a new family of dendrimers with Tyrosine as linker functionalized with radicals on the α amino were synthesized. Tyrosine was chosen because it has a more rigid amino acid chain than Lysine.

Due to the commercially availability of BOC-Tyr-OMe (**91**), we changed the synthetic strategy for Tyrosine dendrimers with respect to the Lysine ones (**Scheme 6.14**). For that synthesis the amino acid was firstly attached to the dendrimer surface and then the amino group of the Tyrosine was bound to the radical.

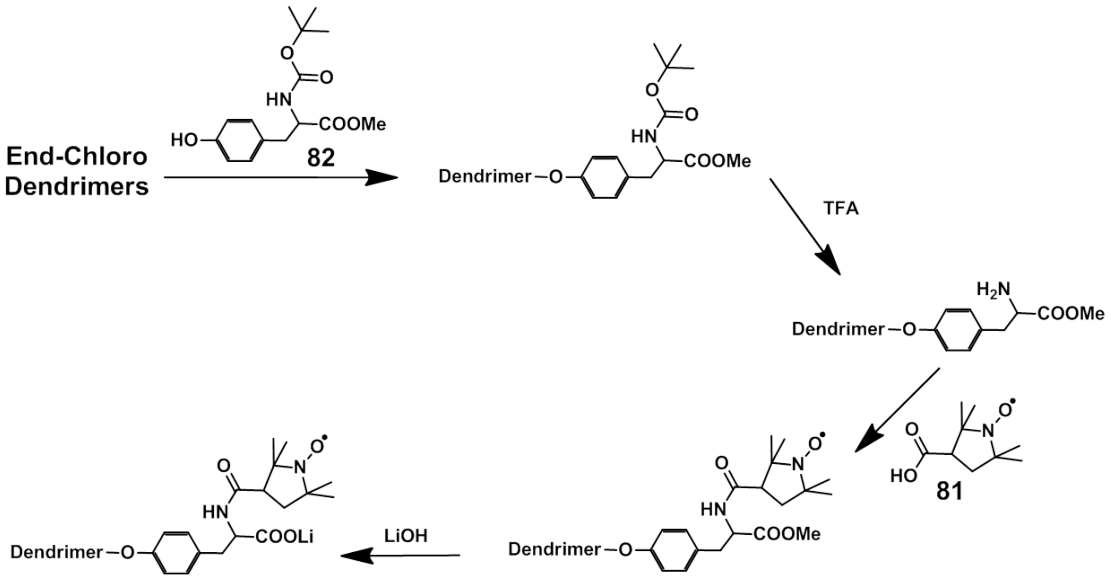

Scheme 6.14: Synthetic route to obtain Tyrosine dendrimers.

Thus, starting from BOC-Tyr-OMe (**82**), which has both α-amino and α-acid functional groups protected, the reaction between the *p*-hydroxyphenyl group of the lateral chain and chloro ended dendrimers, like hexachlorocyclotriphosphazene (**62**), Gc_1 (**65**), or Gc_2 (**67**), were performed under the previously conditions employed for the dendrimers growth.

Following this methodology, the zero, first and second dendrimer generations BOC-Tyr(Gc_0)-OMe (**92**), (BOCTyr(Gc_1)-OMe (**93**) and (BOCTyr(Gc_0)-OMe (**94**) were synthesized (**Scheme 6.15**) obtaining a high yield for the zero (86%) and first generations(90%) and with a moderate (54%) one for the largest one. These reactions were monitored by ^{31}P-NMR since, in contrast to Lysine dendrimers, no radicals are involved in this step. Dendrimers **92**, **93** and **94** were characterized by IR, MALDI-TOF and NMR (^{1}H and ^{31}P).

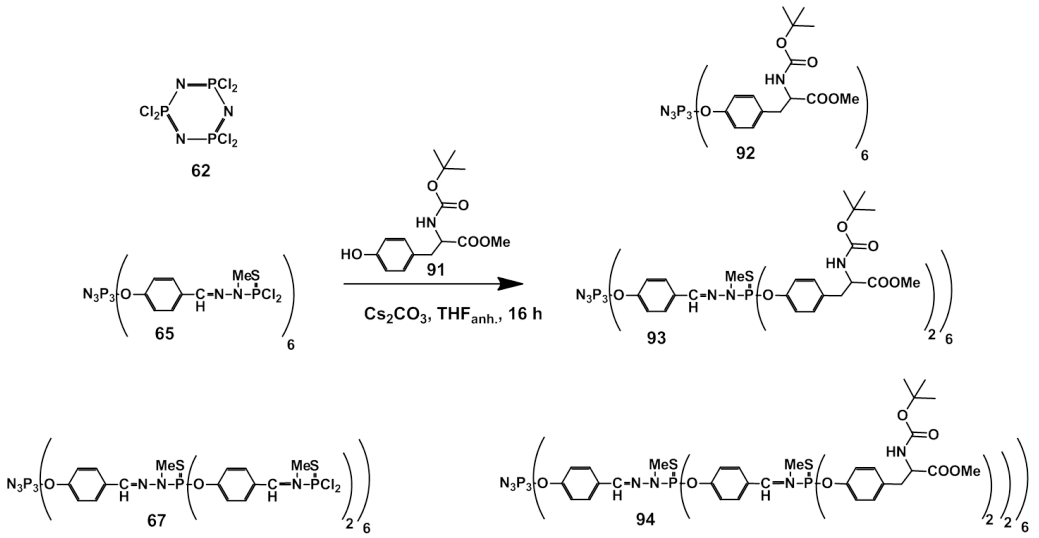

Scheme 6.15: Synthesis of BOC-Tyr(Gc_n)OMe dendrimers, where n= 0 (**92**), 1 (**93**) or 2 (**94**).

Once we had the dendrimers functionalized with protected Tyrosine, the next step consisted of the selective deprotection of the BOC group to yield dendrimers **95**, **96** and **97** (**Scheme 6.16**). The experimental conditions to carry out these reactions were similar than the ones used in the synthesis of Lysine-PROXYL compounds. So, the BOC-protected compound was dissolved in anhydrous dichloromethane, and a slow addition of TFA at 0 °C an excess of TFA was slowly performed. The mixture was then allowed to warm to room temperature and reacted for 6 hours. These reactions were monitored by ^{1}H-NMR, following the disappearance of the ^{t}butyl signal from the BOC group that appears at around 1.4 ppm. Dendrimers **95**, **96**, **97** were characterized by IR, MALDI-TOF and NMR (^{1}H and ^{31}P).

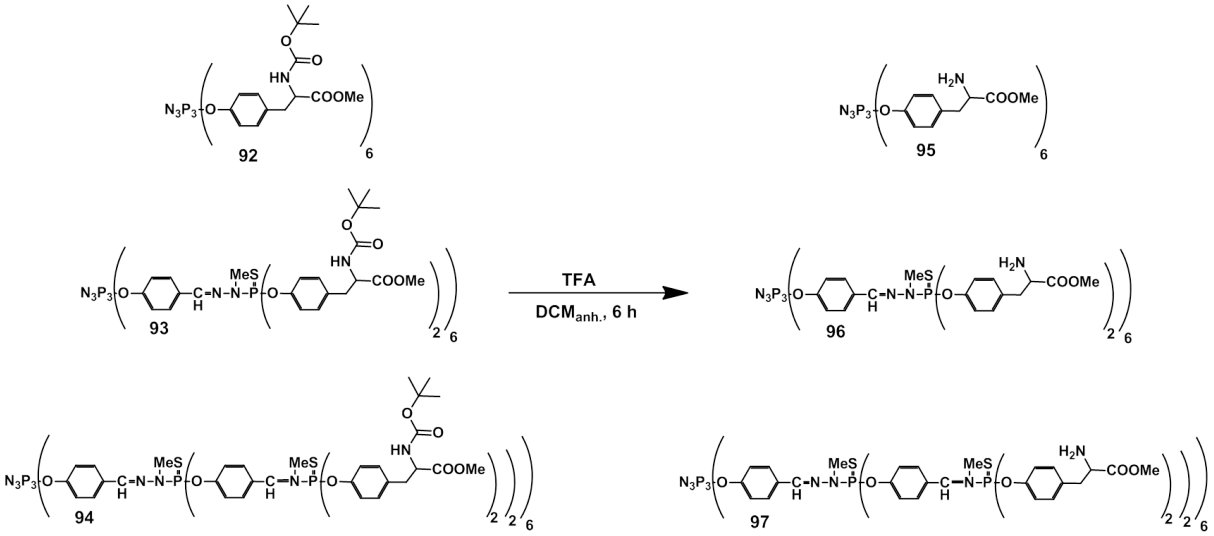

Scheme 6.16: Deprotection of BOC-Tyr(Gc_n)OMe dendrimers, where n= 0, 1 or 2 to afford H-Tyr(Gc_n)OMe, where n= 0 (**95**), 1 (**96**) or 2 (**97**).

In order to carry out the coupling with PROXYL-acid radical, the acid group of 3-carboxy-PROXYL (**81**) and the amino group of Tyrosine dendrimers reacted using HATU as a coupling agent (**Scheme 6.17**). The protected radical dendrimers PROXYL-Tyr(Gc_n)OMe dendrimers, **98** (n= 0), **99** (n= 1) and **100** (n= 2) were obtained with high yields (95, 97 and 95%, respectively) and were characterized by IR, MALDI-TOF and EPR.

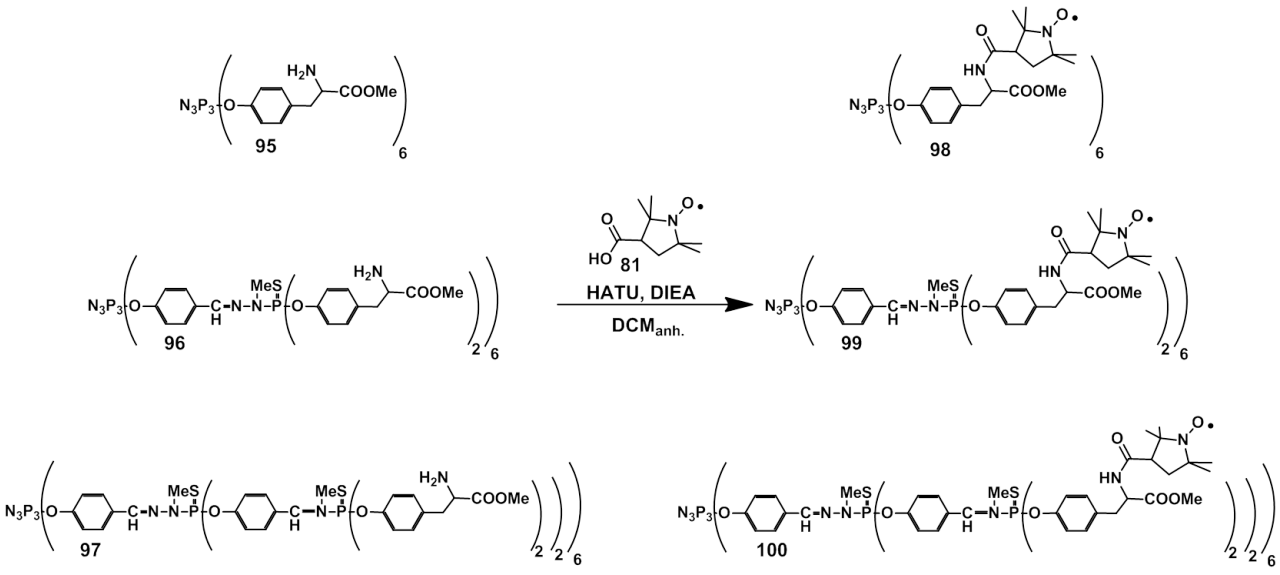

Scheme 6.17: Synthesis of PROXYL-Tyr(Gc_n)OMe dendrimers, where n= 0 (**98**), 1 (**99**) or 2 (**100**).

The EPR spectra of the zero, first and second dendrimer generations of (PROXYL-Tyr(Gc_n)OMe dendrimers were performed in THF. The EPR spectrum of the zero generation (**Figure 6.19a**) shows the three-line pattern, typical of PROXYL radicals, with the high-field line less intense due to the restricted mobility of the radicals anchored on the dendrimer surface. The three-line pattern also indicates a very weak magnetic interaction among neighboring radicals. In fact, it was expected 7 lines corresponding to three interacting radicals (3 radicals on each face of the cyclotryphosphazene plane of the molecule), as it was observed for the zero generation of phosphorous dendrimer based on a cyclotryphosphazene core, with TEMPO radicals.[18] On the other hand, the EPR spectra of the first and second generation (**Figure 6.19b** and **c**) shows a pattern typical of a polyradical which is dominated by a single, intense, broad line overlapping the three narrow lines of PROXYL radical. This broad line results from spin-exchange and dipole-dipole interactions among several PROXYL radicals anchored close together on the dendrimer surface, averaged over different interactions distances. As expected, the second generation EPR spectrum shows this broad line even more intense than in the first generation, as there are twice the number of radicals and hence more spin-exchange and dipole-dipole interactions. However, neither in the first nor in the second generation EPR spectra is visualized any spectral resolution which does not allow us to determine the number of PROXYL interacting radicals. This means that there are several of them interacting with each other, with several hyperfine transitions and hence a decrease of the splitting value a_N/n and an increase of the number of lines 2n+1, were n is the number of interacting radicals. **Table 6.15** summarizes the experimental parameters obtained from the EPR spectra.

In frozen conditions, a $|\Delta m_s|= 2$ half-field transition in diluted conditions is observed for the two larger dendrimer generations (**Figure 6.20**), while this transition was not observed for the zero generation. This gives a direct evidence of the presence of a thermally accessible high-spin states and the intramolecular origin of the dipolar interactions. The half field EPR spectrum of the second generation (**Figure 6.20b**), at the same concentration of radical dendrimer, was found to be double in intensity than in the first generation (**Figure 6.20a**), which is indicative that the dendrimer presents the double amount of radicals on its surface than in the previous generation.

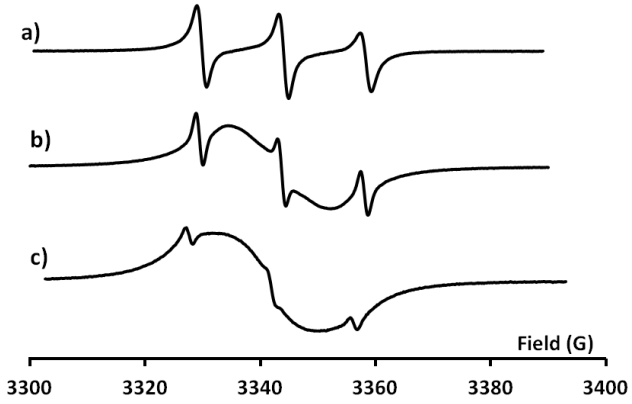

Figure 6.19: EPR spectra of a) PROXYL-Tyr(Gc_0)OMe (**98**), b) PROXYL-Tyr(Gc_1)OMe (**99**) and c) PROXYL-Tyr(Gc_2)OMe (**100**) in THF.

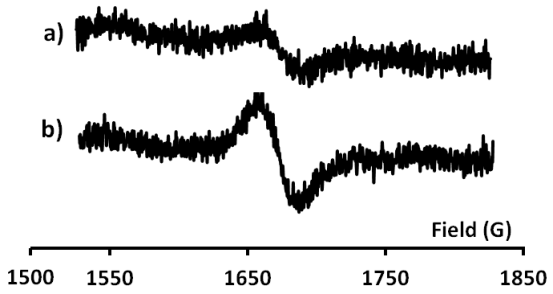

Figure 6.20: EPR Half-Field transition of a) PROXYL-Tyr(Gc_1)OMe (**99**) and b) PROXYL-Tyr(Gc_2)OMe (**100**) in diluted conditions in THF at 120 K.

The last synthetic step consisted of the deprotection of the α-acid group by hydrolisis to obtain the radical dendrimers as a carboxylic salts. This hydrolisis of PROXYL-Tyr(Gc_x)-OMewas performed, as in Lysine dendrimers, using LiOH in THF/H_2O (1/1) (**Scheme 6.18**) for 16 hours and the dendrimers generated in the form of lithium salts **101**, **102** and **103** were characterized by IR, MALDI-TOF and EPR.

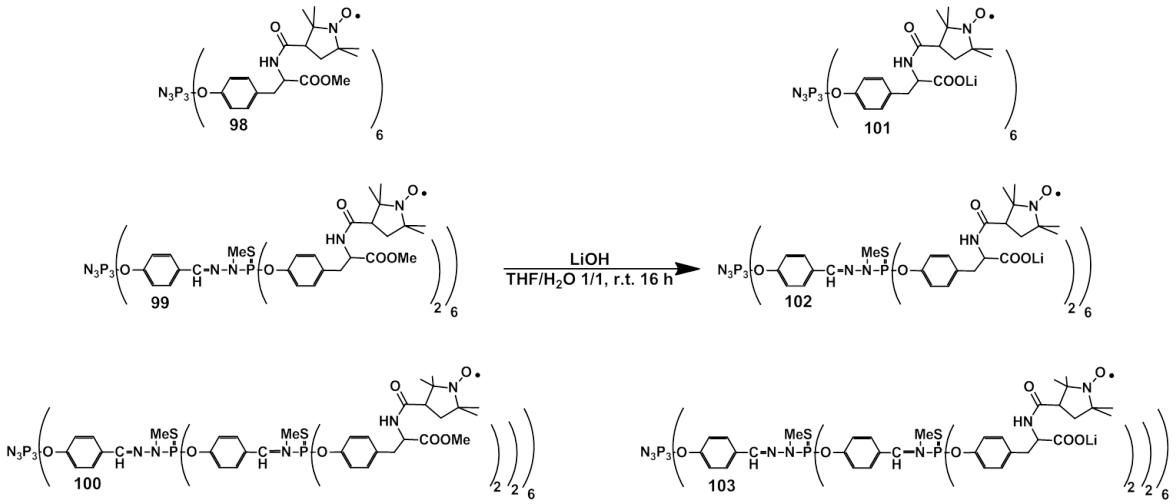

Scheme 6.18: Final deprotection of PROXYL-Tyr(Gc_n)OMe dendrimers, where n= 0, 1 or 2 to afford PROXYL-Tyr(Gc_n)OLi, where n= 0 (**101**), 1 (**102**) or 2 (**103**).

The EPR spectra of PROXYL-Tyr(Gc_x)-OLi salts, in water solution, showed the three line pattern typical of PROXYL radicals and a broad line characteristic of polyradicals. However a sharp decrease of such a broad line corresponding to the exchange and dipole-dipole interactions was observed with respect the protected radicals. The reason

of this decrease of interactions could be explained by the crowded sphere formed by hydrogen bonds on the dendrimer surface among water molecules of the solvated lithium ion and the carboxylate of radical dendrimers hindering their interactions. **Table 6.15** summarizes the experimental parameters obtained for the EPR spectra.

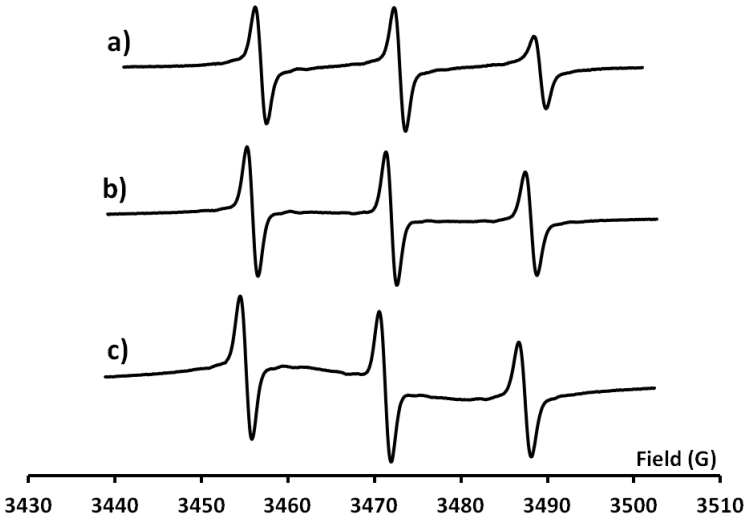

Figure 6.21: EPR spectra of a) PROXYL-Tyr(Gc_0)-OLi **101**, b) PROXYL-Tyr(Gc_1)-OLi **102** and c) PROXYL-Tyr(Gc_2)-OLi **103**, in water.

Table 6.15: Experimental EPR parameters for PROXYL-Tyr(Gc_n)-OMe dendrimers in THF and PROXYL-Tyr(Gc_n)-OLi in H_2O, where n= 0, 1 or 2.

Compound	g	a_N (G)	ΔH_{pp} (G)
PROXYL-TyrGc_0OMe[a] (**98**)	2.0057	14.21	1.67
PROXYL-TyrGc_1OMe[a] (**99**)	2.0064	14.38	-
PROXYL-TyrGc_2OMe[a] (**100**)	2.0061	14.38	-
PROXYL-TyrGc_0OLi[b] (**101**)	2.0055	16.00	1.30
PROXYL-TyrGc_1OLi[b] (**102**)	2.0057	16.15	1.27
PROXYL-TyrGc_2OLi[b] (**103**)	2.0057	16.20	1.36

[a]In THF and [b] In H_2O.

As a main conclusion we can say that it is possible to obtain three different generations of radical dendrimers using a rigid linker like the Tyrosine and PROXYL radical without the presence of defects. Such dendrimers show significant magnetic interactions among neighboring radicals when the carboxilic groups are protected, that decreases considerably when they are deprotected. This fact could be explained by the strong

water binding on the dendrimer surface which hinders the interactions among neighboring radicals.

The possible application of Lysine and Tyrosine bounded dendrimers as contrast agents for MRI are explained in the next Chapter.

6.4 Conclusions

- Four generations of phosphorous dendrimers ended in aldehyde groups (Gc_0 (**63**), Gc_1' (**66**), Gc_2' (**68**), Gc_3' (**70**)) has been successfully synthesized. In the same way, dendrimers ended in chlorine groups (Gc_1 (**65**), Gc_2 (**67**) and Gc_3 (**69**)) were isolated. In the same way dendrimers Gc_0COOH (**71**) and Gc_1COOH (**72**), obtained by modification of dendrimers **63** and **66** using Knoevenagel methodology, were obtained. All dendrimers were fully characterized.

- PTM radical dendrimers **73**, **74**, **75**, and **76** were prepared using the Wittig-Horner-Emmons methodology and their electrochemical and magnetic properties were studied.

- Two generations of amidoTEMPO dendrimers **79** and **80**, were sucessfuly synthesized by reaction of Gc_0COOH (**71**) or Gc_1COOH (**72**) with 4-amino-TEMPO and characterized.

- Two dendrimer generations modified with Lysine and PROXYL radical has been prepared and characterized PROXYL-Lys(Gc_o)-OLi (**89**) and PROXYL-Lys(Gc_1)-OLi (**90**). The EPR of both polyradicals indicated no interaction among radical units. This fact could be attributed to the flexibility of the Lysine chain.

- More rigid amino acid radical dendrimers made with Tyrosine and PROXYL, were sinthesized and characterized, PROXYL-Tyr(Gc_0)-OLi (**101**), PROXYL-Tyr(Gc_1)-OLi (**102**), PROXYL-Tyr(Gc_2)-OLi (**103**). The EPR study showed interaction on the precursors but much less in the salt derivatives.

Bibliography

[1] Slany M., Bardají M., Casanove M.J., Caminade A.M., Majoral J.P., and Chaudret B. *J. Am. Chem. Soc.*, 117:p.9764, **1995**.

[2] Huc V., Boussaguet P., and Mazerolles P. *J. Organomet. Chem.*, 521:p.253, **1996**.

[3] Hawker C.J. and Fréchet J.M.J. *J. Am. Chem. Soc.*, 112:p.7638, **1990**.

[4] Vögtle F. *Synthesis*, 2:p.155, **1978**.

[5] van der Made A.W. and van Leeuwen P.W.N.M. *J. Chem. Soc. Chem. Commun.*, page p.1400, **1992**.

[6] Mekelburger H.-B., Jaworek W., and Vögtle F. *Angew. Chem. Int. Ed Engl.*, 31(12):p.1571, **1992**.

[7] Tomalia D.A., Naylor M.N., and Goddard III W.A. *Angew. Chem. Int. Ed Engl.*, 29:p.138, **1990**.

[8] Launay N. andCaminade A.M., lahana R., and Majoral J.P. *Angew. Chem. Int. Ed Engl.*, 313(15):p.1589, **1994**.

[9] Xu Z., Kahr M., Walker K.L., Wilkins C.L., and Moore J.S. *J. Am. Chem. Soc.*, 116:p.4537, **1994**.

[10] Launay N., Caminade A.M., and Majoral J.P. *J. Am. Chem. Soc.*, 117:p.3282, **1995**.

[11] Lartigue M.L., Donnadieu B., Galliot C., Caminade A.M., Majoral J.P., and Payet J.P. *Macromolecules*, 30:p.7335, **1997**.

[12] Brauge L., Magro G., Caminade A.M., and Majoral J.P. *J. Am. Chem. Soc.*, 123:p.8446, **2001**.

[13] Galliot C.and Larré C., Caminade A.M., and Majoral J.P. *Science*, 277:p.1981, **1997**.

[14] Furer V.L., Kovalenko V.I., Vandyukov A.E., Majoral J.P., and Caminade A.M. *Mol. Biomol. Spectrosc.*, 58:p.2905, **2002**.

[15] Maraval V., Caminade A.M., Majoral J.P., and Blais J.C. *Angew. Chem. Int. Ed Engl.*, 42:p.1822, **2003**.

[16] Bosman A.W., Janssen R.A.J., and Meijer E.W. *Macromolecules*, 30:p.3606, **1997**.

[17] Matyjaszewski K., Shigemoto T., Fréchet J.M.J., and Leduc M. *Macromolecules*, 29(12):p.4167, **1996**.

[18] Badetti E., Lloveras V., Wurst K., Sebastián R.M., Caminade A.M., Majoral J.P., Veciana J., and Vidal-Gancedo J. *Org. Lett.*, 15(14):p.3490, **2013**.

[19] Badetti E., Lloveras V., Muñoz-Gómez J.L., Sebastián R.M., Caminade A.M., Majoral J.P., Veciana J., and Vidal-Gancedo J. *Macromolecules*, 47(22):p.7717, **2014**.

[20] Ottaviani M.F., Bossmann S., Turro N.J., and Tomalia D.A. *J. Am. Chem. Soc.*, 116:p.661, **1994**.

[21] Klajnert B., Cangiotti M., Calici S., Majoral J.P., Caminade A.M., Cladera J., Bryszewska M., and Ottaviani M.F. *Macromol. Biosci.*, 7:p.1065, **2007**.

[22] Poupot M., Griffe L., Marchand P., Maraval A., Rolland O., Martinet L., L' Faqihi-Olive F.-E., Turrin C.-O, Caminade A.M., Fournié J.-J., Majoral J.P., and Poupot R. *Faseb*, 20:p.2339, **2006**.

[23] Caminade A.M. and Majoral J.P. *Accounts of Chemical Research*, 37(6):p.341, **2004**.

[24] Caminade A.M., Turrin C.O., and Majoral J.P. *New J. Chem.*, 34:p.1512, **2010**.

[25] Caminade A.M., Maraval V., Laurent R., Turrin C.O., Sutra P., Leclaire J., Griffe L., Marchand P., Baudoin-Dehoux C., Rebout C., and Majoral J.P. *C.R. Chimie*, 6:p.791, **2003**.

[26] Lei X.G., Jockusch S., Tomalia D.A. Turro N.J., and Ottaviani M. F. *Colloid Interf. Sci.*, 322:p.457, **2008**.

[27] Francese G., Dunand F.A., Loosli C., Merbach A.E., and Decurtins S. *Magn. Reson. Chem.*, 41:p.81, **2003**.

[28] Han H.J., Sebby K. B., Singel D.J., and Cloninger M.J. *Macromolecules*, 40:p.3030, **2007**.

[29] Kashiwagi Y., Kurashima F., Kikuchi C. anf Anzai J.I., and Osa T. *Electrochem Commun.*, 1:p.305, **1999**.

[30] Jansen J.F.G.A., Janssen R.A.J., Brabander van der Berg E.M.M., and Meijer E.W. *Adv. mater.*, 7(6):p.561, **1995**.

[31] Racja A. *Chem. rev.*, 94:p.871, **1994**.

[32] Alonso B., Morán N., C.M. Casado, Lobete P., Losada J., and Cuadrado I. *Chem. Mater.*, 7:p.1440, **1995**.

[33] Tenhu K. and Sundholm F. *Br. Polym. J.*, 23:p.129, **1990**.

[34] Launay N., Caminade A.M., and Majoral J.P. *J. Organomet. Chem.*, 529:p.51, **1997**.

[35] Zou H., Wu H. Zhang X., Zhao Y., Stöckigt J., Lou Y., and Yu Y. *Bioorg. Med. Chem.*, 18:p.6351, **2010**.

[36] Augustine J.K., Naik Y.A., Mandal A.B., Chowdappa N., and Praveen V.B. *J. Org. Chem.*, 72:p.9854, **2007**.

[37] Augustine J.K., Naik Y.A., Mandal A.B., Chowdappa N., and Praveen V.B. *Angew. Chem. Int. Ed.*, 39(23):p.4249, **2009**.

[38] Rovira C., Ruiz-Molina D., Elsner O., Vidal-Gancedo J., Bonvoisin J., Launay J. P., and Veciana J. *J. Chem. Eur. J.*, 7(1):p.240, **2001**.

[39] Sporer C., Ratera I., Ruiz-Molina D., Zhao Y., Vidal-Gancedo J., Wurst K., Jaitner P., Clays K., Persoons A., Rovira C., and Veciana J. *Angew. Chem. Int. Ed.*, 43:p.5266, **2004**.

[40] Crivillers N., Mas-Torrent M., Vidal-Gancedo J., Veciana J., and Rovira C. *J. Am. Chem. Soc.*, 120(16):p.5499, **2008**.

[41] Angell Y.M., Echeverría C.G., and Rich D.H. *Tetrahedron Lett.*, 35:p.5981, **1994**.

[42] Khan F.A., Ahmad S., Kodipelli N., Shivange G., and Anindya R. *Org. Biomol. Chem.*, 12(23):p.3847, **2014**.

[43] Padié C., Maszewska M., Majchrzak K., Nawrot B., Caminade A.M., and Majoral J.P. *New. J. Chem.*, 33:p.318, **2009**.

Chapter 7

Magnetic Resonance Imaging (MRI)

7.1 Introduction

7.1.1 Nuclear Magnetic Spectroscopy and Magnetic Resonance Imaging

As was described in **Chapter 1**, nuclei of atoms present a nuclear spin that is associated with an angular momentum (μ) which, in absence of an external magnetic field shows a random direction. When an external magnetic field (B_0) is applied, the nuclear magnetic moments are oriented preferentially along the magnetic field. As a result, the degenerated energy states from the nucleus are split in different levels which are filled following a Boltzman distribution. Additionally, the nucleus shows a rotational movement around B_0 that depends on the gyromagnetic constant (γ) which is characteristic of each isotope of the nuclei.

By application of an appropriate energy pulse (radiofrequency, E= h $\times$ ν) it is possible to promote nuclei from the low energy state to an excited state, producing a perturbation of the magnetic momentum from the equilibrium. The recovery of the equilibrium state takes place through a relaxation processes changing the magnetization (M) and these data are those which are measured in a magnetic resonance experiment.

The recovery of the transversal magnetization (at the xy plane) and the longitudinal magnetization recovery (in the z axis) are associated with different mechanisms of relaxation and hence their recovery times are different, being the transversal one due to spin-spin interactions and the longitudinal to spin-lattice interactions. The first time is known as T_2 and the longitudinal or spin-lattice relaxation time as T_1. Usually, T_1 presents higher values than T_2.[1–3]

One of the major advances in biomedical imaging in the last century has been the development of MRI techniques, which evolved from the classical NMR. Since the pioneering work of Lauterbur and Mansfield, advances in MR imaging have progressed very rapidly, being now considered critical in the workup of patients suffering from a wide array of disorders.[4]

Briefly, the vast majority of clinical MRI scans observe protons (^{1}H nuclei, spin 1/2), which are highly abundant in the body in the form of H_2O. In a typical NMR experiment, at thermal equilibrium these ^{1}H spins around about the applied magnetic field with a net magnetization, which may be perturbed and detected by an appropriate radiofrequency radiation and detection. Among the potential MR-observable nuclei, only ^{1}H is currently used in clinical practice. Several features of ^{1}H make it the ideal nucleus for MRI/MRS at thermodynamic equilibrium. These include: (1) high natural abundance, (2) high concentration in the body, (3) large gyromagnetic ratio (γ), (4) short T_1 relaxation, and (5) presence in several metabolites that are relevant to human disease.

In MRI, the location of the detected signal in the 3D-space is obtained by applying additional magnetic field gradients during the detection. MRI provides morphometric information about the organs and/or studied disease. Magnetic Resonance Spectroscopy (MRS) is used to study metabolites in tissues, providing functional and biochemical insights. MRS is commonly performed during clinical scans of the brain and prostate gland.[5,6] The brain is ideal for MRS due to its relative lack of motion, and its comparatively high concentrations of metabolites that become altered in cancer, ischemia, and neurodegenerative diseases. MRS is based on the chemical shift, whereby the microenvironment of ^{1}H spins causes a small change in their spin frequency, expressed in parts-per-million (ppm). This frequency information is used to generate metabolite maps with spectra corresponding to various volume elements, or voxels.

Nowadays, MRI plays an important role in cancer diagnosis, staging and treatment planning. With this technique it can be distinguished between normal and diseased[7] tissues and to precisely pinpoint cancerous cells within the body. It is also useful for revealing metastasis. As a result, it is often used for imaging the brain, spine, muscle, connective tissue and also the inside of bones. Some exams require a contrast dye or contrast agent to be injected into a vein before the procedure. This helps certain areas to show up better resolution of the images.

MRI uses the resonance of protons, in general of water, to generate the 3D images. Protons are excited by a radiofrequency pulse of an appropriate frequency and then emit energy in the form of radiofrequency (RF) signal as they return to their original state. The RF signal decays with an exponential curve characterized by the T_1 parameter; *i. e.* the longitudinal relaxation time or spin-lattice relaxation time) (**Figure 7.1**.

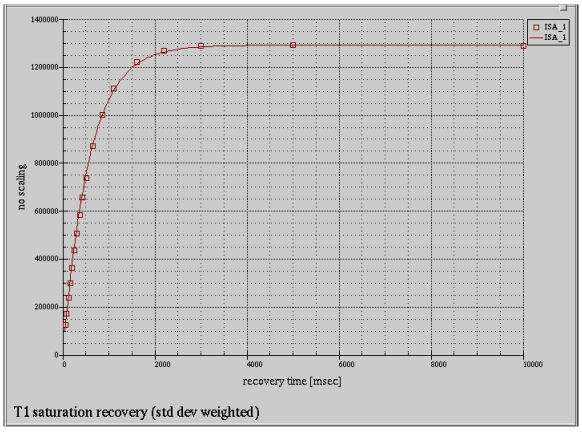

Figure 7.1: Magnetization recovery in the z axis *versus* time to determine the longitudinal relaxation time (T_1).

Longitudinal relaxation time is the mechanism by which the z component of the magnetization vector (M_z) comes into thermodynamic equilibrium with its surroundings (the "lattice") in nuclear magnetic resonance and magnetic resonance imaging techniques. On other words, T_1 characterizes the rate at which the longitudinal M_z component of the magnetization vector recovers exponentially its value towards its thermodynamic equilibrium, according to **Equation 7.1**. By convention it can be defined as the time it takes for the longitudinal magnetization to recover approximately 63 % of its initial value after being flipped into the magnetic transverse plane by a 90^0 radiofrequency pulse.

$$M_z(t) = M_{z,\,eq}(1 - e^{-t/T_1}) \tag{7.1}$$

Different tissues show different T_1 values so it is possible to obtain images of different tissues taking advantage of the different contrast among tissues with this technique. In particular, T_1 is significantly different between grey matter and white matter and is used when undertaking brain scans. Moreover, tumorous tissues show water accumulation and they can be detected and studied by this technique.

7.1.2 Radicals as MRI contrast agents

MRI contrast agents are atoms or molecules or groups of them used to improve the visibility of internal body structures in MRI studies where the desired tissue does not show enough contrast with respect to the surrounding. MRI contrast agents change the relaxation times of atoms within body tissues where they are present after oral or intravenous administration. In general, the parameter that is used to define the ability of a magnetic compound (contrast agent) to change the relaxation rates of the surrounding water proton spins is the relaxivity (r), which are given in $mM^{-1}\times sec^{-1}$.

Overall the relaxivity is determined by two phenomena: First, by short-range dipolar interactions between the unpaired electron spins of the contrast agent and the proton nuclei of water molecules bond in the first coordination sphere (inner-sphere relaxation) of the paramagnetic compound. And second, by long-range dipolar interactions between the paramagnetic centers and the bulk water in the vicinity of the paramagnetic centers (outer-sphere).[8] The relaxivity, therefore, depends on the molecular structure and kinetics of the complex with water molecules. It can be improved the relaxivity value by increasing the number of water molecules that are in the inner sphere of the complex or by slowing down the molecular rotational correlation times.

The most commonly used compounds for contrast enhancements are gadolinium-based compounds, but gadolinium shows a high toxicity so it has to be quelated.[9] Recently some researchers have started to investigate organic radicals, such as stable nitroxides, as MRI contrast agents.[10] To date, the critical obstacle in the development of practical organic radical as contrast agents is the design and synthesis of paramagnetic compounds of moderate size that posses long *in vivo* lifetimes, high ^{1}H water relaxivities (r) and high water solubility. However, the intrinsically low paramagnetic relaxivity of nitroxides (due to their low spin of 1/2) has prevented their widespread application as MRI contrast agents.[11] Attempts have been made to enhance the relaxivity of nitroxides by using nitroxides which have functional groups able of binding proteins.[11] Such protein binding could enhance the inert-sphere contribution to relaxivity and thus improve the profile of nitroxides as relaxation enhancers.

7.1.3 Radical dendrimers as MRI contrast agents

Dendrimers introduce to the contrast agent system the possibility to change the molecule size, as long as we use different generations, providing specific size-biodistribution. In this way, low molecular weight (small size) compounds are quickly eliminated by kidneys. On the other hand, larger molecular weight molecules present low permeability through the vascular walls and remain in blood vessels for longer time. In this sense, radical dendrimers are versatile molecules that allow the control of the final size of the contrast agent to ensure the desired biodistribution, lifetime and excretion. It is important to maintain the contrast agent in the patient enough time to perform the analysis with an appropriate biodistribution but it has to be avoided the accumulation in the body. The upper limit size for glomerular filtration of kidneys is approximately 175 KDa or 25 nm in average. Depending on the size this represents the main excretion mechanism by the metabolism or cell accumulation.[12]

The key points in the development of new contrast agents for MRI are the design and synthesis of paramagnetic compounds with moderate molecular sizes that possess long *in vivo* lifetimes, high water solubility and high ^{1}H water relaxivities. The use of dendrimers makes possible to enhance water solubility by addition of charged polar groups, for instance poly(ethylene glycol) chains.[13] There are only a few examples of radical dendrimers in the literature. Dendrimer scaffolds have been used to enhance paramagnetic relaxation both in gadolinium based paramagnetic relaxation

enhancers (PREs)[8,14] and nitroxide-labeled systems.[15–17] In the case of gadolinium-based dendritic relaxation enhancers, the dendrimer is used to modify the rotational correlation time of the system and thereby to enhance inner-sphere relaxivities.[8,14] In the case of nitroxide-based dendrimers, relaxivity enhancements in aqueous solution are not observed.[17] However, aggregation effects[18] in aqueous solution could complicate the interpretation of relaxivity measurements made in aqueous solution. The dendrimer framework has been shown to be advantageous in decreasing the *in vivo* bioreduction rate of nitroxides, an extremely rapid process which destroys the relaxation enhancer.[16] The potential of dendritic PREs in targeting specific organs has been investigated successfully.[8,17,19] PAMAM dendrimer has been used for the preparation of radical dendrimer for MRI contrast agents as far as they are commercially available. PAMAM dendrimers have been used with nitronyl nitroxide radicals,[17] like TEMPO radical[20] and more recently with derivatives of PROXYL radical[13] with promising results. Moreover, most clinically used MRI contrast agents work through shortening the, T_1, relaxation time of protons located nearby as is the case of radical dendrimers.

In this sense, the purpose of this Chapter was to perform experiments which are named "phantom experiments" to determine the spin-lattice relaxation time T_1 at different concentrations for each of them in order to obtain their relaxivities.

7.2 MRI experiments

With the purpose of having a reference compound, phantom experiments were performed with the monoradicals used to synthesize the corresponding radical dendrimers; *i. e.* the 4-amino-TEMPO (**35**) and 3-carboxy-PROXYL (**81**) radicals.

All experiments were performed in a BIOSPEC 7T (300 MHz) MRI system at 20^0C (spin-echo; repetition time of 100 ms and echo-time of 6 ms). Samples of different concentrations of paramagnetic compounds are introduced in the BIOSPECT MRI spectrometer and a NMR experiment is performed in order to determine the T_1 value of each concentration (which is the output obtained by application of **Equation 7.1**) obtaining a white spot images. The relaxivities (r) were calculated by the linear fit of the inverse of T_1 *vs* the concentrations, being the slope of the linear regression the relaxivity value.[16]

From the phantom experiments (**Figure 7.2**) it could be extracted the T_1 values at each concentration of the radical (**Table 7.1**). The increase in radical concentration implies a reduction in the time necessary to recover the magnetization in the z axis (T_1). With all the phantom data, by linear regression (**Figure 7.3**), we could obtain the relaxivities (r) of the monoradicals. The PROXYL monoradical relaxivity was found to be 538 $M^{-1}S^{-1}$ whereas the obtained TEMPO monoradical relaxivity was lower, with a value of 219 $M^{-1}S^{-1}$.

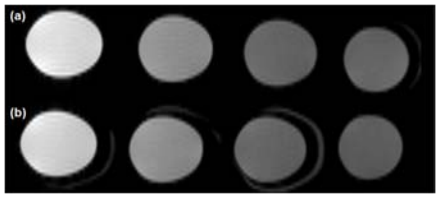

Figure 7.2: T_1 weight images in phantom experiment for (a) 4-amino-TEMPO **35** with concentrations of 5, 2.5, 1 and 0.5 mM. (b) 3-carboxy-PROXYL **81** with concentrations of 5, 2.5, 1 and 0.5 mM.

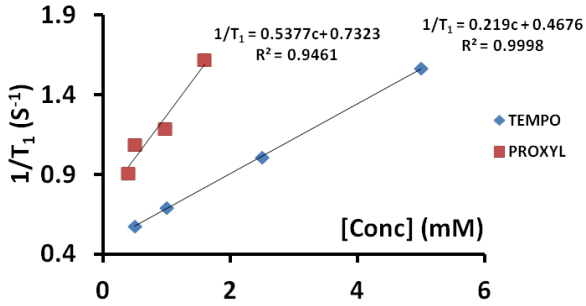

Figure 7.3: Plot of $1/T_1$ *versus* radical concentrations for 4-amino-TEMPO (**35**) in blue and 3-carboxy-PROXYL (**81**), in red, in water.

Table 7.1: T_1 values and relaxivities of radicals 4-amino-TEMPO **35** and 3-carboxy-PROXYL **81**.

	4-amino-TEMPO (**35**)		3-carboxy-PROXYL (**81**)	
	C (mM)	T_1 (ms)	C (mM)	T_1 (ms)
	0.5	1738	0.5	1102
	1	1443	1	921
	2.5	992	2.5	843
	5	639	5	617
r ($M^{-1}s^{-1}$)	219		538	

The relaxivity of the common used Gd (III) complex DOTA (Gadoterate meglumine), at room temperature, is reported to be 4200 $M^{-1}S^{-1}$;[9] a value that is higher than the 538 $M^{-1}S^{-1}$ obtained for 3-carboxy-PROXYL (**81**).

7.2.1 Experiments with TEMPO dendrimers

Only Gc_0-amidoTEMPO (**79**) dendrimer could be used in MRI experiments since the next generation, the Gc_1amidoTEMPO (**80**) was water insoluble at the desired concentrations to perform the phantom experiments.

The phantom experiment with the Gc_0amidoTEMPO (**79**) dendrimer, was performed only at 1.6, 0.98, 0.5 and 0.4 mM concentrations of the radical dendrimer in water since it is only partially soluble at concentrations higher than 2 mM performed. The resulting phantom images can be seen in **Figure 7.4** and, from them, it could be extracted the T_1 values of the radical dendrimer at the different concentrations (see **Table 7.2**) and from them (**Figure 7.5**), the relaxivity which was found to be 540 $M^{-1}s^{-1}$ which corresponds to a relaxivity for each TEMPO unit of the dendrimer of 90 $M^{-1}s^{-1}$. The later value contrast with the value found for the TEMPO radical **35**

which could indicate a poor inner sphere of water or a bad diffusion of the bulk water molecules to the outer sphere of the dendrimer.

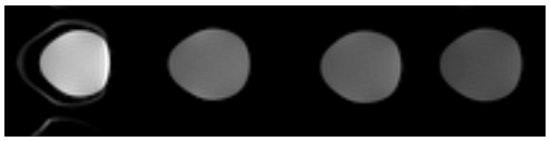

Figure 7.4: T_1 weight images in a phantom experiment for Gc_0amidoTEMPO (**79**) at concentration of 1.6, 0.98, 0.5 and 0.4 mM.

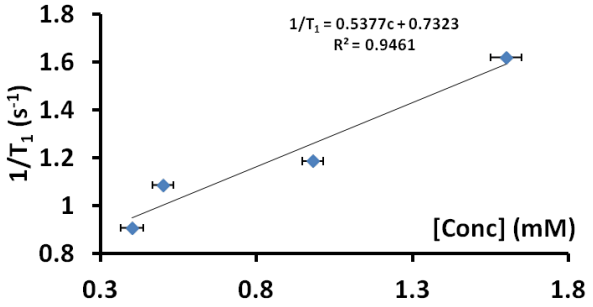

Figure 7.5: Plot of $1/T_1$ *versus* Gc_0amidoTEMPO (**79**) concentrations.

Table 7.2: T_1 values and relaxivity of Gc_0amidoTEMPO (**79**).

	Gc_0amidoTEMPO (**79**)	
	C (mM)	T_1 (ms)
	0.4	1102
	0.5	921
	0.98	843
	1.6	617
r ($M^{-1}s^{-1}$)	538	

Due to the solubility problems with the first generation (Gc_1amidoTEMPO (**80**)) we decided to change the strategy introducing several charges on the dendrimer surface replacing at the surface the TEMPO radical by the PROXYL unit, as the relaxivity of such radicals is higher.

7.2.2 Experiments with PROXYL Dendrimers

7.2.2.1 Lysine dendrimers

The radical dendrimers prepared included negative charged, from a carboxylate group, in each branch with the expectation to increase the water solubility of the radical dendrimers.

For the radical PROXYL-Lys(Gc_0)OLi (**89**) and PROXYL-Lys(Gc_1)OLi (**90**), four solutions in water were prepared at concentration of 4.4, 2.2, 1.1 and 0.55 mM for the zero generation and at 3.39, 1.70, 0.85 and 0.39 mM for the first generation. The phantoms of these samples are shown in **Figure 7.6** from which it could be extracted the T_1 values at the different concentrations (**Table 7.3**) and finally the relaxivity in water by linear regressions (**Figure 7.4**).

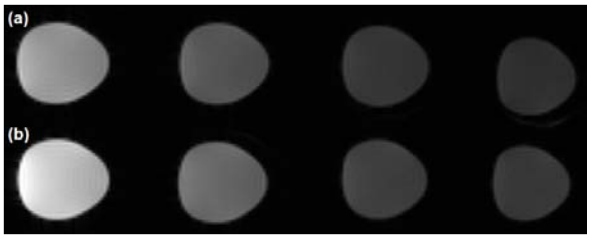

Figure 7.6: T_1 weight images for dendrimers a) PROXYL-Lys(Gc_0)OLi (**89**) at concentrations of 4.4, 2.2, 1.1 and 0.6 mM and b) PROXYL-Lys(Gc_1)OLi (**90**) at concentrations 3.4, 1.7, 0.9 and 0.4 mM.

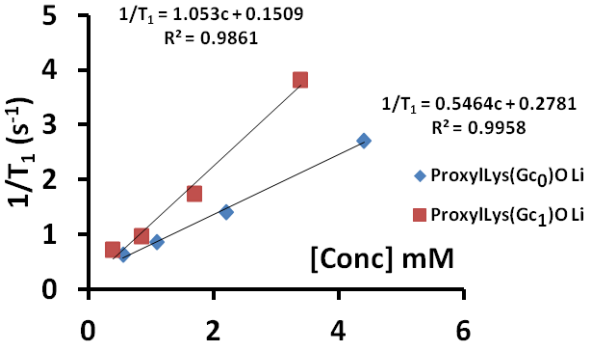

Figure 7.7: Representation of $1/T_1$ *versus* radical concentrations of PROXYL-Lys(Gc_0)OLi (**89**) (in blue) and PROXYL-Lys(Gc_1)OLi (**90**) (in red).

Table 7.3: T_1 values and relaxivities of dendrimers PROXYL-Lys(Gc_0)OLi (**89**) and PROXYL-Lys(Gc_1)OLi (**90**).

	PROXYL-Lys(Gc_0)OLi		PROXYL-Lys(Gc_1)OLi	
	C (mM)	T_1 (ms)	C (mM)	T_1 (ms)
	4.4	368	3.39	262
	2.2	712	1.7	573
	1.1	1164	0.85	1026
	0.55	1565	0.39	1366
r ($M^{-1}s^{-1}$)	546		1053	

The relaxivity for PROXYL-Lys(Gc_0)OLi (**89**) was 546 $M^{-1}s^{-1}$ which indicates that the PROXYL radical unit contributes by 91 $M^{-1}s^{-1}$, which is a very low value compared with the relaxivity of the monoradical **81** of 538 $M^{-1}s^{-1}$. This relaxivity was found to be similar to the monoradical alone. Moreover, the relaxivity by PROXYL unit is low, (91 $M^{-1}s^{-1}$). On the other hand, the first generation dendrimer, PROXYL-Lys(Gc_1)OLi (**90**) shows a total relaxivity of 1053 $M^{-1}s^{-1}$ that is the double of the previous generation 1053 $M^{-1}s^{-1}$ that is in agreement with the fact that there are double number of radical units, but the relaxivity per PROXYL unit is similar to the zero generation (88 $M^{-1}s^{-1}$). Thus, result shows the presence of PROXYL radical on the surface of this family of dendrimers does not enhance their relaxivity value probably because there is a poor inner sphere of water or a poor difusion of the bulk water molecules to the outer sphere of the dendrimers.

7.2.2.2 Tyrosine dendrimers

The radical dendrimers prepared for the next experiments included a negative charge, as in the previous case, from a carboxylate salt, in each branch. Moreover, in this

case the use of Tyrosine as linkers introduces more rigidity to the branches than in the Lysine case.

Four solutions in water were prepared with PROXYL-Tyr(Gc_0)OLi (**101**), PROXYL-Tyr(Gc_1)OLi (**102**) and PROXYL-Tyr(Gc_2)OLi (**103**) at concentrations of 2.22, 1.1, 0.55 and 0.28 mM for the zero generation, at 1.95, 0.97, 0.49 and 0.24 mM for the first generation, and at 0.55, 0.3, 0.14 and 0.07 mM for the second generation.

The phantoms images of these samples are shown in **Figure 7.8a** from which the T_1 values of the radical dendrimers at each concentration was extracted (**Table 7.4**) and finally, by linear regression (**Figure 7.9**), the relaxivities of the Tyrosine dendrimers PROXYL-Tyr(Gc_0)OLi (**101**), PROXYL-Tyr(Gc_1)OLi (**102**) and PROXYL-Tyr(Gc_2)OLi (**103**) were determined.

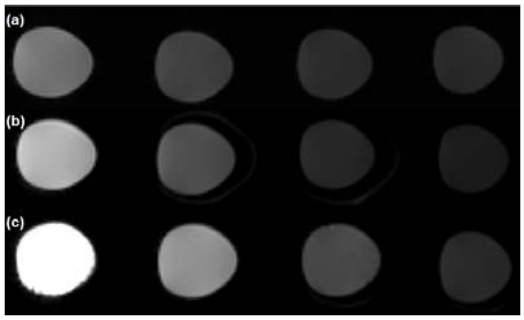

Figure 7.8: T_1 weight images for dendrimers PROXYL-Tyr(Gc_0)OLi (**101**) (a) at concentrations of 2.2, 1.11, 0.55 and 0.28 mM, PROXYL-Tyr(Gc_1)OLi (**102**) (b) at concentrations of 1.95, 0.97, 0.49 and 0.24 mM and PROXYL-Tyr(Gc_2)OLi (**103**) (c) at concentrations of 0.55, 0.3, 0.14 and 0.07 mM.

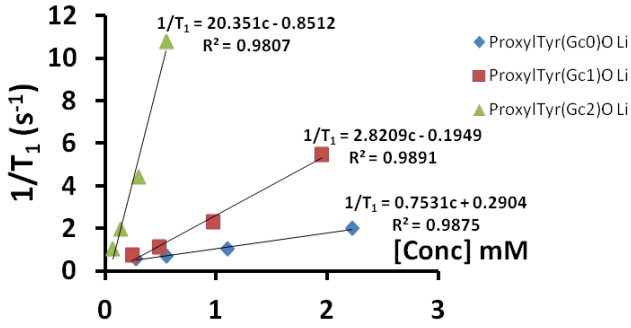

Figure 7.9: Representation of $1/T_1$ *versus* radical concentrations of PROXYL-Tyr(Gc_0)OLi (**101**) (blue), PROXYL-Tyr(Gc_1)OLi (**102**) (red) and PROXYL-Tyr(Gc_2)OLi (**103**) (green).

Table 7.4: T_1 values and relaxivities of dendrimers PROXYL-Tyr(Gc_0)OLi (**101**), PROXYL-Tyr(Gc_1)OLi (**102**) and PROXYL-Tyr(Gc_2)OLi (**103**).

	PROXYL-Tyr(Gc_0)OLi		PROXYL-Tyr(Gc_1)OLi		PROXYL-Tyr(Gc_2)OLi	
	C (mM)	T_1 (ms)	C (mM)	T_1 (ms)	C (mM)	T_1 (ms)
	2.22	499	1.95	184	0.55	93
	1.11	973	0.97	441	0.30	227
	0.55	1469	0.49	906	0.14	508
	0.28	1741	0.24	1408	0.07	961
r ($M^{-1}s^{-1}$)	753		2821		20351	

The relaxivities obtained for the dendrimers **101**, **102** and **103** were 753, 2821 and 20351 $M^{-1}s^{-1}$, respectively what indicated that each PROXYL radical unit at their

surface contributes with a value of 126, 235 and 848 $M^{-1}s^{-1}$. Thus, there is clearly a positive dendritic effect when the Tyrosine linker is present in contrast with the Lysine where there is not dendritic effect. This difference could be attributed to the rigidity of the Tyrosine linker that promotes fixed distances of the radicals units on the surface. A worth notorious point in that relaxivity value for each radical unit of the largest dendrimer **102** generation notoriously overcome the value of the monoradical **81** suggesting that the larger generation of this type of dendrimers would generate extremely large relaxivity values.

7.3 Conclusions

- The relaxivity per TEMPO radical of the Gc_0amidoTEMPO dendrimer (**79**) (90 $M^{-1}s^{-1}$) is lower than TEMPO monoradical **35** (219 $M^{-1}s^{-1}$).
- All the dendrimers which include negative charges on their surfaces (**89**, **90**, **101**, **102** and **103**) are water soluble as initially desired.
- The relaxivity per PROXYL radical unit of dendrimers PROXYL-Lys(Gc_x)OLi **89** and **90** with flexible linkers are small ,90 $M^{-1}s^{-1}$, and lower than that shown by the PROXYL monoradical, 538 $M^{-1}s^{-1}$.
- The relaxivity per PROXYL radical unit of dendrimers PROXYL-Tyr(Gc_x)OLi **101**, **102** and **103** with rigid linkers are 126, 235, and 848 $M^{-1}s^{-1}$, respectively, showing a positive dendritic effect that grow up with the size of the dendrimer.

Bibliography

[1] García J.M. *Espectroscopia in vivo por resonancia magnética nuclear.* EDEMA, **1991**.

[2] Robin A. *In vivo NMR spectroscopy.* Wiley, **2007**.

[3] Caravan P. *Chem. Soc. Rev.*, 35(5):p.512, **2006**.

[4] Macovski A. *J. Magn. Reson.Imaging*, 30:p.919, **2009**.

[5] DeFeo E.M., Wu C.L., McDougal W.S., and Cheng L.L. *Nat. Rev. Urol.*, 8:p.301, **2011**.

[6] Duarte J.M., Lei H., Mlynarik V., and Gruetter R. *Neuroimage*, 61:p.342, **2012**.

[7] Jeong K.K., Seong S.H., Young J.C., Seong H.P., Hanjong A., Choung-Soo K., and Kyoung-Sik C. *J. Magn. Reson. Img.*, 22(5):p.639, **2005**.

[8] Toth E., Pubanz D., Vauthey S., Helm L., and Merbach A.E. *Chem. Eur. J.*, 2(12):p.1607, **1996**.

[9] Caravan P., Ellison J.J., McMurry T.J., and Lauffer R.B. *Chem. Rev.*, 99:p.2293, **1999**.

[10] Brasch R.C., London D.A., Wesbey G.E., Tozer T. N., Nitecki D.E., Williams R.D. anf Doemeny J., Tuck L.D., and Lallemand D.P. *Radiology*, 147(3):p.773, **1983**.

[11] Vallet P., Vanhaverbeke Y., Bonnet P.A., Subra G., Chapat J.P., and Muller R.N. *Magn. Reson. Med.*, 32:p.11, **1994**.

[12] Sato N., Kobayashi H., Hiraga A., Saga T., Togashi K., Konishi J., and Brechbiel M. *Magn. Reson. Med.*, 46:p.1169, **2001**.

[13] Rajca A., Wang Y., Boska M., Paletta J.T., Olankitwanit A., Swanson M.A., Mitchell D.G., Eaton S.S., Eaton G.R., and Rajca S. *J. Am. Chem. Soc.*, 134(38):p.15724, **2012**.

[14] Kobayashi H., Kawamoto S., Jo S., Bryant H., Brechbiel M., and Star R. *Bioconjugate Chem.*, 14:p.388, **2004**.

[15] Bosman A.W., Jasssen R.A.J., and Meijer E.W. *Macromolecules*, 30:p.3606, **1997**.

[16] Winalski C.S., Shortkroff S., Mulkern R.V., Schneider E., and Rosen G.M. *Magn. Reson. Med.*, 48:p.965, **2002**.

[17] Francese G., Dunand F., Loselli C., merbach A., and Decurtins S. *Magn. Reson. Chem.*, 41:p.81, **2003**.

[18] Yordanov A., Yamada K., Krishna M., Mitchell J., Woller E., Cloninger M., and Brechbiel M. *Angew. Chem. Int. Ed.*, 40:p.2690, **2001**.

[19] Jacques V. and Desreux J. *Top. Curr. Chem.*, 221:p.123, **2002**.

[20] Maliakal A.J., Turro N.J., Bosman A.W., Cornel J., and Meijer E.W. *J. Phys. Chem. A*, 107:p.8467, **2003**.

Chapter 8

General Conclusions

The use of monoradicals and biradicals in Dynamic Nuclear Polarizacion has allowed the study of the hyperpolarized nuclei with low gyromagnetic values, such as ^{13}C, obtaining in some cases higher hyperpolarization levels than those obtained with the OX63 radical which is the gold standard compound used commonly in DNP experiments. Morever, with some monoradicals the time of irradiation, and therefore the experimental time, has been reduced and the sample formulation have been simplified by the elimination of sulfolane as glassing agent which makes easier the implimentation of these radicals for *in vivo* experiments.

On the other hand, the use of radical dendrimers as contrast agents for H_2O has been successfully achieved. The reduction of the transversal relaxation time (T_1) by the effect of the radicals was obtained for all the paramagnetic radical dendrimers. Only in the case of water soluble dendrimers, functionalized with Tyrosine was observed a positive dendritic effect that for the second generation containing 24 radical units,provides a relaxivity value comparable to many Gadolinium (III) complexes which are the nowadays the more common contrast agents used in clinical studies.

Chapter 9

Experimental details

9.1 Radicals synthesis

9.1.1 PTM derivatives

4-Methyltriphenylcarbinol (1)

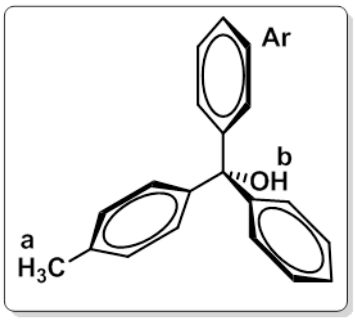

3.2 g (130.7 mmol, 1.1 eq) of magnesium and 0.1 g (0.8 mmol) of iodine were suspended in anhydrous diethyl ether under argon atmosphere at reflux temperature. A solution of 20.0 g (116.95 mmol, 1 eq) of *p*-bromotoluene in 45 ml of diethyl ether was slowly added and constantly stirred over 30 minutes. After 2 hours, a dissolution of 20.8 g (114.2 mmol, 0.98 eq) of benzophenone in 100 ml of diethyl ether was added drop by drop to the mixture reaction and the resulting mixture was refluxed for 1 hour. The reddish solution was constantly stirred for 18 hours. Then, the reaction mixture was poured over an ice bath (50 g of ice) previously acidified with 2.5 ml of sulfuric acid 2 M, and it was extracted with diethyl ether. The organic phase was washed with sodium bicarbonate (5% p/v) and water. Then it was dried over anhydrous magnesium sulfate and filtrated. The solvent was eliminated under vacuum. The yellow solid obtained was crystallized with a mixture of hexane and dichloromethane (3/1) and the desired compound was obtained (13 g, 41%).

Characterization:

- ^{1}H NMR (250 MHz, $CDCl_3$): δ 2.35 (*s*, 3H, H_a), 2.75 (*s*, 1H, H_b), 7.1-7.3 (*m*, 14H, H_{Ar}) ppm.
- MS (MALDI-TOF, negative mode): m/z 274 $[M-H]^-$.

Calculated: $C_{20}H_{18}O$: 274.4.

4-Methyltriphenylmethane (2)

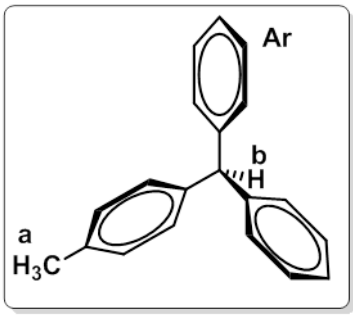

13 g (47.4 mmol, 1 eq) of 4-methyltriphenylcarbinol (**1**) were refluxed in 140 ml (364 mmol) of formic acid under argon atmosphere with constant stirring for 24 hours. The reaction mixture changes from dark green to pale pink. After this time, the mixture was cooled down to room temperature and 100 ml of water were added. The mixture was stirred for 30 minutes. Progressively, a white solid precipitated. It was dissolved with diethyl ether and a solution of saturated sodium bicarbonate was added until the aqueous solution was neutralized. Then, the organic phase was dried over anhydrous magnesium sulfate, filtrated and the solvent was removed under vacuum. The white powder obtained was purified by column chromatography on silica gel with mixtures of hexane and dichlorometane as eluent. A white powder (11 g, 90%) of the desired compound was obtained.

Characterization:

- ^{1}H NMR (250 MHz, $CDCl_3$): δ 2.3 (s, 3H, H_a), 5.5 (s, 1H, H_b), 7.0-7.3 (m, 14H, H_{Ar}) ppm.
- MS (MALDI-TOF, negative mode): m/z 257 $[M\text{-}H]^-$.
  Calculated: $C_{20}H_{18}$: 258.4.

αH-tetradecachloro-4-methyltriphenylmethane (3)

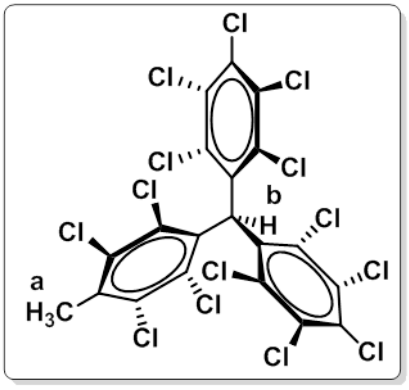

3.85 g (28.6 mmol, 0.37 eq) of $AlCl_3$, 4.5 ml of S_2Cl_2 (56 mmol, 0.72 eq) and 850 ml of SO_2Cl_2 were suspended under argon atmosphere. The orange suspension was refluxed under stirring and 20 g (77.4 mmol, 1 eq) of 4-methyltriphenylmethane (**2**) dissolved in 400 ml of SO_2Cl_2 were added drop by drop obtaining a brown reaction mixture. The mixture was refluxed (65 ^{0}C) for 10 hours. During this time, small quantities of SO_2Cl_2 were added in order to keep the volume of the reacting mixture constant. After that, the solution was cooled down to room temperature and concentrated in vacuum to half the volume. The mixture was poured over an ice bath (400 ml). The mixture was neutralized after slow additions of sodium bicarbonate until the obtaining of pH 7. The mixture was heated to 60 ^{0}C and the mixture was acidified with HCl until pH 2.5 obtaining a green precipitate. This solid was dissolved in $CHCl_3$ and washed with water. Finally, the

organic phase was dried over anhydrous magnesium sulfate, filtrated, and the solvent was eliminated under vacuum. The green solid was purified by digestion with refluxing pentane. The white solid was filtered under vacuum obtaining 40 g (70%) of the desired product.

Characterization:

- ^{1}H NMR (250 MHz, $CDCl_3$): δ 2.63 (s, 3H, H_a), 6.99 (s, 1H, H_b) ppm.
- MS (MALDI-TOF, negative mode): m/z 738 $[M\text{-}H]^-$.
  Calculated: $C_{20}H_4Cl_{14}$: 740.6. The spectrum shows a broad band due to the isotopic abundance of chlorine (^{35}Cl 76% and ^{37}Cl 24%).

αH–(4-bromomethyl)tetradecachloromethyltriphenylmethane (**4**)

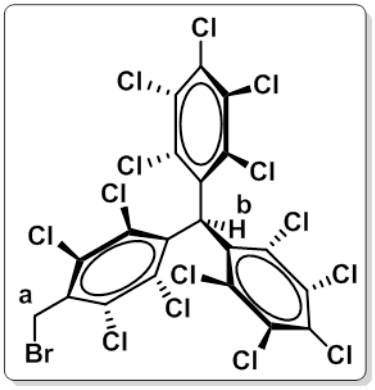

14 g (17 mmol, 1 eq) of αH-tetradecachloro-4-methyltriphenylmethane (**3**) were dissolved in 1.2 l of CCl_4 under argon atmosphere. Then, the solution was heated up to reflux with a white lamp (500 W) and 28 ml (566 mmol, 33.3 eq) of bromine were added. The mixture was refluxed for 6 hours. After this time, the mixture was cooled down to room temperature and the excess of bromine was eliminated by slowly addition of sodium bisulfite. Then, the organic phase was neutralized with sodium bicarbonate until pH 7, extracted with dichlorometane and dried over anhydrous magnesium sulfate. The solvent was removed under vacuum. The white powder obtained was purified by column chromatography on silica gel with mixtures of hexane and dichlorometane as eluent.The product was obtained as white-brown solid (12.8 g, 83%).

Characterization:

- ^{1}H NMR (250 MHz, $CDCl_3$): δ 4.8 (s, 2H, H_a), 7.0 (s, 1H, H_b) ppm.
- MS (MALDI-TOF, negative mode): m/z 740 $[M\text{-}Br]^-$.
  Calculated: $C_{20}H_3BrCl_{14}$: 819.5. The spectrum shows a broad band due to the isotopic abundance of chlorine.

αH–(4-hydroxymethyl)tetradecachloromethyltriphenylmethane (**5**)

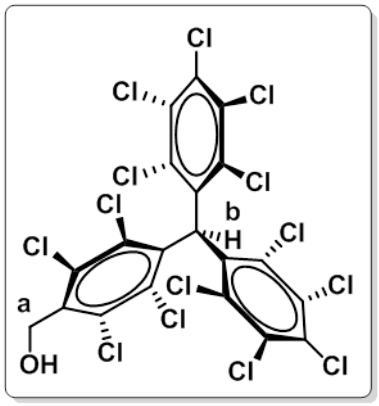

To an 250 ml round-bottom flask equipped with a magnetic stir-bar 0.5 g (0.61 mmol, 1 eq) of αH–(4-bromomethyl)tetradecachloromethyl triphenylmethane) (**4**), 0.6 g (7.3 mmol, 12 eq), 20 ml of MeOH and 30 ml of dioxane were added. The suspension was refluxed for three days. After cooling down to room temperature, the conversion into the acetate derivative was checked by TLC. Then, 7.5 ml of chloridric acid 37% was added and refluxed for 16 hours in order to hydrolyze the esther bond. After that, the mixture was cooled down to room temperature and the organic phase was extracted with dichloromethane. The solvent was removed under vacuum and and solid was purified by column chromatography on silica gel eluting with hexane to hexane:AcOEt 8:2. The pure product was isolated as off white powder (434 mg, 94%).

Characterization:

- ^{1}H NMR (250 MHz, $CDCl_3$): δ 2.19 (*t*, 1H, J= 7 Hz, H_{OH}), 5.07 (*d*, 2H, J= 7 Hz, H_a), 7.01 (*s*, 1H, H_b) ppm.
- MS (MALDI-TOF, positive mode): m/z 755 $[M+H]^+$.
  Calculated: $C_{20}H_4Cl_{14}O$: 756.6. The spectrum shows a broad band due to the isotopic abundance of chlorine.

αH–(4formyl)tetradecachloromethyltriphenylmethane (**6**)

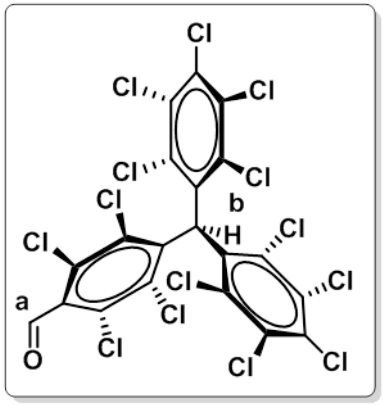

To an oven-dried 100 ml round-bottom flask equipped with a magnetic stir-bar 200 mg of pyridinium chlorochromate (PCC) (932 μmol, 1.5 eq) and 50 ml of dry dichloromethane were added. After suspension of PCC, 470 mg of αH–(4-hydroxymethyl) tetradecachloromethyltriphenyl methane (**5**)(621 μmol, 1 eq) were added to the suspension and the resulting mixture was stirred for 1.5 h. After that, the suspension was filtered in order to eliminate the chromium salts. The solvent was removed under vacuum and solid was purified by column chromatography on silica gel eluting with dichlorometane. The pure product was isolated as off yellow powder (399 mg, 85%).

Characterization:

- ^{1}H NMR (360 MHz, ^{6}d-acetone): δ 7.12 (s, 1H, H_b), 10.39 (s, 1H, H_a) ppm.
- MS (MALDI-TOF, positive mode): m/z 753 $[M+H]^+$.
  Calculated: $C_{20}H_2Cl_{14}O$: 755. The spectrum shows a broad band due to the isotopic abundance of chlorine.

αH–(4-ftalimidomethyl)tetradecachloromethyltriphenylmethane (**7**)

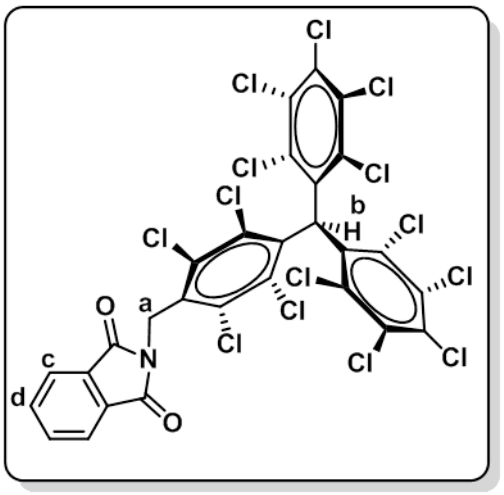

To an oven-dried 100 ml round-bottom flask equipped with a magnetic stir-bar, under argon, 600 mg (732 μmol, 1 eq) of αH–(4-bromomethyl)tetradecachloromethyl triphenylmethane) (**4**), 155 mg (805 μmol, 1.1 eq) and 50 ml of anhydrous DMF were added. The mixture was heated at 80 ^{0}C for 16 hours. After that, the mixture was cooled down to room temperature, the solvent was removed under high vacuum and the solid was purified by column chromatography on silica gel eluting with hexane/dichlorometane. The pure product was isolated as off yellow powder (558 mg, 86%).

Characterization:

- ^{1}H NMR (600 MHz, $CDCl_3$): δ 5.24 (d, 2H, H_a), 7.01 (s, 1H, H_b), 7.72 (m, 2H, H_c), 7.83 (m, 2H, H_d) ppm.
- MS (MALDI-TOF, positive mode): m/z 755 $[(M\text{-}Cl)+H]^+$.
  Calculated: $C_{28}H_7Cl_{14}NO_2$: 786. The spectrum shows a broad band due to the isotopic abundance of chlorine.

αH–(4aminomethyl)tetradecachloromethyltriphenylmethane (**8**)

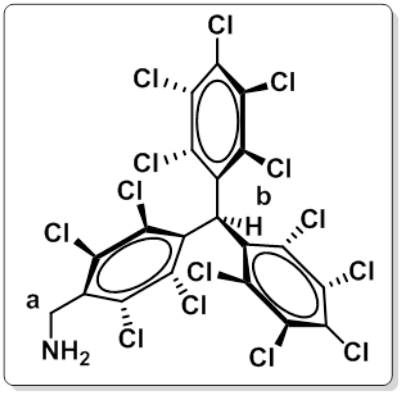

In a 100 ml round-bottom flask equipped with a magnetic stir-bar, 558 mg (630 μmol, 1 eq) of αH–(4-ftalimidomethyl)tetradecachloro methyltriphenylmethane (**7**) was suspended in EtOH, the mixture was heated to reflux and 300 μl (6.3 mmol, 10 eq) of hydrazine were added. The mixture was refluxed for 8 hours and cooled down to room temperature. A white solid of phthalhydrazide subproduct was observed and eliminated by filtration. The solvent was removed under vacuum and the solid was purified by column chromatography on silica gel eluting with dichlorometane. The pure product was isolated as white powder (405 mg, 85%).

Characterization:

- ^{1}H NMR (250 MHz, $CDCl_3$): δ 4.24 (s, 2H, H_a), 6.99 (s, 1H, H_b) ppm.
- MS (MALDI-TOF, positive mode): m/z 756 $[M+H]^+$.
  Calculated: $C_{20}H_5Cl_{14}N$: 756.6. The spectrum shows a broad band due to the isotopic abundance of chlorine.

Diethyl 4-[bis(2,3,4,5,6-pentachlorophenyl)methyl]-2,3,5,6-tetrachlorobenzyl phosphonate (**9**)

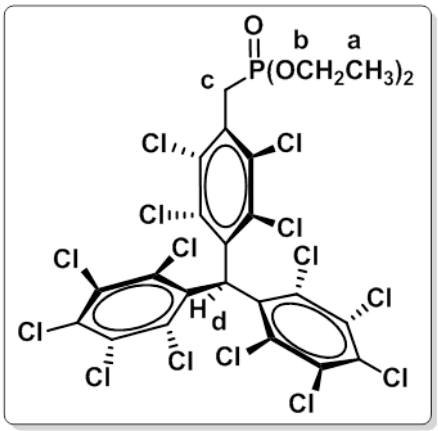

In a 250 ml flask 12.0 g (24.4 mmol, 1 eq) of αH-(4-bromomethyl)tetradecachloromethyl triphenylmethane (**4**) were dissolved in 100 ml (162 mmol) of triethyl phosphite. The mixture was refluxed at 160 ^{0}C with anhydrous $CaCl_2$ tube coupled in the cooling. After three hours it was cooled down to room temperature and 700 ml of water were added. The aqueous phase was extracted with chloroform for 3 times. The combined organic phase was washed with water, dried over anhydrous magnesium sulfate and filtered. The solvent was removed under vacuum. The product was purified by column chromatography on silica gel with mixtures of hexane and ethyl acetate as eluents. The product was isolated as a white powder (10.3 g, 80%).

Characterization:

- ^{31}P $\{^{1}H\}$ NMR (100 MHz, $CDCl_3$): δ 22 (s, P) ppm.
- ^{1}H NMR (250 MHz, $CDCl_3$): δ 1.3 (t, 6H, JH_aH_b=7.5 Hz, H_a),
  3.8 (d, 2H, JH_cP=22.5 Hz, H_c),
  4.1 (td, 4H, JH_bP=7.5 Hz, JH_bH_a=7.3 Hz, H_b),
  7.0 (d, 1H, JH_dP=2.5 Hz, H_d) ppm.
- MS (MALDI-TOF, negative mode): m/z 875 $[M\text{-}H]^-$.
  Calculated: $C_{24}H_{13}Cl_{14}O_3P$: 877. The spectrum shows a broad band due to the isotopic abundance of chlorine.

9.1.2 BDPA derivatives

(9-(4-bromobenzylidene)-9H-fluorene (11)

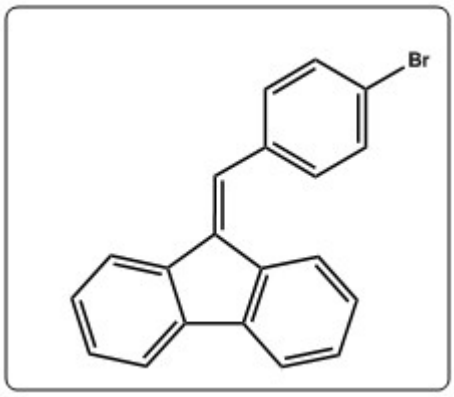

To an oven-dried two necked 100 ml round bottom flask containing a magnetic stir-bar 1.00 g (6 mmol, 1 eq) of fluorene and 1.9 g (16.5 mmol, 2.75 eq) of potassium *tert*-butoxide were added, followed by 60 ml of absolute ethanol. The flask was fitted with a water-cooler reflux condenser and a rubber septum. The mixture were heated to reflux with vigorous stirring and then 1.34 g (7.22 mmol, 1.2 eq) of 4-bromobenzaldehyde was added. The flask was allowed to reflux overnight. After cooling to room temperature, the mixture was poured into a flask containing excess of cold 1 M HCl. This mixture was extracted with 3 portions of ethyl acetate. The combined organic phase was dried over anhydrous magnesium sulfate and the solvent was removed under vacuum. The product was purified by column chromatography on silica gel eluting with a gradient from pure hexane to 98:2 Hx:EtOAc. The pure product was isolated as yellow powder (1.8 g, 90%).

Characterization:

- ^{1}H NMR (400 MHz, ^{6}d-dimethylsulfoxide): δ 7.15 (*t*, 1H, J= 8 Hz), 7.35-7.44 (*m*, 3H), 7.48 (*d*, 1H, J= 8 Hz), 7.56 (*d*, 2H, J=8 Hz), 7.72 (*d*, 2H, J= 8 Hz), 7.86 (*s*, 1H), 7.88 (*d*, 2H, J= 8 Hz), 7.97 (*d*, 1H, J=8 Hz) ppm.
- ^{13}C NMR (100 MHz, ^{6}d-dimethylsulfoxide): δ 140.8, 138.8, 138.4, 136.0, 135.6, 135.5, 131.7, 131.3, 129.0, 128.6, 127.3, 127.0, 123.69, 123.68, 121.5, 120.9, 120.3, 119.9 ppm.
- MS (MALDI-TOF, positive mode): m/z 332 $[M+H]^{+}$.
  Calculated: $C_{20}H_{13}Br$: 332/334.
- IR-ATR (cm^{-1}): 1482, 1448, 1435, 1065, 1008 and 729.

9-bromo-9-(bromo(4-bromophenyl)methyl)-9H-fluorene (**12**)

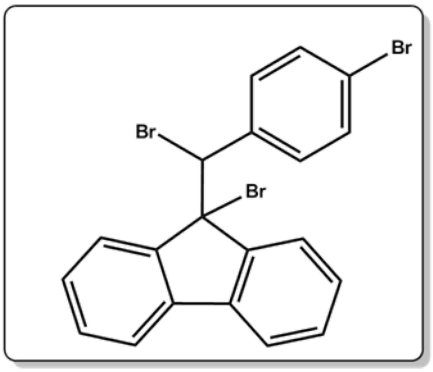

To an oven-dried 100 ml round-bottom flask equipped with a magnetic stir-bar 0.8 g of compound **11** (2.4 mmol, 1 eq), and 32 ml of AcOH were added. The resulting suspension was introduced in an ultrasound bath for 5 minutes and then, bromine was added (0.5 ml, 1.53 g, 9.6 mmol, 4 eq). The solution became a homogeneous red solution and was stirred for 5 minutes at room temperature. After this time, the mixture was poured into a flask containing excess of cold 1 M $NaHSO_3$ in order to eliminate the excess of bromine. The pH was adjusted to 7 with Na_2CO_3, and the solution was extracted with dichloromethane. The organic phase was dried over anhydrous magnesium sulfate and the solvent was removed under vacuum. The product was purified by column chromatography on silica gel eluting with hexane. The pure product was isolated as white powder (1.17 mg, 99%).

Characterization:

- ^{1}H NMR (400 MHz, ^{6}d-dimethylsulfoxide): δ 6.53 (*s*, 1H), 6.86 (*d*, 2H, J= 8 Hz), 7.2 (*d*, 2H, J= 8 Hz), 7.32 (*m*, 2H), 7.50 (*m*, 2H), 7.63-7.65 (*m*, 1H), 7.75-7.78 (*m*, 1H), 7.80 (*m*, 1H), 8.3 (*d*, 1H, J= 8 Hz) ppm.
- ^{13}C NMR (100 MHz, ^{6}d-dimethylsulfoxide): δ 144.6, 144.5, 139.0, 138.0, 136.1, 130.9, 130.3, 130.2, 129.7, 128.1, 126.4, 125.9, 121.6, 120.6, 120.4, 66.3, 60.3 ppm.
- MS (MALDI-TOF, positive mode): m/z 491 $[M+H]^+$.
  Calculated: $C_{20}H_{13}Br_3$: 493.
- IR-ATR (cm^{-1}): 2922, 1616, 1575, 1476, 1442, 1391, 1070, 1008, 773 and 722.

9-(bromo(4-bromophenyl)methylene)-9H-fluorene (**13**)

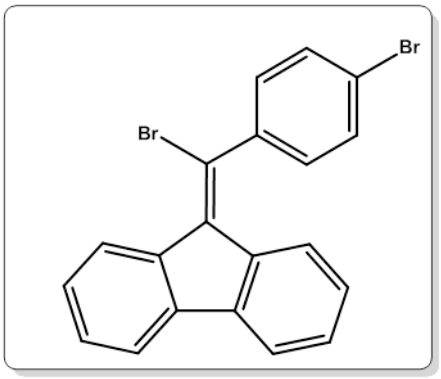

To an oven-dried two necked 250 ml round-bottom flask equipped with a magnetic stir-bar 1.2 g of compound **12** (2.4 mmol, 1 eq) and 30 ml of absolute ethanol were added. The flask was fitted with a water-cooler reflux condenser and with a rubber septum. In a 100 ml round-bottom flask equipped with a magnetic stir-bar 4.87 g of NaOH (122 mmol, 50 eq) and 60 ml of absolute ethanol were added. After dissolution of NaOH in ethanol, it was added to the 250 ml flask and refluxed for 1 hour. Then, it was

allowed to cool down to room temperature and the mixture was acidified with diluted hydrochloric acid. Afterwards, it was extracted with dichloromethane. The organic phase was dried over anhydrous magnesium sulfate and the solvent was removed under vacuum. The product was purified by column chromatography on silica gel eluting with hexane. The pure product was isolated as yellow powder (0.950 g, 95%).

Characterization:

- ^{1}H NMR (400 MHz, ^{6}d-dimethylsulfoxide): δ 6.20 (*d*, 1H, J= 8 Hz), 6.99 (*t*, 1H, J= 8 Hz), 7.31 (*t*, 1H, J= 8 Hz), 7.49-7.44 (*m*, 3H), 7.53 (*t*, 1H, J= 8 Hz), 7.80 (*d*, 2H, J= 8 Hz), 8.86 (*d*, 1H, J= 8 Hz), 7.94 (*d*, 1H, J= 8 Hz), 8.76 (*d*, 1H, J= 8 Hz) ppm.
- ^{13}C NMR (100 MHz, ^{6}d-dimethylsulfoxide): δ 141.7, 141.1, 139.7, 137.5, 137.3, 135.9, 133.0, 130.87, 130.1, 129.2, 127.9, 127.6, 125.9, 124.4, 123.43, 123.42, 120.6, 120.4 ppm.
- MS (MALDI-TOF, positive mode): m/z 412.0 $[M+H]^{+}$.
  Calculated: $C_{20}H_{12}Br_2$: 412.
- IR-ATR (cm^{-1}): 2922, 1590, 1488, 1488, 1407, 1071, 1010, 737 and 737.

9-((4-bromophenyl)(9H-fluoren-9-yl)methylene)-9H-fluorene (**14**)

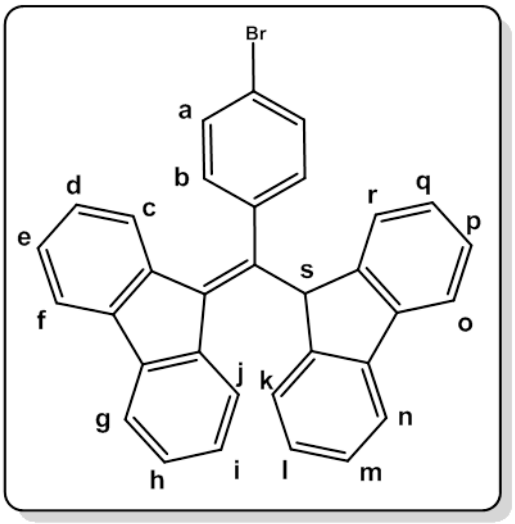

To an oven-dried 25 ml Schlenk flask equipped with a stir-bar and a rubber septum 0.3 g (728 μmol, 1 eq) of compound **13** was added. The flask was evacuated under vacuum and refilled with argon for three times and then 5 mL of dry dimethylacetamide (DMA) were added. In a separate oven-dried 25 ml Schlenk flask equipped with a stir-bar and a rubber septum 242 mg (1.46 mmol, 2 eq) of fluorene and 327 mg (2.91 mmol, 4 eq) of potassium *tert*-butoxide were added. The flask was also evacuated under vacuum and refilled with argon for three times and 10 mL of dry dimethylacetamide (DMA) were added. The solution appeared dark red. The dark red solution was slowly added to the compound **13** flask by cannulation. The reaction turned deep blue and then it was stirred for 2 hours at room temperature. After that, the flask was cooled down in an ice bath and 1 M HCl in diethyl ether was added until the blue color disappeared. The solution was diluted with water and extracted with dichloromethane. The organic phase was dried over anhydrous magnesium sulfate, the solvent was removed under vacuum and then with high vacuum to eliminate the

dimethylacetamide. The organic solid obtained was purified by column chromatography on silica gel eluting with hexane. The pure product was isolated as yellow powder (351 mg, 97%).

Characterization:

- ^{1}H NMR (500 MHz, ^{8}d-tetrahydrofuran): δ 5.95 (*d*, 1H, J= 8 Hz, H_c), 6.52 (*s*, 1H, H_s), 6.59 (*d*, 2H, J= 8 Hz, H_b), 6.79 (*t*, 1H, J= 8 Hz, H_d), 7.13 (*d*, 2H, J= 8 Hz, H_a), 7.18 (*t*, 1H, J= 8 Hz, H_e), 7.24 (*t*, 2H, J= 8 Hz, H_l, H_q), 7.29-7.36 (*m*, 3H, H_i, H_m, H_p), 7.43 (*t*, 1H, J= 8 Hz, H_h), 7.59 (*d*, 2H, J= 8 Hz, H_k, H_r), 7.69 (*d*, 2H, J= 8 Hz, H_n, H_o), 7.77 (*d*, 1H, J= 8 Hz, H_f), 7.90 (*d*, 1H, J= 8 Hz, H_g), 8.48 (*d*, 1H, J= 8 Hz, H_j) ppm.
- ^{13}C NMR (125 MHz, ^{8}d-tetrahydrofurane): δ 144.8, 144.1, 142.8, 142.2, 140.8, 139.4, 139.3, 138.6, 137.2, 131.5, 131.2, 129.0, 128.24, 128.20, 128.0, 127.6, 127.1, 126.5, 126.0, 125.9, 121.9, 120.7, 120.5, 119.8, 53.2 ppm.
- MS (MALDI-TOF, negative mode): m/z 497.5 $[M-H]^-$.
  Calculated: $C_{33}H_{21}Br$: 497.
- IR-ATR (cm^{-1}): 2989, 1444, 1075, 1006 and 729.
- UV-Vis(Anion): 610nm (ε = 28600 M^{-1} cm^{-1})

9-((4-bromophenyl)(fluoren-9-yl)methylene)-fluorene radical (15)

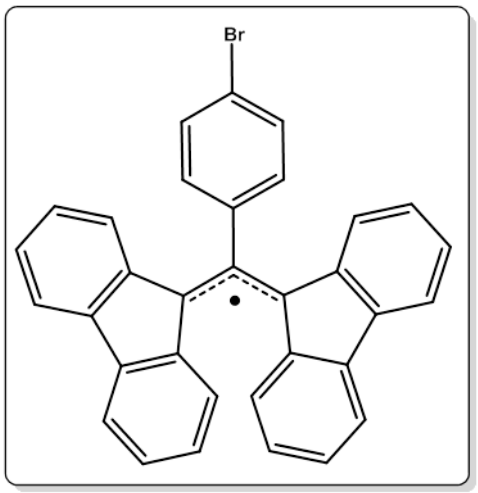

To an oven-dried 25 ml Schlenk flask equipped with a stir-bar and a rubber septum, 100 mg (201 μmol, 1 eq) of Br-BDPA (**14**) was added The flask was evacuated under vacuum and refilled with argon for three times and then 5 mL of dry DCM were added. After that, 60 μL (402 μmol, 2 eq) of 1,8-Diazabicyclo[5.4.0]undec-7-ene (DBU) were slowly added. The reaction turned into deep blue. The blue solution was stirred at room temperature for five minutes. Then, a solution of $AgNO_3$ (137 mg, 802 μmol, 4 eq) in ACN were added, and the oxidation was monitored by UV-Visible. The organic phase was removed under vacuum and the organic solid obtained was purified by column chromatography on silica gel eluting with hexane to hexane:dichlorometane 8:2. The pure product was isolated as a red powder (98 mg, 98%).

Characterization:

- EPR (Dichlorometane): g: 2.0024; a(4H).1.988 G, a(4H): 1.827 G, a(4H): 0 .539 G, a(4H): 0.365 G, a(2H): 0.065 G and a(2H): 0.062 G, ΔH_{pp}: 0.31 G.
- UV-Vis: 494 nm (ε = 29200 M^{-1} cm^{-1}), 859 nm (ε = 1410 M^{-1} cm^{-1})

4-((9H-fluoren-9-ylidene)methyl)benzonitrile (16)

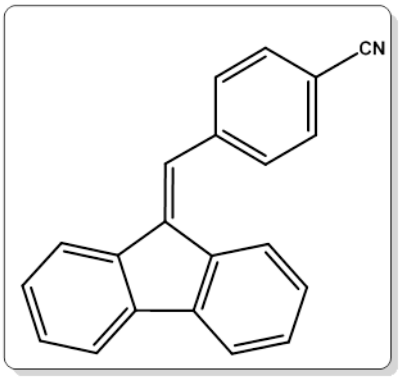

To an oven-dried two necked 1000 ml round bottom flask containing a magnetic stir-bar 3.00 g (18 mmol, 1 eq) of fluorene and 5.56 g (49.6 mmol, 2.75 eq) of potassium *tert*-butoxide were added, followed by 300 ml of absolute ethanol. The flask was fitted with a water-cooler reflux condenser and a rubber septum. The mixture was heated to reflux with vigorous stirring and then 2.8 g (21 mmol, 1.2 e) of 4-formylbenzonitrile were added. The flask was allowed to reflux overnight. After cooling to room temperature, the mixture was poured into a flask containing excess of cold 1 M HCl. This mixture was extracted with 3 portions of ethyl acetate. The organic phase was dried over anhydrous magnesium sulfate and the solvent was removed under vacuum. The product was purified by column chromatography on silica gel eluting with a gradient from pure hexane to 98 Hx: 5 EtOAc. The pure product was isolated as a yellow powder (4.5 g, 90%).

Characterization:

- ^{1}H NMR (400 MHz, ^{6}d-dimethylsulfoxide): δ 7.07 (*t*, 1H, J= 8 Hz), 7.34 (*t*, 2H, J= 8Hz), 7.42 (*t*, 2H, J= 8 Hz), 7.58 (*s*, 1H), 7.68-7.77 (*m*, 7H) ppm.
- ^{13}C NMR (100 MHz, ^{6}d-dimethylsulfoxide): δ 141.9, 141.4, 139.0, 139.0, 137.5, 135.6, 133.0, 130.5, 129.8, 129.3, 127.8, 127.5, 126.7, 124.2, 121.5, 120.8, 120.4, 119.2, 111.0 ppm.
- MS (MALDI-TOF, positive mode): m/z 279 $[M+H]^{+}$.
  Calculated: $C_{21}H_{13}N$: 279.
- IR-ATR (cm^{-1}): 2223, 1602, 1502, 1446 and 1433.

4-(bromo(9-bromo-9H-fluoren-9-yl)methyl)benzonitrile (17)

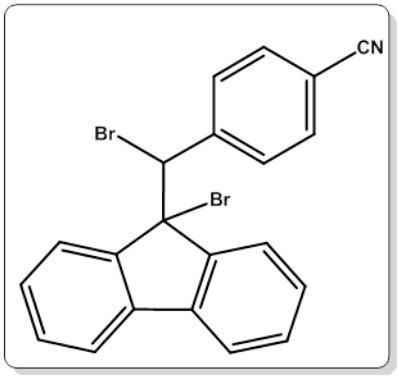

To an oven-dried 100 ml round-bottom flask equipped with a magnetic stir-bar, 2.5 g of compound **16** (8.9 mmol, 1 eq) and 50 ml of CCl_4 were added. The resulting suspension was introduced in an ultrasound bath for 5 minutes and then, bromine was added (1.83 ml, 5.7 g, 35,8 mmol, 4 eq). The solution became a homogeneous red solution and was stirred for 5 minutes at room temperature. After this time, the mixture was poured into a flask containing excess of cold 1 M $NaHSO_3$ in order to eliminate the excess of bromine. The pH was adjusted to 7 with Na_2CO_3, and the solution was extracted with dichloromethane. The organic phase was dried over anhydrous magnesium sulfate and the solvent was removed under vacuum. The product was purified by column chromatography on silica gel eluting with hexane. The pure product was isolated as white powder (3.8 g, 97%).

Characterization:

- ^{1}H NMR (400 MHz, ^{6}d-dimethylsulfoxide): δ 6.63 (s, 1H), 7.06 (d, 2H, J= 8 Hz), 7.31-7.33 (m, 2H), 7.49 (d, 2H, J= 8 Hz), 7.51-7.53 (m, 2H), 7.62-7.64 (m, 1H), 7.75-7.78 (m, 1H), 7.80-7.83(m, 1H), 8.23 (d, 1H, J= 8 Hz) ppm.
- ^{13}C NMR (100 MHz, $CDCl_3$): δ 144.4, 144.3, 141.9, 139.0, 138.01, 137.99, 131.3, 130.4, 129.9, 129.7, 128.2, 126.5, 125.9, 120.7, 120.5, 118.1, 111.0, 65.8 and 59.7 ppm.
- MS (MALDI-TOF, positive mode): m/z 441 $[M+H]^+$.
  Calculated: $C_{21}H_{13}Br_2N$: 439.
- IR-ATR (cm^{-1}): 2223, 1602, 1502, 1446 and 1433.

4-(bromo(9H-fluoren-9-ylidene)methyl)benzonitrile (18)

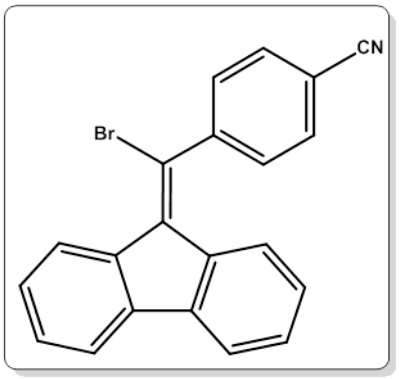

To an oven-dried two necked 500 ml round-bottom flask equipped with a magnetic stir-bar, 3.5 g of compound **17** (8 mmol, 1 eq) and 85 ml of absolute ethanol were added. The flask was fitted with a water-cooler reflux condenser and a rubber septum. In a 250 ml round-bottom flask equipped with a magnetic stir-bar 16 g of NaOH (399 mmol, 50 eq) and 175 ml of absolute ethanol were added. After dissolution of NaOH in ethanol, were added into the 500 ml flask and refluxed for 15 minutes. After letting it to cool down to room temperature, the mixture

was acidified with diluted hydrochloric acid and then extracted with dichloromethane. The organic phase was dried over anhydrous magnesium sulfate and the solvent was removed under vacuum. The product was purified by column chromatography on silica gel eluting with a gradient from pure hexane to Hx: EtOAc 95:5. The pure product was isolated as yellow powder (2. 56 g, 90%).

Characterization:

- ^{1}H NMR (400 MHz, ^{6}d-dimethylsulfoxide): δ 6.1 (*d*, 1H, J= 8 Hz), 6,97 (*t*, 1H, J= 8 Hz), 7.32 (*t*, 1H, J= 8 Hz), 7.47 (*t*, 1H, J= 8 Hz), 7.55 (*t*, 1H, J= 8 Hz), 7.74 (*d*, 2H, J= 8 Hz), 7.87 (*d*, 1H, J= 8 Hz), 7.95 (*d*, 1H, J= 8 Hz), 8.06 (*d*, 2H, J= 8 Hz), 8.77 (*d*, 1H, J= 8 Hz) ppm.
- ^{13}C NMR (100 MHz, ^{6}d-dimethylsulfoxide): δ 146.3, 140.8, 139.4, 136.8, 136.76, 135.8, 133.6, 130.0, 129.4, 129.0, 127.5, 127.4, 125.6, 124.1, 121.7, 120.3, 120.1, 118.4, 112.3 ppm.
- MS (MALDI-TOF, positive mode): m/z 359 $[M+H]^{+}$.
  Calculated: $C_{21}H_{12}BrN$: 357/359.
- IR-ATR (cm^{-1}): 2223, 1645, 1602, 1502 and 1444.

4-((9H-fluoren-9-yl)(9H-fluoren-9-ylidene)methyl)benzonitrile (**19**)

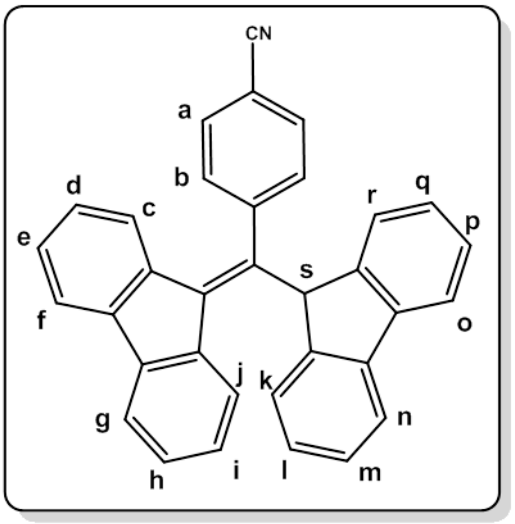

To an oven-dried 250 ml Schlenk flask equipped with a stir-bar and a rubber septum, 2.2 g (6.14 mmol, 1 eq) of compound **18** were added. The flask was evacuated under vacuum and refilled with argon for three times and then 32 mL of dry dimethylacetamide (DMA) were added. In a separate oven-dried 250 ml Schlenk flask equipped with a stir-bar and rubber septum, 1.53 g (9.2 mmol, 1.5 eq) of fluorene and 2.76 g (24.6 mmol, 4 eq) of potassium *tert*-butoxide were added. The flask was also evacuated under vacuum and refilled with argon for three times and 92 mL of dry dimethylacetamide (DMA) were added. The solution appeared dark red. The dark red solution was slowly added to the compound **18** flask by cannulation. The reaction turned deep green and was stirred for 2 hours at room temperature. After that, the flask was cooled down in an ice bath and then 1M HCl in diethyl ether was added until the green color disappeared. The solution was diluted with water and extracted with dichloromethane. The organic phase was dried over anhydrous magnesium sulfate, the solvent was removed under vacuum and then, with high vacuum to eliminate the

dimethylacetamide. The product was purified by column chromatography on silica gel eluting with a gradient from pure hexane to Hx:EtOAc 95:5. The pure product was isolated as yellow powder (2.66 g, 97%).

Characterization:

- ^{1}H NMR (600 MHz, ^{8}d-tetrahydrofuran): δ 5.70 (*d*, 1H, J= 8 Hz, H_c), 6.50 (*s*, 1H, H_s), 6.84 (*d*, 2H, J= 8 Hz, H_b), 6.88 (*t*, 1H, J= 8 Hz, H_d), 7.28 (*t*, 1H, J= 8 Hz, H_e), 7.31 (*t*, 2H, J= 8 Hz, H_l, H_q), 7.39 (*t*, 2H, J= 8 Hz, H_m, H_p), 7.43 (*t*, 1H, J= 8 Hz, H_i), 7.54 (*t*, 1H, J= 8 Hz, H_h), 7.57 (*d*, 2H, J= 8 Hz, H_a), 7.62 (*d*, 2H, J= 8 Hz, H_k, H_r), 7.82 (*d*, 2H, J= 8 Hz, H_n, H_o), 7.92 (*d*, 1H, J= 8 Hz, H_f), 8.05 (*d*, 1H, J= 8 Hz, H_g), 8.54 (*d*, 1H, J= 8 Hz, H_j) ppm.
- ^{13}C NMR (125 MHz, $CDCl_3$): δ 144.5, 144.2, 143.4, 142.8, 142.2, 140.9, 139.1, 139.0, 137.1, 132.1, 130.3, 129.3, 128.5, 128.4, 128.1, 127.7, 127.1, 126.6, 126.0, 125.8, 120.7, 120.6, 119.9, 118.7, 112.2, 53.0 ppm.
- MS (MALDI-TOF, negative mode): m/z 444 $[M-H]^-$.
  Calculated: $C_{34}H_{21}N$: 443.5.
- IR-ATR (cm^{-1}): 2223, 1645, 1602, 1498 and 1445.
- UV-Vis(Anion): 610 nm (ε = 21000 M^{-1} cm^{-1})

4-((fluoren-9-yl)(fluoren-9-ylidene)methyl)benzonitrile radical (20)

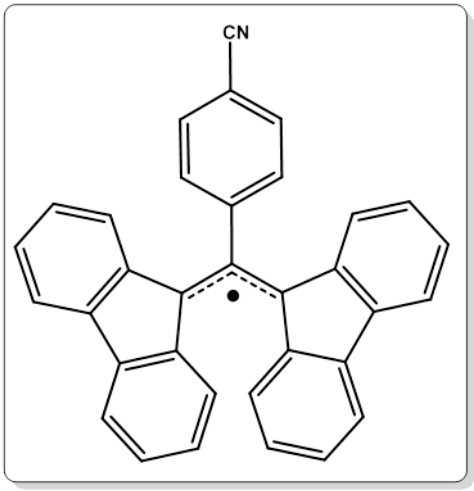

To an oven- dried 25 ml schlenk flask equipped with a stir-bar and a rubber septum, 100 mg (225 μmol, 1 eq) of CN-BDPA **19** was added. The flask was evacuated under vacuum and refilled with argon for three times and then 5mL of dry DCM were added. After that, 70 μL (451 μmol, 2 eq) of 1,8-Diazabicyclo[5.4.0]undec-7-ene (DBU) were slowly added. The reaction turned into deep green. The green solution was stirred at room temperature for five minutes. Then, a solution of $AgNO_3$ (153 mg, 902 μmol, 4 eq) in ACN were added, and the oxidation was monitored by UV-Visible. The organic phase was removed under vacuum and the organic solid obtained was purified by column chromatography on silica gel eluting with hexane to hexane:dichlorometane 8:2. The pure product was isolated as a red powder (97 mg, 97%).

Characterization:

- EPR (solvent): g: 2.0024; a(4H).1.988 G, a(4H): 1.827 G, a(4H): 0 .539 G, a(4H): 0.365 G, a(2H): 0.065 G and a(2H): 0.062 G, ΔH_{pp}: 0.31 G.
- UV-Vis: 495 nm (ε = 33300 M^{-1} cm^{-1}), 860 nm (ε = 2300 M^{-1} cm^{-1})

(4-((9H-fluoren-9-yl)(9H-fluoren-9-ylidene)methyl)phenyl)methanamine (21)

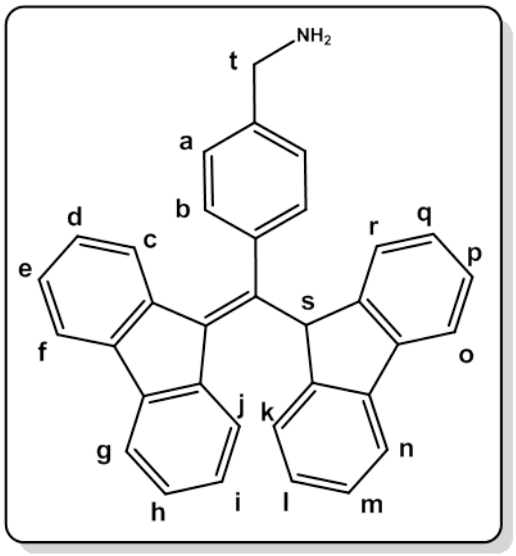

To an oven-dried 250 ml Schlenk flask equipped with a stir-bar and a rubber septum, 2.5 g (5.6 mmol, 1 eq) of CN-BDPA **19** were added. The flask was evacuated under vacuum and refilled with argon for three times and 80 mL of dry tetrahydrofuran (THF) were added. The mixture was cooled in an ice bath and 22.54 mL of a solution of $LiAlH_4$ in THF 1 M (22.56 mmol, 4 eq) were slowly added. The reaction turned deep blue and was stirred for 4 hours at room temperature. After that, the flask was cooled in an ice bath and 1 M HCl in diethyl ether was added until the blue color disappeared. The solution was diluted with 1 M $KHCO_3$/DCM and extracted with dichloromethane. The organic phase was dried over anhydrous magnesium sulfate and the solvent was removed under vacuum. The product was purified by column chromatography on silica gel eluting with a dichlorometane. The pure product was isolated as dark red powder (1.76 g, 70%).

Characterization:

- ^{1}H NMR (500 MHz, CD_2Cl_2): δ 3.77 (*s*, 2H, H_t), 5.85 (*d*, 1H, J= 8 Hz, H_c), 6.53 (*s*, 1H, H_s), 6.69 (*d*, 2H, J= 8 Hz, H_b), 7.84 (*t*, 1H, J= 8 Hz, H_d), 7.01 (*d*, 2H, J= 8 Hz, H_a), 7.23 (*t*, 1H, J= 8 Hz, H_e), 7.31 (*t*, 2H, J= 8 Hz, H_l, H_q), 7.36-7.41 (*m*, 3H, H_i, H_m, H_p), 7.51 (*t*, 1H, J= 8 Hz, H_h), 7.65 (*d*, 2H, J= 8 Hz, H_k, H_r), 7.71 (*d*, 2H, J= 8 Hz, H_k, H_r), 7.79 (*d*, 2H, J= 8 Hz, H_n, H_o), 7.92 (*d*, 1H, J= 8 Hz, H_g), 8.46 (*d*, 1H, J= 8 Hz, H_j) ppm.
- ^{13}C NMR (125 MHz, $CDCl_3$): δ 145.1, 144.3, 142.4, 141.4, 140.0, 139.1, 138.8, 137.0, 139.3, 128.7, 128.3, 127.59, 127.55, 127.4, 127.1, 126.8, 126.6, 126.1, 125.6, 125.23, 125.29, 120.1, 120.1, 119.2, 52.9, 45.9 ppm.
- MS (MALDI-TOF, positive mode): m/z 448 $[M+H]^+$.
  Calculated: $C_{34}H_{25}N$: 447.6.

- IR-ATR (cm^{-1}): 2926, 2855, 1610, 1510 and 1444.
- UV-Vis(Anion): 602 nm (ε = 228000 M^{-1} cm^{-1})

(4-((fluoren-9-yl)(fluoren-9-ylidene)methyl)phenyl)methanamine radical, BAm-BDPA (22)

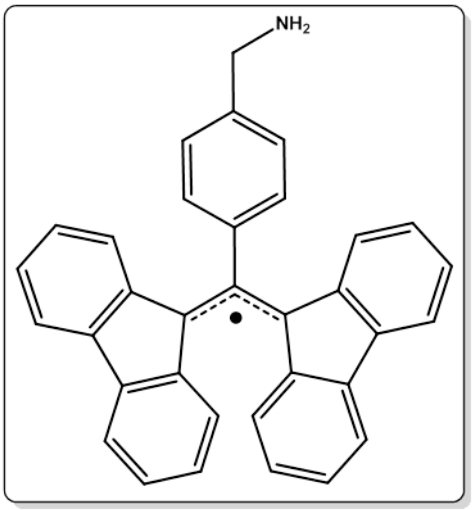

To an oven- dried 25 ml Schlenk flask equipped with a stir-bar and a rubber septum, 100 mg (223 μmol, 1 eq) of $BDPACH_2NH_2$ (**21**) was added The flask was evacuated under vacuum and refilled with argon for three times and then 5mL of dry DCM were added. After that, 67 μL (447 μmol, 2 eq) of 1,8-Diazabicyclo[5.4.0]undec-7-ene (DBU) were slowly added. The reaction turned into deep blue. The blue solution was stirred at room temperature for five minutes, then, a solution of $AgNO_3$ (152 mg, 894 μmol, 4 eq) in ACN were added, and the oxidation was monitored by UV-Visible. The organic phase was removed under vacuum and the organic solid obtained was purified by column chromatography on silica gel eluting with hexane to dichlorometane: methanol 98:2. The pure product was isolated as a red powder (98 mg, 98%).

Characterization:

- EPR (solvent): g: 2.0024; a(4H).1.988 G, a(4H): 1.827 G, a(4H): 0 .539 G, a(4H): 0.365 G, a(2H): 0.065 G and a(2H): 0.062 G. Linewidth 0.31.
- UV-Vis: 493 nm (ε = 32300 M^{-1} cm^{-1}), 855 nm (ε = 1150 M^{-1} cm^{-1})

4-((9H-fluoren-9-ylidene)methyl)benzoic acid (23)

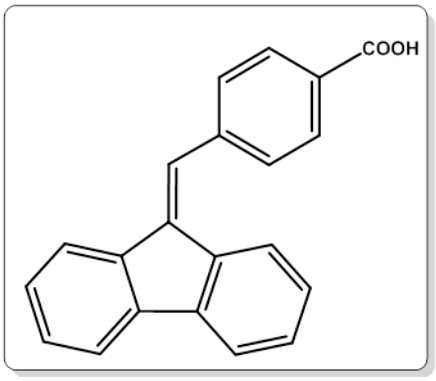

To an oven-dried two necked 250 ml round bottom flask containing a magnetic stir-bar, 2.68 g (16.2 mmol, 1 eq) of fluorene and 6.0 g (53.3 mmol, 2.75 eq) of *tert*-butoxide were added, followed by 150 ml of absolute ethanol. The flask was fitted with a water-cooler reflux condenser and a rubber septum. The mixture was heated to reflux with vigorous stirring and then 3.0 g (19.4 mmol, 1.2 eq) of 4-formylbenzoic acid was added. The flask was allowed to reflux overnight. After cooling to room temperature, the mixture was poured into a flask containing excess of cold 1 M HCl. This mixture was

extracted with 3 portions of ethyl acetate. The organic phase was dried over anhydrous magnesium sulfate and the solvent was removed under vacuum. The product was purified by recristalization on toluene. The pure product was isolated as yellow powder (4.4 g, 91%).

Characterization:

- ^{1}H NMR (600 MHz, ^{6}d-acetone): δ 7.13 (*t*, 1H, J= 6 Hz), 7.39 (*t*, 2H, J= 6Hz), 7.44 (*t*, 1H, J= 6 Hz), 7.56 (*d*, 1H, J= 6 Hz), 7.77 (*d*, 1H, J= 6 Hz), 7.85 (*d*, 2H, J= 6 Hz), 7.91 (*s*, 1H), 7.96 (*d*, 1H, J= 6 Hz), 8.20 (*d*, 2H, J= 6 Hz), 11.28 (*br*, 1H) ppm.
- ^{13}C NMR (125 MHz, ^{6}d-dimethylsulfoxide): δ 167.4, 140.9, 140.7, 138.8, 138.5, 136.5, 135.5, 130.9, 129.7, 129.3, 129.1, 128.7, 127.37, 127.35, 127.1, 123.9, 121.0, 120.3, 119.9. ppm.
- MS (MALDI-TOF, positive mode): m/z 299 $[M+H]^{+}$.
  Calculated: $C_{21}H_{14}O_2$: 298.
- IR-ATR (cm^{-1}): 1679, 1602, 1445, 1422, 1290, 722.

4-(bromo(9-bromo-9H-fluoren-9-yl)methyl)benzoic acid (24)

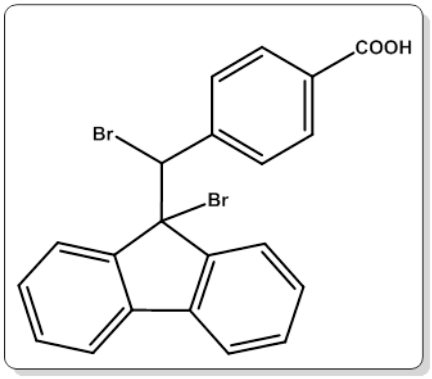

To an oven-dried 100 ml round-bottom flask equipped with a magnetic stir-bar 3 g of compound **23** (10.1 mmol, 1 eq), and 60 ml of CCl_4 were added. The resulting suspension was introduced in an ultrasound bath for 5 minutes and then, 0.62 ml of bromine (1.93 g, 12.1 mmol, 1.2 eq) was added. The solution became a homogeneous red solution and was stirred for 10 minutes at room temperature. After this time, the mixture was poured into a flask containing excess of cold 1 M $NaHSO_3$ in order to eliminate the excess of bromine. The pH was adjusted to 4 with Na_2CO_3, and the solution was extracted with dichloromethane. The organic phase was dried over anhydrous magnesium sulfate and the solvent was removed under vacuum. The pure product was isolated as white powder (4.05 g, 88%) and was used in the next step without further purification.

Characterization:

- ^{1}H NMR (400 MHz, ^{6}d-acetone): δ 6.36 (*s*, 1H), 7.12 (*d*, 2H, J= 7.2 Hz), 7.31-7.38 (*m*, 2H), 7.53 (*t*, 2H, J= 7.2 Hz), 7.58 (*d*, 1H, J= 7.2 Hz), 7.65 (*d*, 2H, J= 7.2

Hz), 7.72 (*d*, 1H, J= 7.2 Hz), 7.84 (*d*, 1H, J= 7.2 Hz), 8.3 (*d*, 1H, J= 7.2 Hz), 11.28 (*br*, 1H) ppm.

- ^{13}C NMR (100 MHz, ^{6}d-dimethylsulfoxide): δ 166.6, 144.7, 144.4, 141.2, 139.0, 138.1, 130.5, 130.2, 129.8, 129.1, 128.2, 128.09, 129.05, 126.4, 126.0, 120.5, 120.4, 66.2, 60.4 ppm.
- MS (MALDI-TOF, positive mode): m/z 456/458 $[M+H]^+$.
  Calculated: $C_{21}H_{14}Br_2O_2$: 458.
- IR-ATR (cm^{-1}): 1688, 1610, 1426, 1288, 741, 728.

4-(bromo(9H-fluoren-9-ylidene)methyl)benzoic acid (25)

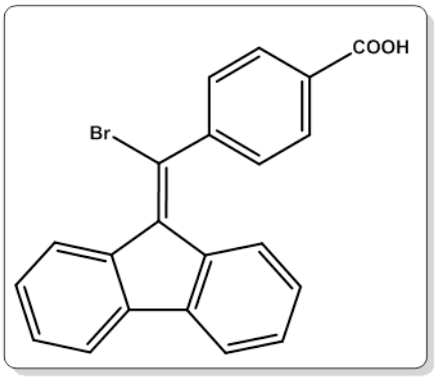

To an oven-dried two necked 250 ml round-bottom flask equipped with a magnetic stir-bar, 3.0 g of compound **24** (6.5 mmol, 1 eq) and 60 ml of absolute ethanol were added. The flask was fitted with a water-cooler reflux condenser and with a rubber septum. In a 100 ml round-bottom flask equipped with a magnetic stir-bar 1.05 g of NaOH (26.2 mmol, 4 eq) and 75 ml of absolute ethanol were added. After dissolution of NaOH in ethanol, it was added to the 250 ml flask and refluxed for 1 hour. Then it was allowed to cool down to room temperature and the mixture was acidified with diluted hydrochloric acid. Afterwards, it was extracted with dichloromethane. The organic phase was dried over anhydrous magnesium sulfate and the solvent was removed under vacuum. The pure product was isolated without further purification as a yellow powder (2.42 g, 98%).

Characterization:

- ^{1}H NMR (400 MHz, ^{6}d-acetone): δ 6.26 (*d*, 1H, J= 8 Hz), 6,93 (*t*, 1H, J= 8 Hz), 7.30 (*t*, 1H, J= 8 Hz), 7.47 (*t*, 1H, J= 8 Hz), 7.54 (*t*, 1H, J= 8 Hz), 7.68 (*d*, 2H, J= 8 Hz), 7.82 (*d*, 1H, J= 8 Hz), 7.91 (*d*, 1H, J= 8 Hz), 8.27 (*d*, 2H, J= 8 Hz), 8.87 (*d*, 1H, J= 8 Hz), 11.28 (*br*, 1H) ppm.
- ^{13}C NMR (100 MHz, ^{6}d-dimethylsulfoxide): δ 166.7, 146.0, 140.7, 139.3, 137.0, 136.8, 135.5, 131.6, 130.5, 129.8, 128.8, 128.6, 127.3, 125.5, 124.0, 123.0, 120.3, 120.0 ppm.
- MS (MALDI-TOF, positive mode): m/z 377/379 $[M+H]^+$.
  Calculated: $C_{21}H_{13}BrO_2$: 377.
- IR-ATR (cm^{-1}): 1673, 1418, 1268, 1177, 776, 765, 726.

4-((9H-fluoren-9-yl)(9H-fluoren-9-ylidene)methyl)benzoic acid (**26**)

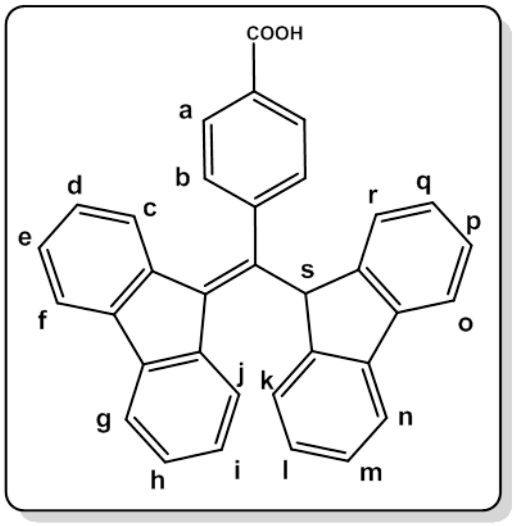

To an oven-dried 250 ml schlenk flask equipped with a stir-bar and a rubber septum, 0.5 g (1.33 mmol, 1 eq) of compound **25** was added. The flask was evacuated under vacuum and refilled with argon for three times and then 18.5 mL of dry dimethylacetamide (DMA) were added. In a separate oven-dried 100 ml Schlenk flask equipped with a stir-bar and a rubber septum, 330 mg (1.99 mmol, 1.5 eq) of fluorene and 744 mg (6.63 mmol, 5 eq) of potassium *tert*-butoxide were added. The flask was also evacuated under vacuum and refilled with argon for three times and 68.5 mL of dry dimethylacetamide (DMA) were added. The solution appeared dark red. The dark red solution was slowly added to the compound **25** flask by cannulation. The mixture turned deep blue and then, it was stirred for 1.5 hours at room temperature. After that, the flask was cooled down in an ice bath and 1 M HCl in diethyl ether was added until the blue color disappeared. The solution was diluted with water and extracted with dichloromethane. The organic phase was dried over anhydrous magnesium sulfate, the solvent was removed under vacuum and then with high vacuum to eliminate the dimethylacetamide. The organic solid obtained was purified by column chromatography on silica gel eluting with dichloromethane. The pure product was isolated as a yellow powder (330 mg, 54%).

Characterization:

- ^{1}H NMR (400 MHz, CD_2Cl_2): δ 5.89 (*d*, 1H, J= 8 Hz, H_c), 6.53 (*s*, 1H, H_s), 6.78-6.82 (*m*, 3H, H_b, H_d), 7.23 (*t*, 1H, J= 7.6 Hz, H_e), 7.29 (*t*, 2H, J= 7.6 Hz, H_l, H_q), 7.35-7.41 (*m*, 3H, H_i, H_m, H_p), 7.49 (*t*, 1H, J= 7.6 Hz, H_h), 7.62 (*d*, 2H, J= 7.6 Hz, H_a), 7.76 (*m*, 4H, H_k, H_n, H_o, H_r), 7.8 (*d*, 1H, J= 7.6 Hz, H_f), 7.90 (*d*, 1H, J= 7.6 Hz, H_g), 8.46 (*d*, 1H, J= 7.6 Hz, H_j) ppm.
- ^{13}C NMR (125 MHz, $CDCl_3$): δ 169.9, 144.3, 143.7, 143.4, 141.9, 141.4, 139.9, 138.4, 138.4, 136.1, 129.6, 128.7, 128.5, 127.74, 127,69, 127.4, 127.1, 126.7, 125.9, 125.28, 125.26, 125.1, 120.1, 120.0, 119.2, 52.3 ppm.
- MS (MALDI-TOF, negative mode): m/z 461 $[M-H]^-$.
  Calculated: $C_{34}H_{22}O_2$: 462.5.
- IR-ATR (cm^{-1}): 1589, 1444, 1075, 1006 and 729.
- UV-Vis(Anion): 610 nm (ε = 28600 M^{-1} cm^{-1})

4-((fluoren-9-yl)(fluoren-9-ylidene)methyl)benzoic acid radical (**27**)

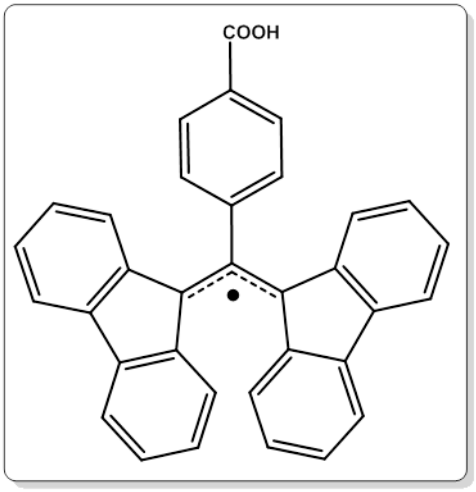

To an oven- dried 25 ml Schlenk flask equipped with a stir-bar and a rubber septum, 100 mg (216 μmol, 1 eq) of COOH-BDPA (**26**) was added. The flask was evacuated under vacuum and refilled with argon for three times and then 5mL of dry DCM were added. After that, 64 μL (432 μmol, 2 eq) of 1,8-Diazabicyclo[5.4.0]undec-7-ene (DBU) were slowly added. The reaction turned into deep blue. The blue solution was stirred at room temperature for five minutes, then, a solution of $AgNO_3$ (147 mg, 865 μmol, 4 eq) in ACN were added, and the oxidation was monitored by UV-Visible. The organic phase was removed under vacuum and the organic solid obtained was purified by column chromatography on silica gel eluting with hexane to dichlorometane: methanol 98:2. The pure product was isolated as a red powder (98 mg, 98%).

Characterization:

- EPR (solvent): g: 2.0024; a(4H).1.988 G, a(4H): 1.827 G, a(4H): 0 .539 G, a(4H): 0.365 G, a(2H): 0.065 G and a(2H): 0.062 G, ΔH_{pp}: 0.31 G.
- UV-Vis: 494 nm (ε = 29200 M^{-1} cm^{-1}), 859 nm (ε = 1410 M^{-1}, cm^{-1})

(4-((9H-fluoren-9-yl)(9H-fluoren-9-ylidene)methyl)phenyl)methanol (**28**)

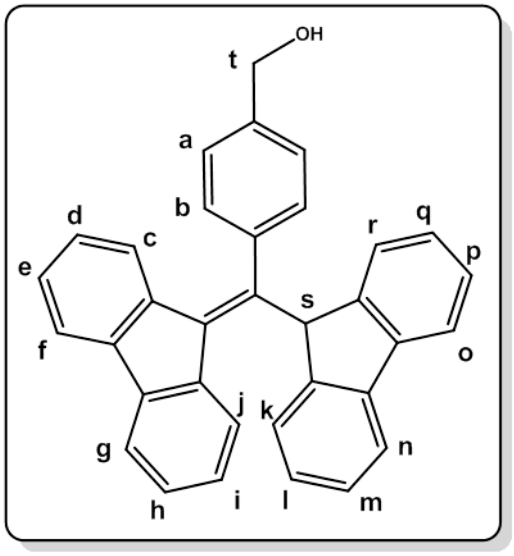

To an oven-dried 100 ml Schlenk flask equipped with a stir-bar and a rubber septum, 500 mg (1.08 mmol, 1 eq) of COOH-BDPA (**26**) was added. The flask was evacuated under vacuum and refilled with argon for three times and then, 40 mL of dry tetrahydrofuran (THF) were added. The Schlenk was cooled down in an ice bath and, after that, 5.4 ml (5.40 mmol, 5 eq) of diisobutylaluminium hydride (DIBAL-H) were slowly added. The reaction was allowed to warm to room temperature and was stirred for 1.5 hours at this temperature. After that, the flask was cooled down in an ice bath and 1 M HCl in diethyl ether was added until pH of 4. The solution was diluted with water and extracted with dichloromethane. The organic phase was dried over anhydrous magnesium sulfate, the solvent was removed under vacuum and the organic solid obtained was purified by column chromatography on silica gel eluting with dichloromethane. The pure product was isolated as a off yellow powder (430 mg, 90%).

Characterization:

- ^{1}H NMR (500 MHz, ^{6}d-acetone): δ 4.13 (*t*, 1H, J= 6 Hz, H_{OH}), 4.51 (*d*, 2H, J= 8 Hz, H_t), 5.86 (*d*, 1H, J= 8 Hz, H_c), 6.55 (*s*, 1H, H_s), 6.71 (*d*, 2H, J= 8 Hz, H_b) 6.80 (*t*, 1H, J= 8 Hz, H_d), 7.05 (*d*, 2H, J= 8 Hz, H_a),7.25 (*t*, 1H, J= 8 Hz, H_e), 7.34 (*t*, 2H, J= 8 Hz, H_l, H_q),7.39 (*t*, 2H, J= 8 Hz, H_m, H_p), 7.45 (*t*, 1H, J= 8 Hz, H_i), 7.53 (*t*, 1H, J= 8 Hz, H_h), 7.70 (*d*, 2H, J= 8 Hz, H_k, H_r), 7.78 (*d*, 2H, J= 8 Hz, H_n, H_o), 7.87 (*d*, 1H, J= 8 Hz, H_f), 8.02 (*d*, 1H, J= 8 Hz, H_g), 8.56 (*d*, 1H, J= 8 Hz, H_j) ppm.
- ^{13}C NMR (125 MHz, ^{6}d-acetone): δ 145.7, 144.7, 142.2, 142.1, 141.6, 140.2, 139.3, 138.9, 137.7, 136.5, 128.68, 128.67,127, 95, 127.93, 127.90, 127.4, 126.8, 126.4, 126.1, 125.8, 125.7, 120.4, 120.3, 119.5, 63.7, 53.1 ppm.
- MS (MALDI-TOF, negative mode): m/z 447 $[M-H]^-$.
  Calculated: $C_{34}H_{24}O$: 448.6.
- IR-ATR (cm^{-1}): 2923, 1444, 1013, 1006, 782 and 727.
- UV-Vis(Anion): 610 nm (ε = 28600 M^{-1} cm^{-1})

(4-((fluoren-9-yl)(fluoren-9-ylidene)methyl)phenyl)methanol radical, BA-BDPA (**29**)

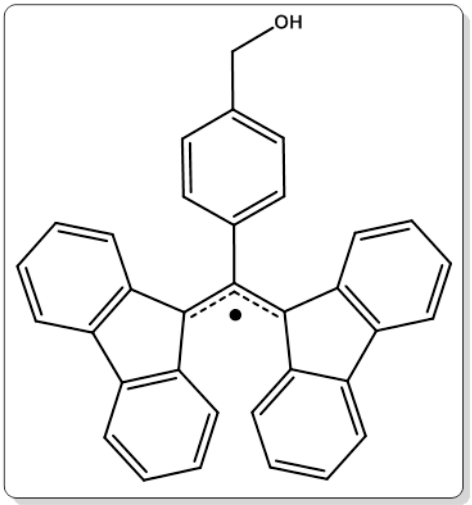

To an oven-dried 25 ml Schlenk flask equipped with a stir-bar and a rubber septum, 100 mg (223 μmol, 1 eq) of BA-BDPA **28** was added. The flask was evacuated under vacuum and refilled with argon for three times and then 5 mL of dry DCM were added. After that 70 μl (468 μmol, 2 eq) of 1,8-Diazabicyclo[5.4.0]undec-7-ene (DBU) were slowly added. The reaction turned into a deep blue color. The blue solution was stirred at room temperature for five minutes, then a solution of $AgNO_3$ (151 mg, 892 μmol, 4 eq) in ACN was added. The oxidation was monitored by UV-Visible. The organic phase was removed under vacuum and the organic solid obtained was purified by column chromatography on silica gel eluting with dichloromethane to dichloromethane /methanol 98:2. The pure radical product was isolated as a off red powder (98 mg, 98%).

Characterization:

- EPR (solvent): g: 2.0024; a(4H).1.988 G, a(4H): 1.827 G, a(4H): 0 .539 G, a(4H): 0.365 G, a(2H): 0.065 G and a(2H): 0.062 G, ΔH_{pp}:h 0.31 G.
- UV-Vis: 491 nm (ε = 29200 M^{-1} cm^{-1}), 859 nm (ε = 1410 M^{-1}, cm^{-1})

4-((9H-fluoren-9-yl)(9H-fluoren-9-ylidene)methyl)benzaldehyde (**30**)

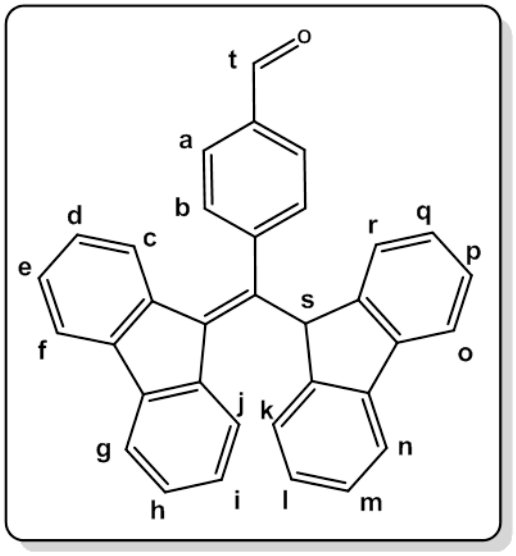

To an oven-dried 100 ml round-bottom flask equipped with a magnetic stir-bar, 290 mg of pyridinium chlorochromate (PCC) (134 mmol, 1.5 eq) and 40 ml of dry dichloromethane were added. After suspension of PCC, 400 mg of BA-BDPA (**28**) (896 μmol, 1 eq) were added to the suspension and the resulting mixture was stirred for 1.5 h. After that, the suspension was filtered with silica gel and the organic phase was removed under vacuum. The organic solid obtained was purified by column chromatography on silica gel eluting with hexane to hexane:Ethyl acetate 8:2. The pure product was isolated as off yellow powder (384 mg, 96%).

Characterization:

- ^{1}H NMR (600 MHz, ^{6}d-acetone): δ 5.86 (*d*, 1H, J= 8 Hz, H_c), 6.56 (*s*, 1H, H_s), 6.79 (*t*, 1H, J= 8 Hz, H_d) 6.94 (*d*, 2H, J= 8 Hz, H_b), 7.25 (*t*, 1H, J= 8 Hz, H_e), 7.32 (*t*, 2H, J= 8 Hz, H_l, H_q), 7.37 (*t*, 2H, J= 8 Hz, H_m, H_p), 7.45 (*t*, 1H, J= 8 Hz, H_i), 7.53 (*t*, 1H, J= 8 Hz, H_h), 7.58 (*t*, 2H, J= 8 Hz,H_a), 7.72 (*d*, 2H, J= 8 Hz, H_k, H_r), 7.75 (*d*, 2H, J= 8 Hz, H_n, H_o), 7.87 (*d*, 1H, J= 8 Hz, H_f), 8.01 (*d*, 1H, J= 8 Hz, H_g), 8.57 (*d*, 1H, J= 8 Hz, H_j), 9.88 (*s*, 1H, H_t) ppm.
- ^{13}C NMR (125 MHz, ^{6}d-acetone): δ 192.2, 145.3, 143.8, 143.3, 142.1, 141.5, 140.2, 138.6, 138.5, 136.3, 135.1, 129.4, 129.3, 128.8, 128.0, 127.9, 127.6, 127.3, 126.8, 126.1, 125.4, 125.3, 120.3, 120.2, 119.5, 52.4 ppm.
- MS (MALDI-TOF, positive mode): m/z 445 $[M+H]^+$.
  Calculated: $C_{34}H_{22}O$: 446.5.
- IR-ATR (cm^{-1}): 1699, 1602, 1444, 1205, 1006, 784 and 729.

9-((4-(bromomethyl)phenyl)(9H-fluoren-9-yl)methylene)-9H-fluorene (**31**)

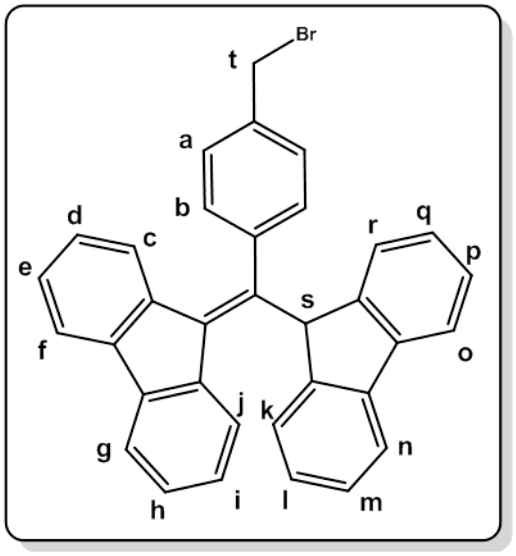

To an oven-dried 50 ml round-bottom flask equipped with a magnetic stir-bar, 1.0 g of BA-BDPA (**28**) (2.23 mmol, 1 eq) and 20 ml of dry dichloromethane were added. The solution was cooled down in an ice bath and 84 μl of PBr_3 (0.89 mmol, 1.2 eq) were added drop by drop. The mixture was allowed to warm to room temperature and was stirred for 3 hours at this temperature. After that, The solution was diluted with water and extracted with dichloromethane. The organic phase was dried over anhydrous magnesium sulfate, the solvent was removed under vacuum and the organic solid obtained was purified by column chromatography on silica gel eluting with hexane to henane:Ethyl acetate 95:5. The pure product was isolated as a off yellow powder (855 mg, 75%).

Characterization:

- ^{1}H NMR (400 MHz, ^{6}d-acetone): δ 4.5 (*s*, 2H, J= 8 Hz, H_t), 5.79 (*d*, 1H, J= 8 Hz, H_c), 6.52 (*s*, 1H, H_s), 6.73 (*d*, 2H, J= 8 Hz, H_b) 6.77 (*t*, 1H, J= 8 Hz, H_d), 7.15 (*d*, 2H, J= 8 Hz, H_a), 7.25 (*t*, 1H, J= 8 Hz, H_e), 7.34 (*t*, 2H, J= 8 Hz, H_l, H_q), 7.38 (*t*, 2H, J= 8 Hz, H_m, H_p), 7.45 (*t*, 1H, J= 8 Hz, H_i), 7.52 (*t*, 1H, J= 8 Hz, H_h), 7.69 (*d*, 2H, J= 8 Hz, H_k, H_r), 7.78 (*d*, 2H, J= 8 Hz, H_n, H_o), 7.87 (*d*, 1H, J= 8 Hz, H_f), 8.01 (*d*, 1H, J= 8 Hz, H_g), 8.56 (*d*, 1H, J= 8 Hz, H_j) ppm.
- ^{13}C NMR (125 MHz, ^{6}d-acetone): δ 144.5, 144.0, 141.9, 141.2, 139.9, 138.9, 138.6, 138.4, 137.6, 136.2, 128.8, 128.6, 128.4, 127.6, 128.58, 127.0, 126.4, 125.9, 125.3, 125.3, 120.0, 119.9, 119.2, 52.5 and 32.9 ppm.
- MS (MALDI-TOF, negative mode): m/z 431 $[M\text{-}Br]^{-}$.
  Calculated: $C_{34}H_{23}Br$: 511.5.
- IR-ATR (cm^{-1}): 2950, 1445, 1070, 1014 and 730.

Diethyl 4-((9H-fluoren-9-yl)(9H-fluoren-9-ylidene)methyl)benzylphosphonate (32)

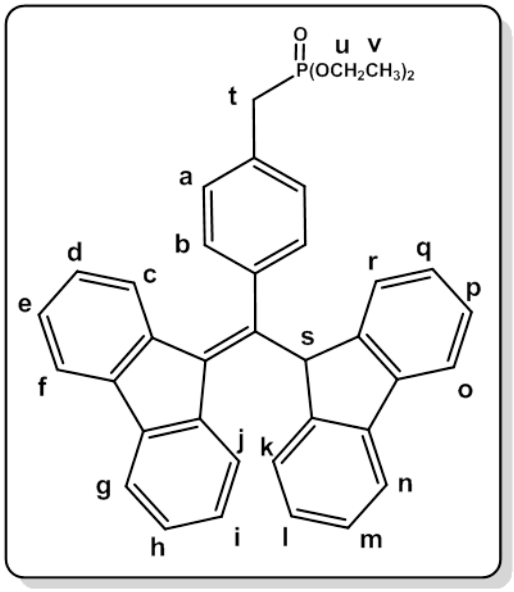

In a 50 ml round-bottom flask equipped with a magnetic stir-bar and anhydrous $CaCl_2$ tube coupled in the cooling, 844 mg (1.65 mmol, 1 eq) of BDPA-CH_2Br (**31**) were dissolved in 20 ml (115 mmol) of triethyl phosphite. The mixture was refluxed at 160 ^{0}C . After four hours, it was cooled down to room temperature and the solvent was removed under vacuum. The solution was diluted with water and extracted with dichloromethane. The organic phase was dried over anhydrous magnesium sulfate, the solvent was removed under vacuum and the organic solid obtained was purified by column chromatography on silica gel eluting with pure hexane to pure ethyl acetate. The pure product was isolated as a off brown powder (845 mg, 90%).

Characterization:

- ^{1}H NMR (600 MHz, ^{6}d-acetone): δ 1.14 (*s*, 6H, J= 6 Hz, H_v), 2.99 (*d*, 1H, J= 24 Hz, H_t), 3.81 (*dq*, 4H, H_u), 5.90 (*d*, 1H, J= 6 Hz, H_c), 6.51 (*s*, 1H, H_s), 6.65 (*d*, 2H, J= 6 Hz, H_b), 6.77 (*t*, 1H, J= 6 Hz, H_d), 7.0 (*dd*, 2H, J= 6 Hz, H_a), 7.23 (*t*, 1H, J= 6 Hz, H_e), 7.30 (*t*, 2H, J= 6 Hz, H_l, H_q), 7.35 (*t*, 2H, J= 6 Hz, H_m, H_p), 7.42 (*t*, 1H, J= 6 Hz, H_i), 7.49 (*t*, 1H, J= 8 Hz, H_h), 7.65 (*d*, 2H, J= 6 Hz, H_k, H_r), 7.74 (*d*, 2H, J= 6 Hz, H_n, H_o), 7.84 (*d*, 1H, J= 6 Hz, H_f), 7.98 (*d*, 1H, J= 6 Hz, H_g), 8.53 (*d*, 1H, J= 6 Hz, H_j) ppm.
- ^{31}P {^{1}H} NMR (100 MHz, $CDCl_3$): δ 23.2 (*s*, P) ppm.
- ^{13}C NMR (125 MHz, $CDCl_3$): δ 145.5, 144.6, 142.4, 141.6, 140.3, 139.2, 138.9, 137.6, 137.5, 136.4, 132.2, 129.8, 129.7, 128.76, 128.71, 127.97, 127.94, 127.4, 126.8, 126.4, 125.8, 125.7, 120.4, 120.3, 119.5, 62.6 (JC_uP= 6.3 Hz), 53.0, 33.2 (JC_tP= 133 Hz), 16.1 (JC_v=5 Hz) ppm.
- MS (MALDI-TOF, negative mode): m/z 567 [M-H]$^-$.
  Calculated: $C_{38}H_{33}O_3P$: 568.6.
- IR-ATR (cm^{-1}): 2978, 1445, 1254, 1242, 1025, 960.

9.1.3 TEMPO derivatives

4-Methoxycarbonylmethylidene-2,2,6,6-tetramethyl-1-piperidyloxyl (37)

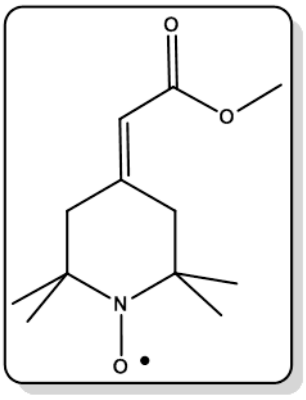

1.80 ml of lithium diisopropilamide (1.82 mmol, 1.03 eq) was added to a three-necked oven-dried 100 ml round-bottom flask equipped with a magnetic stir-bar containing 14 ml of anfhydrous THF at -78 ^{0}C under Ar atmosphere. Then, 307 μl of methyl 2-(trimethylsilyl)acetate (1.82 mmol, 1.03 eq) dissolved in 5 ml of dry THF were slowly added. After the addition was completed, the reaction was maintained at -78 ^{0}C for 20 minutes before 0.3 g (1.76 mmol, 1 eq) of 2,2,6,6,-tetramethyl-4-oxo-1-piperidinyloxyl (**36**) in 5 ml of dry THF were slowly added. After 20 minutes, the mixture was warmed to room temperature. Cold HCl 5% was added to attain a pH of 3-4, and the mixture was extracted with pentane/diethyl ether. The organic phase was dried over anhydrous magnesium sulfate, the solvent was removed under vacuum and the organic red oil obtained was purified by column chromatography on silica gel eluting with pure hexane to hexane/ethyl acetate 4/1. The pure product was isolated as off orange solid (399 mg, 75%).

Characterization:

- EPR (THF): g: 2.0058, a_{N}: 15.5 G, $\Delta \mathrm{H}_{\mathrm{pp}}$: 0.86 G.
- MS (MALDI-TOF, positive mode): m/z 226 $[\mathrm{M+H}]^+$.
  Calculated: $\mathrm{C_{12}H_{20}NO_3^{\bullet}}$: 226.
- IR-ATR ($\mathrm{cm^{-1}}$): 1720, 1660.

4-Carboxymethylidene-2,2,6,6-tetramethyl-1-piperidyloxyl (38)

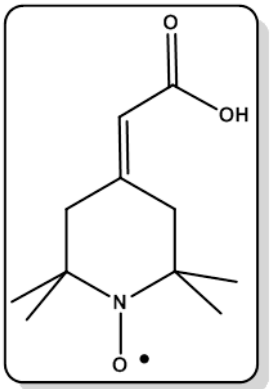

To a solution of 1 g (4.42 mmol, 1 eq) of 4-Methoxycarbonylmethylidene-2,2,6,6-tetramethyl-1-piperidiyloxyl (**37**) in 25 ml of methanol a dissolution of 298 mg (5.3 mmol, 1.2 eq) KOH in 2 ml of water were added. The reaction was warmed at 35-38 ^{0}C of 6 hours. The progress of hydrolysis was monitored by TLC. Once the reaction was completed, the solvent was removed under vacuum. The solid was solved in water and extracted with dichloromethane. The aqueous phase was then cooled in an ice bath, and the pH was reduced to 3 with HCl 10%. The solution was then extracted with ether, dried over over anhydrous magnesium sulfate, the solvent was removed under vacuum to yield the desired product as

a red oil, that eventually solidifies (795 mg, 85%).

Characterization:

- EPR (THF): g: 2.0056, a_N: 15.4 G, ΔH_{pp}: 1.07 G.
- MS (MALDI-TOF, positive mode): m/z 212 $[M+H]^+$.
  Calculated: $C_{11}H_{18}NO_3^{\bullet}$: 212.
- IR-ATR (cm^{-1}): 1708, 1643

9.2 Diradicals synthesis

9.2.1 Homodiradicals

9.2.1.1 PTM=PTM diradical

bis αH-PTM=PTM (**39**) and **PTM = PTM$^{2\bullet}$** (**40**)

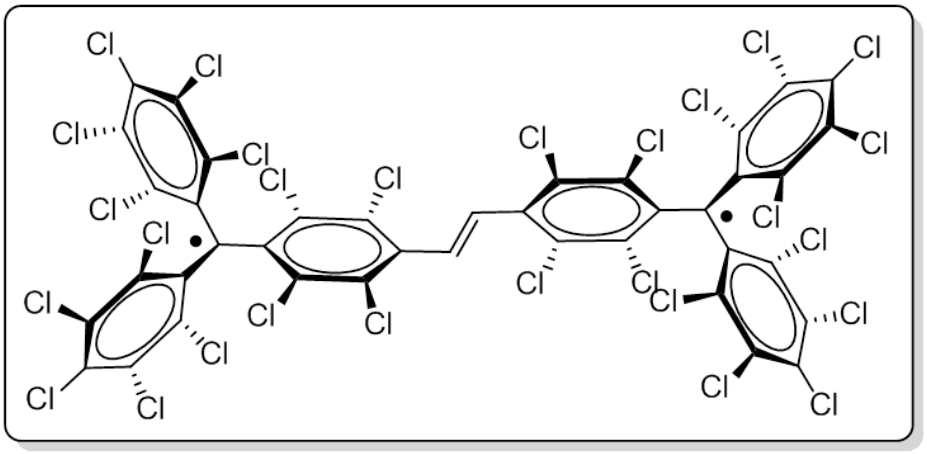

In a 25 ml Schlenk, under argon atmosphere, 150 mg (172.3 μmol, 1.3 eq) of diethyl 4-[bis(2,3,4,5,6-pentachlorophenyl)methyl]-2,3,5,6-tetrachlorobenzyl phosphonate (**9**), and 238 mg (199 μmol, 1.5 eq) of potassium *tert*-butoxide were dissolved in 5 ml of anhydrous THF at -78 ^{0}C. The reaction mixture changed its color to violet. It was stirred for 10 minutes and 0.1 g (132.5 μmol, 1 eq) of αH–(4-formyl)tetradecachloromethyl triphenylmethane) (**6**) in 5 ml of anhydrous THF were added, drop by drop, with a cannula. The mixture reaction was stirred 20 minutes at -78 ^{0}C. Then, the mixture was warmed to room temperature and stirred for 16 hours. After a reaction control by TLC, 5% aqueous HCl was added until the violet color disappeared. The mixture was extracted with dichlorometane/water. The organic phase was dried over anhydrous magnesium sulfate, the solvent was removed under vacuum to obtain a white powder that was purified by column chromatography on silica gel eluting with pure hexane to hexane/ethyl acetate 4/1. The pure bis αH compound **39** was isolated as white solid (20 mg, 10%).

A small quantity of bis αH compound **39** was dissolved in THF, and a solution of tetrabutylammonium hydroxide 2 M in water was added. The colorless solution became homogeneous purple and an excess of $AgNO_3$ were added. The conversion of the anion into the radical was monitored by UV-Vis. Once the anion was fully converted into radical, the reaction mixture was filtered and the EPR spectrum was registered.

Characterization of compound **39**:

- ^{1}H NMR (250 MHz, $CDCl_3$) (αH- form): δ 7.03 (s, 2H), 7.04 (s, 2H, H_α) ppm.
- MS (MALDI-TOF, negative mode): m/z 1474 [M-H]$^-$, 1402 [M-2Cl]$^-$
  Calculated: $C_{40}H_4Cl_{28}$: 1477, $C_{40}H_4Cl_{26}{}^{2\bullet}$: 1476.
- IR-ATR (cm^{-1}): 2946, 1618, 1440, 1351, 1291, 960, 808.

Characterization of compound **40**:

- EPR (THF): g: 2.0036, $a_{C_{orto/bridge}}$: 6 G, a_{C_α}: 14.4 G, a_H: 0.32 G, ΔH_{pp}: 0.6 G (220 K).

9.2.1.2 BDPA=BDPA diradical

bis αH-BDPA=BDPA (**41**) and **BDPA = BDPA$^{2\bullet}$** (**42**)

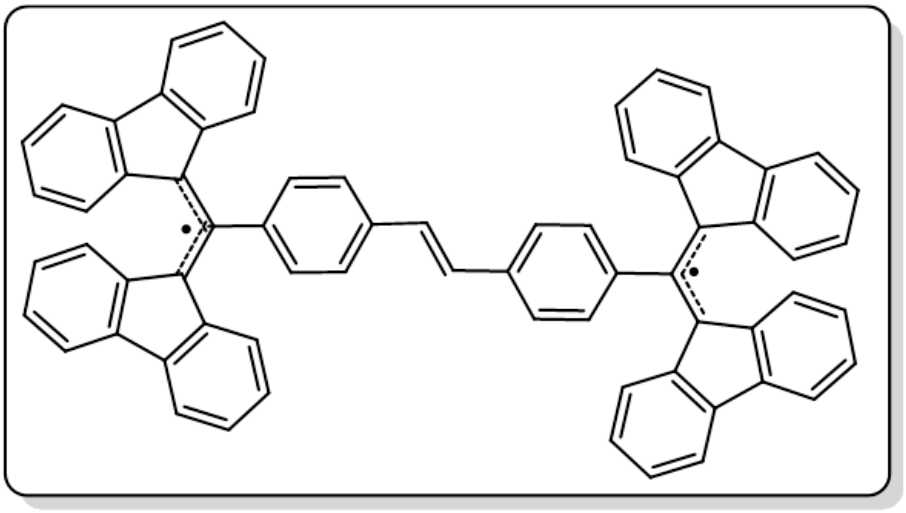

In a 25 ml Schlenk, under argon atmosphere, 150 mg (264 μmol, 1 eq) of diethyl 4-((9H-fluoren-9-yl)(9H-fluoren-9-ylidene)methyl)benzylphosphonate (**32**), and 118 mg (1.06 mmol, 4 eq) of potassium *tert*-butoxide were dissolved in 5 ml of anhydrous THF at -78 ^{0}C, the reaction mixture changed its color to deep blue. The mixture was stirred for 10 minutes and 141 mg (317 μmol, 1.2 eq) of 4-((9H-fluoren-9-yl)(9H-fluoren-9-ylidene)methyl)benzaldehyde (**30**) in 5 ml of anhydrous THF were added, drop by drop, with a cannula. The reaction mixture was stirred 20 minutes at -78 ^{0}C and then, it was warmed to room temperature and stirred for 16 hours. After a reaction control by TLC, 5% aqueous HCl was added until the blue color disappeared. The mixture was extracted with dichlorometane/water and the organic phase was dried over over anhydrous magnesium sulfate. The solvent was removed under vacuum to obtain a orange solid that was purified by column chromatography on silica gel eluting with pure

hexane to hexane/ethyl acetate. The isolated orange powder (110 mg, 48%) contained radical traces so the ^{1}H NMR could not be registered.
A small amount of orange solid previously obtained was dissolved in dichloromethane, and DBU was added. The colorless solution became homogeneous blue and then $AgNO_3$ were added. The conversion of the anion into the radical was monitored by UV-Vis. Once the anion was fully converted into radical, the reaction mixture was filtered and the EPR spectrum was registered.

Characterization of compound **41**:

- MS (MALDI-TOF, negative mode): m/z 859.3 $[M-H]^-$
  Calculated: $C_{68}H_{44}$: 861.$C_{68}H_{42}{}^{2\bullet}$: 859.
- IR-ATR (cm^{-1}): 2930, 1620, 1442, 1332, 1290, 970.

Characterization of compound **42**:

- EPR (THF/benzene): g: 2.0026 , a_H(4H): 1.8 G, a_H(4H): 1.5 G, a_H(4H): 0.57 G, a_H(4H): 0.39 G, a_H(2H): 0.067 G, ΔH_{pp}: 0.25 G.

9.2.1.3 TEMPO-TEMPO diradicals

2,2,2',2',6,6,6',6'-octamethyl-4,4'-bipiperidylidene (**43**)

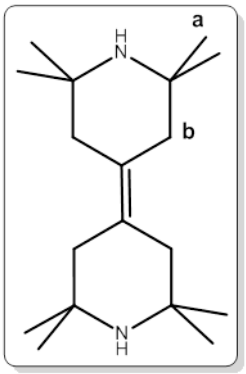

To an oven-dried two necked 100 ml round bottom flask containing a magnetic stir-bar, 1.55 g of 2,2,6,6,-tetramethyl-4-piperidone (**42**) (9.5 mmol, 1 eq), 10 ml of anhydrous dioxane and 0.6 ml of AcOH were stirred under argon atmosphere. A solution of $TiCl_4$ (2.84 g, 15 mmol, 1.6 eq) in 15 ml of anhydrous dioxane was slowly added. The mixture was stirred for 30 minutes and a suspension of 1.95 g of Zn (29.8 mmol, 3 eq) in 5 ml of anhydrous THF was added. The mixture was stirred for an hour at room temperature in order to form the pinacol intermediate. After that, the mixture was refluxed for 8 hours in order to eliminate the pinacol. Then, the mixture was allowed to warm to room temperature, and it was neutralized with 10 % aqueous potassium carbonate solution, then made strongly alkaline with 20 % aqueous sodium hydroxide solution and extracted with toluene. The organic phase was dried over anhydrous magnesium sulfate, the solvent was removed under vacuum and the organic solid obtained was purified by column chromatography on silica gel eluting with dichlorometane to dichlorometane:MeOH 95:5. The pure product was isolated as a off white powder (1.15 g, 87%).

Characterization:

- ^{1}H NMR (400 MHz, $CDCl_3$): δ 1.1 (s, 24H, H_a), 2.1 (s, 8H, H_b) ppm.
- ^{13}C NMR (125 MHz, $CDCl_3$: δ 128.0, 52.8, 43.5, 31.4 ppm.
- MS (MALDI-TOF, positive mode): m/z 278.5 $[M+H]^+$.
  Calculated: $C_{18}H_{34}N_2$: 278.
- IR-ATR (cm^{-1}): 2959, 1485, 1435, 1374 and 1363.

2,2,2',2',6,6,6',6'-octamethyl-4,4'-bipiperidyliden-oxyl (**44**)

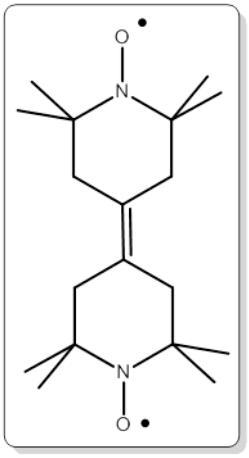

To a 10 ml round-bottom flask equipped with a magnetic stir-bar, 0.2 g of 2,2,2',2',6,6,6',6'-octamethyl-4,4'-bipiperidylidene (**43**) (718 μmol, 1 eq) and 3 ml of dry dichloromethane were added. The solution was cooled down in an ice bath and 620 mg (3.59 mmol, 5 eq) of *meta*chloroperbenzoic acid were added. The mixture was allowed to warm to room temperature and was stirred for 2 hours at this temperature. After that, the mixture was treated with a 5% NaOH dissolution in order to eliminate the benzoic acid and extracted with dichloromethane. The organic phase was dried over anhydrous magnesium sulfate, the solvent was removed under vacuum and the organic solid obtained was purified by column chromatography on silica gel eluting with dichlorometane to dichlorometane:MeOH 95:5. The pure product was isolated as a red oil that eventually solidifies (168 mg, 76%).

Characterization:

- EPR (DCM/Toluene 1/1, 300 K): g: 2.0058, a_N: 7.65 G, ΔH_{pp}: 1.3-1.4 G.
- MS (MALDI-TOF, positive mode): m/z 311 $[M+3H]^+$.
  Calculated: $C_{18}H_{32}N_2O_2{}^{2\bullet}$: 308.
- IR-ATR (cm^{-1}):2978, 2933, 1727, 1541, 1454, 1363, 1337, 1239, 1189, 1170.

4-(2,2,6,6-tetramethyl-1-piperidiyloxyl)oxycarbonylmethylidene-2,2,6,6-tetramethyl-1-piperidiyloxyl (**45**)

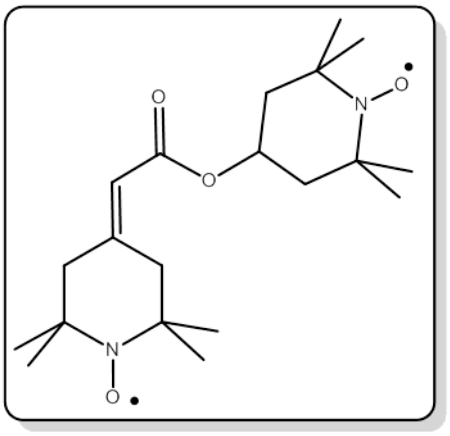

To a 10 ml round-bottom flask equipped with a magnetic stir-bar 0.1 g of 4-carboxymethylidene-2,2,6,6-tetramethyl-1-piperidiyloxyl (**38**) (471 μmol, 1 eq), 63 mg (518 μmol, 1.1 eq)of dimethylaminopiridine (DMAP), 107 mg (518 μmol, 1.1 eq) of diciclohexylcarbodiimide and 3 ml of dry dichloromethane were added under Ar atmosphere. The solution was stirred for 10 minutes and then, 97 mg (565 μmol, 1.2 eq) of 4-hydroxy-TEMPO (**34**) were added. The mixture was stirred at room temperature for 16 hours. After that, the mixture was extracted with water/dichloromethane. The organic phase was dried over anhydrous magnesium sulfate, the solvent was removed under vacuum and the organic solid obtained was purified by column chromatography on silica gel eluting with dichlorometane to dichlorometane:MeOH 95:5. The pure product was isolated as

a orange oil that eventually solidifies in a off orange solid (120 mg, 70%).

Characterization:

- EPR (DCM/Toluene 1/1, 300 K): g: 2.0067, a_N: 15.4 G, ΔH_{pp}: 1.2 G.
- MS (MALDI-TOF, positive mode): m/z 366 $[M+H]^+$.
  Calculated: $C_{20}H_{34}N_2O_4{}^{2\bullet}$: 367.
- IR-ATR (cm^{-1}): 2978, 2929, 2851, 1736, 1625, 1575, 1155.

4-(2,2,6,6-tetramethyl-1-piperidiyloxyl)carbamoilmethylidene-2,2,6,6-tetramethyl-1-piperidiyloxyl (**46**)

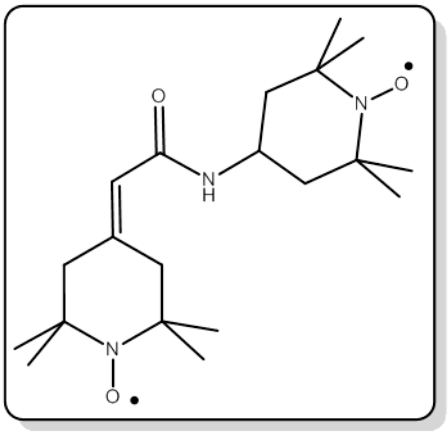

To a 10 ml round-bottom flask equipped with a magnetic stir-bar 0.1 g of 4-carboxymethylidene-2,2,6,6-tetramethyl-1-piperidiyloxyl (**38**) (471 μmol, 1 eq), 63 mg (518 μmol, 1.1 eq) of dimethylaminopiridine (DMAP), 107 mg (518 μmol, 1.1 eq) of diciclohexylcarbodiimide and 3 ml of dry dichloromethane were added under Ar atmosphere. The solution was stirred for 10 minutes and then, 97 mg (565 μmol, 1.2 eq) of 4-amino-TEMPO (**35**) were added. The mixture was stirred at room temperature for 16 hours. After that, the mixture was extracted with water/dichloromethane. The organic phase was dried over anhydrous magnesium sulfate, the solvent was removed under vacuum and the organic solid obtained was purified by column chromatography on silica gel eluting with dichlorometane to dichlorometane:MeOH 95:5. The pure product was isolated as a off orange solid (168 mg, 76%).

Characterization:

- EPR (DCM/Toluene 1/1, 300 K): g: 2.0068, a_N: 5.6 G, ΔH_{pp}: 1.2 G.
- MS (MALDI-TOF, positive mode): m/z 388 $[M+Na]^+$.
  Calculated: $C_{20}H_{35}N_3O_3{}^{2\bullet}$: 365.
- IR-ATR (cm^{-1}): 3271, 2974, 2933, 2855, 1640, 1556, 1359, 1242.

9.2.2 Heterodiradicals

9.2.2.1 PTM-BDPA diradical

αH-PTM=BDPA (**47**) and **PTM = BDPA$^{2\bullet}$** (**48**)

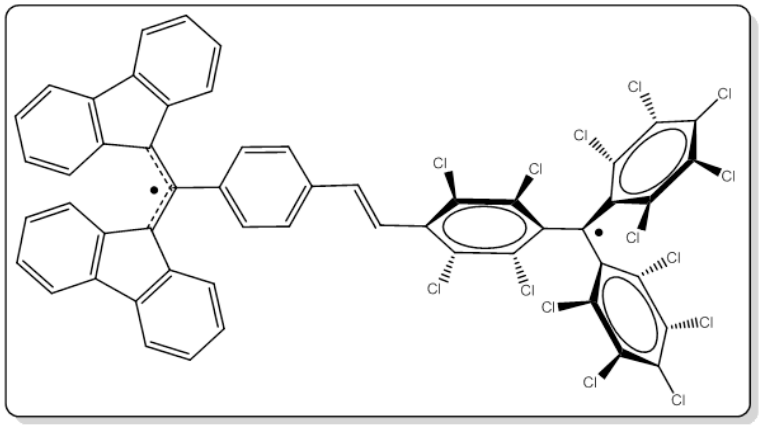

In a 25 ml Schlenk, under argon atmosphere, 236 mg (269 μ, 1.2 eq) of diethyl 4-[bis(2,3,4,5,6-pentachlorophenyl)methyl]-2,3,5,6-tetrachlorobenzyl phosphonate (**9**), and 50 mg (448 μmol, 2 eq) of potassium *tert*-butoxide were dissolved in 5 ml of anhydrous THF at -78 ^{0}C, the reaction mixture changed its color to violet. The mixture was stirred for 10 minutes and 0.1 g (224 μmol, 1 eq) of 4-((9H-fluoren-9-yl)(9H-fluoren-9 ylidene)methyl)benzaldehyde (**32**) in 5 ml of anhydrous THF were added, drop by drop, with a cannula. It was maintained at -78 ^{0}C for 20 minutes and then, the mixture was warmed to room temperature and stirred for 16 hours. After a reaction control by TLC, 5% aqueous HCl was added until the color disappeared and it was extracted with ethyl acetate. The organic phase was dried over anhydrous magnesium sulfate, the solvent was removed under vacuum and the organic solid obtained was purified by column chromatography on silica gel eluting with mixtures of hexane and ethyl acetate. The αH-PTM=BDPA **47** radical product was isolated as red powder (160 mg, 61%)

The treatment of a small amount of monoradical αH-PTM=BDPA **47** in anhydrous THF/Benzene with tetrabutylammonium hydroxyde and $AgNO_3$ allowed the full conversion into the diradical **48**. Once the anion was fully converted into radical, the reaction mixture was filtered and the EPR spectrum was registered.

Characterization of compound **47:**

- EPR (THF/Benzene): g: 2.0023, a_H(4H): 1.99 G, a_H(4H): 1.86 G, a_H(4H): 0.48 G, a_H(4H): 0.37 G, a_H(2H): 0.073 G, ΔH_{pp}: 0.22 G.
- MS (MALDI-TOF, positive mode): m/z 1167 $[M+H]^+$, 1095 $[M-2Cl]^+$
  Calculated: $C_{54}H_{24}Cl_{14}$: 1169, $C_{54}H_{22}Cl_{14}{}^{2\bullet}$: 1167.
- IR-ATR (cm^{-1}): 2926, 2851, 1623, 1445, 1359, 1337, 1296, 1242, 1138, 807.

Characterization of compound **47:**

- EPR (THF/Benzene): g: 2.0033, a_H(4H): 0.849 G, a_H(4H): 0.848 G, a_H(4H): 0.139 G, a_H(4H): 0.135 G, a_H(2H): 2.220 G, a_H(2H): 2.219 G, ΔH_{pp}: 0.1 G.

9.2.2.2 PTM-TEMPO diradicals

PTM = TEMPO$^{2\bullet}$(49)

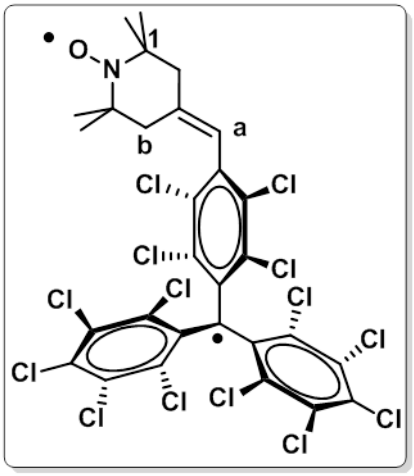

In a 250 ml Schlenk, under argon atmosphere, 566 mg (646 μ, 1.1 eq) of diethyl 4-[bis(2,3,4,5,6-pentachlorophenyl)methyl]-2,3,5,6- tetrachlorobenzyl phosphonate (**9**), and 73 mg (646 μmol, 1.1 eq) of potassium *tert*-butoxide were dissolved in 80 ml of anhydrous THF at -78 ^{0}C. The reaction mixture changed its color to light violet. The mixture was stirred for 10 minutes and 100 mg (587 μmol, 1 eq) of 2,2,6,6,-tetramethyl-4-oxo-1-piperidinyloxyl (**36**) in 20 ml of anhydrous THF were added, drop by drop, with a cannula. The reaction mixture was stirred 20 minutes at -78 ^{0}C. Then, the mixture was warmed to room temperature and stirred for 16 hours. After a reaction control by TLC, 400 mg (2.35 mmol, 4 eq) of $AgNO_3$ were added and the conversion of the anion into the radical was monitored by UV-Vis. Once the anion was fully converted into radical, the reaction mixture was filtered and the solvent was removed under vacuum. The product was purified by column chromatography on silica gel with mixtures of hexane/Ethyl acetate. The product was isolated as red powder (430 mg, 82%).

Characterization:

- EPR (Dichlorometane): PTM subunit: g: 2.0023 G; a_{Ha}: 7.89 G, a_{Hb}: 1.24 G, $a_{C_{orto}}$: 10.5 G, $a_{C_{bridge}}$: 12.0 G, a_{C_α}: 29.0 G, ΔH_{pp}: 0.6 G. TEMPO subunit: g: 2.0063; a_N: 14.6 G, a_{C1}: 5.7 G, ΔH_{pp}:0.6 G.
- MS (MALDI-TOF, positive mode): m/z 899.6 $[M+H]^+$
  Calculated: $C_{29}H_{17}Cl_{14}NO^{2\bullet}$: 892.
- IR-ATR (cm^{-1}): 2929, 1021, 808.

PTM = TEMPE$^{\bullet}$(48)

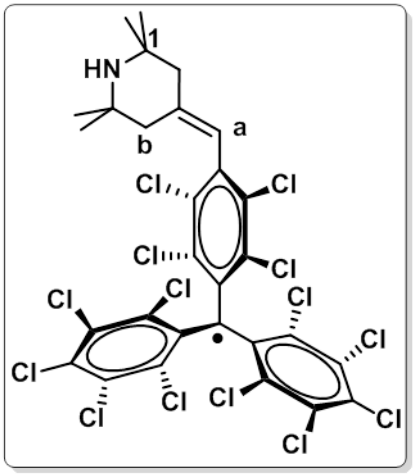

In a 25 ml Schlenk, under argon atmosphere, 100 mg (115 μmol, 1 eq) of diethyl 4-[bis(2,3,4,5,6-pentachlorophenyl)methyl]-2,3,5,6- tetrachlorobenzyl phosphonate (**9**), and 39 mg (345 μmol, 2.2 eq) of potassium *tert*-butoxide were dissolved in 5 ml of anhydrous THF at -78 ^{0}C. The mixture was stirred for 10 minutes and 35 mg (224 μmol, 1.3 eq) of 4-oxo-2,2,6,6,-tetramethylpiperidine in 5 ml of anhydrous THF were added, drop by drop, with a cannula. It was stirred 20 minutes at -78 ^{0}C and then, the mixture was warmed to room temperature. After that, it was stirred for 16 hours. After a reaction control by TLC, 5% aqueous HCl was added and extracted with dichloromethane. The organic phase was dried over anhydrous magnesium sulfate, the solvent was removed under vacuum and the organic solid obtained was purified by column chromatography on silica gel eluting with mixtures of dichlorometane and methanol. The treatment of the compound in anhydrous THF with tetrabutylammonium hydroxyde and 390 mg (2.30 mmol, 2 eq) of $AgNO_3$ was monitored by UV-Vis. Once the anion was fully converted into radical, the reaction mixture was filtered and the solvent was removed under vacuum. The product was purified by column chromatography on silica gel with mixtures of dichlorometane/methanol. The product was isolated as red powder (106 mg, 70%).

Characterization:

- EPR (Dichlorometane): g: 2.0026; a_{Ha}: 6.94 G, a_{Hb}: 1.40 G, $a_{C_{orto}}$: 10.3 G, $a_{C_{bridge}}$: 12.7 G, $a_{C\alpha}$: 29.0 G, ΔH_{pp}: 0.9 G.
- MS (MALDI-TOF, positive mode): m/z 875 $[M+H]^{+}$
  Calculated: $C_{29}H_{18}Cl_{14}N^{\bullet}$: 876.
- IR-ATR (cm^{-1}): 2929, 1021, 808.

αH – PTMesterTEMPO$^{\bullet}$ (**51**) and PTMesterTEMPO$^{2\bullet}$ (**52**)

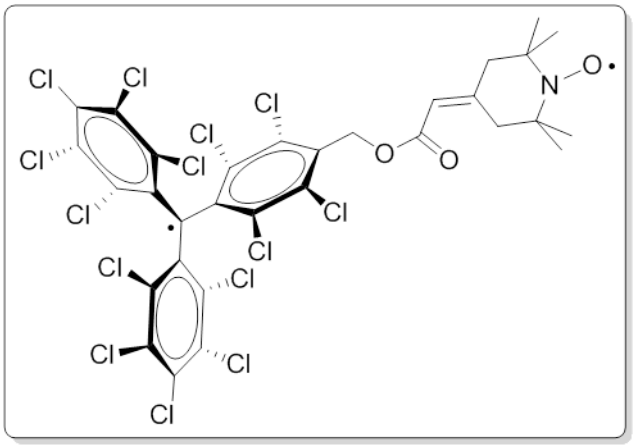

To a 10 ml round-bottom flask equipped with a magnetic stir-bar, under Ar atmosphere, 31 mg of 4-Carboxymethylidene-2,2,6,6-tetramethyl-1-piperidyloxyl (**38**) (146 μmol, 1.1 eq), 18 mg (146 μmol, 1.1 eq)of dimethylaminopiridine (DMAP), 30 mg (146 μmol, 1.1 eq) of diciclohexylcarbodiimide and 3 ml of dry dichloromethane were added. The solution was stirred for 10 minutes and then, 0.1 g of αH–(4-hydroxymethyl)tetradecachloromethyltriphenylmethane (**5**) (132 μmol, 1 eq) were added. The mixture was stirred at room temperature for 16 hours. After that, the mixture was extracted with water/dichloromethane. The organic phase was dried over anhydrous magnesium sulfate, the solvent was removed under vacuum and the organic solid obtained was purified by column chromatography on silica gel eluting with mixtures of hexane and ethyl acetate.The pure monoradical **51** was isolated as a off orange solid (83 mg, 66%).
The treatment of a small among of monoradical **51** in anhydrous THF with tetrabutylammonium hydroxyde and $AgNO_3$ was monitored by UV-Vis. Once the anion was fully converted into diradical **52**, the reaction mixture was filtered and characterized by EPR.

Characterization of compound **51:**

- EPR (THF, 300 K): g_{TEMPO}: 2.0059, a_{N}: 15.1 G, $a_{^{13}\mathrm{C}}$: 5.0 G, $\Delta \mathrm{H_{pp}}$: 1.1 G.
- MS (MALDI-TOF, positive mode): m/z 951 $[\mathrm{M+H}]^+$.
  Calculated: $\mathrm{C_{31}H_{19}Cl_{14}NO_3}^{2\bullet}$: 950.
- IR-ATR ($\mathrm{cm^{-1}}$): 2926, 2855, 1723, 1333, 1260, 1153, 810.

Characterization of compound **52:**

- EPR (THF, 300 K): Conformer I: g_{TEMPO}: 2.0059, a_{N}: 15.2 G, $a_{^{13}\mathrm{C}}$: 5.0 G, $\Delta \mathrm{H_{pp}}$: 1.0 G, g_{PTM}: 2.0027, $\Delta \mathrm{H_{pp}}$: 1.4 G. Conformer II: g: 2.0043, a_{N}: 7.6 G, $\Delta \mathrm{H_{pp}}$: 1.4 G.

αH – PTMamidoTEMPO$^{\bullet}$ (**53**) and PTMamidoTEMPO$^{2\bullet}$ (**54**)

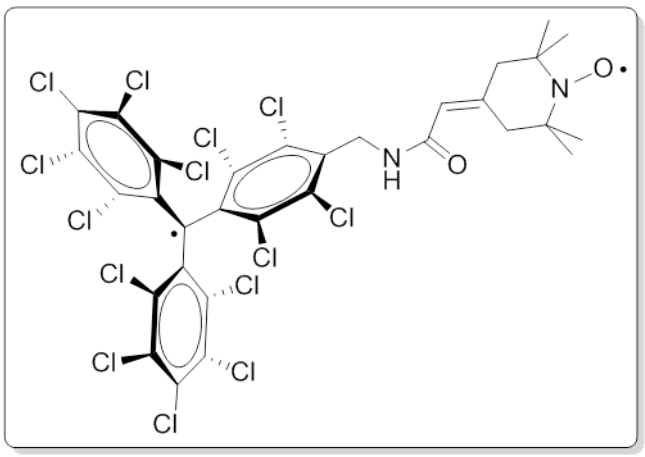

To a 10 ml round-bottom flask equipped with a magnetic stir-bar, 42 mg (199 μmol, 1.5 eq) of 4-Carboxymethylidene-2,2,6,6-tetramethyl-1-piperidyloxyl (**38**), 24 mg (199 μmol, 1.5 eq) of dimethylaminopiridine (DMAP), 41 mg (199 μmol, 1.5 eq) of diciclohexylcarbodiimide and 2 ml of dry dichloromethane were added under Ar atmosphere. The solution was stirred for 10 minutes and then, 0.1 g of αH–(4aminomethyl) tetradecachloromethyltriphenylmethane (**8**) (132 μmol, 1 eq) were added. The mixture was stirred at room temperature for 16 hours. After that, the mixture was extracted with water/dichloromethane. The organic phase was dried over anhydrous magnesium sulfate, the solvent was removed under vacuum and the organic solid obtained was purified by column chromatography on silica gel eluting with dichlorometane to dichlorometane:MeOH 98:2. The pure monoradical **53** was isolated as a off orange powder (73 mg, 58%).
The treatment of a small amount of the obtained monoradical **53** in anhydrous THF with tetrabutylammonium hydroxyde and $AgNO_3$ was monitored by UV-Vis. Once the anion was fully converted into diradical **54**, the reaction mixture was filtered and characterized by EPR.

Characterization of compound **53:**

- EPR (THF, 300 K): g_{TEMPO}: 2.0064, a_{N}: 15.1 G, $a_{^{13}\mathrm{C}}$: 5.0 G, $\Delta \mathrm{H_{pp}}$: 1.2 G.
- MS (MALDI-TOF, positive mode): m/z $[\mathrm{M+H}]^+$.
  Calculated: $\mathrm{C_{31}H_{20}Cl_{14}N_2O_2}^{2\bullet}$: 949.
- IR-ATR ($\mathrm{cm^{-1}}$):3327, 2929, 2855, 1743, 1658, 1626, 1572, 1334, 1337, 1299, 1242, 810

Characterization of compound **54:**

- EPR (THF, 300 K): Conformer I: g_{TEMPO}: 2.0064, a_{N}: 15.1 G, $a_{^{13}\mathrm{C}}$: 5.0 G, $\Delta \mathrm{H_{pp}}$: 1.2 G, g_{PTM}: 2.0048, a_{N}: 7.6 G, $\Delta \mathrm{H_{pp}}$: 1.4 G. Conformer II: g: 2.0048, a_{N}: 7.6 G, $\Delta \mathrm{H_{pp}}$: 1.6 G.

9.2.2.3 BDPA-TEMPO diradicals

αH – BDPA = TEMPO$^{\bullet}$ (55) and **BDPA = TEMPO$^{2\bullet}$ (56)**

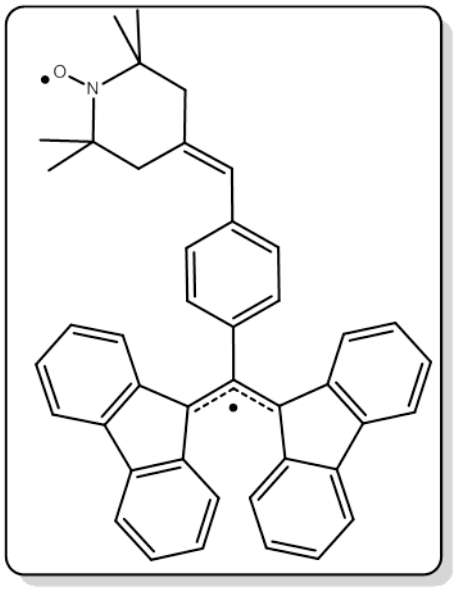

In a 25 ml Schlenk, under argon atmosphere, 100 mg (176 μmol, 1 eq) of diethyl 4-((9H-fluoren-9-yl)(9H-fluoren-9-ylidene)methyl) benzylphosphonate (**32**) were dissolved in 5 ml of anhydrous THF and cooled down to -78 ^{0}C under Ar. Then, dropside, 920 μl (458 μmol, 2.6 eq) of Lithium diisopropylamide 2M in THF were added. The mixture became deep blue. It was stirred for 10 minutes and 39 mg (229 μmol, 1.3 eq) of 2,2,6,6,-tetramethyl-4-oxo-1-piperidinyloxyl (**36**) solid were added. The mixture was stirred 20 minutes at -78 ^{0}C. Then, it was allowed to warm to room temperature and stirred for 16 hours. After a reaction control by TLC, 5% aqueous HCl was added and extracted with dichloromethane. The organic phase was dried over anhydrous magnesium sulfate, the solvent was removed under vacuum. The organic solid obtained was purified by column chromatography on silica gel eluting with mixtures of dichlorometane/methanol. The monoradical **55** was isolated as red powder (65 mg, 63%).
The treatment of the obtained monoradical in dichlorometane with 1,8-Diazabicyclo[5.4.0]undec-7-ene (DBU) and 60 mg (352 μmol, 2 eq) of $AgNO_3$ was monitored by UV-Vis. Once the anion was fully converted into radical, the reaction mixture was filtered and the solvent was removed under vacuum. The product was purified by column chromatography on silica gel with mixtures of dichlorometane/methanol affording the diradical **56**.

Characterization of compound **55:**

- EPR (DCM/Benzene, 300 K): g_{TEMPO}: 2.0053, a_N: 14.8 G, ΔH_{pp}: 0.78 G.
- MS (MALDI-TOF, positive mode): m/z 582.3 $[M+H]^+$
  Calculated: $C_{34}H_{38}NO^{2\bullet}$: 585.
- IR-ATR (cm^{-1}): 2921, 2855, 1736, 1446, 1140, 1041 .

Characterization of compound **55:**

- EPR (DCM/Benzene, 300 K): g_{TEMPO}: 2.0053, a_N: 14.8 G, ΔH_{pp}: 0.78 G, g_{BDPA}: 2.0020, a_H(4H): 1.92 G, a_H(4H): 1.91 G, a_H(4H): 0.41 G, a_H(4H): 0.37 G and ΔH_{pp}: 0.5 G.

αH – BDPAesterTEMPO$^{\bullet}$ (**57**) and BDPAesterTEMPO$^{2\bullet}$ (**58**)

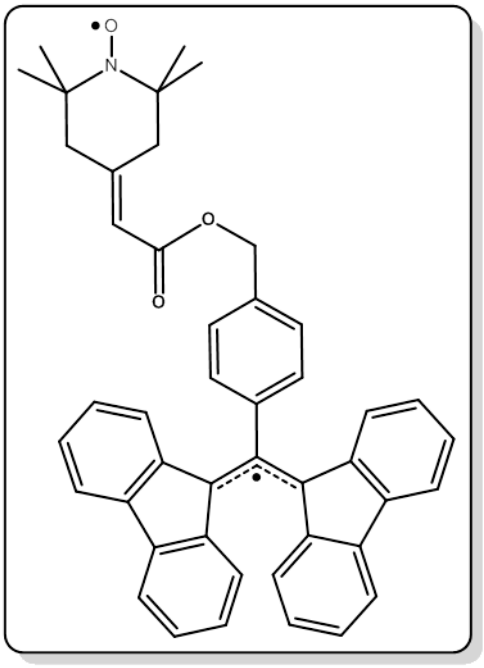

To a 10 ml round-bottom flask equipped with a magnetic stir-bar, 57 mg (269 μmol, 1.2 eq) of 4-carboxymethylidene-2,2,6,6,-tetramethyl-1-piperidyloxyl (**38**), 33 mg (269 μmol, 1.2 eq) of dimethylaminopiridine (DMAP), 56 mg (269 μmol, 1.2 eq) of diciclohexylcarbodiimide and 5 ml of dry dichloromethane were added under Ar atmosphere. The solution was stirred for 10 minutes and then, 0.1 g of 4-((9H-fluoren-9-yl)(9H-fluoren-9-ylidene)methyl)phenyl) methanol (**28**) (224 μmol, 1 eq) were added. The mixture was stirred at room temperature for 16 hours. After that, the mixture was extracted with water/dichloromethane. The organic phase was dried over anhydrous magnesium sulfate, the solvent was removed under vacuum and the organic solid obtained was purified by column chromatography on silica gel eluting with mixtures of hexane and ethyl acetate. The monoradical **57** was isolated as an off orange powder.
The treatment of the obtained monoradical **57** in dichlorometane with 1,8-Diazabicyclo[5.4.0]undec-7-ene (DBU) and 76 mg (448 μmol, 2 eq) of $AgNO_3$ was monitored by UV-Vis. Once the anion was fully converted into radical, the reaction mixture was filtered and the solvent was removed under vacuum. The product was purified by column chromatography on silica gel with mixtures of dichlorometane/methanol. The diradical **58** was isolated as red powder (79 mg, 46%).

Characterization:

- EPR (THF/Benzene, 300 K): TEMPO subunit: g_{TEMPO}: 2.0065, a_{N}: 15.1 G, $a_{^{13}\mathrm{C}}$: 5.0 G, $\Delta \mathrm{H_{pp}}$: 1.0 G), interaction: g: 2.0049, a_{H}(4H): 1.0 G, a_{H}(4H): 0.92 G, a_{H}(4H): 0.23 G, a_{H}(4H): 0.36 G, a_{N}: 7.74 G, $\Delta \mathrm{H_{pp}}$: 0.4 G.
- MS (MALDI-TOF, positive mode): m/z 642.4 $[\mathrm{M+H}]^+$.
  Calculated: $\mathrm{C_{45}H_{40}NO_3^{\bullet}}$: 643.
- IR-ATR ($\mathrm{cm^{-1}}$): 2922, 2855, 1733, 1688, 1445, 1150.

αH – BDPAamidoTEMPO$^{\bullet}$ (**59**) and BDPAamidoTEMPO$^{2\bullet}$ (**60**)

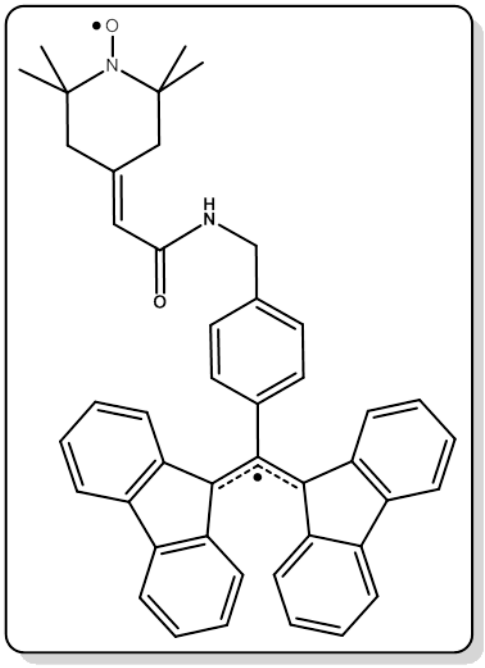

To a 10 ml round-bottom flask equipped with a magnetic stir-bar, 107 mg (503 μmol, 1.5 eq) of 4-carboxymethylidene-2,2,6,6,-tetramethyl-1-piperidyloxyl (**38**), 62 mg (503 μmol, 1.5 eq) of dimethylaminopiridine (DMAP), 104 mg (503 μmol, 1.5 eq) of diciclohexylcarbodiimide and 10 ml of dry dichloromethane were added under Ar atmosphere. The solution was stirred for 10 minutes and then, 0.15 g of 4-((9H-fluoren-9-yl)(9H-fluoren-9-ylidene)methyl)phenyl) methanamine (**21**) (335 μmol, 1 eq) were added. The mixture was stirred at room temperature for 16 hours. After that, the mixture was extracted with water/dichloromethane. The organic phase was dried over anhydrous magnesium sulfate, the solvent was removed under vacuum and the organic solid obtained was purified by column chromatography on silica gel eluting with dichlorometane to dichlorometane:MeOH 99:1. The monoradical **59** was isolated as an off orange powder.

The treatment of the obtained monoradical **59** in dichlorometane with 1,8-Diazabicyclo-[5.4.0]undec-7-ene (DBU) and 114 mg (2 mmol, 2 eq) of $AgNO_3$ was monitored by UV-Vis. Once the anion was fully converted into radical, the reaction mixture was filtered and the solvent was removed under vacuum. The product was purified by column chromatography on silica gel with mixtures of dichlorometane/methanol. The diradical **60** was isolated as red powder (128 mg, 89%).

Characterization:

- EPR (THF/Benzene, 300 K): g_{TEMPO}: 2.0062, a_N: 15.4 G, $a_{^{13}C}$: 5.0 G, ΔH_{pp}: 1.0 G, interaction: g: 2.0049, a_H(4H): 1.0 G, a_H(4H): 0.92 G, a_H(4H): 0.23 G, a_H(4H): 0.36 G, a_N: 7.74 G, ΔH_{pp}: 0.4 G.
- MS (MALDI-TOF, positive mode): m/z 642 $[M+H]^+$.
  Calculated: $C_{45}H_{40}N_2O_2^{\bullet}$: 642.
- IR-ATR (cm^{-1}): 3120, 2926, 2851, 1627, 1565, 1441, 1242.

9.3 Polyradicals synthesis

9.3.1 Dendrimers synthesis

Gc'_0 (63)

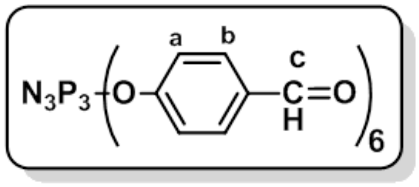

In a 250 ml round-bottom flask 2 g (5.76 mmol, 1 eq) of hexachlorocyclotryphosphazene (**62**), 30 g (92 mmol, 16 eq) of Cs_2CO_3 and 5.6 g (46 mmol, 8 eq) of *p*-hydroxybenzaldehyde were mixed under argon atmosphere with 80 ml of anhydrous THF at 0 ^{0}C for 10 min. The mixture was stirred about 5 hours at room temperature. After a NMR reaction control, the organic phase was transferred under argon atmosphere to a 500 ml round-bottom flask with a filtration cannula. The solvent was removed under vacuum and the solid was dissolved with the minimum amount of anhydrous THF under argon atmosphere. Then, anhydrous pentane was added to precipitate and purify the product; the solvent was removed with a filtration cannula under argon atmosphere. The last operation had to be done two more times. The final solid was dried under vacuum and the product was isolated as a white powder (4.8 g, 97%).

Characterization:

- ^{31}P $\{^1$H$\}$ NMR (100 MHz, $CDCl_3$): δ 7.2 (*s*, P_0) ppm.
- ^{1}H NMR (250 MHz, $CDCl_3$): δ 7.1 (*d*, 12H, JH_aH_b=10 Hz, H_a), 7.7 (*d*, 12H, JH_aH_b=10 Hz, H_b), 9.9 (*s*, 6H, H_c) ppm.
- Ms (MALDI-TOF, positive mode): m/z 862.3 $[M+H]^+$.
  Calculated: $C_{42}H_{30}N_3O_{12}P_3$: 861.6.
- IR-ATR (cm^{-1}): 1700 ν(C=O), 1598 ν(CCAr) and δ(CCH), 1274 ν(PN), 1205 δ(PNN), 1100 δ(NCH), 943 ν(P-O).

Dichlorophosphonomethylhydrazide (64)

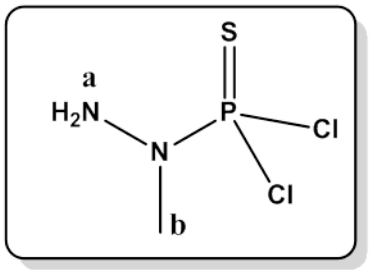

In a three necked 500 ml round-bottom flask equipped with a thermometer and a dropping funnel 250 ml of anhydrous $CDCl_3$ were added under argon atmosphere. The system was cooled to -60 ^{0}C in a chloroform/N_2 bath. At this temperature 9 ml (88.6 mmol, 1 eq) of thiophosphorylchloride were added. Drop by drop, with the dropping funnel, it was added a solution of 9.33 ml (177.2 mmol, 2 eq) of methylhydrazine in 150 ml of anhydrous $CDCl_3$ controlling the temperature, which could not exceed -55 ^{0}C. After the addition, the mixture was kept at -60 ^{0}C for half an hour and for 18 hours at room temperature. The organic phase was filtered with a filtration cannula and analyzed by NMR of ^{1}H and ^{31}P.

Characterization:

- ^{31}P {^{1}H} NMR (100 MHz, $CDCl_3$): δ 68.5 (s, P) ppm.
- ^{1}H NMR (250 MHz, $CDCl_3$): δ 4.0 (brs, 2H, H_a), 3.3 (d, 3H, JPH_b=15 Hz, H_b) ppm.

Gc_1 (65)

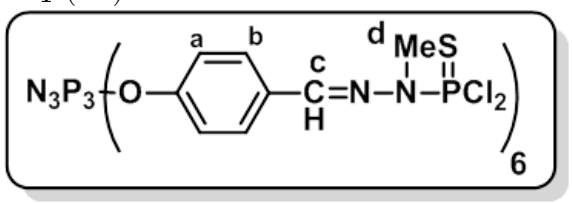

In a three necked 100 ml round-bottom flask equipped with a dropping funnel and under argon atmosphere 2.6 g (3 mmol, 1 eq) of Gc_0 (**63**) and 40 ml of anhydrous THF were added. The solution was cooled down to 0 ^{0}C in an ice bath. At this temperature, with the dropping funnel and drop by drop, 57 ml (22.5 mmol, 7.5 eq) of a solution of dichlorophosphonomethylhydrazide (**64**) in $CDCl_3$ (0.4 M) were added. After the addition, the mixture was kept at room temperature for 5 hours. Then, a NMR reaction control was performed to determine the full conversion. After that, the solvent was removed under vacuum and the solid was dissolved with the minimum amount of anhydrous THF under argon atmosphere. Then, anhydrous pentane was added and the product precipitated. The solvent was removed with a filtration cannula under argon atmosphere. The last operation had to be done two more times. The final solid was dried under vacuum and the product was isolated as a white powder (5.4 g, 98%).

Characterization:

- ^{31}P {^{1}H} NMR (100 MHz, $CDCl_3$): δ 8.4 (s, P_0), 62.5(s, P_1) ppm.
- ^{1}H NMR (250 MHz, $CDCl_3$): δ 3.5 (d, 18H, JH_dP_1=15 Hz, H_d),
  7.0 (d, 12H, JH_3H_b=10 Hz, H_a),
  7.6 (d, 12H,JH_aH_b=7.5 Hz, H_b), 7.6 (d, 6H, JH_bH_c=2.5 Hz, H_c) ppm.
- MS (MALDI-TOF, positive mode): m/z 1827 $[M+H]^+$.
  Calculated: $C_{48}H_{48}N_{15}O_6P_9S_6Cl_{12}$: 1827.6.
- IR-ATR (cm^{-1}): 1598 ν(CCAr), δ(CCH) and ν(C=N), 1264 (PN), 1205 δ(PNN), 1100 δ(NCH), 943ν(P-O), 786 (P=S).

Gc_1' (66)

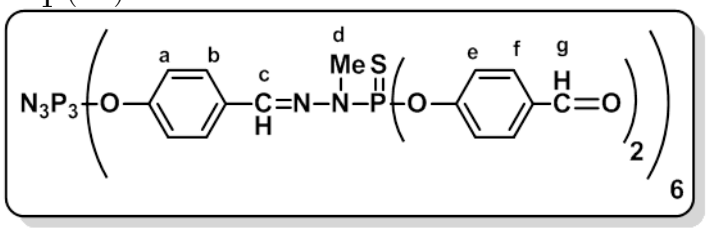

In a 250 ml round-bottom flask 5 g (2.7 mmol, 1 eq) of Gc_1 (**65**), 28.5 g (87.5 mmol, 32 eq) of Cs_2CO_3 and 5.35 g (43.7 mmol, 16 eq) of *p*-hydroxybenzaldehyde were mixed under argon atmosphere with 75 ml of anhydrous THF at 0 ^{0}C. The mixture was stirred for 4 hours at room temperature. After a NMR reaction control, the organic phase was transferred under argon atmosphere to a 500 ml round-bottom flask with a filtration cannula. The solvent was removed under vacuum and the solid was dissolved with the minimum amount of anhydrous THF under argon atmosphere. Anhydrous pentane was added and the product precipitated; the solvent was removed with a filtration cannula under argon atmosphere. The last operation had to be done two more times. The final solid was dried under vacuum and the product was isolated as a white powder (7.6 g, 97%).

Characterization:

- ^{31}P $\{^1$H$\}$ NMR (100 MHz, $CDCl_3$): δ 8.2 (*s*, P_0), 60.7(*s*, P_1) ppm.
- ^{1}H NMR (250 MHz, $CDCl_3$): δ 3.3 (*d*, 18H, JH_dP_d=10 Hz, H_d), 7.0 (*d*, 12H, JH_aH_b=10 Hz, H_a), 7.3 (*d*, 24H, JH_eH_f=7.5 Hz, H_e), 7.6 (*d*, 12H, JH_bH_a=7.5 Hz, H_b), 7.6 (*br*, 6H, H_c), 7.8 (*d*, 24H, JH_fH_e=10 Hz, H_f), 9.9 (*s*, 12H, H_g) ppm.
- MS (MALDI-TOF, positive mode): m/z 2870 $[M+Na]^+$ and picks of breakage of 1, 2 and 3 hydrazone bonds (2535, 2200, 1865).
  Calculated: $C_{132}H_{108}N_{15}O_{30}P_9S_6$: 2855.6.
- IR-ATR (cm^{-1}): 1700 ν(C=O), 1598 ν(CCAr), δ(CCH) and ν(C=N), 1264 ν(PN), 1205 δ(PNN), 1100 δ(NCH), 943 ν(P-O), 786 ν(P=S).

Gc_2 (67)

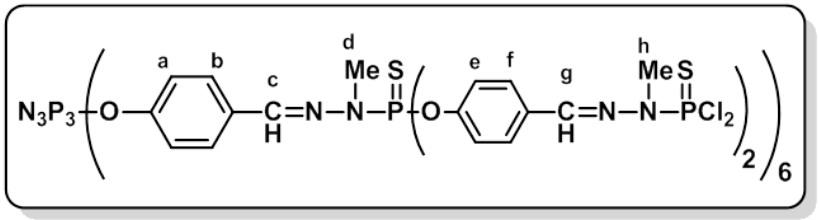

In a three necked 100 ml round-bottom flask equipped with a dropping funnel and under argon atmosphere 2.6 g (1.26 mmol, 1 eq) of Gc_1' (**66**) and 70 ml of anhydrous THF were added. The solution was cooled down to 0 ^{0}C in an ice bath. At this temperature, with the dropping funnel and drop by drop, 47 ml (18.9 mmol, 15 eq) of a solution of dichlorophosphonomethylhydrazide (**64**) in $CDCl_3$ (0.4 M) were added. After the

addition, the mixture was kept at room temperature for 4 hours. Then, a NMR reaction control was performed to determine the full conversion. After that, the solvent was removed under vacuum and the solid was dissolved with the minimum amount of anhydrous THF under argon atmosphere. Anhydrous pentane was added and the product precipitated; the solvent was removed with a filtration cannula under argon atmosphere. The last operation had to be done two more times. The final solid was dried under vacuum and the product was isolated as a white powder (5.9 g, 99%).

Characterization:

- ^{31}P $\{^{1}$H$\}$ NMR (100 MHz, $CDCl_3$): δ 8.4 (s, P_0), 62.1(s, P_1), 62.9 (s, P_2) ppm.
- ^{1}H NMR (250 MHz, $CDCl_3$): δ 3.3 (d, 18H, JH_dP_1=10 Hz, H_d), 3.4 (d, 36H, JH_hP_2=12.5 Hz, H_h), 7.0 (d, 12H, JH_aH_b=10 Hz, H_a), 7.2 (d, 24H, JH_eH_f=7.5 Hz, H_e), 7.6-7.7 (m, 54H, H_b, H_c, H_f, H_g) ppm.
- MS (MALDI-TOF, positive mode): m/z does not fly. Calculated: $C_{144}H_{144}N_{39}O_{18}P_{21}S_{18}Cl_{24}$: 4772.4.
- IR-ATR (cm^{-1}): 1598 ν(CCAr), δ (CCH) and ν(C=N), 1264 ν(PN), 1205 δ(PNN), 1100 δ(NCH), 943 ν(P-O), 786 ν(P=S).

Gc_2' (68)

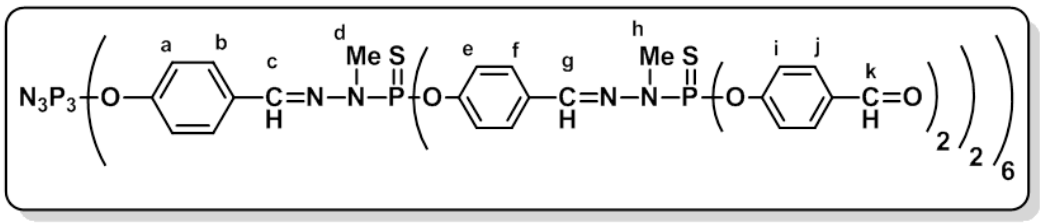

In a 250 ml round-bottom flask 5.5 g (1.2 mmol, 1 eq) of Gc_2' (**67**), 24 g (73.8 mmol, 62 eq) of Cs_2CO_3 and 4.5 g (36.9 mmol, 31 eq) of p-hydroxybenzaldehyde were mixed under argon atmosphere with 58 ml of anhydrous THF at 0 ^{0}C. Then, the mixture was stirred for 4 hours at room temperature. After a NMR reaction control, the organic phase was transferred under argon atmosphere, to a 250 ml round-bottom flask with a filtration cannula. The solvent was removed under vacuum and the solid was dissolved with the minimum amount of anhydrous THF under argon atmosphere. Anhydrous pentane was added and the product precipitated; the solvent was removed with a filtration cannula under argon atmosphere. The last operation had to be done two more times. The final solid was dried under vacuum and the product was isolated as a white powder (7.8 g, 97%).

Characterization:

- ^{31}P $\{^1H\}$ NMR (100 MHz, $CDCl_3$): δ 8.4 (s, P_0), 60.4 (s, P_2), 62.4 (s, P_1) ppm.
- ^1H NMR (250 MHz, $CDCl_3$): δ 3.2 (d, 18H, JH_dP_1=12.5 Hz, H_d) 3.3 (d, 36H, JH_hP_2=10 Hz, H_h), 6.9 (d, 12H, JH_aH_b=7.5 Hz, H_a), 7.2 (d, 24H, JH_eH_f=7.5 Hz,H_e), 7.3 (d, 24H, JH_iH_j=7.5 Hz, H_i), 7.55-7.62 (m, 54H, H_b, H_c, H_f, H_g), 7.8 (d, 48H, JH_iH_j=10 Hz, H_j), 9.9 (s, 24H, H_k) ppm.
- MS (MALDI-TOF, positive mode): m/z does not fly. Calculated: $C_{312}H_{264}N_{39}O_{66}P_{21}S_{18}$: 6843.3.
- IR-ATR (cm^{-1}): 1700 ν(C=O), 1598 ν(CCAr), δ(CCH) and ν(C=N), 1264 ν(PN), 1205 δ(PNN), 1100 δ(NCH), 943 ν(P-O), 786 ν(P=S).

Gc_3 (**69**)

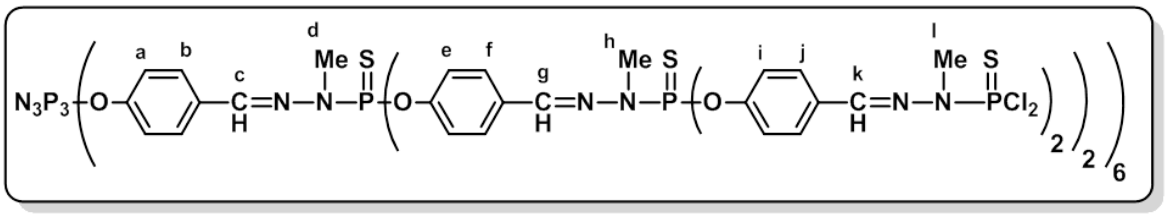

In a three necked 100 ml round-bottom flask equipped with a dropping funnel and under argon atmosphere 0.5 g (73 μmol, 1 eq) of Gc_2' (**68**) and 20 ml of anhydrous THF were added. The solution was cooled down to 0 ^{0}C in an ice bath. At this temperature, with the dropping funnel and drop by drop, 5.5 ml (2.2 mmol, 30 eq) of a solution of dichlorophosphonomethylhydrazide (**64**) in $CDCl_3$ (0.4 M) were added. After this addition, the mixture was kept at room temperature for 4 hours. Then, a NMR reaction control was performed to determine the full conversion. After that, half of the solvent was removed under vacuum. Anhydrous pentane was added and the product precipitated; the solvent was removed with a filtration cannula under argon atmosphere. The solid was dissolved with the minimum amount of anhydrous THF under argon atmosphere and anhydrous pentane was added. The product precipitated and the solvent was removed with a filtration cannula under argon atmosphere. The last operation had to be done one more time. The final solid was dried under vacuum and the product was isolated as a white powder (780 mg, 99%).

Characterization:

- ^{31}P $\{^1H\}$ NMR (100 MHz, $CDCl_3$): δ 8.6 (s, P_0), 62.1 (s, P_2), 62.5 (s, P_1), 63.0 (s, P_3) ppm.

- ^{1}H NMR (250 MHz, $CDCl_3$): δ 3.2 (d, 18H, JH_dP_1=12.5 Hz, H_d), 3.3 (d, 36H, JH_hP_2=10 Hz, H_h), 3.4 (d, 72H, JH_lP_3=15 Hz, H_l), 6.9 (d, 12H, JH_aH_b=7.5 Hz, H_a), 7.1-7.2 (m, 72H, H_e, H_i), 7.5-7.7 (m, 126H, H_b, H_c, H_f, H_g, H_j, H_k) ppm.
- MS (MALDI-TOF, positive mode): m/z does not fly. Calculated: $C_{336}H_{336}N_{87}O_{42}P_{45}S_{42}Cl_{48}$: 10707.1.
- IR-ATR (cm^{-1}): 1598 ν(CCAr), δ(CCH) and ν(C=N), 1264 ν(PN), 1205 δ(PNN), 1100 δ(NCH), 943 ν(P-O), 786 ν(P=S).

Gc_3' (70)

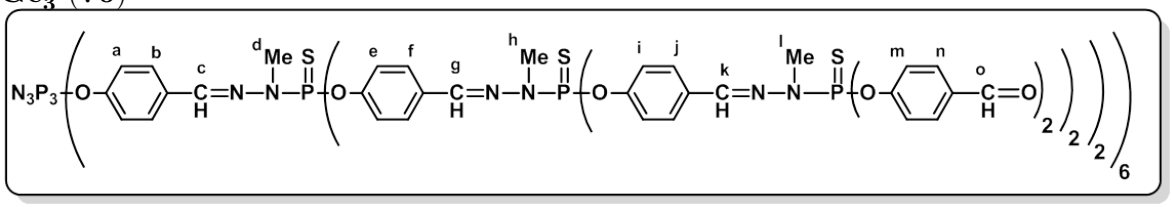

In a 250 ml round-bottom flask 780 mg (73 μmol, 1 eq) of Gc_3 (**69**), 3.05 g (9.4 mmol, 130 eq) of Cs_2CO_3 and 571 mg (4.7 mmol, 64 eq) of p-hydroxybenzaldehyde were mixed under argon atmosphere with 20 ml of anhydrous THF at 0 ^{0}C. The mixture was stirred for 4 hours at room temperature. After a NMR reaction control, the organic phase was transferred under argon atmosphere to a 250 ml round-bottom flask with a filtration cannula. The solvent was removed under vacuum and the solid was dissolved with the minimum amount of anhydrous THF under argon atmosphere. Anhydrous pentane was added and the product precipitated; the solvent was removed with a filtration cannula under argon atmosphere. The last operation had to be done two more times. The final solid was dried under vacuum and the product was isolated as a white powder (1.0 g, 93%).

Characterization:

- ^{31}P $\{^{1}$H$\}$ NMR (100 MHz, $CDCl_3$): δ 8.4 (s, P_0), 60.4 (s, P_3), 62.4 (s, P_2), 62.7 (s, P_1) ppm.
- ^{1}H NMR (250 MHz, $CDCl_3$): δ 3.2 (d, 18H, JH_dP_1=10 Hz, H_d), 3.27 (d, 36H, JH_hP_2=12.5 Hz, H_h), 3.32 (d, 72H, JH_lP_3=12.5 Hz, H_l), 6.9 (d, 12H, JH_aH_b=10 Hz, H_a), 7.2 (d, 72H, JH_eH_f (H_iH_j)= 7.5 Hz, H_e, H_i), 7.3 (d, 96H, JH_mH_n=7.5 Hz, H_m), 7.5-7.6 (m, 126H, H_b, H_c, H_f, H_g, H_j, H_k), 7.8 (d, 96H, JH_mH_n=7.5 Hz, H_n), 9.9 (s, 48H, H_o) ppm.
- MS (MALDI-TOF, positive mode): m/z does not fly. Calculated: $C_{672}H_{576}N_{87}O_{138}P_{45}S_{42}$: 14818.8.
- IR-ATR (cm^{-1}): 1700 ν(C=O), 1598 ν(CCAr), δ(CCH) and ν(C=N), 1264 ν(PN), 1205 δ(PNN), 1100 δ(NCH), 943 ν(P-O), 786 ν(P=S).

Gc_0COOH (71)

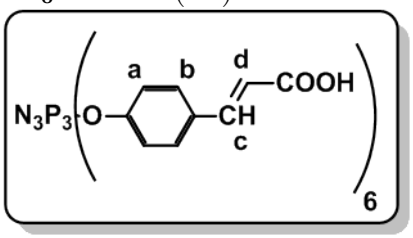

In a 10 ml round-bottom flask, under Ar atmosphere, a mixture of 200 mg (224 μmol, 1 eq) of Gc_0 (**63**) and 91 mg of malonic acid (1.74 mmol, 7.5 eq) were added. The mixture was dissolved in anhydrous pyridine (3 ml) and 34 μl of anhydrous piperidine (340 μmol, 1.5 eq) were added. The mixture was heated at 95 °C for 4 hours. Then, the solution was refluxed for 15 minutes to complete the carbon dioxide removal. The yellow solution was then allowed to cold down, and once the solution was at room temperature, was cooled in an ice bath. After that, the cold solution was poured onto 10 M HCl (6 ml). The precipitate of dendrimer was the washed with water (2 ml) and dried under vacuum. finally, the white crude powder was washed with diethylether. The final solid was dried under vacuum and the product was isolated as a white powder (258 mg, 99%).

Characterization:

- ^{31}P $\{^1H\}$ NMR (100 MHz, ^{6}d-dimethylsulfoxide): δ 8.4 (s, P_0) ppm.
- ^1H NMR (250 MHz, ^{6}d-dimethylsulfoxide): δ 6.5 (d, 6H, JH_cH_d=16 Hz, H_d), 6.9 (d, 12H, JH_aH_b=8.75 Hz, H_a), 7.55 (d, 6H, JH_cH_d= 16 Hz, H_c), 7.6 (d, 12H, JH_aH_b= 8.75 Hz, H_b) ppm.
- MS (MALDI-TOF, negative mode): m/z 1114 $[M-H]^-$. Calculated: $C_{54}H_{42}N_3O_{18}P_3$: 1114.
- IR-ATR (cm^{-1}): 1682 ν(C=O), 1598 ν(CCAr), δ(CCH) and ν(C=N), 1270 ν(PN), 1205 δ(PNN), 1100 δ(NCH), 943 ν(P-O),

Gc_1COOH (72)

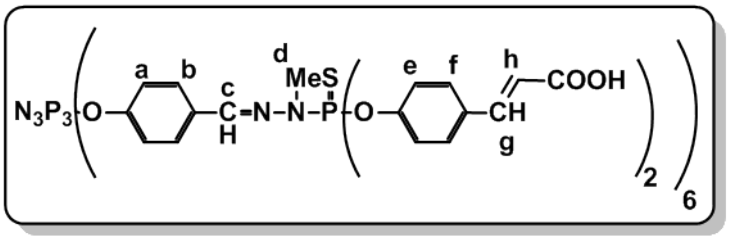

In a 10 ml round-bottom flask, under Ar atmosphere, a mixture of 100 mg (35 μmol, 1 eq) of Gc'_1 (**66**) and 55 mg of malonic acid (525 μmol, 15 eq) were added. The mixture was dissolved in anhydrous pyridine (3 ml) and 6 μl of anhydrous piperidine (53 μmol, 1.5 eq) were added. The mixture was heated at 95 °C for 4 hours. Then, the solution was refluxed for 15 minutes to complete the carbon dioxide removal. The yellow solution was then allowed to cold down, and once the solution was at room temperature, was cooled in an ice bath. After that, the cold solution was poured onto 10 M HCl (6 ml). The precipitate of dendrimer was the washed with water (2 ml) and dried under vacuum. finally, the white crude powder was washed with diethylether. The final solid was dried under vacuum and the product was

isolated as a white powder (118 mg, 99%).

Characterization:

- ^{31}P $\{^{1}H\}$ NMR (100 MHz, 100 MHz, ^{6}d-dimethylsulfoxide): δ 8.4 (s, P_0), 60.4 (s, P_1) ppm.
- ^{1}H NMR (250 MHz, 100 MHz, ^{6}d-dimethylsulfoxide): δ 3.3 (d, 18H, JH_dP_1=11 Hz, H_d),
  6.4 (d, 12H, JH_gH_h=16 Hz, H_h), 7.0 (d, 12H, JH_aH_b=8.5 Hz, H_a),
  7.1 (d, 24H, JH_eH_f = 8 Hz, H_d), 6.5 (d, 12H, JH_gH_h=16 Hz, H_e),
  7.6 (s, 6H, H_c), 7.7 (d, 36H, JH_eH_f (JH_aH_b)=8.5 Hz, H_b, H_f) ppm.
- MS (MALDI-TOF, positive mode): m/z does not fly.
  Calculated: $C_{156}H_{132}N_{15}O_{42}P_9S_6$: 3360.
- IR-ATR (cm^{-1}): 1700 ν(C=O), 1598 ν(CCAr), δ(CCH) and ν(C=N), 12764 ν(PN), 1205 δ(PNN), 1100 δ(NCH), 943 ν(P-O), 786 ν(P=S).

9.3.2 Radical dendrimers synthesis

9.3.2.1 PTM dendrimers

$Gc_0(PTM^{\bullet})_6$ (73)

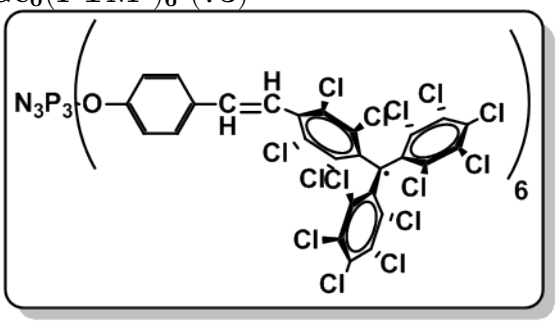

In a 25 ml schlenk, under argon atmosphere, 733 mg (836 μmol, 7.2 eq) of **9**, and 188 mg (1.67 mmol, 14 eq) of potassium *tert*-butoxide were dissolved in 2 ml of anhydrous THF were added. The mixture was stirred for 10 minutes and 0.1 g (116 μmol, 1 eq) of Gc_0 (**63**) in 3 ml of anhydrous THF drop by drop with a cannula. The reaction mixture changed its color from orange to violet and was stirred for 18 hours. After a reaction control by IR-ATR and NMR, 158 mg (928 μmol, 8 eq) of $AgNO_3$ were added and the conversion of the anion into the radical was monitored by UV-Vis. After 5 minutes, 158 mg (928 μmol, 8 eq) of extra $AgNO_3$ were added. Once the anion was fully converted into radical, the reaction mixture was filtered and the solvent removed under vacuum. The product was purified by column chromatography on Bio-Beads^{TM}gel (size exclusion chromatography) with HPLC grade THF as eluent and column chromatography on silica gel with HPLC grade THF as eluent. The product was isolated as brown-green powder (229 mg, 38%).

Characterization:

- EPR (DCM/Toluene 1/1): g: 2.0030, a_H: 1.65 G, $a_{C_{orto}}$: 10.0 G, $a_{C_{bridge}}$: 12.0 G, a_{C_α}: 29.0 G, ΔH_{pp}: 1.3 G, ΔH_{sp}: 3.1 G.
- ^{31}P $\{^1H\}$ NMR (100 MHz, $CDCl_3$): 9.3 (s, P_0) ppm.
- ^1H NMR (250 MHz, $CDCl_3$): No signals.
- MS (MALDI-TOF, positive mode): m/z 5198 $[M+H]^+$.
  Calculated: $C_{162}H_{36}Cl_{84}N_3O_6P_3$: 5191. The spectrum shows a broad band due to the isotopic abundance of chlorine.
- IR-ATR (cm^{-1}): 1660 ν(C=C), 1598 ν(CCAr) and δ(CCH), 1274 ν(PN), 1205 δ(PNN), 1100 δ(NCH), 943 ν(P-O).

$Gc_1(PTM^{\bullet})_{12}$ (74)

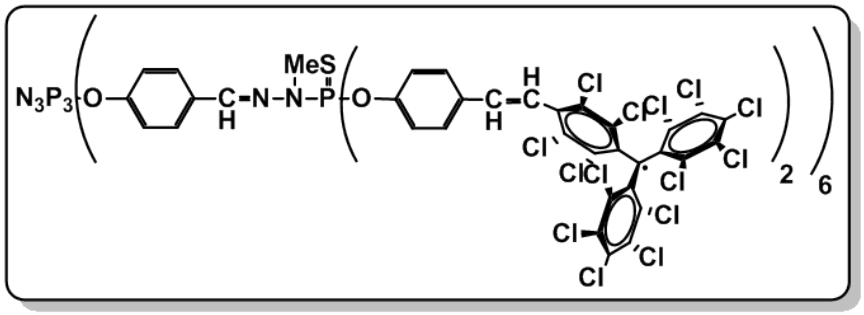

In a 25 ml schlenk, under argon atmosphere, 442 mg (504 μmol, 14.4 eq) of diethyl 4-[bis(2,3,4,5,6-pentachlorophenyl)methyl]-2,3,5,6-tetrachlorobenzyl phosphonate (**9**), and 118 mg (1.1 mmol, 31 eq) of potassium *tert*-butoxide were dissolved in 2 ml of anhydrous THF. The mixture was stirred for 10 minutes and 0.1 g (35 μmol, 1 eq) of $Gc_1^{'}$ (**66**) in 3 ml of anhydrous THF were added, drop by drop, with a cannula. The reaction mixture changed its color from orange to violet and was stirred for 18 hours. After a reaction control by IR-ATR and NMR, 94 mg (560 μmol, 16 eq) of $AgNO_3$ were added and the conversion of the anion into the radical was monitored by UV-Vis. After 5 minutes, 94 mg (560 μmol, 16 eq) of extra $AgNO_3$ were added. Once the anion was fully converted into radical, the reaction mixture was filtered and the solvent was removed under vacuum. The product was purified by column chromatography on Bio-Beads^{TM}gel with HPLC grade THF as eluent and then by column chromatography on silica gel with HPLC grade THF as eluent. The product was isolated as brown-green powder (220 mg, 55%).

Characterization:

- EPR (DCM/Toluene 1/1): g: 2.0034, the line is too broad to determine the hyperfine splitting constants a_{H}, $a_{C_{orto}}$, $a_{C_{bridge}}$ and $a_{C_{\alpha}}$, ΔH_{sp}: 2.7 G.
- ^{31}P $\{^1H\}$ NMR (100 MHz, $CDCl_3$): δ 8.5 (s, P_0), 62.7 (s, P_1) ppm.
- ^1H NMR (250 MHz, $CDCl_3$): No signals.
- MS (MALDI-TOF, positive mode): m/z 11537 $[M+H]^+$, and peaks of breakage of 1, 2, 3 and 4 hydrazone bonds (9786, 7990, 6220, 4425).
  Calculated: $C_{372}H_{118}Cl_{168}N_{15}O_{18}P_9S_6$: 11512.
- IR-ATR (cm^{-1}): 1660 ν(C=C), δ(CCH) and ν(C=N), 1274 ν(PN), 1205 δ(PNN), 1100 δ(NCH), 943 ν(P-O), 786 ν(P=S).

$Gc_2(PTM^{\bullet})_{24}$ (75)

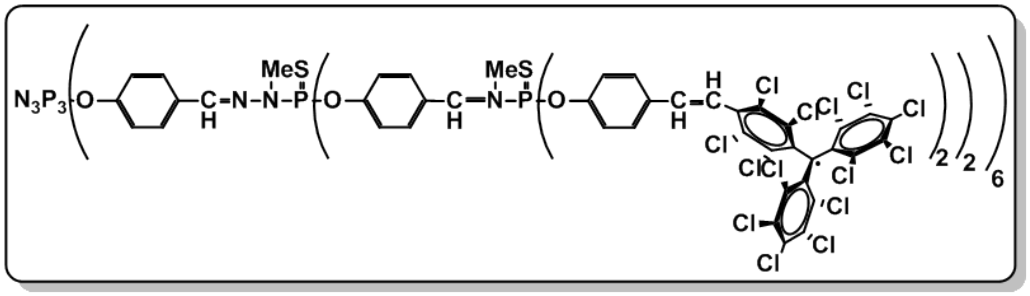

In a 10 ml schlenk, under argon atmosphere, 369 mg (421 mmol, 28.8 eq) of diethyl 4-[bis(2,3,4,5,6-pentachlorophenyl)methyl]-2,3,5,6-tetrachlorobenzyl phosphonate (**9**), and 94 mg (842 mmol, 57.6 eq) of potassium *tert*-butoxide were dissolved in 2 ml of anhydrous THF. The mixture was stirred for 10 minutes and 0.1 g (14.6 μmol, 1 eq) of Gc_2' (**68**) in 3 ml of anhydrous THF were added, drop by drop, with a cannula. The reaction mixture changed its color from orange to violet and was stirred for 18 hours. After a reaction control by IR-ATR and NMR, 75 mg (438 μmol, 28.8 eq) of $AgNO_3$ were added and the conversion of the anion into the radical was monitored by UV-Vis. After 5 minutes, 75 mg (438 μmol, 28.8) of extra $AgNO_3$ were added. Once the anion was fully converted into radical, the reaction mixture was filtered and the solvent was removed under vacuum. The product was purified by column chromatography on Bio-Beads^{TM} gel with HPLC grade THF as eluent and then by column chromatography on silica gel with HPLC grade THF as eluent. The product was isolated as brown-green powder (141 mg, 40%).

Characterization:

- EPR (DCM/Toluene 1/1): g: 2.0034, the line is too broad to determine the hyperfine splitting constants a_{H}, $a_{C_{orto}}$, $a_{C_{bridge}}$ and a_{C_α}, ΔH_{sp}: 2.7 G.
- ^{31}P $\{^1H\}$ NMR (100 MHz, $CDCl_3$): No signals.
- ^1H NMR (250 MHz, $CDCl_3$): No signals.
- MS (MALDI-TOF, positive mode): The molecule breaks.
  Calculated: $C_{792}H_{288}Cl_{336}N_{39}O_{42}P_{21}S_{18}$: 24161.
- IR-ATR (cm^{-1}): 1660 ν(C=C), δ(CCH) and ν(C=N), 1264 ν(PN), 1205 δ(PNN), 1100 δ(NCH), 943 ν(P-O), 786 ν(P=S).

$Gc_3(PTM^{\bullet})_{48}$ (76)

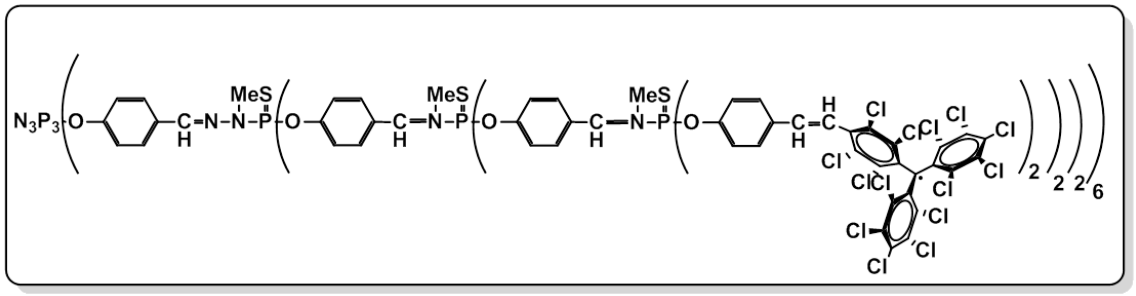

In a 10 ml schlenk, under argon atmosphere, 171 mg (194 μmol, 57.6 eq) of diethyl 4-[bis(2,3,4,5,6-pentachlorophenyl)methyl]-2,3,5,6-tetrachlorobenzyl phosphonate (**9**), and 44 mg (390 μmol, 115.6 eq) of potassium *tert*-butoxide were dissolved in 2 ml of anhydrous THF. The mixture was stirred for 10 minutes and 50 mg (3.4 μmol, 1 eq) of Gc_3' (**70**) in 3 ml of anhydrous THF were added, drop by drop, with a cannula. The reaction mixture changed its color from orange to violet and was stirred for 48 hours. After a reaction control by IR-ATR, 34 mg (202 μmol, 60 eq) of $AgNO_3$ were added and the conversion of the anion into the radical was monitored by UV-Vis. After 5 minutes, 34 mg (202 μmol, 60 eq) of extra $AgNO_3$ were added. Once the anion was fully converted into radical, the reaction mixture was filtered and the solvent was removed under vacuum. The product was purified by column chromatography on Bio-Beads^{TM} gel with HPLC grade THF as eluent and then by column chromatography on silica gel with HPLC grade THF as eluent. The product was isolated as brown-green powder (59 mg, 35%).

Characterization:

- EPR (DCM/Toluene 1/1): g: 2.0028, the line is too broad to determine the hyperfine splitting constants a_{H}, $a_{C_{orto}}$, $a_{C_{bridge}}$ and a_{C_α}, $\Delta \mathrm{H_{sp}}$: 2.7 G.
- ^{31}P $\{^1$H$\}$ NMR (100 MHz, $CDCl_3$): No signals.
- ^{1}H NMR (250 MHz, $CDCl_3$): No signals.
- MS (MALDI-TOF, positive mode): m/z The molecule breaks.
  Calculated: $C_{1632}H_{624}Cl_{672}N_{87}O_{90}P_{45}S_{42}$: 49488.
- IR-ATR (cm^{-1}): 1660 ν(C=C), δ(CCH) and ν(C=N), 1274 ν(PN), 1205 δ(PNN), 1100 δ(NCH), 943 ν(P-O), 786 ν(P=S).

4-(Benzyloxy)benzaldehyde (**77**)

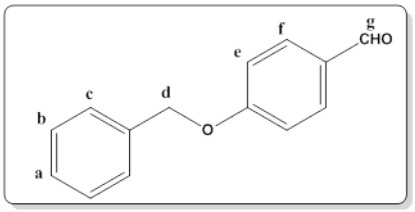

In a 100 ml flask 200 mg (1.64 mmol, 1 eq) of *p*-hydroxybenzaldehyde, 55 mg of NaH over mineral oil (2.29 mmol) and 60 mg of TBAI (0.16 mmol, 0.1 eq) were dissolved in 5 ml of anhydrous THF under argon atmosphere. 234 μl (1.96 mmol, 1.2 eq) of benzyl bromide were added and the mixture was stirred for 18 hours at room temperature. After this time 20 ml of water were added. The aqueous phase is extracted with dichloromethane for 3 times. The combined organic phase was dried over anhydrous magnesium sulfate and filtered, and the solvent was removed under vacuum. The product was purified by column chromatography on silica gel with mixtures of hexane and ethyl acetate as eluents. The product was isolated as a white powder (320 mg, 92%).

Characterization:

- ^{1}H NMR (250 MHz, $CDCl_3$): δ 5.1 (s, 2H, H_d), 7.1(d, JH_eH_f=7.5 Hz, 2H, H_e), 7.3-7.4 (m, 5H, H_c, H_b, H_a), 7.8 (d, JH_fH_e=7.5 Hz, 2H, H_f), 9.9 (s, 1H, H_g) ppm.
- MS (MALDI-TOF, positive mode): m/z 211 $[M+H]^+$.
  Calculated: $C_{14}H_{12}O_2$.: 212.

(E)-1-((4-(4-(benzyloxy)styryl)-2,3,5,6-tetrachrorophenyl-4-methyl--[bis(2,3,4,5,6-pentachlorophenyl)] (**78**)

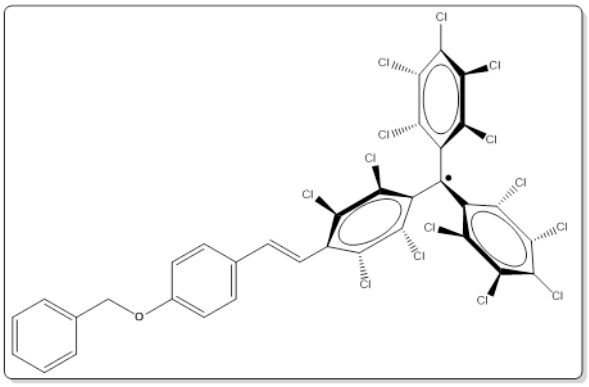

In a 25 ml schlenk, under argon atmosphere, 397 mg (452 μmol, 1.2 eq) of Diethyl 4-[bis(2,3,4,5,6-pentachlorophenyl)methyl]-2,3,5,6-tetrachlorobenzyl phosphonate (**9**), and 110 mg (980μmol, 2.6 eq) of potassium *tert*-butoxide were dissolved in 3 ml of anhydrous THF. The mixture was stirred for 10 minutes, and 80 mg (377 μmol, 1 eq) of 4-(benzyloxy)benzaldehyde (**77**) in 2 ml of anhydrous THF, drop by drop, with a cannula. The reaction mixture changed its color from orange to violet and was stirred for 18 hours. After a reaction control by IR-ATR and NMR, 89 mg (452 μmol, 1.2 eq) of $AgNO_3$ were added and the conversion of the anion into the radical was monitored by UV-Vis. After 2 minutes, 94 mg (560 μmol, 1.5 eq) of extra $AgNO_3$ were added. Once the anion was fully converted into radical, the reaction mixture was filtered and the solvent was removed under vacuum. The product was purified by column chromatography on silica gel with mixtures of hexane and ethyl acetate as eluents.

The product was isolated as a brown-green powder (275 mg, 78%).

Characterization:

- EPR (DCM/Toluene 1/1): g: 2.0030, a_{H}: 1.92 G, $a_{\mathrm{C}_{orto}}$: 10.20 G, $a_{\mathrm{C}_{bridge}}$: 12.45 G, $a_{\mathrm{C}_{\alpha}}$: 29.20 G, $\Delta \mathrm{H}_{\mathrm{pp}}$: 1.10 G, $\Delta \mathrm{H}_{\mathrm{sp}}$: 3.1 G.
- MS (MALDI-TOF, negative mode): m/z 933 $[\mathrm{M\text{-}H}]^{-}$.
  Calculated: $\mathrm{C_{34}H_{13}Cl_{14}O}$: 934.

9.3.2.2 TEMPO dendrimers

$\mathbf{Gc_0}$(amidoTEMPO$^{\bullet}$)$_6$ (79)

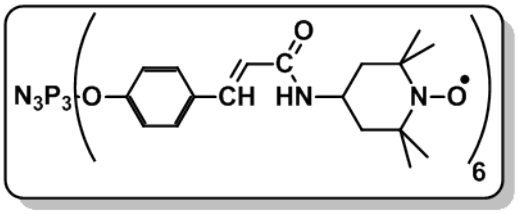

To a 10 ml round-bottom flask equipped with a magnetic stir-bar, and under argon atmosphere, 50 mg of $\mathrm{Gc_0COOH}$ (**71**) (45 μmol, 1 eq) and 65 mg (314 μmol, 7 eq) of diciclohexylcarbodiimide were dissolved in 3 ml of dry dichloromethane. The solution was stirred for 10 minutes and then, 54 mg (314 μmol, 7 eq) of 4-aminoTEMPO (**35**) were added. The mixture was stirred at room temperature for 16 hours (the disappearance of the acid was monitored by IR). After that, the mixture was dried under vacuum. The solid residue was suspended in EtOAc and filtered. The solid was washed two times with fresh EtOAc to afford the pure product as a off orange solid (49 mg, 54%).

Characterization:

- $^{31}\mathrm{P}$ $\{^{1}\mathrm{H}\}$ NMR (100 MHz, ^{6}d-dimethylsulfoxide): 7 ppm ($\mathrm{P_0}$).
- $^{1}\mathrm{H}$ NMR (250 MHz, ^{6}d-dimethylsulfoxide): No signals.
- EPR (water): g: 2.0055, $\mathrm{a_N}$: 16.9 G, $\Delta \mathrm{H}_{\mathrm{pp}}$: 1.7 G.
- MS (MALDI-TOF, positive mode): m/z Does not fly.
  Calculated: $\mathrm{C_{108}H_{144}N_{15}O_{18}p_3}^{6\bullet}$: 2033.
- IR-ATR ($\mathrm{cm^{-1}}$): 2977, 2930, 2851, 1640, 1600, 1502, 1200, 1372, 1160.

Gc_1(amidoTEMPO$^\bullet$)$_{12}$ (80)

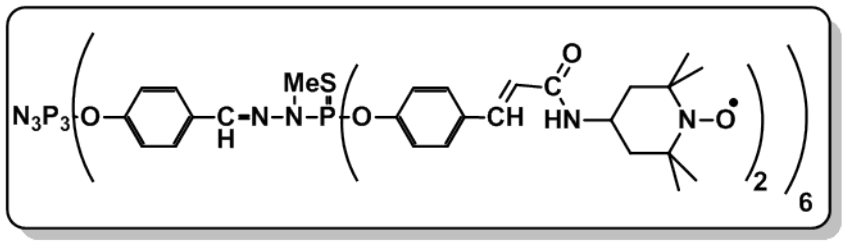

To a 10 ml round-bottom flask equipped with a magnetic stir-bar, and under argon atmosphere, 100 mg of Gc_1COOH (**72**) (30 μmol, 1 eq) and 92 mg (446 μmol, 15 eq) of diciclohexylcarbodiimide were dissolved in 5 ml of dry dichloromethane. The solution was stirred for 10 minutes and then, 77 mg (446 μmol, 15 eq) of 4-aminoTEMPO (**35**) were added. The mixture was stirred at room temperature for 16 hours (the disappearance of the acid was monitored by IR). After that, the mixture was dried under vacuum. The solid residue was suspended in EtOAc and filtered. The solid was washed two times with fresh EtOAc to afford the pure product as a off orange solid (105 mg, 68%).

Characterization:

- ^{31}P $\{^1$H$\}$ NMR (100 MHz, ^{6}d-dimethylsulfoxide): No signals.
- ^{1}H NMR (250 MHz, ^{6}d-dimethylsulfoxide): No signals.
- EPR (Water): g: 2.0056, a_N: 16.9 G, ΔH_{pp}: 1.7 G.
- MS (MALDI-TOF, positive mode): m/z Does not fly.
  Calculated: $C_{264}H_{336}N_{39}O_{42}P_9S_6{}^{12\bullet}$: 5199.
- IR-ATR (cm^{-1}): 2977, 2930, 2851, 1636, 1600, 1502, 1372, 1160.

9.3.2.3 PROXYL dendrimers

9.3.2.3.1 Lysine-PROXYL dendrimers

6-((tert-butoxycarbonyl)amino)-2-(1-oxo-2,2,5,5- tetramethylpyrrolidine- 3-carboxamido)hexanoate (**85**)

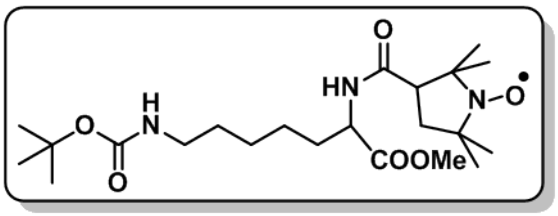

In a 10 mL schlenk bottom flask, under Ar atmosphere, 77 mg of 3-carboxy-PROXYL (**81**) (414 μmol, 1.2 eq) and mg of HATU (414 μmol, 1.2 eq) were dissolved in anhydrous dichloromethane (3 mL). Then, DIEA was added and the mixture was stirred for 10 minutes. After that, 0.1 g of H-Lys(BOC)OMe (**84**) (334, μmol, 1.0) were added. the mixture was stirred at room temperature for 16 hours (until all the H-Lys(BOC)OMe was consumed, which could be monitored by TLC using ninhydrin as a developer. Then, water was added (4 mL). The two phases were separated, the aqueous phase was extracted with dichloromethane (3 X 5 mL) and the total organic phase was dried over $MgSO_4$. The product was purified by column chromatography with mixtures of dichloromethane/MeOH. The pure product was isolated as yellow pale solid (116 mg, 81%).

Characterization:

- EPR (solvent): g: 2.0054, a_N: 14.7 G, ΔH_{pp}: 1.0 G.
- MS (MALDI-TOF, positive mode): m/z 443.2 $[M+H]^+$.
  Calculated: $C_{22}H_{40}N_3O_6^{\bullet}$: 442.6.
- IR-ATR (cm^{-1}): 3320 (NH carbamate), 2981 2937 (NH amide), 2732, 1742, 1714, 1673, 1612, 1517 (N-C=O amide), 1456, 1385, 1361, 1313, 1250, 1207, 1168, 1151, 1090, 1063, 1113, 865, 798, 660.

6-(amino)-2-(1-oxo-2,2,5,5- tetramethylpyrrolidine-3-carboxamido)hexanoate (**86**)

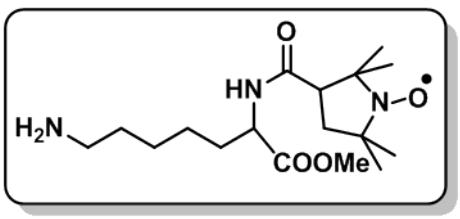

In a 10 mL schlenk bottom flask, under argon atmosphere, 150 mg of Proxyl-Lys(Boc)OMe (**85**) (341 μmol, 1 eq) was dissolved in 4 mL of anhydrous dichloromethane. The solution was cold to 0 °C using an ice bath. Then, 590 μL of TFA (7.66 mmol, 2200 eq) was added to the reaction (the solution turns from yellow to red). The reaction was warmed and then, was stirred at room temperature for six hours. After a TLC control, using 4-anisaldehyde as a developer, of the total deprotection, the volatile byproducts were removed by solvent evaporation

under one day of vacuum. The pure product was isolated as orange oil (111 mg, 99%).

Characterization:

- EPR (solvent): g: 2.0054, a_N: 14.7 G, ΔH_{pp}: 1.0 G.
- MS (MALDI-TOF, negative mode): m/z 342 $[M-H]^-$.
  Calculated: $C_{17}H_{32}N_3O_4^{\bullet}$: 342.5.
- IR-ATR (cm^{-1}): 2957, 2919 (NH amide), 2852, 1778, 1738, 1671, 1466, 1436, 1401, 1318, 1293, 1175, 1128, 1068, 1025, 925, 880, 798, 720, 705.

Proxyl-Lys(Gc_0)-OMe (**87**)

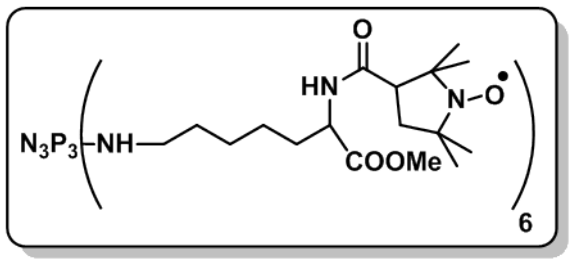

In a 10 ml schlenk bottom flask, under argon atmosphere, 93 mg (26.75 μmol, 1 eq) of hexachlorocyclotryphosphazene (**62**), 204 mg (627 μmol, 24 eq) of Cs_2CO_3 were added and the mixture was suspended in anhydrous THF. In another schlenk bottom flask, under Ar atmosphere, 110 mg of Proxyl-Lys-OMe (**86**) (249 μmol, 9 eq) were dissolved in freshly distilled. Then, the solution of the second schlenk was transferred by cannula to the first one. The mixture was stirred 16 hours at room temperature. After that, the solvent was removed by cannula and the residual white solid was washed with anhydrous pentane three times. The final residue was purified by column chromatography with mixtures of dichlorometane/methanol and GPC in THF. The pure product was isolated as yellow pale oil (216 mg, 36%).

Characterization:

- EPR (THF): g: 2.0055, a_N: 14.3 G, ΔH_{pp}: 1.1 G.
- MS (MALDI-TOF, positive mode): m/z $[M+Na]^+$.
  Calculated: $C_{102}H_{186}N_{21}O_{24}P_3{}^{6\bullet}$: 2183.6.
- IR-ATR (cm^{-1}): 3280, 2932, 2862, 1741 (C=O ester), 1658 (C=O amide), 1543, 1461, 1443, 1368, 1308, 1200, 1173, 1153, 1135, 973, 833, 800, 720.

Proxyl-Lys(Gc_0)-OH (**89**)

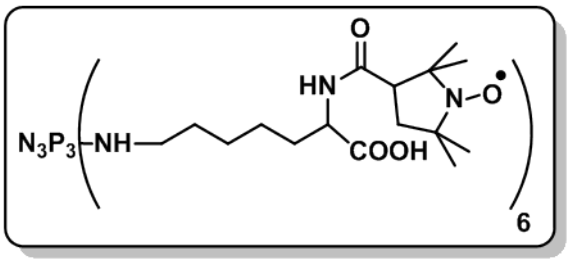

In a 10 ml schlenk bottom flask, 20 mg of Proxyl-Lys(Gc_0)-OMe (**87**) (8.9 μmol, 1 eq) and 230 mg of LiOH monohydrate(540 μmol, 60 eq) were added. Both reagents were dissolved in 3 ml of a THF/H_2O 2/1 solution . The reaction was stirred for 16 hours at room After that, the solvent was removed and the product was dried under vacuum. The lithium salt was isolated as pale yellow solid (19 mg, 99%).

Characterization:

- EPR (water): g: 2.0058, a_N: 15.96 G, ΔH_{pp}: 1.44 G.
- MS (MALDI-TOF, positive and negative modes): m/z Does not fly. Calculated: $C_{96}H_{174}N_{21}O_{24}P_3{}^{6\bullet}$: 2099.5.
- IR-ATR (cm^{-1}): 3678, 3322, 2933, 1658, 1594, 1496, 1440, 1409, 1308, 1205, 14179, 1137, 1084, 1059, 1039, 863.

Proxyl-Lys(Gc_1)-OMe (**88**)

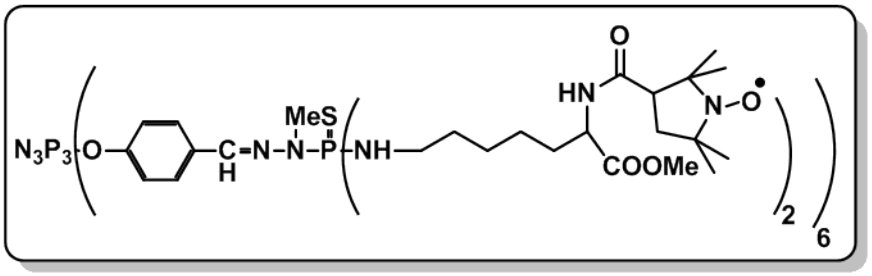

In a 10 ml schlenk bottom flask, under argon atmosphere, 163 mg (9 μmol, 1 eq) of Gc_1 (**65**), 119 mg (365 μmol, 40 eq) of Cs_2CO_3 were added and the mixture was suspended in anhydrous THF (2 ml). In another 10 ml schlenk bottom flask, under Ar atmosphere, 54 mg of Proxyl-Lys-OMe (**86**) (164 μmol, 18 eq) were dissolved in freshly distilled THF (4 ml). Then, the solution of the second schlenk was transferred by cannula to the first one. The mixture was stirred 16 hours at room temperature. After that, the solvent was removed by cannula and the residual white solid was washed with anhydrous THF three times. The combined organic phase was dried under vacuum. The final residue was purified by Gel Permeation Chromatography with THF. The pure product was isolated as yellow pale oil (400 mg, 85%).

Characterization:

- EPR (THF): g: 2.0059, a_N: 14.3 G, ΔH_{pp}: 1.14 G.

- MS (MALDI-TOF, positive and negative modes): m/z Does not fly. Calculated: $C_{252}H_{420}N_{51}O_{54}P_9S_6^{12\bullet}$: 5499.5.
- IR-ATR (cm^{-1}): 3300 (NH amine), 2952 2877 (NH amide + CH dendrimer), 1741, 1666 (C=O ester + amide), 1546, 1506 (N=P core), 1463, 1438, 1423, 1396, 1298, 1198, 1168, 1123, 1033, 948, 885, 828, 798, 720.

Proxyl-Lys(Gc_1)-OH (**90**)

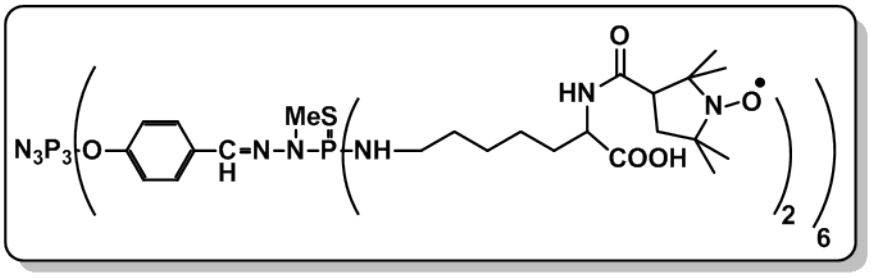

In a 10 ml schlenk bottom flask, 35 mg of Proxyl-Lys(Gc_1)-OMe (**88**) (6.8 μmol, 1 eq) and 400 mg of LiOH monohydrate (934 μmol, 138 eq) were added. Both reagents were dissolved in 6 ml of a THF/H_2O 2/1 solution . The reaction was stirred for 16 hours at room temperature and, after that, the solvent was removed and the product was dried under vacuum. The lithium salt was isolated as pale orange oleaginous solid (34 mg, 99%).

Characterization:

- EPR (water): g: 2.0051, a_N: 16.06 G, ΔH_{pp}: 1.20 G.
- MS (MALDI-TOF, positive and negative modes): m/z Does not fly. Calculated: $C_{240}H_{396}N_{51}O_{54}P_9S_6^{12\bullet}$: 5331.2.
- IR-ATR (cm^{-1}): 3353, 2944, 2878, 1681, 1597, 1420, 1373, 1205, 1182, 1135, 1053, 953, 868, 838, 801, 723.

9.3.2.3.2 Tyrosine-PROXYL dendrimers

Boc-Tyr(Gc_0)-OMe (**92**)

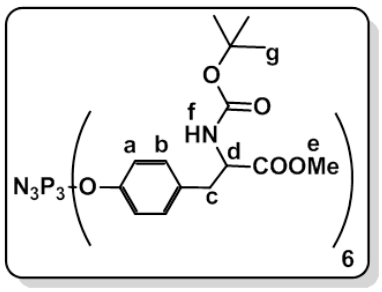

In a schlenk bottom flask, under Ar atmosphere, 50 mg of hexachlorocyclotryphosphazene (**62**) (144 μmol, 1 eq), 690 mg of Cs_2CO_3 (2.12 mmol, 15 eq) and 260 mg of BOC-Tyr-OMe (**91**) (884 μmol, 6.2 eq) were added. The mixture of reagents was suspended in anhydrous THF, just distilled over Na. The reaction mixture was stirred at room temperature for 16 hours. Once the reaction was finished (the reaction was monitored by ^{31}P), the solid residue was separated of the organic face with a filtration cannula, the residual solid

was washed with anhydrous THF and filtered two times. The whole organic phase was dried in vacuum. The obtained solid was dissolved in the minimum amount of anhydrous THF (1 ml), and then, the product was precipitated with anhydrous pentane (30 mL). The organic phase was separated of the solid with a filtration cannula obtaining the product as a solid. The precipitation process was carried out two more times. Finally, the pure product was further dried under vacuum. The pure product was isolated as white powder (234 mg, 86%).

Characterization:

- ^{31}P {^{1}H} NMR (100 MHz, $CDCl_3$): δ 9.4 (s, P_0) ppm.
- ^{1}H NMR (400 MHz, $CDCl_3$): δ 1.4 (s, 54H, H_g), 3.0 (m, 12H, H_c), 3.7 (s, 18H, H_e), 4.5 (s, 6H, H_d), 5.1 (s, 6H, H_f), 6.9-7.1 (m, 24H, H_a, H_b) ppm.
- MS (MALDI-TOF, positive mode): m/z $[M+Na]^+$. Calculated: $C_{84}H_{108}N_9O_{30}O_3$: 1816.7.
- IR-ATR (cm^{-1}): 3357 (NH carbamate), 2974, 1741 (C=O ester), 1708 (C=O carbamate), 1606, 1503 (N=P core), 1438, 1391, 1363, 1258, 1250, 1195, 1158, 1105, 1055, 1017, 953, 883, 835, 778, 760, 695.

H-Tyr(Gc$_0$)-OMe (95)

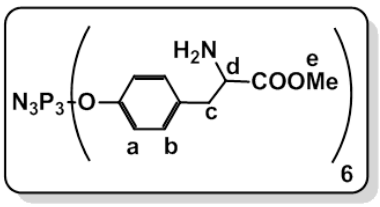

In a 10 mL schlenk bottom flask, under Ar atmosphere, 41 mg of BocTyr(Gc$_0$)OMe (**92**) (21.5 μmol, 1 eq) was dissolved in 2.2 ml of anhydrous dichloromethane. The dissolution was cooled to 0°C with an ice-bath, then 200 μl of TFA (2.6 mmol, 30 eq for each Boc group) was added dropwise. After the addition, the reaction mixture was warmed to room temperature and stirred for six hours. Then, the solvent and the excess of acid were evaporated under vacuum. The pure product was isolated as trifuoroacetic salt (425 mg, 93%).

Characterization:

- ^{31}P {^{1}H} NMR (100 MHz, D_2O): δ 9.0 (s, P_0) ppm.
- ^{1}H NMR (400 MHz, D_2O): δ 3.0 (m, 12H, H_c), 3.8 (s, 18H, H_e), 4.4 (m, 6H, H_d), 7.0 (m, 12H, H_a), 7.2 (m, 12H, H_b) ppm.
- MS (MALDI-TOF, positive mode): m/z $[M+Na]^+$. Calculated: $C_{54}H_{60}N_9O_{18}p_3$: 1216.0.
- IR-ATR (cm^{-1}): 3352, 2979, 1743 (C=O ester), 1708, 1693, 1503 (N=P core), 1441, 1366, 1248, 1155, 1058, 1018, 950, 885, 833.

Proxyl-Tyr(Gc_0)-OMe (**98**)

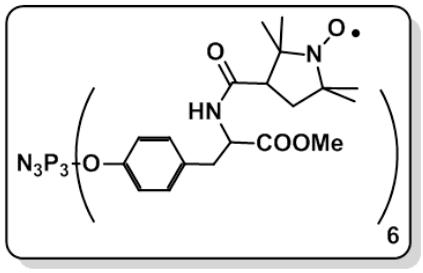

In a 25 ml schlenk bottom flask, under Ar atmosphere, 220 mg of 3-carboxy-PROXYL (**81**) (117 μmol, 7 eq, 1.16 eq for each α amino group) and 50 mg eg HATU (127 μmol, 7.7 eq, 1.3 eq for each α amino group), as a coupling agent were dissolved in in 6 ml of anhydrous dichloromethane. Then, 90 μl of DIEA (517 μmol, 10 eq for each α amino group) was added. The mixture was stirred for 15 min. After that, the mixture was transferred with dropwise to a schlenk, under Ar atmosphere, that contains 324 mg of H-Tyr(Gc_0)OMe (**95**) dendrimer (16.4 μmol, 1 eq). The reaction mixture was stirred at room temperature until total consumption of the primary dendrimer-amine (the reaction control was carried out by TLC, using anisaldehide as a developer). Once the reaction finished, 5 ml of water was added and the phases were separated; the aqueous phase was extracted with dichlorometane. The whole organic phase was dried over $MgSO_4$ and the solvent was removed under vacuum. The final protected radical dendrimer was purified by column chromatography using mixtures of CH_2Cl_2 as solvent. The pure product was isolated as yellow pale oil (359 mg, 95%).

Characterization:

- EPR (THF): g: 2.0057, a_N: 14.21 G, ΔH_{pp}: 1.67 G.
- MS (MALDI-TOF, positive mode): m/z $[M+Na]^+$.
  Calculated: $C_{114}H_{156}N_{15}O_{30}P_3{}^{6\bullet}$: 2309.5.
- IR-ATR (cm^{-1}): 3397, 3209 (NH amide), 2954, 2882, 2336, 1721 (C=O ester), 1663 (C=O amide), 1530, 1503 (N=P core),1461, 1443, 1391, 1371, 1306, 1268, 1183, 1165, 1130, 1040, 955, 843, 743.

Proxyl-Tyr(Gc_0)-OH (**101**)

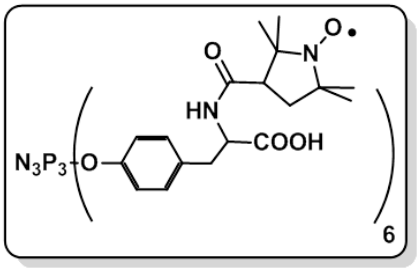

In a 10 ml bottom flask, 36 mg of Proxyl-Tyr(Gc_0)OMe (**98**) (16 μmol, 1 eq) and 532 mg of LiOH monohydrate(1.24 mmol, 78 eq) were added. Both reagents were dissolved in 6 ml of a THF/H_2O 2/1 solution . The reaction was stirred for 16 hours at room temperature. After that, the solvent was removed and the product was dried under vacuum. The lithium salt was isolated as pale yellow solid (35 mg, 98%).

Characterization:

- EPR (water): g: 2.0055, a_N: 16.00 G, ΔH_{pp}: 1.30 G.
- MS (MALDI-TOF, positive mode): m/z $[M+Na]^+$.
  Calculated: $C_{108}H_{144}N_{15}O_{30}P_3{}^{6\bullet}$: 2225.3
- IR-ATR (cm^{-1}): 3562, 2864, 2325, 1570, 1506, 1408, 1368, 1271, 1180, 1163, 980, 837.

Boc-Tyr(Gc_1)-OMe (**93**)

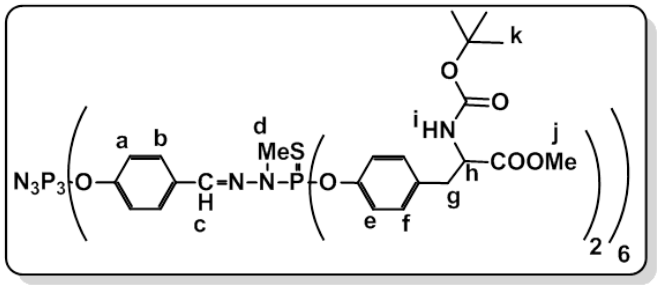

In a 10 ml schlenk bottom flask, under Ar atmosphere, 4000 mg of Gc_1 (**65**) (21.7 μmol, 1 eq), 290 mg of Cs_2CO_3 (883 μmol, 42 eq) and 85 mg of BOC-Tyr-OMe (**91**) (286 μmol, 13.2 eq) were added. The mixture of reagents was suspended in 4 ml of anhydrous THF, just distilled over Na. The reaction mixture was stirred at room temperature for 16 hours. Once the reaction was finished (the reaction was monitored by ^{31}P), the solid residue was separated of the organic face with a filtration cannula, the residual solid was washed with anhydrous THF and filtered two times. The whole organic phase was dried in vacuum. The obtained solid was dissolved in the minimum amount of anhydrous THF (1 ml), and then, the product was precipitated with anhydrous pentane (30 mL). The organic phase was separated of the solid with a filtration cannula obtaining the product as a solid. The precipitation process was carried out two more times. Finally, the pure product was further dried under vacuum. The pure product was isolated as white powder (107 mg, 90%).

Characterization:

- ^{31}P $\{^1H\}$ NMR (100 MHz, $CDCl_3$): δ 8.3 (s, P_0), 62.6 (s, P_1) ppm.
- ^1H NMR (400 MHz, $CDCl_3$): δ 1.4 (s, 108H, H_k), 3.0 (m, 24H, H_g), 3.22 (m, 18H, H_d), 3.63 (s, 36H, H_j), 4.51 (s, 12H, H_h), 5.1 (s, 12H, H_i), 7.0-7.1 (m, 60H, H_a, H_e, H_f), 7.6 (m, 18H, H_b, H_c) ppm.
- MS (MALDI-TOF, positive mode): m/z $[M+Na]^+$.
  Calculated: $C_{228}H_{288}N_{27}O_{66}P_9S_6$: 4934.0
- IR-ATR (cm^{-1}): 3362 (NH carbamate), 2974, 1746 (C=O ester), 1706 (C=O carbamate), 1603, 1501 (N=P core), 1441, 1394, 1366, 1245, 1190, 1155, 1105, 1055, 1018, 943, 920, 1888, 838, 780, 750, 663.

H-Tyr(Gc$_1$)-OMe (**96**)

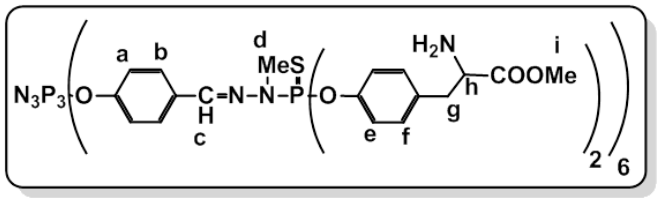

In a 10 mL schlenk bottom flask, under Ar atmosphere, 255 mg of BocTyr(Gc$_1$)OMe (**93**) (52 μmol, 1 eq) was dissolved in 1 ml of anhydrous dichloromethane. The dissolution was cooled to 0°C with an ice-bath, then 130 μl of TFA (1.7 mmol, 32 eq for each Boc group) was added dropwise. After the addition, the reaction mixture was warmed to room temperature and stirred for five hours. Then, the solvent and the excess of acid were evaporated under vacuum. The pure product was isolated as trifuoroacetic salt (174 mg, 90%).

Characterization:

- ^{31}P {^{1}H} NMR (100 MHz, $CDCl_3$): δ 9.1 (s, P_0), 62.7 (s, P_1) ppm.
- ^{1}H NMR (400 MHz, $CDCl_3$): δ 3.2 (m, 24H, H_g), 3.3 (m, 18H, H_d), 3.72 (s, 36H, H_i), 4.3 (s, 12H, H_h), 7.8-7.7 (m, 60H, H_a, H_b, H_e, H_f), 7.8 (s, 6H, H_c) ppm.
- MS (MALDI-TOF, positive mode): m/z $[M+Na]^+$. Calculated: $C_{216}H_{264}N_{27}O_{66}P_9S_6$: 4765.7.
- IR-ATR (cm^{-1}): 2997, 1751 (C=O ester), 1666, 1603, 1506 (N=P core), 1466, 1426, 1406, 1238, 1193, 1178, 1165, 1123, 1018, 945, 920, 890, 833, 800, 785, 718.

Proxyl-Tyr(Gc$_1$)-OMe (**99**)

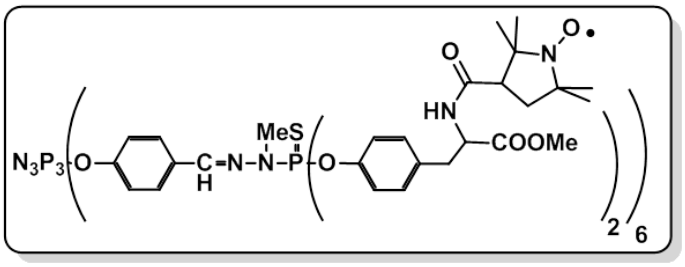

In a 25 ml schlenk bottom flask, under Ar atmosphere, 171 mg of 3-carboxy-PROXYL (**81**) (92 μmol, 23.3 eq, 1.9 eq for each α amino group) and 31 mg of HATU (80 μmol, 20 eq, 1.7 eq for each α amino group), as a copling agent were dissolved in in 4 ml of anhydrous dichloromethane. Then, 100 μl of DIEA (574 μmol, 1.2 eq for each α amino group) was added. The mixture was stirred for 15 min. After that, the mixture was transferred with dropwise to a schlenk, under Ar atmosphere, that contains 20 mg of H-Tyr(Gc$_1$)OMe (**96**) dendrimer (4 μmol, 1 eq). The reaction mixture was stirred at room temperature until total consumption of the primary dendrimer-amine (the reaction control was carried out by TLC, using p-anisaldehido as a developer). Once the reaction finished, 5 ml of water was added and the phases were separated; the aqueous phase was extracted with 10 ml of dichlorometane. The whole organic phase was dried over $MgSO_4$ and the solvent was removed under vacuum. The final protected radical

dendrimer was purified by GPC using THF as solvent. The pure product was isolated as white oil (218 mg, 97%).

Characterization:

- EPR (THF): g: 2.0064, a_N: 14.38 G, ΔH_{pp}: To much broad to be measured.
- MS (MALDI-TOF, positive and negative modes): m/z Does not fly.
  Calculated: $C_{276}H_{360}N_{39}O_{66}P_9S_6{}^{12\bullet}$: 5751.2.
- IR-ATR (cm^{-1}): 3407 (NH amide), 2979, 2687, 1746 (C=O ester), 1668 (C=Oamide), 1603, 1506, 1466, 1378, 1193, 1163, 420, 838, 783.

Proxyl-Tyr(Gc_1)-OH (**102**)

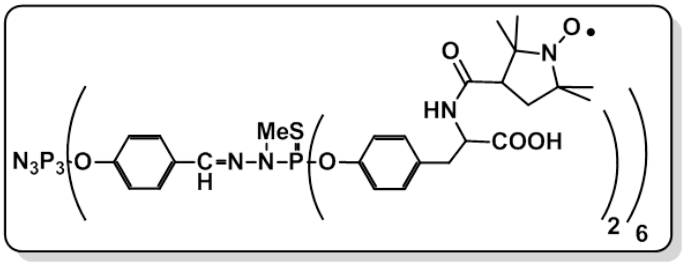

In a 10 ml bottom flask, 20 mg of Proxyl-Tyr(Gc_1)OMe (**99**) (3.5 μmol, 1 eq) and 20 mg of LiOH monohydrate(462 μmol, 133 eq) were added. Both reagents were dissolved in 3 ml of a THF/H_2O 2/1 solution . The reaction was stirred for 16 hours at room temperature. After that, the solvent was removed and the product was dried under vacuum. The lithium salt was isolated as pale yellow solid (20 mg, 98%).

Characterization:

- EPR (water): g: 2.0057, a_N: 16.15 G, ΔH_{pp}: 1.27 G.
- MS (MALDI-TOF, positive and negative modes): m/z Does not fly
  Calculated: $C_{264}H_{336}N_{39}O_{66}P_9S_6{}^{12\bullet}$: 5582.9.
- IR-ATR (cm^{-1}): 3633, 3398, 2980, 1602, 1504, 1415, 1196, 1160, 1056, 947, 837.

Boc-Tyr(Gc_2)-OMe (**94**)

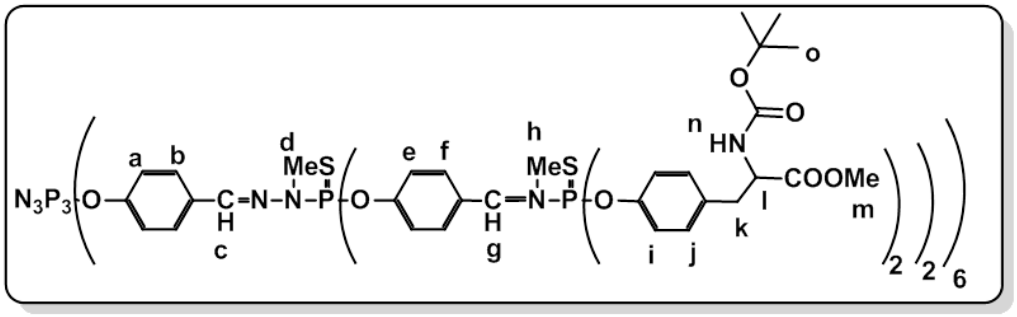

In a schlenk bottom flask, under Ar atmosphere, 83 mg of Gc_2 (**67**) (17.4 μmol, 1 eq), 334 mg of Cs_2CO_3 (1.03 mmol, 59 eq) and 151 mg of BOC-Tyr-OMe (**91**) (512 μmol, 29 eq) were added. The mixture of reagents was suspended in 9 ml of anhydrous THF, just distilled over Na. The reaction mixture was stirred at room temperature for 48 hours. Once the reaction was finished (the reaction was monitored by ^{31}P), the solid residue was separated of the organic face with a filtration cannula, the residual solid was washed with anhydrous THF and filtered two times. The whole organic phase was dried in vacuum. The obtained solid was dissolved in the minimum amount of anhydrous THF (1 ml), and then, the product was precipitated with anhydrous pentane (30 mL). The organic phase was separated of the solid with a filtration cannula obtaining the product as a solid. The precipitation process was carried out two more times. Finally, the product was dried under vacuum and purified by GPC using THF as solvent and by preparative thin layer chromatography (mixtures of CH_2Cl_2/MeOH). The pure product was isolated as brown pale oil (104 mg, 54%).

Characterization:

- ^{31}P $\{^1H\}$ NMR (100 MHz, $CDCl_3$): δ 8.3 (s, P_0), 68.6 (m, P_1, P_2) ppm.
- ^1H NMR (400 MHz, $CDCl_3$): δ 1.4 (s, 216H, H_o), 3.26 (s, 18H, H_d), 3.28 (s, 36H, H_h), 3.6 (s, 72H, H_m), 4.0 (m, 48H, H_k), 4.5 (s, 24H, H_l), 5.1 (s, 24H, H_n), 6.9-7.6 (m, 186H, H_a, H_b, H_c, H_e, H_f, H_g, H_i, H_j) ppm.
- MS (MALDI-TOF, positive and negative modes): m/z Does not fly
  Calculated: $C_{504}H_{624}N_{63}O_{138}P_{21}S_{18}$: 11000.3.
- IR-ATR (cm^{-1}): 3355 (NH carbamate), 2977, 2954, 2932, 2869, 1746 (C=O ester), 1706 (C=O carbamate), 1601, 1503 (N=P core), 1441, 1366, 1240, 1190, 1155, 1053, 1015, 915, 840, 780.

H-Tyr(Gc_2)-OMe (97)

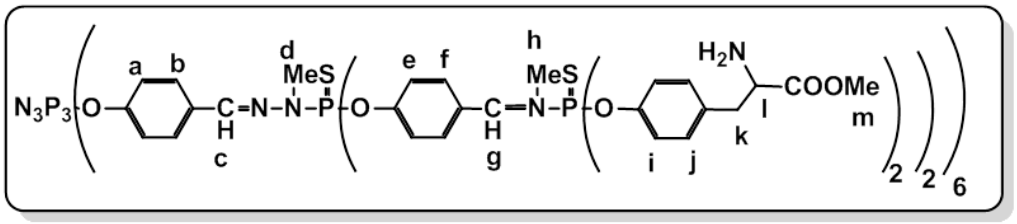

In a 10 mL schlenk bottom flask, under Ar atmosphere, 41 mg of BocTyr(Gc_2)OMe (**94**) (3.7 μmol, 1 eq) was dissolved in 1 ml of anhydrous dichloromethane. The dissolution was cooled to 0°C with an ice-bath, then 200 μl of TFA (2.6 mmol, 30 eq for each Boc group) was added dropwise. After the addition, the reaction mixture was warmed to room temperature and stirred for six hours. Then, the solvent and the excess of acid were evaporated under vacuum. The pure product was isolated as trifuoroacetic salt (355 mg, 85%).

Characterization:

- ^{31}P $\{^1$H$\}$ NMR (100 MHz, CD_3OD): δ 9.0 (s, P_0), 62.2 (m, P_1), 62.8 (s, P_2) ppm.
- ^{1}H NMR (400 MHz, CD_3OD): δ 3.26 (s, 18H, H_d), 3.28 (s, 36H, H_h), 3.5 (m, 48H, H_k), 3.9 (s, 72H, H_m), 4.4 (s, 24H, H_l), 6.9-7.8 (m, 186H, H_a, H_b, H_c, H_e, H_f, H_g, H_i, H_j) ppm.
- MS (MALDI-TOF, positive and negative modes): m/z Does not fly. Calculated: $C_{384}H_{432}N_{63}O_{90}P_{21}S_{18}$: 8597.5.
- IR-ATR (cm^{-1}): 2928, 1784 (C=O ester), 1747 (C=O carbamate), 1660, 1604, 1506, (N=P core), 1467, 1444, 1371, 1293, 1189, 1133, 1018, 917, 835, 779, 720, 701.

Proxyl-Tyr(Gc_2)-OMe (100)

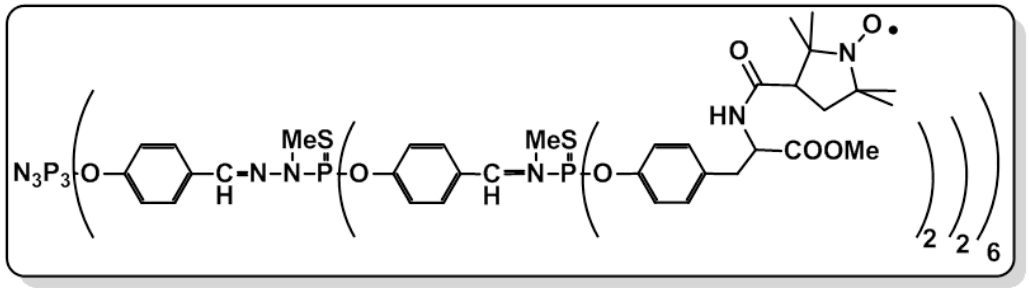

In a 25 ml schlenk bottom flask, under Ar atmosphere, 210 mg of 3-carboxy-PROXYL (**81**) (113 μmol, 30 eq, 1.3 eq for each α amino group) and 48 mg eg HATU (123 μmol, 33 eq, 1.4 eq for each α amino group), as a coupling agent were dissolved in in 6 ml of anhydrous dichloromethane. Then, 770 μl of DIEA (4.4 mmol, 50 eq for each α amino group) was added. The mixture was stirred for 15 min. After that, the mixture

was transferred with dropwise to a schlenk, under Ar atmosphere, that contains 32 mg of H-Tyr(Gc_2)OMe (**97**) dendrimer (3.7 μmol, 1 eq). The reaction mixture was stirred at room temperature until total consumption of the primary dendrimer-amine (the reaction control was carried out by TLC, using *p*-anisaldehide as a developer). Once the reaction finished, 7 ml of water was added and the phases were separated; the aqueous phase was extracted with dichlorometane. The whole organic phase was dried over $MgSO_4$ and the solvent was removed under vacuum. The final protected radical dendrimer was purified by GPC using THF as solvent. The pure product was isolated as yellow oil (36 mg, 95%).

Characterization:

- EPR (THF): g: 2.0061, a_N and ΔH_{pp}: Could not be measured.
- MS (MALDI-TOF, positive and negative modes): m/z Does not fly
  Calculated: $C_{600}H_{768}N_{87}O_{138}P_{21}S_{18}{}^{24\bullet}$: 12634.6.
- IR-ATR (cm^{-1}): 3207 (NH amide), 2967, 1736 (C=O ester), 1673 (C=O amide), 1603, 1506 (N=P core), 1466, 1391, 1368, 1306, 1193, 1180, 1163, 1135, 1060, 1020, 943, 925, 828, 783, 740.

General synthesis of Proxyl-Tyr(Gc_2)-OH (**103**)

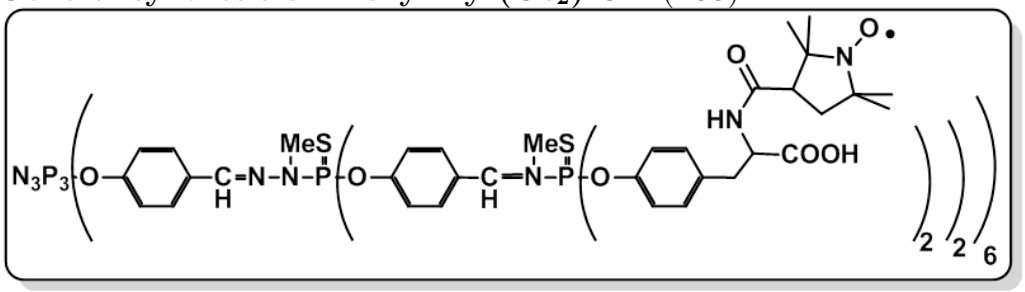

In a 10 ml bottom flask, 40 mg of Proxyl-Tyr(Gc_2)OMe (**100**) (3.2 μmol, 1 eq) and 37 mg of LiOH monohydrate(857 μmol, 270 eq) were added. Both reagents were dissolved in 4.5 ml of a THF/H_2O 2/1 solution . The reaction was stirred for 16 hours at room temperature. After that, the solvent was removed and the product was dried under vacuum. The lithium salt was isolated as pale yellow solid (35 mg, 98%).

Characterization:

- EPR (water): g: 2.0057, a_N: 16.20 G, ΔH_{pp}: 1.36 G.
- MS (MALDI-TOF, positive and negative modes): m/z Does not fly.
  Calculated: $C_{576}H_{720}N_{87}O_{138}P_{21}S_{18}{}^{24\bullet}$: 12298.
- IR-ATR (cm^{-1}): 3224, 2958, 1602, 1586, 1501, 1443, 1415, 1367, 1305, 1241, 1191, 1163, 1079, 1059, 1034, 978, 961, 866, 843, 712, 656.

Appendix A

Publications and Patents

- 2014 **Novel PTM-TEMPO Biradical for Fast Dissolution Dynamic Nuclear Polarization**
  Muñoz-Gómez J.L., Marín-Montesinos I., Lloveras V., Pons M., Vidal-Gancedo J., and Veciana, J., *Org. Lett.*, 16:p.5402, **2014**.

- 2014 **Derivados de 1,3-bisdifenilen-2-fenilalilo y su aplicación en Polarización Dinámica Nuclear**
  Muñoz-Gómez J.L., Monteagudo E., LLoveras V., Parella T., Veciana J., Vidal-Gancedo J., Spanish Patent P201431388.

- 2014 **Radical Dendrimers: A Family of Five Generations of Phosphorus Dendrimers Functionalized with TEMPO Radicals**
  Badetti E., Lloveras V., Muñoz-Gómez J.L., Sebastián R.M., Caminade A.M., Majoral J.P., Veciana J. and Vidal-Gancedo J., *Macromolecules*, 47:p.7717, **2014**.

- 2014 **A Benzyl Alcohol Derivative of BDPA radical for Fast Dissolution Dynamic Nuclear Polarization NMR spectroscopy**
  Muñoz-Gómez J.L., Monteagudo E., LLoveras V., Parella T., Veciana J., Vidal-Gancedo J., *Org. Biomol. Chem*, DOI: 10.1039/c4ob02356k.

Appendix B

Materials and Methods

5.1 Reagents and solvents.

Commercial reagents have been directly used.
Commercial solvents have been used directly, except for the following:

- THF has been distilled over metallic sodium and benzophenone under N_2.
- $CHCl_3$ has been distilled over CaH_2 and under N_2.
- Pyridine has been distilled over CaH_2 and under N_2.
- Piperidine has been distilled over CaH_2 and under N_2.
- Pentane has been distilled over P_2O_5 and under N_2.

5.2 Intrumentation.

5.2.1 Nuclear magnetic resonance.

The NMR spectra were performed in SeRMN of UAB using the next spectrometers: Bruker Avance DRX-250, Bruker DXP-360 MHz, Bruker Advance III-400 MHz, Bruker Advance-500 MHz or Bruker Advance II-600 MHz.

The chemical shifts of $^{31}P\{^1H\}$ spectra are expressed in ppm using as an internal reference H_3PO_4 85% in water for ^{31}P NMR (0 ppm).

The chemical shifts of ^1H spectra are expressed in ppm using as an internal reference tetramethylsilane (TMS) (0 ppm).

The chemical shifts of ^{13}C spectra are expressed in ppm using as an internal reference the canbon traces of the solvent.

5.2.2 UV-Vis.

The UV-Vis spectra were recorded in a Varian Cary 5000 spectrophotometer with double beam, the cuvettes used are made of quartz of 3 ml of volume and 1 cm of optical path length. The scanning for our work was from 200 to 900.

5.2.3 Infrared.

The infrared spectra were recorded in a Perkin Elmer spectrophotometer with ATR (Attenuated Total Reflectance) system. The scan range was 4000 cm^{-1} to 650 cm^{-1}.

5.2.4 Electron Paramagnetic Resonance.

The EPR spectra were obtained at room temperature using a Bruker ELEXYS E500 X band spectrometer equipped with a field-frequency (F/F) lock accessory and built in NMR Gaussmeter. A rectangular TE102 cavity was used for the measurements. Precautions to avoid undesirable spectral distortions and line broadenings, such as those arising from microwave power saturation and magnetic field over modulation, were also taken into account. To avoid dipolar line broadening from dissolved oxygen, solutions were always carefully degassed with pure Argon.

5.2.5 Mass spectrometry.

The mass spectra have been recorded in a MALDI-TOF Bruker Daltonic without matrix or using a matrix of 9-Nitroantracene.

5.2.5 Dynamic Nuclear Polarizarion.

The Fast Dissolution DNP were performed in an Hypersense 3.35 T vertical bore Oxford magnet that contains a microwave source of 94 GHz and controllable power of 100 mW. The sample is accommodated in a cryogenic chamber (VTI, variable temperature insert) maintaining the samples at 1.4 K using a mixture of vacuum cooling and a liquid helium bath.
The Magic Angle Spinning-DNP experiments were performed in an ADVANCE Bruker 9.4 T spectrometer for DNP-MAS equipped with a gyrotron generating a continuous wave. The μwaves irradiation was transmitted through a corrugated wave guide to a triple resonance $^{1}H/X/Y$ MAS probe for 3.2 mm rotors.[? ?] NMR spectra with μwave irradiation "on" or "off" were acquired at a temperature of 100 K, which was stabilized using a BioSpin MAS cooling system. The one dimensional (1D) cross-polarization magic angle spinning (CP-MAS) $^{1}H \rightarrow ^{13}C$ and $^{1}H \rightarrow ^{15}N$ experiments were performed in the ADVANCE Bruker 9.4 T spectrometer for DNP-MAS.

5.2.6 SQUID.

The magnetic susceptibility measurements were obtained in a Quantum Design MPMS XL magnetometer with a ramp of temperatures among 2-300k with a 5 T field. The samples were put in a gelatin capsule of low diamagnetic response.

5.2.7 Cyclic Voltamperometry.

The electric properties were studied with a potentiostat VersaSTAT 3 between -0.5 V and 1.5 V with a three-electrode cell.

5.3 Chromatographic techniques.

- Thin layer chromatography (TLC): The TLC was performed over chromatoplates of silica gel with aluminum support (60F, 0.2 mm, Merk), revealed with UV-Vis for high conjugated systems or tetrabutylammonium hydroxide for radicals.
- Column chromatography: The purification by column chromatography has been carried out with silica gel (Chromatogel 60 ÅCC, 230-400 mesh).
- Size exclusion chromatography: The purification by size exclusion was performed using THF HPLC grade and Bio-Beads^{TM}S-X3 as stationary phase.

Appendix C

Cyclic Voltamperometry

It is a type of potentiodynamyc electrochemical technique in which it is used three electrodes (**Figure C.1**):

- The reference electrode is an electrode that maintains a virtually invariant potential under the conditions prevailing in an electrochemical measurement, that permits the observation, measurement, or control of the potential of the indicator or working electrode (a).

- The auxiliary electrode serves to carry the current flowing through the cell (b).

- The working electrode serves as a transducer responding to the excitation signal and the concentration of the substance of interest in the solution being investigated (c).

In CV the analyte is dissolved in an appropriated solvent with an electrolyte that reduces the electronic resistance of the solution and is degassed with argon in order eliminate the O_2, an electroactive compound.

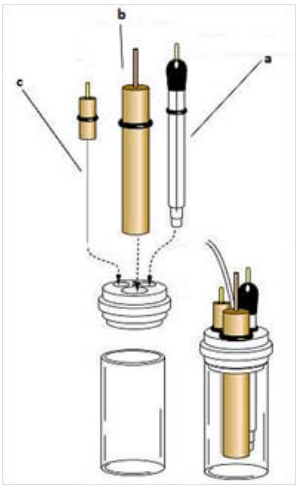

Figure C.1: Voltamperometric cell.

In CV experiments the working electrode potential is ramped linearly versus time. When the potential reaches a set potential the working electrodes potential ramp is inverted. The current at the working electrode is plotted versus the applied voltage to give the cyclic voltammogram (**Figure C.2**).

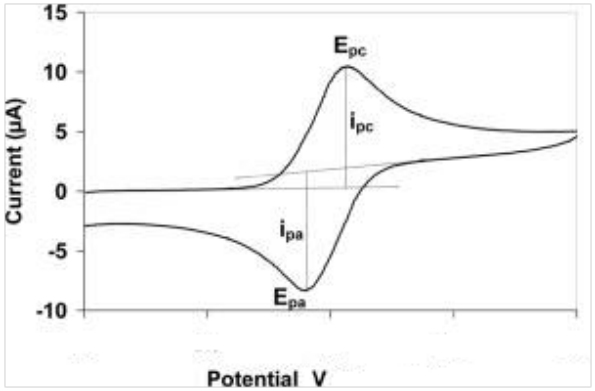

Figure C.2: Voltamperogram of redox specie.

References

Bard, Allen J.; Larry R. Faulkner, *Electrochemical Methods : Fundamentals and Applications*, **2001**, Jonh Wiley & Sons, New York.

Appendix **D**

Electron Paramagnetic Resonance (EPR)

To describe a paramagnetic isolated system under a magnetic field B, in EPR is used the formalism of Spin Hamiltonian. If we consider the paramagnetic system with, a part from the unpaired electron, some nuclei with angular momentum I$\neq$ 0, the spin Hamiltonian can be written as follows:

$$H = \mu_B \overline{BgS} - \mu_N \overline{Bg_N I} + \overline{IAS} + \overline{SDS} \tag{D.1}$$

In this expression appears the electronic Zeeman interaction between the unpaired electron and the magnetic field, the nuclear interaction between the nuclei with I$\neq$0 and the magnetic field, the hyperfine interaction between the electron spin and the nuclei with I$\neq$0 and, finally, the dipolar interaction or zero field splitting between two or more unpaired electrons.

EPR spectra in solution. Hyperfine structure.

EPR spectra of radicals in solution, especially those of organic radicals, are the easiest to interpret. In the case of a radical with an unpaired electron and in isotropic conditions, the expression of the spin Hamiltonian is reduced to:

$$H = \mu_B B g \overline{S} \tag{D.2}$$

and since the energy E is proportional to the magnetic moment, the quantization of spin angular momentum ($M_S = \pm\frac{1}{2}$) determines the quantization of the electron energy levels in a magnetic field, obtaining in this case two levels:

$$E_\alpha = +\frac{1}{2} g\mu_B \; and \; E_\beta = -\frac{1}{2} g\mu_B \tag{D.3}$$

being the resonance equation corresponding to the transition between the α and β states (**Figure D.1**) as follows:

$$\Delta E = E_\alpha - E_\beta = g\mu_B = h\nu \tag{D.4}$$

Therefore, the EPR spectrum will consist of a single line centered at the resonance field corresponding to the g factor and with a linewidth (ΔH_{pp}) characteristics of the radical. For technical reasons, the EPR spectra are always represented as a first derivative of the absorption signal.

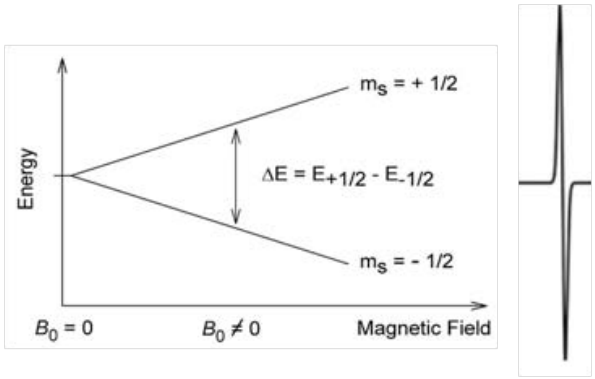

Figure D.1: Representation of the energy separation of an electron spin under a magnetic field B and the corresponding EPR spectrum.

If in the paramagnetic system, for example an organic radical, there are nuclei with I≠0, we also must take into account the hyperfine interaction. A radical having a nucleus with I=$\frac{1}{2}$, as a hydrogen atom, manifests a hyperfine splitting, a, which is proportional to the electron spin density on that atom. It presents an energy diagram and spectrum as that depicted in **Figure D.2a** which shows two lines with the same intensity 1:1. A nucleus with I=1, as a nitrogen atom, presents an energy diagram and spectrum as that depicted in **Figure D.2b** which shows three lines with the same intensity 1:1:1. In general, the rules for calculating the number of signals and their relative intensities are similar to those used in NMR.

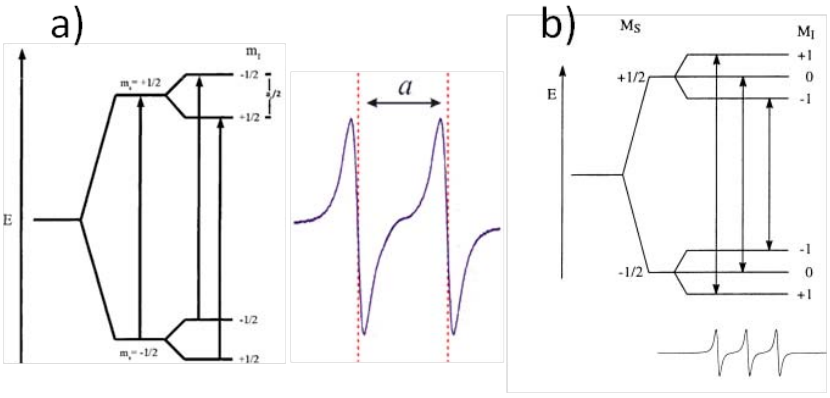

Figure D.2: Energy states of a system with one unpaired electron and one nucleus with a) I=$\frac{1}{2}$, b) I=1 and its corresponding EPR spectrum.

A radical system can have atoms of the same type with different hyperfine splitting due to its different position in the molecule and groups of atoms that show the same hyperfine constant because they are equivalent. The number of lines (2I+1) in the spectrum and their intensity can be predicted with the Pascal triangle **Figure D.3** (*e.g.*, one unpaired electron that interacts with three equivalent nuclei of spin I=$\frac{1}{2}$ generates an EPR spectrum with 4 lines with relatives intensities 1:3:3:1).
In general, there are some rules to interpret the EPR spectra in solution when the conditions

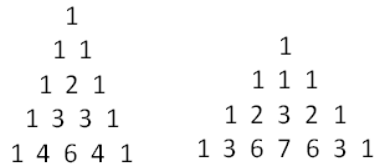

Figure D.3: Pascal triangle for nucleus I=$\frac{1}{2}$ (left) and for I=1 (right).

are isotropic and the splitting is of first order:

1. The spectrum must be symmetrical with respect to a central point.
2. The absence of a central line indicates an odd number of equivalent nuclei.
3. The separation between the two outer lines, always give the value of the smallest hyperfine splitting.
4. When in the molecule only appears nuclei with spin I=$\frac{1}{2}$, the sum $\sum_j n_j|a_j|$ is equal to the total extension of the spectrum; where nj is the number of nuclei with hyperfine splitting a_j.
5. The maximum possible number of lines is given by the expression $\prod_j(2n_jI_j+1)$ where n_j is the number of equivalent nuclei with spin I_j.
6. The best proof of the correct interpretation is the simulation of the spectrum.

Zero field splitting. Fine-structure.

These contributions may appear in systems with S>$\frac{1}{2}$ and express the energy splitting between different levels that take place in the absence of applied magnetic field. The simplest case corresponds to a biradical.

When a system contains two unpaired electrons that interact between them, appear two states of different energy, a symmetric one (triple state, S=1) and an antisymmetric one (singlet state, S=0). These two states present relative energies that depends on the sign and magnitude of the exchange integral J. The three different configurations of the triplet state present different energies even in absence of an external magnetic field due to the magnetic field generated by each electron over the other (zero field splitting).

We can say that, in the simplest case of system with S=1, the zero field splitting component of the spin Hamiltonian is:

$$H_{zfs} = \overline{SDS} \tag{D.5}$$

Where $\bar{D}$ is a symmetrical tensor of zero trace. The resolution of the corresponding secular determinant shows that the solution can be written in function of two parameters, D and E and they define completely the system. It is important to highlight the dependence of D parameter with the average distance between the two electrons which are interacting, while E parameter only depends on the wave function symmetry.

References

1. Weil John A., Bolton James R. and Wertz, *Electron Paramagnetic Resonance*, **1994**, Jonh Wiley & Sons, New York.

2. Atherton N.M., *Principles of Electron Resonance*, **1993**, Ellis Horwood Limited, London.

Appendix E

SQUID magnetometry

A superconducting quantum device (SQUID) is a very sensitive magnetometer used to measure extremely subtle magnetic fields. It is based on superconducting loops containing Josephson junctions (**Figure E.1**). In absence of any external magnetic field the input current, I, split into two branches equally. If a small external magnetic field (sample) is applied to the superconducting loop, a screening current, I_s, begins circulating in the loop which generates a magnetic field canceling the applied external flux, and a voltage appears across the junction that is proportional to the magnetic flux.

The magnetic susceptibility measurement with this device is carried out with a constant magnetic field. The temperature of the sample is decreased and the long moment of the system is measured. After some diamagnetic corrections, and taking into account the sample mass and its molecular weight, the molecular susceptibility can be determined and plotted versus temperature (**Figure E.2**). The ferromagnetic, antiferromagnetic or paramagnetic behavior can be determined since the magnetic susceptibility increases or decreases respect to the value predicted by the Curie law ($\chi = C/T$) where C is the Curie constant. The simplest expression that takes into account this effect is the Curie-Weiss law ($\chi = C/(T-\theta)$) where θ is the Weiss temperature and its positive or negative value indicates the type of the magnetic interaction ($\theta > 0$ ferromagnetic behavior, $\theta < 0$ antiferromagnetic behavior).

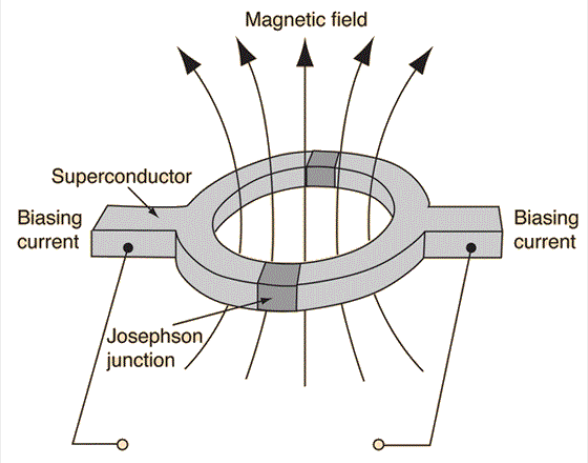

Figure E.1: Schematic representation of a Josephson junction in a SQUID system.

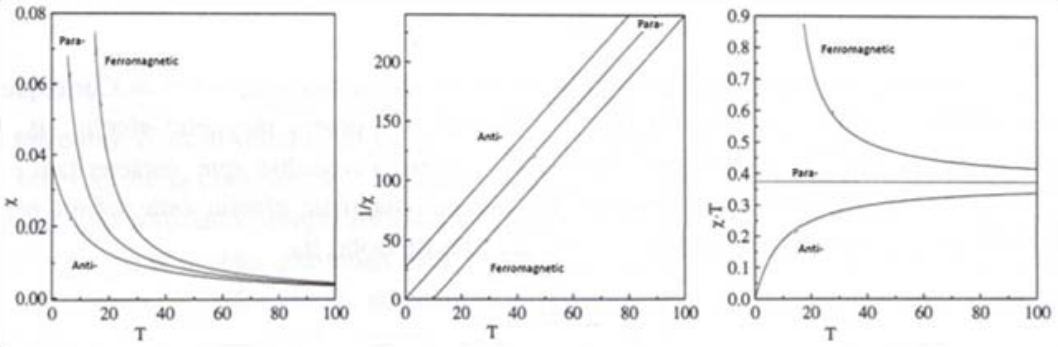

Figure E.2: Magnetic behavior versus temperature in the three classical plots, χ vs T, $1/\chi$ vs T and χT vs T.

References

John Clarke and Alex I. Braginski, *The SQUID Handbook : Applications of SQUIDs-and SQUID Systems, VolumeII*, **2006**, WILEY-VCH Verlag GmbH & Co. KGaA, Germany.